The Nigerian Institution of Mechanical Engineers,

Minna Chapter.

(A Division of the Nigerian Society of Engineers)

PROCEEDINGS

OF THE

5th INTERNATIONAL VIRTUAL CONFERENCE AND PAPER PRESENTATION

ON

THEME:

ECONOMIC DOWNTURN AS A RESULT OF COVID-19: THE ROLE OF MECHANICAL ENGINEERS IN RECOVERY.

DECEMBER, 2020.

The

NIGERIAN INSTITUTION OF MECHANICAL ENGINEERS,

Minna Chapter

(A Division of the Nigerian Society of Engineers)

PROCEEDINGS OF THE

5th INTERNATIONAL VIRTUAL CONFERENCE AND PAPER PRESENTATION.

Theme:

ECONOMIC DOWNTURN AS A RESULT OF COVID-19: THE ROLE OF MECHANICAL ENGINEERS IN RECOVERY.

Date: 19th December, 2020.

Edited by:

Engr. Prof. Olugboji A. Oluwafemi, Engr. Dr. Alkali Babawuya, Engr. Akonyi Nasiru Sule, Engr. Ayuba Jatau.

Organising Committee

Engr. Akonyi Nasiru Sule
Chairman

Scientific Equipment Development Institttute. SEDI, Minna.

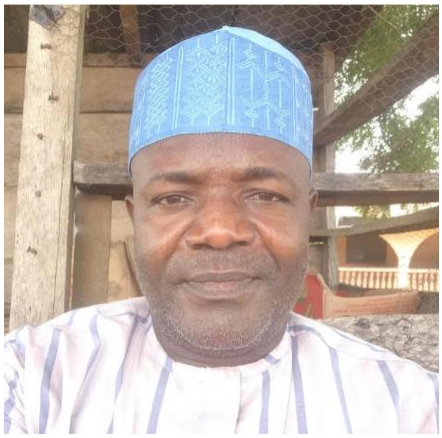

Engr. Dr. Babawuya Alkali
Coordinator

Department of Mechatronics
Federal University of Technology, Minna.

Engr. Ayuba Jatau
Secretary

Mechanical Engineering Department
The Polytechnic, Zungeru.
Niger State.

Welcome to NIMechE, Minna Chapter, 2020.

The 5th International (Virtual) Conference of Nigerian Institution of Mechanical Engineers, Minna chapter, Niger state, Nigeria (NIMechE-MC 2020) was successfully held on 19th December 2020. More than 30 papers were submitted and 22 was scheduled for presentations via the internet at the conference and published in this proceeding. Opening and Closing Remarks was witnessed by about 50 participants, who included authors, non-authors, and invited guests. The Opening speech by the Chapter Chairman was very brief and scintillating. He addressed the participants with a very warm welcome message to the conference. It is one of the highlights of the event. Another highlight was the **lead paper** presented by **Dr. Jack Hale, (**Visiting Fellow**),** School of Engineering, Newcastle University, United Kingdom. The title of Paper is **Recovery from COVID-19 – The Role of Engineers.**

Despite the short notice of this conference (less than one month), it attracted close to 30 researchers from different mechanical engineering options. This reflects the topical nature of the ***Theme*** of this conference. If we had announced earlier, it would have attracted more papers, no doubt. We are very proud of it. Each paper went through reviewing process. We appreciate the help of reviewers who made it possible. We are very proud of you. We worked hardly and Sincerely as a team to make this possible within the one-month period. There is definitely an impact that we believe this conference has achieved.

Worthy of appreciation is Engr. Dr. Alkali Babawuya, the workaholic maestro for his untiring efforts throughout the conference planning and execution. We appreciate the efforts and advice from all members, especially the National Chairman, Engr. Prof. M. B. Ndaliman, the Chapter Chairman and the Executive committee members, past Chairmen of the institution and friends of the institution. We look forward to your future contributions.

Akonyi Nasiru Sule

Chairman, Organising Committee.

Table of Contents

Proceedings

SUITABILITY OF BIDA BASIN KAOLIN FOR INDUSTRIAL APPLICATION: PRELIMINARY INVESTIGATION

[1]Dutsun M.A and [2]Agboola J.B.

[1]abdullahdutsun@gmail.com, [2]joeagboola@gmail.com

Department of Materials & Metallurgical Engineering, School of Infrastructure, Process Engineering and Technology (SIPET), Federal University of Technology, Minna, Nigeria

Corresponding Author's email and phone: *abdullahdutsun@gmail.com, +2348066546806.*

Abstract: Kaolin deposits from three deposits (Sakpe, Lemu and Kpaki) in Bida basin of Niger state has been investigated using XRD, XRF and TGA/DTA methods. The analyses suggest that they are Kaolinite in nature with the presence of quartz, muscovite and anatase. The Chemical composition of the deposits were observed as Lemu (85.16% SiO_2, 7.65% Al_2O_3, 1.13% Fe_2O_3 and others less than 1%), Kpaki (74.86% SiO_2, 15.6% Al_2O_3, 1.32% Fe_2O_3 and others less than 1%) and Sakpe (55.73% SiO_2, 29.65% Al_2O_3, 0.92% Fe_2O_3 and others less than 1%). The deposits were observed to be thermally unstable as they lost very high weight and could be useful for zeolite and silica synthesis, high temperature environments like furnace lining, low temperature environments like microwaves and ovens, Tiles and bricks making due to its chemical composition after an upgrade.

Key words: Kaolin, Characterisation, Thermal, Mineralogical, clay

1. INRODUCTION

Nigeria continues to import almost everything from items used in our daily life to vehicles; porcelain; drilling fluids; ceramic industry to produce household wares like plates, cups, electrical sockets (insulators), toilet seats, bath tubs, flower verses, refractory bricks; and as raw materials for manufacture of paints, paper, fertilizer and plastics fillers, despites the availability of different kaolin deposits spread all over the country (Abuh *et al.*, 2018). Kaolin minerals are important industrial minerals. Millions of tons are used annually in several applications. These applications include uses in the process industries as mentioned above, agriculture, construction and geology (Aramide *et al.*, 2014; Mudi *et al*., 2018 ; Abuh *et al.*, 2018).

To determine the profitability of utilizing clay of a particular deposit for industrial application, it is necessary to determine the mineralogical composition, examine the microstructural morphology and analyse the various available phases in such clay deposit (Olokode *et al*., 2010).

Clays from Odukpani, south eastern Nigeria has also been characterized by researchers. It was established through X-ray diffraction studies that the clay deposits consist predominantly of kaolinite and quartz with illites and biotite minerals traces. The comparison of this clay with some industrial clays shows that the samples can be used in industries such as plastics, paint, ceramics, refractory and fertilizer among others (Osabor *et al.*, 2009).

Clay deposits from Abeokuta region has been characterised using scanning electron microscopy, X-ray diffraction and thermal analysis (DTA/TG). It was observed that Ajebo clay belongs to the kaolin group with the mine having a hydrothermal geological formation (Olokode *et. al*. 2010).

The characterized Kaolin clay from Ejigbo (Lagos) was reported to possesses high crystallinity with orderly arranged structures that can provide a base for supporting nanoparticles with the presence of hydroxyl group which provides active sites for anchoring catalyst substrates. High thermal stability, good morphology, and high surface area were also noticed in the clay (Mudi *et al*. 2018).

Ndia clay deposits from Takum Local Government Area of Taraba State investigated for industrial application using physicochemical, XRF and TGA techniques showed some weight loss on heating and thermal stability of the clay at high temperature, moderate physical properties such as plasticity, shrinkage and a bulk density (Malu *et al.*, 2018).

The major reason for the utilization of certain clay minerals in specific application is due to the fact that their physical and chemical properties are dependent on their structure and composition (Aramide *et al*., 2014). Hence their application in electrical porcelain, sanitary-wares, glazes, high quality tableware, or tiles.

The geotechnical investigation, geology and mineralogy, geochemical and reserve estimation of Kutigi clay deposits has been studied (Akhirevbulu and Ogunbajo, 2011). The aim of this study is to characterize clay from central Bida basin, determine their physical and thermal properties with a view to predicting their engineering behaviour and evaluating their economic potentials, for the nation's industrial raw materials data base. Akhirevbulu and Ogunbajo (2011) also stated that the scope of investigations of these clays from Niger state have not gone beyond geotechnical studies and reserve estimation of the clay deposits and comparative study of them with the popularly studied deposits within the country is yet to be ascertained.

This study is focused on Sakpe, Lemu and Kpaki deposits in Niger state. The study will be focused on determination of Thermogravimetric analysis (TGA), Differential Thermal analysis (DTA), XRD, XRF and SEM analysis of clay samples from these deposits.

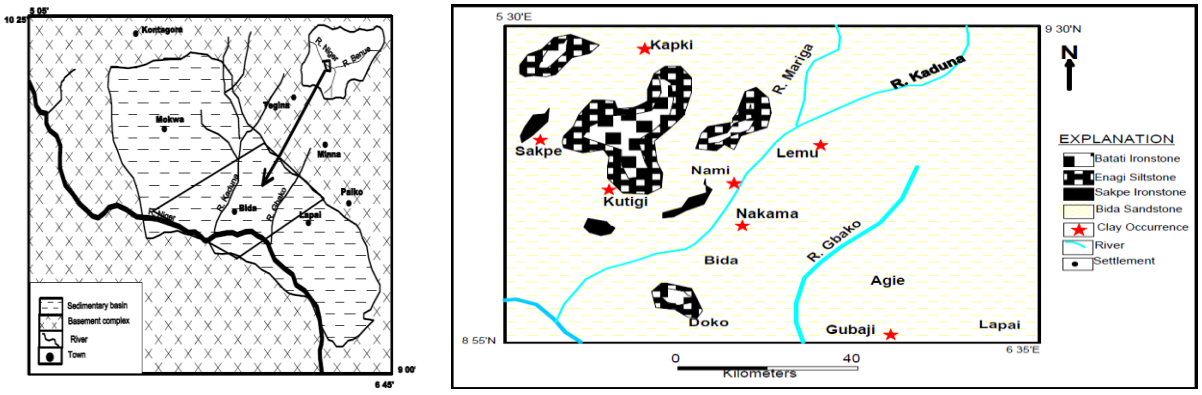

Figure 1: Outline of the study area within the sedimentary Bida basin and Map of Central Bida Basin Showing Clay Occurrences (Alabi, 2015).

The buried Precambrian basement complex is directly overlain by rounded to sub-rounded coarse conglomerates, clay-sand-pebble admixtures and cross- stratified sandstones locally with scattered pebbles, cobbles and boulders (Alabi, 2015).

2. MATERIAL AND METHODS

The materials (clay) used in this research work was collected from Kpaki, Sakpe and Lemu all in Bida basin, Niger State. It is locally used by the people around the area for painting, moulding and bricks making.

Clay samples were randomly collected from different points. The clay samples were collected at a depth of 2m for each of the pits. The collected clay samples were placed in a dry clean polythene bag in line with Osabor *et al*., 2009 and Malu *et al*., 2018.

The clay samples were sun-dried for five days and crushed using ceramic Crusher, mortar and pestle. The pulverized clay was sieved using 2mm mesh and packaged in a plastic container.

The powdered clay was soaked and thoroughly mixed in a plastic bath of water to get a slurry of clay, which was left for two days to settle and water drained off and slurry poured into a stack of sieves connected to a mechanical vibrator to sieve through clay of particles of size of 100μm. The clays were finally washed with de-ionized water and dried for days under open shade and then pulverized (grind into powder) to 100μm and poured in a clean-dried plastic bags.

Some clay samples were set aside for XRD, XRF and Thermal (TGA/DTA)analyses, while specific quantity was mixed with 7 - 8% de-ionized water and kept in plastic bags for two days and stirred to form homogeneous plastic paste. These samples were kept in a plastic (air-tight) bag for two days for a homogenous wetting and then formed into the appropriate shapes for further analysis.

Structural and Microstructural Characterization

The crystalline phases present in samples were identified by X-ray diffraction (XRD), performed in a Rigaku diffractometer (model DMAX III-C3 kW) at room temperature with Cu-ka radiation. A scanning electron microscope, Zeiss (model DSM 962) was used to observe the microstructure (morphology) and to carry out X-ray chemical microanalysis of the samples.

Thermal Analysis (TGA/DTA)

In this study, a Perkin Elmer STA 4000 analyzer at Step-B Lab of Federal University of Technology Minna was used to test the thermal stability of the samples. A known weight of samples was put into a ceramic pan placed in the machine, heated from room temperature to 900^0C at 10^0C/min under nitrogen gas flow at 20 ml/min and Pressure of 2.5 bar. Traces were recorded as weight loss versus temperature for Thermal Gravimetric Analysis (TGA) and Differential Thermal Analysis (DTA).TGA/DTA curve generate the corresponding data with the help of Pyris manager software.

3. RESULTS AND DISCUSSION

Chemical composition of clay deposits

The chemical analysis result of clay samples from the study area show high value of SiO_2 ranging from 54.91% to 87.37 %, moderate to high Al_2O_3 ranging from 7.65 % to 29.65 %, and a low value of Fe_2O_3 ranging from 0.92 % to 1.32wt %. Also, the samples are low in CaO, Na_2O and K_2O. Lost of Ignition (LOI), range from 3.56% to 11.36 in all the studied clays (Table 1)

Table1: Percentage major oxides distribution of clays in the study area

%	SiO_2	Al_2O_3	Fe_2O_3	MnO	MgO	CaO	Na_2O	K_2O	TiO_2	P_2O_5	LOI	Total
Lemu	85.16	7.65	1.13	0.010	0.10	0.12	0.04	0.14	0.863	0.02	3.56	98.80
Kpaki	74.86	15.60	1.32	0.011	0.09	0.06	0.10	0.58	1.830	0.04	5.70	100
Sakpe	55.73	29.65	0.92	0.006	0.05	0.07	0.05	0.31	1.793	0.05	11.36	99.99

The relatively higher total alkalis average (45%) and K_2O/Na_2O ratio (1.59) is indication of abundance K-feldspar (microcline and orthoclase). Lower concentration of Fe_2O_3, MnO, MgO, CaO and P_2O_5 reflect felsic character of these rocks. These compositions are similar to those of Kutigi (Akhirevbulu &Ogunbajo 2011) and Mbom (Abuh et. al, 2018).

All these clays have high silica contents of 85% (Lemu), 75% (Kpaki) and approximately 56% (Sakpe) respectively with small to moderate alumina content which is comparable to that of Ejigbo in Lagos state.

Mineralogical composition of clay deposits

X-Ray Diffraction (XRD) analysis result is presented in Table 2 and corresponding curves. The mineralogy of the clay is composed of quartz with range of 27.8wt% to 75.3wt%, Kaolinite $\{Al_2Si_2O_2(OH)_4\}$ muscovite $\{KAl_2(AlSi_3O_{10})(F,OH)_2\}$ and anatase (TiO_2) as the non clay minerals components with percentage of each as shown in table 2 below and are comparable to Ajebo clay.

Table 2: Mineralogical Composition of the Clay from Central Bida Basin

Location	Quartz	Kaolinite	Muscovite	Anatase	Total
Lemu	75.3	22.1	2.2	0.04	100
Kpaki	55.9	37.5	5.7	0.9	100
Sakpe	27.8	66.2	4.7	1.3	100

The clay occurrence is dominated by kaolinite clay mineral (average 42%) with little concentration of muscovite. This confirms the studied clays to be kaolin.

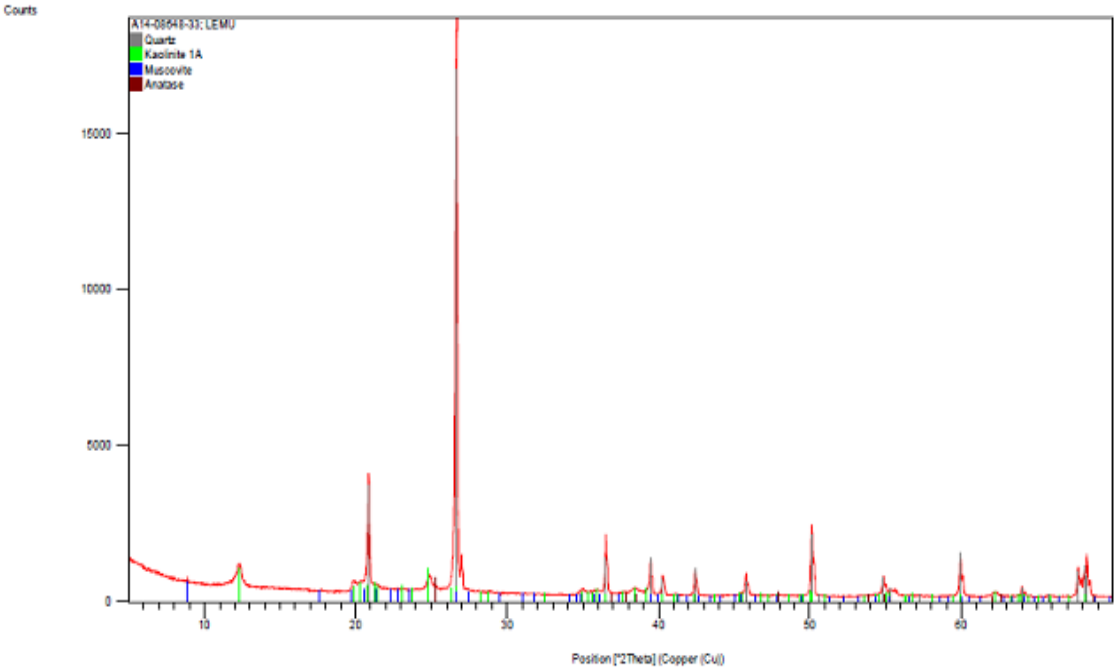
Counts
A14-08648-33; LEMU
Quartz
Kaolinite 1A
Muscovite
Anatase
15000
10000
5000
0
10
20
30
40
50
60
Position [°2Theta] (Copper (Cu))

(a)

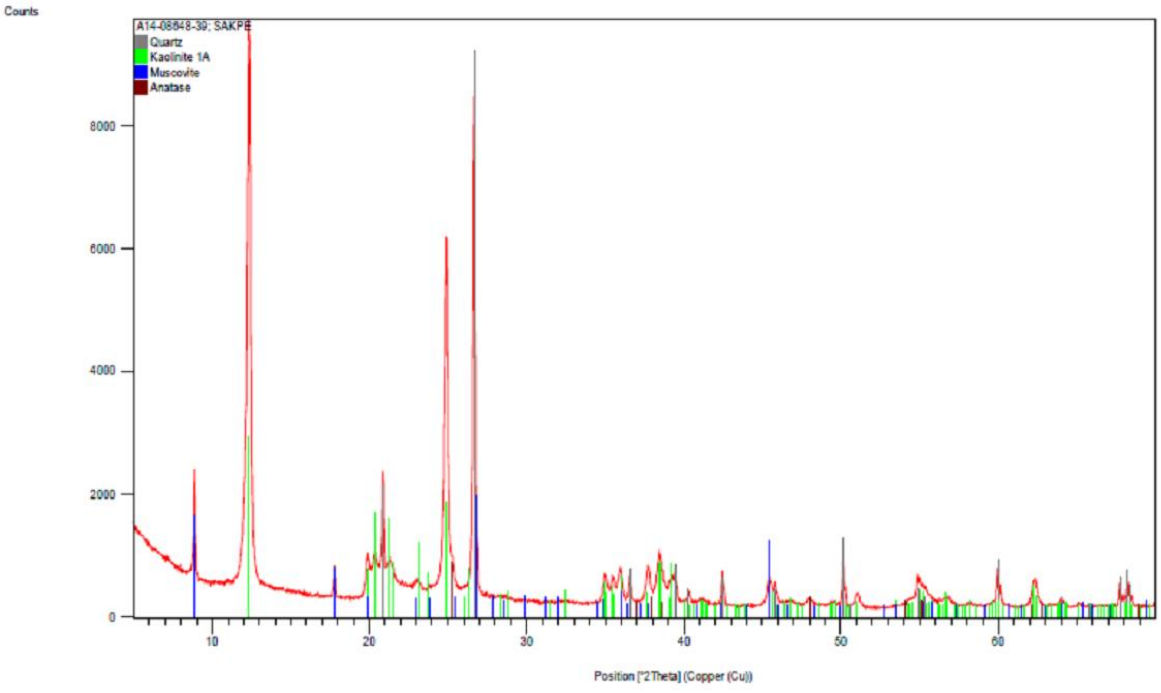
Counts
A14-08648-39; SAKPE
Quartz
Kaolinite 1A
Muscovite
Anatase
8000
6000
4000
2000
0
10
20
30
40
50
60
Position [°2Theta] (Copper (Cu))

(b)

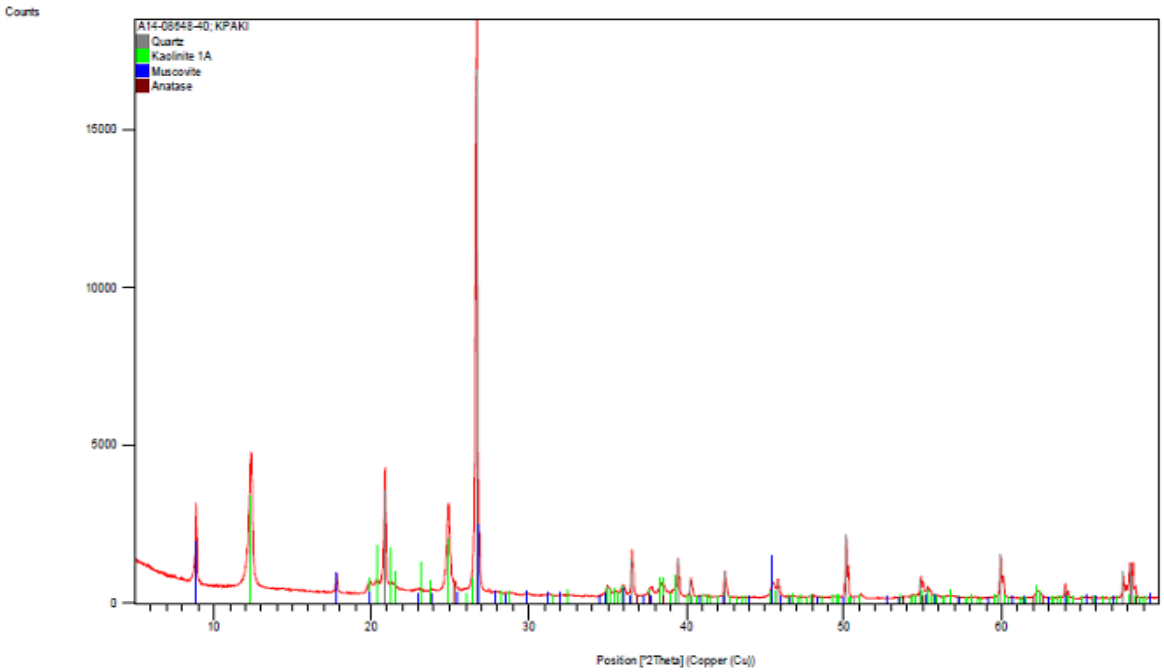

(c)

Figure 2: X-ray Diffractogram of (a)Lemu, (b)Sakpe and (c) Kpaki Clay Samples

SEM analysis

The micro-structural observation of the clay surface shows a distributed-finely uniform surface having isolated patches of granulated texture as shown in Figure 3 below.

(a)

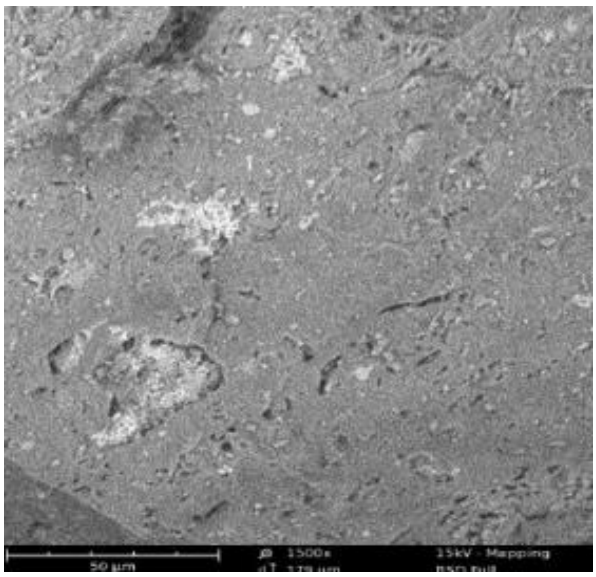

(b)

(c) 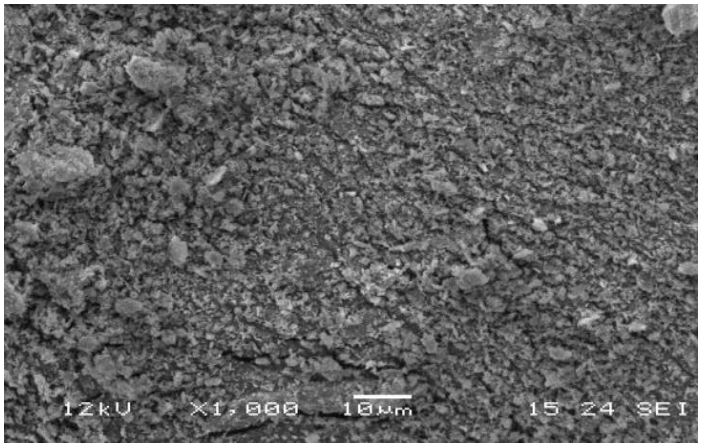

Figure 3: SEM image of (a)Lemu, (b)Sakpe and (c) Kpaki Clay Samples moulded into shape

Thermal Analysis (TGA/DTA)

The first reaction occurred around100°C and is related to elimination of water of hydration (i.e. the release of water absorbed in pores and on the surfaces at drying stage) as shown in figure 4.The hydration phenomenon occurred below 250°C, and the mass loss is attributed to the reorganisation in the octahedral layer.

The rather abrupt change in mass loss rate for all clay samples studies (Figure 4) starting at around 300ºC and continuing until 520°C is an indication of dehydroxylation kaolinite to form Metakaolin.

The DTA curve also shows a peak around 400°C and the peaks corresponding to the multi-step and double stage decomposition of the kaolin (endothermic release of constitutional water from the interlayer octahedral sheets), immediately followed by an exothermal event beyond that temperature at around 600 °C attributable to the recrystallization into spinel, as also observed in Ndia (Taraba state) clay.

The differential thermal analysis (DTA) result manifested material reactions of exothermic beyond 600 °C (exothermic peaks). The dehydroxylation of the minerals in the clay ensues at these temperatures signified the initial step in the oxidative degradation of the clay material. The flux components (oxides) like CaO, P_2O_5 and K_2O manifested reaction from around 600 °C and above which signified the beginning of sintering process, material crystallization and phase change .

There is high weight loss in all samples studied. Lemu kaolin was observed to have weight loss of 32.7% at 325°C and 44.8% at 522.72°C, Kpaki where observed to be 36.72% at 325.5°C and 532.15°C and those of Sakpe were observed to between 47% at 210°C and 39.4% at 493.6°C respectively.

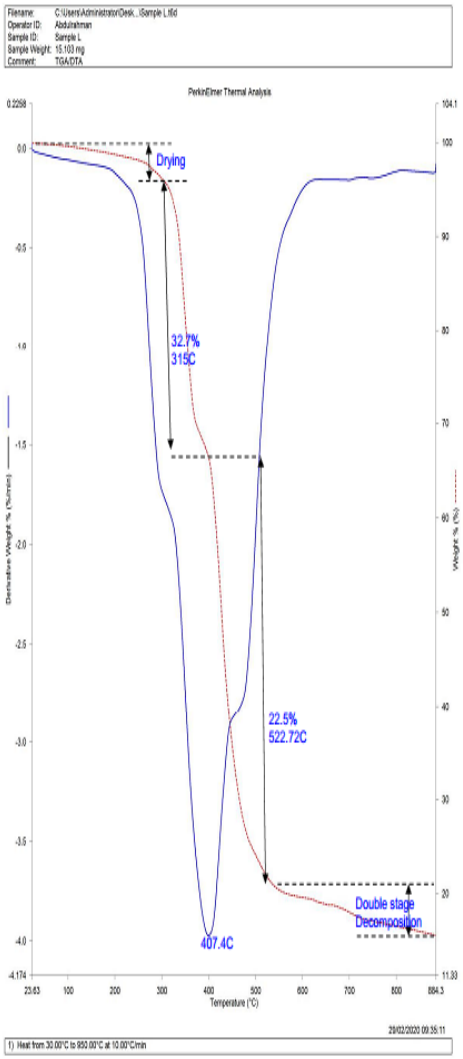
Filename: C:\Users\Administrator\Desk...\Sample L.tfd
Operator ID: Abdulrahman
Sample ID: Sample L
Sample Weight: 15.103 mg
Comment: TGA/DTA
PerkinElmer Thermal Analysis
Drying
32.7%
315C
22.5%
522.72C
Double stage
Decomposition
407.4C
Temperature (°C)
Derivative Weight % (%/min)
Weight % (%)
28/02/2020 09:55:11
1) Heat from 30.00°C to 950.00°C at 10.00°C/min

(a)

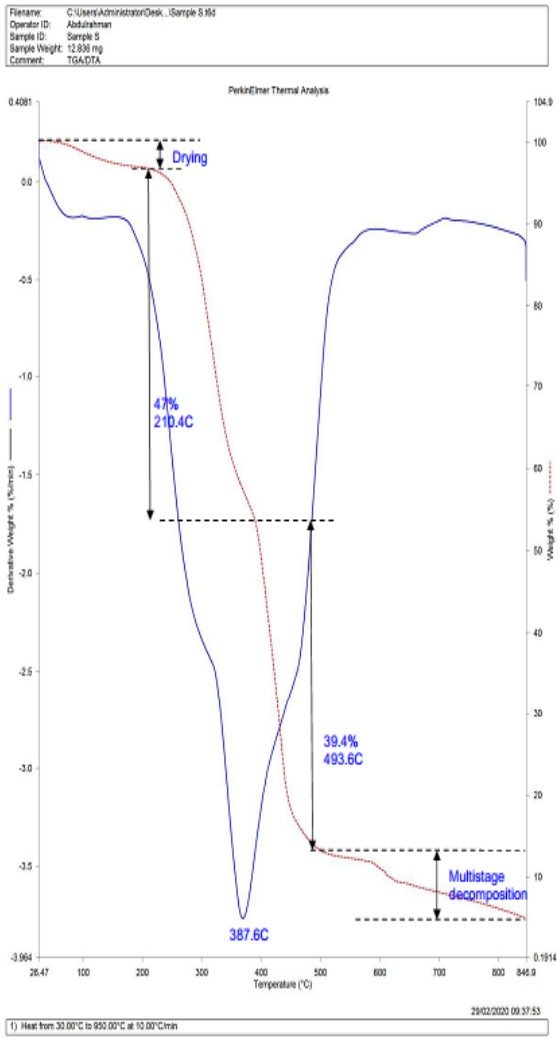
Filename: C:\Users\Administrator\Desk...\Sample S.tfd
Operator ID: Abdulrahman
Sample ID: Sample S
Sample Weight: 12.836 mg
Comment: TGA/DTA
PerkinElmer Thermal Analysis
Drying
47%
210.4C
39.4%
493.6C
Multistage
decomposition
387.6C
Temperature (°C)
Derivative Weight % (%/min)
Weight % (%)
28/02/2020 09:57:53
1) Heat from 30.00°C to 950.00°C at 10.00°C/min

(b)

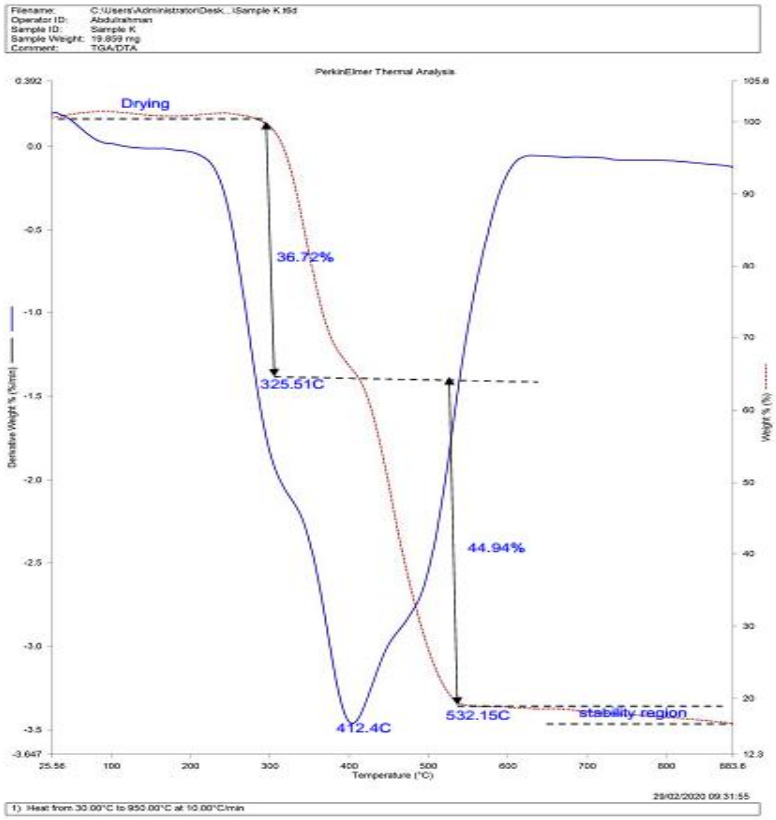

(c)

Figure 4: TGA/DTA curves of (a)Lemu, (b)Sakpe and (c) Kpaki clay Samples

The above results shows that all the kaolin deposits investigated were found to be less stable thermally and therefore not suitable for high temperature ceramic applications until upgraded except for low temperature applications like microwaves and ovens/kilns .

The presence of oxides in kaolin plays important role in their applications of clay. Oxides (SiO_2, Al_2O_3, Na_2O, K_2O, Fe_2O_3, TiO_2 and CaO) play a significant role in the industrial application of kaolin. High SiO_2 and Al_2O_3 play important roles in the production of refractories after an upgrade and removal of volatile matters. Silica content also makes it a good material for synthesis of zeolite, amorphous silica alumina, tiles and bricks production. Na_2O and K_2O are fluxing agents in ceramic and as functional filler in paint, rubber, plastic and adhesives, it also serves helps to reduce the melting temperature of quartz and help to control viscosity of glass. Free or low Fe_2O_3 content in these clays make it suitable for use in pottery, tiles and sanitarywares. Their lightness and whiteness and opacity for paints, coating in plastic and paper.

The composition of the studied clays compared with industrial specifications makes the clay deposit important raw material for the production of Refractory bricks by upgrading Al_2O_3 level/content to meet raw material for the production of Refractory bricks, Pottery production and Ceramics.

4. CONCLUSION

Kaolin deposits from deposits (Sakpe, Lemu and Kpaki) in Bida basin of Niger state has been investigated using XRD, XRF and TGA/DTA methods. The deposits were found to be kaolinite in nature with high percentage of silica but low alumina content. These deposits were found to be thermally unstable as they loss very high weight

rapidly as observe from the TGA/DTA curve and can be upgraded for use in high temperature environments like furnace lining, in low temperature environments like microwaves ovens, and other areas such paper making, paint and fillers. These clay deposits can also be used in Tiles and bricks making due to its chemical composition after an upgrade and suitable for zeolite and silica synthesis.

References

1. Akhirevbulu O.E. and Ogunbajo M.I (2011). The Geotechnical Properties Of Clay Occurrences Around Kutigi Central Bida Basin, Nigeria. *Ethiopian Journal of Environmental Studies and Management, 4(1).* doi: 10.4314/ejesm.v4i1.3
2. Alabi, A.A. (2015). *Mineralogy and Geochemical Characteristics of Clay Occurrence in Central Bida Basin Northwestern Nigeria. Journal of Natural Sciences Research www.iiste.org ISSN 2224-3186 (Paper) ISSN 2225-0921 (Online) Vol.5, No.20, 2015.*
3. Aramide Fatai O., Kenneth K. Alaneme, Peter A. Olubambi, and Joseph O. Borode (2014). Characterization of some clay deposits in South West Nigeria, Leonardo Electronic Journal of Practices and Technologies, Issue 25, p. 46-57
4. Abuh Mark Agaba, Ndubuisi Edennaya IDENYI, Arit Beka ETUKUDOH, Chijioke Gideon ITUMA, ChidubemIgnatus OBIOHA and Christian Oluchukwu ASADU (2018). Ceramics application of Mgbom clay: Characterization and micro-structural studies. Leonardo Electronic Journal of Practices and Technologies, Issue 33, p. 105-122
5. Malu S. P., J. T. Ugye and R. B. Donatus (2018). Characterization Of Clay For Industrial Application By Physicochemical, XRF, and TGA Methods. FUW Trends in Science & Technology Journal, www.ftstjournal.com, 3(1) pp. 314 – 318.
6. Mudi, K.Y, Akande, H.F and Oyawoye, M.R (2018). Characterization of Kaolin Clay from Ejigbo, Lagos, South-Western Nigeria, IJISET - International Journal of Innovative Science, Engineering & Technology, 5(11).
7. Olokode O.S., P.O Aiyedun, S.I. Kuye, N.O Adekunle And W.E. Lee (2010). Evaluation Of A Clay Mineral Deposit In Abeokuta, South-West Nigeria, Journal of Natural Sciences, Engineering and Technology, 9(1):132-136.
8. Osabor V. N., P. C. Okafor, K. A. Ibe and A. A. Ayi (2009). Characterization of clays in Odukpani, south eastern Nigeria, African Journal of Pure and Applied Chemistry, 3 (5), pp. 079-085.

Development and Economic Analysis of a Hybrid Power of Photovoltaic and Wind Turbine System.

A. Yusuf[1], A. Nasir[1], B. Alkali[2], J. Y. Jiya[1] and Nasir Akonyi[2]

Department of Mechanical Engineering, Federal University of Technology, Minna, Nigeria,
Department of Mechatronics Engineering, Federal University of Technology, Minna, Nigeria,

Corresponding author:a.nasir@futminna.edu.ng

Abstract

Energy is essential for economic and social development and are generated both by conventional and non-conventional means. However, because of greenhouse effect from conventional means, renewable means of photovoltaic and wind turbine hybrid power generating system was considered in this research. Different means of generating energy from renewable energy were reviewed and the hybrid power of this renewable energy was developed using mild steel as the foundation plate, steel pipe as the structural pole for the solar panel and wind turbine while the control system were mounted on the wall for easy operation and accessibility. The designed and fabricated part involved wind turbine blades, photovoltaic panel hanger. The maximum voltage and current generated during the experiment were 16.5V and 3.6A for photovoltaic power while that of wind turbine were 18.2V and 8.8A, The maximum power generated by hybrid power system when the output of photovoltaic power was connected to wind turbine output in series and parallel was 152.9W while the minimum power generated in series connection was 54.8W and in parallel was 86.4W. The mechanical and overall efficiencies of wind turbine power system were 54.2% respectively while the overall efficiency of photovoltaic power system was 16.9%.

Keywords: Renewable energy, Hybrid, Photovoltaic, wind power

1.0 INTRODUCTION

Energy plays a very vital role in human life and is required generally by the people in both urban and rural areas for various activities and access to affordable energy is essential for economic and social development. This energy may be obtained conventionally from fossils fuels and from renewable. The problems associated to this non-renewable energy generation (thermal power energy) have been on increase, these problems are on increase in oil price, limitation of fossil fuels and environmental pollution (Perkins, 2018). According to (Idris, Lamin, Ladan, & Yusuf, 2012), upon the availability of renewable energy sources in Nigeria, there is a wide energy deficit due to under- utilization of these energy potentials and to inherent fluctuation and intermittency of most renewable energy sources which have a negative impact on the smooth operation of energy generation. In (Ding, et al., 2018), there is need to improve renewable energy generation quality and quantity at a particular period which is very important. According to Elie et al., (2017), most energy expert agree that the energy generated from renewable source of about IMW can power 630 households and prevents carbon iv oxide (CO_2) emission of about 2500 ton/yr to the atmosphere and for this reason, more of the these type of energy generation are being developed and commissioned around the world. Wind energy is manifestation of solar energy which transforms the air in motion. The energy in wind is converted into rotary mechanical energy by the wind turbine invariably generating electricity by the generator attached to the turbine (Lacho & Avram, 2015) while that of solar PV cells convert the incident solar light energy directly to electricity in direct current (DC) form and the power generated by PV cells are subject to climatic conditions at the location (Prashant, Sanjay, & Kumar, 2018). The hybrid of solar and wind power with micro grid technology was designed for a remote area in Japan with pump storage technology

to alleviate the problem of carbon II oxide and other toxic substance from Fukushima nuclear accident (Ma, Yang, Lu, & Peng, 2015).

According to (Anoune, Laknizi, Bouya, Astito, & Abdellah, 2018) a deterministic approach of sizing a hybrid of photovoltaic and wind power system was established using TRANSYS software to determine the electrical load while (Jain, Choi, & Kim, 2002) used discrete state algorithm method to develop a hybrid power plant of photovoltaic and wind in South Korea without storage system and also used PID regular analysis to develop a hybrid power of wind-diesel without storage system. Figure 1 below shows a schematic diagram of hybrid photovoltaic and wind power system

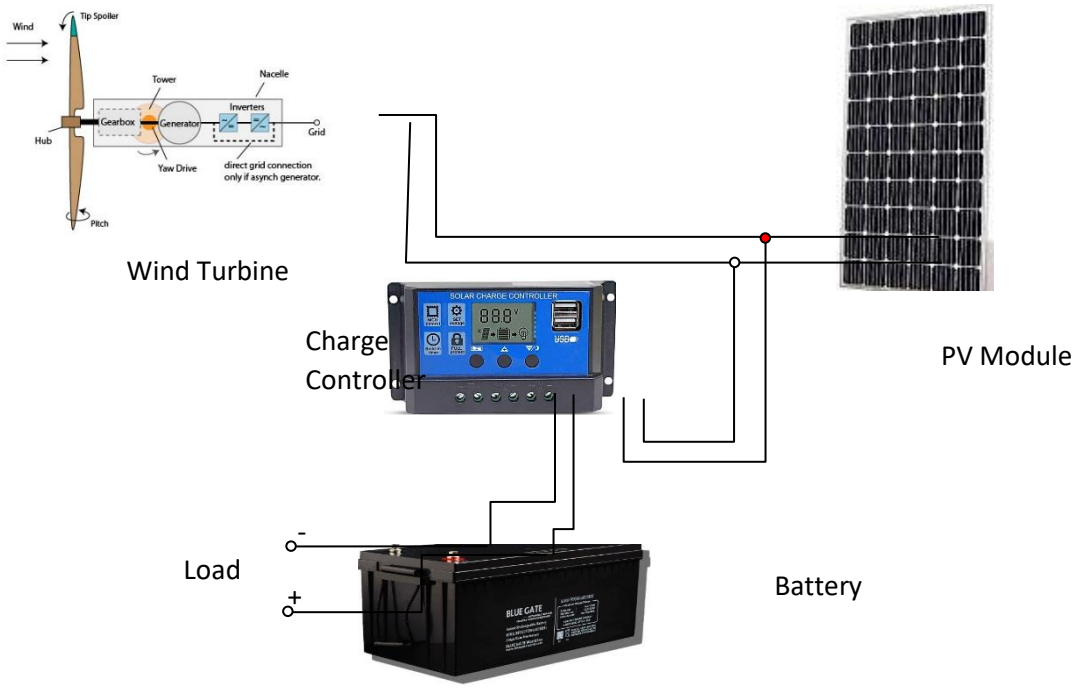

Figure 1: Hybrid of photovoltaic and wind power system

2.0 MATERIALS AND METHOD

2.1 Design Analysis

2.1.1Angle of Tilt (β) for PV

The maximum PV module tilting angle to enable maximum performance are calculated in the following section. The average time for sun rays in Minna between January and December is 7.5 hours starting from 9.00 am to 4.30 pm (Idris, Lamin, Ladan, & Yusuf, 2012)

2.1.2 Angle of inclination (θ) of the PCV

This is the sun rays inclined angle to the photovoltaic and the equation for estimating angle of inclination according to (Nag, 2011)

$$\cos\theta = \sin\phi(\sin\delta.\cos\beta + \cos\delta.\cos\gamma.\cos\omega.\sin\beta) + \cos\varphi(\cos\delta.\cos\omega.\cos\beta - \sin\delta.\cos\gamma.\sin\beta) + (\cos\delta.\sin\gamma.\sin\omega.\sin\beta) \quad (1)$$

2.1.3 Angle of declination (δ)

The angle of declination is estimated using the equation 2 as presented in (Nag, 2011).

$$\delta = 23.45 \times \text{Sin}[360/365\ (284 + n)] \quad (2)$$

2.1.4 Solar irradiance (S)

Solar irradiance (S) is the quantity of energy radiated to the earth crust; 1000W/m^2. Solar Insolation (I_s) is a measure of solar radiation received on a given surface area at a given time and is calculated by the equation

$$I_N = \text{Scos}\, Z_\theta \quad (3)$$

Where $Z_\theta = \cos^{-1}(\sin\phi \sin\delta + \cos\phi \cos\delta \cos\omega)$ (4)

2.2 Wind Turbine Design Analysis

Location determines the wind speed necessary to operate wind turbine power system. The location of the power system in Nigeria determines the type of wind turbine to be installed. According to (Nag, 2011) the average wind speed of Minna is 5.36 m/s and maximum extractable power density was 55.12 W/m^2.Wind power is the maximum extractable power realized by a specific wind turbine in a particular location and this wind power were calculated using equation 5,the wind turbine swept area was estimated.

$$P_w = \rho \times A_r \times V_i^3 \quad (5)$$

Where P_w is wind power, (W)
ρ is air density
A_r is rotor area (m^2)
$V_i$is wind speed at entrance to wind turbine (m/s)

2.2.1 Mechanical power in the rotor (P_T)

This is the available power generated by the rotor and transmitted same to the generator. The mechanical power of the rotor is calculated with the equation 6 as used by (Nag, 2011)

$$P_T = \rho \times A_s \times V_t^3 \quad (6)$$

where V_t is turbine rotor speed.

2.2.2 Wind turbine electrical power (P_{wt})

The wind turbine power is the electrical power generated by dynamo which is the useful energy required to power electrical equipment. It was calculated using equation 7 as used by (Nag, 2011)

$$P_{wt} = \sqrt{3} \times I \times V \times \cos\varphi \quad (7)$$

2.3 Tower Design

The pole or tower that carries both the PV panel and the wind turbine is been subjected to axial loading and therefore was designed as a column with one end free and the other end fixed. According to (Rao & Parulekar, 2005) the critical load on a short column can be determined from equation 8

$$P_{cr} = \frac{C\pi^2 EI}{L^2} \quad (8)$$

Where,

Pcr - critical load on the tower.
C – the column end condition.
E – young modulus of elasticity.
I – moment of inertia of the column cross section
L – effective column length.

2.3.1 Turbine Shaft Design

The turbine shaft conducted torsional energy from the rotor blade to the turbine generator and therefore, it is subjected to twisting moments only. The diameter, d of a shaft is related to the torque, T by equation 9

$$T = \frac{\pi d^3}{4}\tau \quad (9)$$

Where
τ- Material shear stress. The diameter of the turbine shaft was estimated as 12 mm

Table 1: Specification of Dynamo

S/No	Item/Part	Specification
1	Generator type	Dynamo
2	Power rating	350W
3	Body material	Plain carbon steel
	Core material	Cast iron
4	Number of poles	4
5	No load current	35.6 A
6	Voltage	12V
7	Rated speed	2700 rpm
8	Gear ratio	15
9	Size	$\emptyset 150 \times 120$

10	Gearing system	Inbuilt and speed increaser
11	Type of speed	Variable speed constant frequency

2.4 Test running and Operation of the Power System

After the assembling of the major components of the hybrid power system, a field test was conducted and the following readings were recorded for one day, this includes the voltage, current and the power was calculated and displayed on the LCD. These readings were recorded for parallel and series connections. The time interval for the recording of the output data was two hours while the total time taken for the overall operation was twenty four hours. The power plant was first operated and recorded appropriately without load, later with load. The tables 2 and 3 present the results of testing the power plant without and with load. The data in table 2 was recorded at an interval of two hours.

Table 2: Voltage Generated by PV and Wind Power Plant without Load

S/No.	Time (Hrs)	PVC Voltage	WT Voltage	Total in series
1.	08 – 10	20	18.7	38.7
2	10 – 12	20.5	10.5	31.0
3	12 – 14	21.6	12.8	34.4
4	14 – 16	20.8	12.0	32.8
5	16 – 18	18.1	15.2	33.3
6	18 –20	0	15.2	15.2
7	20 – 22	0	18.5	18.5
8	22 – 00	0	20.2	20.2
9	00 – 02	0	20.5	20.5
10	02 – 04	0	22.0	22.0
11	04 – 06	0	19.9	19.9
12	06 – 08	5.4	18.5	23.9

The power output wires from the photo cells and wind turbine were connected to the charge controller and the results were recorded without load and later used to power two 3V bulbs. The voltage and current of hybrid power system was recorded from power controller. The output voltage and current of photovoltaic cell system were recorded from 08:00 hrs in the morning till 18:00 hrs (6'Oclock in the evening) when there was sunlight while the voltage and current generated by the wind turbine power were taken throughout the day and night but the wind speed to turbine rotor was not recorded. It can be seen that, the wind turbine performed better than the PV module with an average voltage of 17 V to 9 V during the testing period. The average voltage output for the test period is 26 V.

Table 3: Voltage Generated by PV and Wind Turbine Power Plant with load

S/No	Time (Hrs)	PVC voltage (V)	WTvoltage (V)	Total in Series Generated (V)
1	08 – 10	15.2	14.6	29.8
2	10 – 12	16.5	7.2	23.7
3	12 – 14	15.6	8.8	24.4
4	14– 16	14.8	8.2	23.0
5	16 – 18	14.3	12.2	26.5
6	18– 20	0	11.8	11.8
7	20– 22	0	14.6	14.6
8	22 – 00	0	16.8	16.8
9	00 –02	0	15.6	15.6
10	02 – 04	0	18.2	18.2
11	04 –06	0	14.2	14.2
12	06 – 08	2.8	13.8	16.6

When the output power from charge controllers from the two power systems were connected in series, the total output voltage was the sum of two results from each power systems but the current recorded was the smallest result gotten from the two systems. In table 4, at the time between 08 – 10 hrs, the result from photovoltaic system was 15.2 V while that from wind turbine was 14.6 V and the total voltage output was 29.8 V as presented table 4

Table 4: Current Generated by PV and Wind Turbine Power System without Load.

S/No	Time (Hrs)	PV (A)	WT (A)
1	08 – 10	3.6	8.2
2	10 – 12	3.6	8.3
3	12 – 14	3.2	8.6
4	14– 16	3.3	8.2
5	16 – 18	3.4	8.3
6	18– 20	0	8.2
7	20– 22	0	8.6
8	22 – 00	0	8.6
9	00 –02	0	8.6

10	02 – 04	0	8.2
11	04 –06	0	8.4
12	06 – 08	3.2	8.2

Wind turbine produce fairly steady current as compared with that of the PV module. this may because during the test period the wind current were more steady and stronger as compare to the fluctuating solar radiation.

4.0 CONCLUSION

The mounting of photovoltaic panel at 10m height and at the tilting angle of 15^{o} to the horizontal making the angle of inclination to be between 13.2^{o} and 25^{o} from sunrise to the sunset. During test a maximum rotor speed was 76 rev/min while the output speed of the turbine generator was 1140 rev/min. The maximum voltage and current generated during the experiment were 16.5 V and 3.6 A for photovoltaic power while that of wind turbine were 18.2 V and 8.8 A. The maximum power generated by hybrid power system when the output of photovoltaic power was connected to wind turbine output in series and parallel was 152.9 W while the minimum power generated in series connection was 54.8 W and in parallel was 86.4 W.The mechanical and overall efficiencies of wind turbine power system were 54.2% respectively while the overall efficiency of photovoltaic power system was 16.9%.

REFERENCES

Anoune, K., Laknizi, A., Bouya, M., Astito, A., & Abdellah, B. A. (2018). Sizing a PV-Wind based Hybrid system using Deterministic Approach. *Energy conversion and management*, 137-148.

Ding, Z., Hou, H., Yu, Z., Hu, E., Duan, L., & Zhao, J. (2018). Performances Analysis of a Wind – Solar Hybrid Power. *Energy Conversion and Management, 1811*(5), 223-234.

Elie, B. K., Oumrau, H., & Jean, N. (2017). Methodology of Feasibility Studies of Micro – Hydropower PlantsMethodology of Feasibility Method of Feasibility Studies of Micro-Hydropower plant in Cameroun: A case Study of the Micro – Hydro of KEMKEN,. *International Conference on Technologies and Materials for Renewable Energy, Environment and Sustainability*, 17-28.

Idris, N. A., Lamin, H. S., Ladan, M. J., & Yusuf, B. H. (2012). Nigeria's Wind Energy Potentials: The Path to a Diversified Electricity Generation Mix. *International Journal of Modern Engineering Research*, 2434-2437.

Jain, A., Choi, J., & Kim, B. (2002). Impact of integrating the photovoltaic and wind Energy Sources on Generation System Reliability and Operation Economics. *Proceeding of IEEE International Conference of Power System Technology*, 2437-2442.

Lacho, P., & Avram, D. (2015). The New Simple and Practical Solar Component Guide. *USA Digital Publishing Limited. Kindle edition*, 50-62.

Ma, T., Yang, H., Lu, L., & Peng, J. (2015). Optimal Design of an Autonomous Solar-wind pumped Storage Power supply System . *Journal of Applied Energy*, 728-736.

Nag, P. K. (2011). *Power Plant Engineering* (3rd ed.). New Delhi India: Tata McGraw Hill.

Perkins, G. (2018). Techno-Economic Comparison of the Levelised Cost of Electricity Generation from Solar PV and Battery Storage with Solar PV and Combustion of Bio - Crude using fast Pyrolysis of Biomass. *Energy Conversion and Management*, 1573-1588.

Prashant, K., Sanjay, D., & Kumar, S. (2018). Designing and Simulation Tools of Renewable Energy Systems: Review Literature. *Progress in Advanced Computing and Intelligent Engineering*, 132-143.

Rao, S., & Parulekar, B. B. (2005). *Energy Technology; Non Conventional, Renewable & Conventional*. (3rd Revised and updated ed.). NaiSarak Delhi, India: Khana Publishers.

Design of In-situ Load Bearing Capacity Mechanism

[1]Umaru I., [2]Babawuya A., [3]Alhaji M. M., [3]Alhassan M., [3]Adejumo T. W. and S. S. [4]Lawal.

[1] *Department of Civil Engineering, Abubakar Tafawa Balewa University, Bauchi, Nigeria,*
[2]Department of Mechatronics Engineering, Federal University of Technology, Minna, Nigeria
[3]*Department of Civil Engineering,* Federal University of Technology, Minna, Nigeria. [3]Department of Mechanical Engineering, Federal University of Technology, Minna, Nigeria

Corresponding Author: *ibropopoi@yahoo.com*

Abstract:
Major causes of structural failure are associated with bearing capacity and settlement of foundation soil. These bearing capacity and settlement are determined in laboratory and on field. The parameter obtained from the tests will either lead to under design or over design of the intended structure. The design of In-situ Load Bearing Capacity Mechanism was chosen follow by the design analysis and calculations, material selection and development of CAD model. The concept was conceived to allow for incremental loadings for each loading on the in-situ load bearing capacity mechanism for 24 hours so that the settlement will be insignificant before another loading is applied. The process will continue for the period of seven (7) days so as to allow for gradual dissipation of pore water from clay soil. The results from this test will provides civil engineers the real problem of soil on site which will help in design for the bearing capacity and settlement of foundation.

Key words:

1. INTRODUCTION

The common and traditional method of testing for bearing capacity of shallow foundations rely mainly on the collection of in-situ soil sample transfer of the sample to the laboratory and carrying out requisite tests to determine the shear strength parameters of soil. The parameters (Cohesion, C and angle of internal friction, φ) are then used to calculate bearing capacity through the use of terzaghi's equation. A lot of errors have been observed from sample collection through laboratory tests to the terzaghi's equation used for the calculation. Therefore, the bearing capacity obtained from this method is grossly inaccurate.

Attempts have been made at field and laboratory medium scale level (Dasaka 2012, Dasaka et. al 2013, Warmate, T., 2014, Warmate and Nwankwola 2014, Barnard and Heymann 2015, Shirvani and Shooshpasha 2015, Gul and Ceylanoglu 2016, Araujo *et al*. 2017, Sultana and Dey 2018 and Barnard 2019) to develop and applied In-situ and laboratory plate load test to determine the bearing capacity of soil deposits. Most of these plate load tests uses heavy but special automobile jack mounted with pressure gauges and deformation dial gauges. These mechanisms usually require a rigid supporting medium (Anchored grillage or heavy lorry truck) to prevent upward movement of the jack and hence records the deformation due to specified applied load. This test is usually rapid and the mechanism does not allow for long time duration of loading which does not aid dissipation of pore water in saturated clay deposits during testing. This can also result in to errors when used to obtain bearing capacity in clay soils

It is on these that the concept of designing a load bearing capacity mechanism that is field operated (in-situ test) was conceive. The load bearing mechanism will be loaded incrementally through a lever arm for 24 hours before the next loading and reading taken at time interval, that will allowed for gradual dissipation of pore water from the soil on site as against the use of hydraulic jack and anchored grillage or heavy loaded truck in determine bearing capacity and settlement of soil on field.

2.0 MATERIAL AND METHODS

2.1 Materials Used

The materials used for the design and their specification are listed in Table 1.

Table 1: Materials Used and Their Specifications

S/No	Components	Specification	Function and Reason
1	Lever Arm	1 meter length and tapered	Transfer load through fulcrum to the column
2	Dead loads	5kg, 10kg, 15kg, 20kg and 25kg and 50 kg	Used in loading the lever arm
3.	Frame	Made of I-section, D= B= t	Used to carry the lever arm and loads
4.	Loading Arm	Length and circular in shape	For loading the mechanism
5.	Loading Plate	Circular and 300 mm in diameter	Transfer load to the foundation soil.

2.2 Equipment

2.2.1 Linear Variable Differential Transformer (LVDT)

Linear variable differential transformer LVDT is a device that was used to observe the settlement of the plate during testing period. It enable recording of displacement continuously with the help of LVDTs at time interval. As shown in figure 1.

Figure 1. Linear Variable Differential Transformer (LVDT)

2.2.2 Tensiometer

Tensiometer was used to monitor Matric suction during the loading tests. Four (4) tensiometers was installed at the bottom of the pit besides the loading plate at depths of 100, 300, 600, and 800 mm. The tensiometers were installed in predrilled holes with a slightly smaller diameter than the tube diameter (20 mm). In order to facilitate a full contact of the porous element with the soil, the tensiometers were driven into the soil for a few centimeters. The tensiometers were equipped with a porous ceramic cup of 10^{-3}-m/s hydraulic conductivity and a Bourdon type vacuum gage, which was used for negative pore water pressure measurements. Readings were taken prior to and after each plate load test. As shown in figure 2

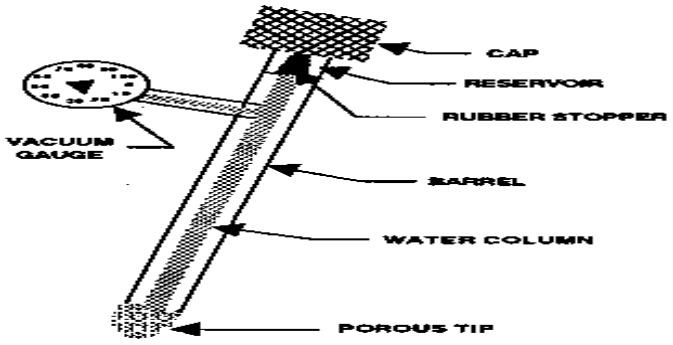

Figure 2. Tensiometer

2.3 Method

This section presented the method used for the design of the load bearing probe. Design consideration was made on the chosen concept follow by the design analysis and calculations, material selection and development of CAD model.

2.3.1 Description of Load Bearing Probe

The in-situ load bearing mechanism shown in figure 3. is a field in-situ test device that was used to determine the bearing capacity and settlement of foundation on site so as to improve on the existing/conventional plate load test and traditional laboratory test method as shown in Figure 3.

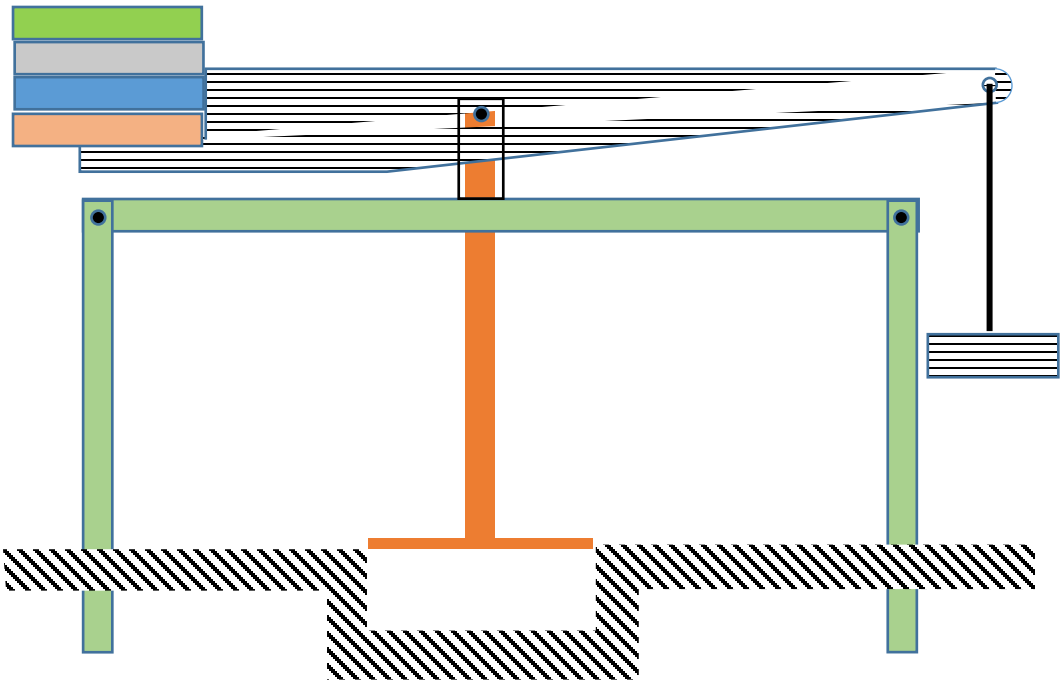

Figure 3. Sketch of Load Bearing Probe

The load bearing capacity mechanism is a straight lever with a parallel forces acting in the same plane as shown in figure 3.

The device was loaded incremental through the load hanger known as effort, P attached to lever arm and balance load W, at the opposite end to produce equilibrium of the weight on a fulcrum which was then transmit to the square base plate at the foundation level with the base plate of 300mm diameter and 25mm thickness. The load applied at the lever arm through load hanger was in order of 10kg, 10kg, 20kg, 40kg, 80kg, 160kg and 320kg. Each load placed on the lever arm was maintained for the period of 24 hours before the next incremental loadings.

2.3.2 Design of Lever Arm

A first class type of lever mechanism (Figure 4) were used in the load bearing probe because the fulcrum is located in between the load and the effort. An I-section were used for the lever arm so as to minimize the twisting due to the over hand loads. The dimensions of the lever arm are determined in the following analysis and results are presented in table 2.

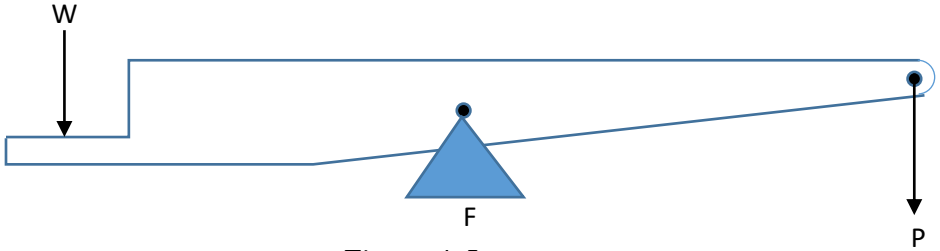

Figure 4. Lever arm

The lever that has a fulcrum F, in between the load and effort is termed first type of lever. In this case effort arm is greater than the load arm. The mechanical advantage, M.A obtained in this case should be more than one.

$$W\ x\ X_1 = P\ x\ L \qquad (1)$$ (Khurmi and Gupta 2005)

Where,

P = Loads (N),

W = balancing load (N),

X_2 distance from P to the fulcrum R_1 (mm),

X_1 = Distance from Balancing load W to fulcrum (mm).

R_2 = reaction from balancing weight taken as fixed end.

P = 500,000 kg =5,000 N, L = 1,000 mm, X_1 = 350 mm, X_2 = 650 mm, W = ?

To calculate for weight of lever arm,

The total volume of the lever arm was calculated as,

V_T = 1,745,507.19 mm^3 = 0.00174550719 m^3 .

The mass, M of the lever arm is:

$$M=\rho \text{ x } V_T \qquad (2)$$

Where, M is mass of the lever arm,

.ρ is density of mild steel

V_T is total volume of lever arm.

7850 x 0.00174550719= 13.7 kg.

If the fulcrum is placed at x_1 = 650 mm and weight along x_1 is 2.28kg. x_2 = 350 mm and weight at end 1.67 kg.

Provide additional load of 2.584 kg at the end of x_1.

From equation 1,

For equilibrium of the lever arm, $PxX_2 = W\ x\ X_1 = 4.234 \text{ x } 350 \ = \ 2.28 \text{ x } 650 = 0$

And therefore, the moment, M is =P x L= 5,000 x 1000 = 5,000,000 N/mm.

According to Khurmi and Gupta (2005). The sectional modulus of the I-section in figure 5, was computed using equation 3 and 4.

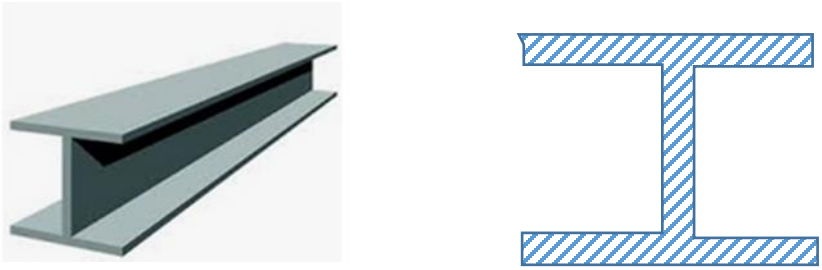

Figure 5. Proportion of I- section

Width B = 2.5t, depth D = 6t and thickness t.

Therefore,

Sectional modulus, Z

$$Z = \frac{\frac{1}{12}[2.5t(6t)^3 - 1.5t(4t)^3]}{\frac{6t}{2}} \qquad (3)\ (Kurmi\ and\ Gupta\ 2005)$$

$= \frac{37t^3}{3t} = \mathbf{12.3t^3}$

Yield stress of mild steel is 220Mpa in table 2.5 (Kurmi and Gupta 2005)

The bending stress σ_b

$$\sigma_b = \frac{m}{z} \qquad (4)\ (Khurmi\ and\ Gupta\ 2005)$$

Where,

M= moment in N mm, Z= sectional modulus of the material in mm^3.

$$220 = \frac{m}{Z} = 220 = \frac{5{,}000{,}000}{12.3t^3} = t = \mathbf{15\ mm}$$

Therefore, from Lingaiah (2004), the I-section ISMB 125 was chosen from the table (24.31). the values of I-section is tabulated in table 2.

Table 2. Showing Dimension of I-section

Sections	Value (units)
Depth of I-section D	125 mm
Breath B	75 mm
Thickness of web t_w	4.4 mm
Thickness of flanges t_f	7.6 mm
Area of section A	1660 mm^2
Sectional Modulus Z_{xx}	71800 cm^3

Therefore, the bending stress, σ, for the I-section was computed from equation 4;

$\sigma = \frac{m}{Z}$ (4)

$= \frac{5{,}000{,}000}{71800} = \mathbf{70}\frac{\boldsymbol{N}}{\boldsymbol{mm^2}}$

According to (Khurmi and Gupta 2005) the allowable bending stress, $/\sigma_b/$ is given by equation 4;

$$\sigma_b = \frac{\sigma}{FS} \qquad (5)$$

$$= \frac{70}{4} = \mathbf{17.5 N/mm^2}$$

And the mechanical advantage, M. A of the lever arm is given in equation 6;

M. A = $\frac{W}{P}$ $\qquad eq.6\,.(Khurmi\ and\ Gupta\ 2005)$

$M.A = \frac{W}{P} = \frac{L_1}{L_1} = \frac{650}{350} = \mathbf{1.9\ ok}$ (According to Khurmi and Gupta 2005, mechanical advantage M. A must be less than 2. So the 1.9 is ok.)

2.3.4. Design for Pin at Fulcrum

The fulcrum pin connect the lever arm and the load transfer column via a revolute joint. Therefore, the pin is subjected to shearing stress as shown in Figure 6. And the pin load is given by equation 7. While equations 8, 9 and 10are for length of pin, maximum bending moment and sectional modulus of the materials respectively

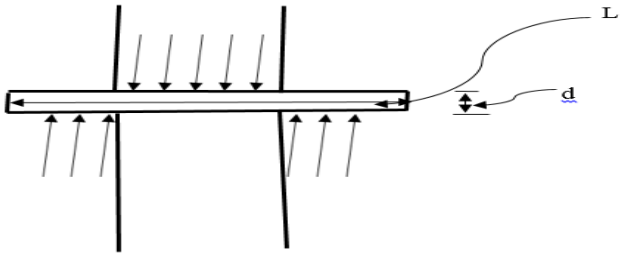

Figure 6. Pin at the fulcrum

$$P = d_1\ x\ l_1 x\ p_b \qquad (7)\ (Khurmi\ and\ Gupta\ 2005)$$

Where, d_1 =diameter of pin at fulcrum and l_1 = length of the pin at fulcrum. P =dead load applied at load hanger and p_b = shear stress of the material.

If the pin is going to fail due to bearing of the pin of the fulcrum, then the pin diameter is determine as follows:

5,000 = $d_1\ x\ l_1 x\ p_b = d_1 1.25\ d_1 x\ 17.5 = 21.875\ d^2 =\ d_1 = \sqrt{228.57} = \mathbf{15\ mm}$

$$l_1 = 1.25\ d_1 = 1.25x17 = \mathbf{20\ mm}$$

$$l = 1.25\ d \qquad (8)\ (Khurmi\ and\ Gupta\ 2005)$$

$1.25\ x\ 15 = 20\ \boldsymbol{mm}$

$$5{,}000 = 2\ x\ \frac{\pi}{2} x\ d^2\ x\ \tau = 2\ x\ \pi\ x\ \left(\frac{15}{2}\right)^2\ x\ \tau = \tau = \mathbf{14\ N - mm^2}$$

Since the end is forked and therefore thickness of each eye

$$t_1 = \frac{l_1}{2} = \frac{20}{2} = \mathbf{10\ mm}$$

Inner diameter of each eye,

$$d_1 + 2x3 = 15 + 6 = \mathbf{21\ mm}$$

$$D = 2d_1 = 2\ x\ 15 = \mathbf{30\ mm}$$

Maximum bending moment at Y-Y

$$m = \frac{w}{2}\left(\frac{l_1}{2} + \frac{l_1}{3}\right) - \frac{w}{2} x \frac{l_1}{4} = \frac{5}{24}\ w\ x\ l_1 \qquad (9)\ (Khurmi\ and\ Gupta\ 2005)$$

Where,

$\frac{5}{24}5{,}000\ x\ 20 = \mathbf{20{,}833.33\ \ Nmm}$

Sectional modulus, as given in equation 10

$$Z = \frac{\pi}{32}(d_1)^3 \qquad (10)\ (Khurmi\ and\ Gupta\ 2005)$$

$\frac{\pi}{32}x15^3 = \mathbf{331.34\ mm^3}$

Bending stress induced,

$$\sigma_b = \frac{m}{z} = \frac{20{,}833.33}{331.34} = \mathbf{63\ MPa}$$

2.3.5 Design of the frame.

The frame is an assembly where the lever arm and the load is placed, the frame consist of I-beam and I-section column. The load are transferred to the crossing beam and in turn transfer to the column as shown in figure 3.

a. Design of Crossing Beam that Support Lever Arm

The cross beam is used to support the load from lever arm and transfer to the column. It is design using equation 11 and is shown in figure 7. The proportion of the support beam is taken as t =thickness, h = depth as 5t. the result is shown in table 3.

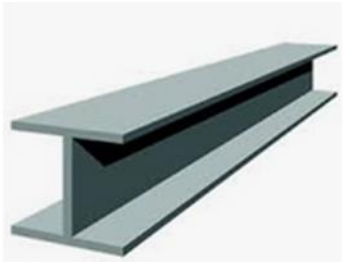

Figure 7. Crossing Beam

Moment of inertial I,

$$I = \frac{1}{12}[BxD^3 - bxd^3] \qquad (11)(Khurmi\ and\ Gupta\ 2005$$

$$I_{xx} = \frac{1}{12}[4t\ (5t)^3 - 3t(3t)^3] = \frac{\mathbf{419}}{\mathbf{12}}\boldsymbol{t^4\ mm^4}$$

Sectional Modulus Z,

$$Z = \frac{I_{xx}}{\frac{5t}{2}} = \frac{419t^4}{12}x\frac{2}{5t} = \frac{419}{30}t^3 = \mathbf{13.97}\boldsymbol{t^3}$$

(From table 2.5 Khurmi and Gupta 2005) yield stress of 220 Mpa

However, bending stress σ_b,

$$\sigma_b = \frac{m}{Z} = 220 = \frac{5{,}000{,}000}{13.97t^3} = t = \sqrt[3]{1{,}626.86}\ = \mathbf{12}\ \boldsymbol{mm}$$

$$Z = 13.97x\ 12^3 = 24{,}140.61\ mm^3$$

(From table 24.41 Lingaiah 2004) I-section chosen for the crossing beam is ISLB 75. As shown in table 3

Table 3. Showing Dimension of section

Sections	Value (units)
Depth of I-section	75 mm
Breath	50 mm
Thickness of web t_w	3.7 mm
Thickness of flanges t_f	5.0 mm
Area of section A	7.71 cm^2
Sectional Modulus Z_{xx}	19.4 cm^3

b. Load Transfer Column

The load transfer column is attached with the fulcrum that transfer the dead load to base of the foundation. The proportioning of load transfer column is shown in figure 8. Using Rankine's method to design for the cripple load as shown in equation 12, 13 and 14. Shear stress at equation 15 and the results is shown in table 4.

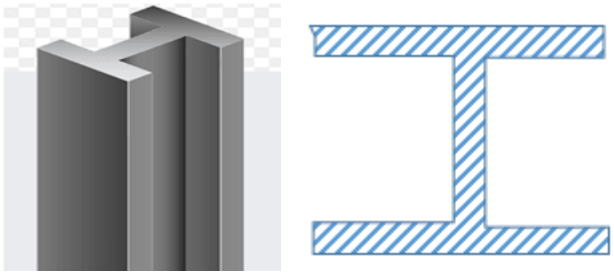

Figure 8. I-section column.

Area of the section, A =LxB (12) (*Khurmi and Gupta* 2005)

A = 2(4txt) + 3t x t =$11t^3$

Moment of inertial in X-axis, I_{xx}

$$I_{xx} = \frac{1}{12}[4t\ (5t)^3 - 3t(3t)^3] = \mathbf{\frac{419}{12}t^4\ mm^4}$$

Moment of inertia in Y-axis, $I_{yy.}$

$$I_{yy} = \left[2x\frac{1}{12}tx(4t)^3 + \frac{1}{12}3txt^3\right] = \mathbf{\frac{131}{12}t^4\ mm^4}$$

Therefore,

$$\frac{I_{xx}}{I_{yy}} = \frac{419}{131}x\frac{12}{131} = \mathbf{3.2}$$

Since the value of I_{xx}/I_{yy} lies between 3 and 3.5. The I-section is quite satisfactory (kurmi and Gupta 2005).

Also, (table 4.3 of Kurma and Gupta 2005) factor of safety was taken as 4 for cripple load on column.

$W_{cr} = \frac{\sigma_c A}{1+a\left(\frac{L}{2K_{xx}}\right)}$ (13) (*Kurmi and Gupta* 2005)

Where,

W_{cr} = cripple load

.σ_c = compressive yield stress

A = cross sectional area of the column

.a = Rankine's constant

K = least radius of gyration

L = equivalent length of column

However, since the column is fixed, effective length is L = L/2 =2,000mm/2 = **1,000 mm**

.σ_c = 320 MPa = 320 N/mm^2 and a = 1/7,500.

$$w_{cr} = w\ x\ factor\ of\ safety = 5{,}000x4 = \mathbf{20{,}000N}$$

Consider list moment of inertia,

$$I_{xx} = \frac{1}{12}[4t\ (5t)^3 - 3t(3t)^3] = \frac{\mathbf{419}}{\mathbf{12}}\boldsymbol{t^4\ mm^4}$$

And radius of gyration k_{xx} of the least moment of inertia, as given in equation 14

$$K_{xx} = \sqrt{\frac{I_{xx}}{A}} \qquad (14)\ (Kurmi\ and\ Gupta\ 2005)$$

$$k_{xx} = \sqrt{\frac{I_{xx}}{A}} = \sqrt{\frac{419t^4}{12}\,x\,\frac{1}{11t^2}} = \mathbf{1.78}\boldsymbol{t}$$

Equivalent length of column for both ends fixed.

$$L = \frac{L}{2} = l = \mathbf{1,000}\ \boldsymbol{mm}$$

From eq.13. Rankine's cripple load, W_{cr},

$$w_{cr} = \frac{\sigma_c x A}{1 + a\left(\frac{L/2}{k_{xx}}\right)^2}$$

$$20{,}000 = \frac{320x11t^2}{1 + \frac{1}{7{,}500}\,x\left(\frac{1000}{1.78t}\right)^2}$$

Thickness, t = **4.3 mm**

However, (Table 24.31 Lingaiah 2004). I-section chosen for the column is ISLB 75. As shown in table 4.

Table 4. Showing Dimension of section

Sections	Value (units)
Depth of I-section	75 mm
Breath	50 mm
Thickness of web t_w	3.7 mm
Thickness of flanges t_f	5.0 mm
Area of section A	7.71 cm^2
Sectional Modulus Z_{xx}	19.4 cm^3

Shear Stress τ,

$$\tau = \frac{F}{A} \qquad (15)\ (Kurmi\ and\ Gupta\ 2005)$$

$$\tau = \frac{5{,}000}{771} = \mathbf{7}\ \boldsymbol{N/mm^2}$$

c. Design of anchor Leg

The anchor column legs is made up an I-section mild steel with the crushing stress of $\sigma_c = 320\,Mpa$ with Rainkine constant, $a = {}^{1}/_{7500}$

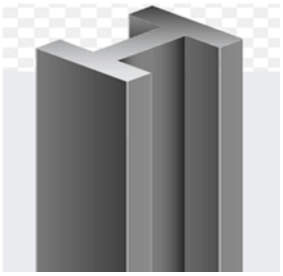

Figure 8. Anchor column legs

Radius of gyration for an I-section, K, from eq. 14 and results at table 5

$$K = \sqrt{\frac{I_{xx}}{A}}$$

Moment of inertia about x-axias

$$I_{xx} = \frac{1}{12}[4t\,(5t)^3 - 3t(3t)^3] = \mathbf{\frac{419}{12}\,t^4\ mm^4}$$

The factor of safety is taken as 4

$$k_{xx} = \sqrt{\frac{I_{xx}}{A}} = \sqrt{\frac{419t^4}{12}\,x\,\frac{1}{11t^2}} = 1.78t$$

From eq. 13

$$w_{cr} = \frac{\sigma_c x A}{1 + a\left(\frac{L/2}{k_{xx}}\right)^2} = 20{,}000 = \frac{320x11t^2}{1 + \frac{1}{7{,}500}\,x\left(\frac{2000}{1.78t}\right)^2}$$

Thickness, t = 8 mm

(From table 24.41 Lingaiah 2004) I-section chosen for the anchor leg ISLB75 is shown on table 5

Table 5. Showing Dimension of section

Sections	Value
Depth of I-section	75 mm
Breath	50 mm
Thickness of web t_w	3.7 mm
Thickness of flanges t_f	5.0 mm
Area of section A	7.71 cm^2
Sectional Modulus Z_{xx}	19.4 cm^3

Shear stress τ,

$$\tau = \frac{F}{A} = \frac{5{,}000}{771} = \frac{5{,}000}{771} = 6\ \boldsymbol{N/mm^2}$$

2.3.6. Design of Loading Arm

Loading arm is circular mild steel rod attached to the lever arm through a pin and was used in loading the load bearing probe. Using equation 7

P = area of rod x $shear\ stress. \sigma_t$

$5{,}000 = \frac{\pi}{4} d^2 x 220,\ d = \boldsymbol{6mm}$

Safe tensile load = stress area x σ_t

Shear area A = $\frac{\pi}{4} x 6^2 = 28.27\ mm^2$

Safe tensile load = 28.27 x 220 = **6,219N**

Design of Loading Arm Pin.

From equation 7.

$P = d_1\ x\ l_1 x\ p_b$

Let, d_1 =diameter of pin at loading arm

And l_1 = length of the pin at loading arm

Let consider bearing of the pin at loading arm

$5{,}000 = d_1\ x\ l_1 x\ p_b = d_1 1.25\ d_1 x\ 17.5 = 21.875 d_1^2 = d_1 = \boldsymbol{15\ mm}$

$$l_1 = 1.25\ d_1 = 1.25 x 15 = \boldsymbol{18.75\ mm}$$

Check for shear stress, from equation 15.

$P = 2x\frac{\pi}{4}\ x\ d^2\tau$

$$5{,}000 = 2x\frac{\pi}{4}\ x\ 15^2\tau$$

$\tau = \boldsymbol{14.15\ MPa\ is\ ok}$ (According to Khurmi and Gupta 2005)

Since the end is forked and therefore thickness of each eye

$$t_1 = \frac{l_1}{2} = \frac{18.75}{2} = \mathbf{9.375\ mm}$$

Inner diameter of each eye,

$$d_1 + 2x3 = 15 + 6 = \mathbf{21\ mm}$$

$$D = 2d_1 = 2\ x\ 15 = \mathbf{30\ \ mm}$$

Maximum bending moment at Y-Y

$m = \frac{w}{2}\left(\frac{l_1}{2} + \frac{l_1}{3}\right) - \frac{w}{2} x \frac{l_1}{4} = \frac{5}{24}\ w\ x\ l_1$

Where,

$\frac{5}{24} 5{,}000\ x\ 18.75 = \mathbf{19{,}531.25\ Nmm}$

Sectional modulus,

$Z = \frac{\pi}{32}(d_1)^3$

$\frac{\pi}{32} x 15^3 = \mathbf{331.34\ mm^3}$

Bending stress induced, A

$$\sigma_b = \frac{m}{z} = \frac{19{,}531.25}{331.34} = \mathbf{5.83\ MPa}$$

3. Results and Discussion of the Results

3.1 Results of Lever Arm Design Analysis

The result of the design analysis are presented in tables 6 – 8. Table 6, shows the design results of the lever arm. The minimum safe dimensions of the lever arm presented for the I-section used.

Table 6: Lever Arm Results

Sections	Value (units)
Depth of I-section D	125 mm
Breath B	75 mm
Thickness of web t_w	4.4 mm
Thickness of flanges t_f	7.6 mm
Area of section A	1660 m^2
Sectional Modulus Z_{xx}	71800 cm^3

The anchor legs provide support for the entire frame of the load bearing capacity probe. The design results are presented in Table 7. The results shows that maximum shear stress during working is far less that the yield stress of the mild steel.

Table 7: Results Leg Anchor

Sections	Value
Depth of I-section	75 mm
Breath	50 mm
Thickness of web t_w	3.7 mm
Thickness of flanges t_f	5.0 mm
Area of section A	771 mm^2
Sectional Modulus Z_{xx}	19400 mm^3

Table 8: Other results includes.

Sections	Value
Area of load bearing arm	28.27 mm^2
Length of the load bearing arm	600 mm
Diameter of the pin	6 mm
Length of the pin	18.75 mm

4. Conclusion

The design analysis of in-situ load bearing capacity mechanism was successfully conducted, which will facilitate the fabrication and final performance evaluation of the mechanism. The similar mechanism presently in use are laboratory and field models for sand soils only. They don't facilitate testing at the site of the project for long period of time. Therefore, this design is mainly for site experimentation for long time as against the previous tests. A CAD model of the design concept was developed, followed by design analysis and synthesis of the required dimensions of the components of the load bearing capacity mechanism. The minimum thickness and load area of the lever arm and anchor legs are 4.4mm, 3.7mm and 16.60 mm^2, 7.71mm^2 respectively.

REFERENCES

ASTM D1194-94 (2003). *Standard test method for bearing capacity of soil for static load and spread footings*. American Society for Testing Materials, Philadelphia, USA.

Barnard, H. F. T., Heyman, G. (2015). The Effect of Bedding Errors on the Accuracy of Plate Load Tests. Journal of the South Africa Institution of Civil Engineering, 57(1), 1-23.

Barnard, H.F.T., (2019). The Importance of Plate Load Tests in Geotechnical Engineering Practice. *Proceedings of the 17th African Regional Conference on Soil Mechanics and Geotechnical Engineering. Cape Town.*

Dasaka, S. M. (2012). Risk Analysis of Bearing Capacity of Shallow Foundations. *Workshop on Emerging Trends in Geotechnical Engineering (ETGE 2012) 8th June 2012*, Guwahati, 89-97.

Dasaka, S. M., Jain, A., and Kolekar, Y. A. (2013). Effect of Uncertainties in the Field Load Testing on the Observed Load-Settlement Response. *Indian Geotechnical Journal*, 44(3), 294-304.

Gul, Y. and Cellanoglu, A. (2016). Evaluation of Ground Bearing Capacity Estimation Method Based on Plate Loading Tests. *IOP Conference Series: Earth and Environmental Science*.,**44**, 1-12.

Khurmi R. S, and Gupta J. K., (2005) A Text Book of Machine Design. Eurasia Publishing House (PVT.) LTD. Ram, Nagar, New Delhi-110 055.

Lingaiah K, (2004) Machine Design Data Book, McGraw-Hill Handbooks. Second edition. Downloaded from Digital Engineering Library.

Shirvani, R. A. and Shooshpashpasha, I. (2015). Experimental Study on Load-Settlement Behavious of Cement Stabilized Footing with Different Dimension on Sandy Soil. Arab Journal of Science and Engineering, 40, 397-406.

Sultana, P. and Dey, A. K. (2018). Estimation of Ultimate Bearing Capacity of Footings on Soft Clay from Plate Load Test Data Considering Variability. *Indian Geotechnical Journal*, 49, 170–183.

Warmate, T., (2014). Bearing Capacity Determination using Plate Load Test in Calabar, South Eastern Nigeria. *EJGE*, 19(bundle T), 4577-4588.

Warmate, T. and Nwankwola, H. O. (2014). Determination of Elastic Modulus using Plate Load Test in Calabar, South Eastern Nigeria. International Journal of Natural Sciences Research. 2(11), 237-248.

IMPROVEMENT ON SOME PHYSICAL PROPERTIES OF SELECTED NIGERIAN CLAY

[1]Rabiu O. I., [2]Bala K. C.

[1]Department of Mechanical Engineering, School of Infrastructure and Process Engineering Technology Federal University of Technology Minna, Niger State. Nigeria, rabobreezeoladimeji@gmail.com

[2]Department of Mechanical Engineering, School of Infrastructure and Process Engineering Technology Federal University of Technology Minna, Niger State. Nigeria, katsina.bala@futminna.edu.ng

Corresponding author, rabobreezeoladimeji@gmail.com 08123456853

Abstract

In metallurgical industries the quality of refractory clay depends largely on the physical properties of clay and proper selection of clay affect these physical properties which include Porosities, Compressive strength, Linear shrinkage, Thermal shock resistance, and refractoriness. This gives need on the improvement on some physical properties of selected Nigerian clays. Clay collected from Bida, Chanchaga, Kpakungu and Maikunkele areas of Niger State were analysed to determine the chemical composition of the clays samples and raw clay were beneficiated and mixed with additives which include ash of Sawdust, Ricehusk and Cornhusk in a ratio of 5, 10, 15, 20, 25 & 30% weight to produce clay bars which were subjected to tests to determine the effect of the additives on the physical properties of the clay samples. The result revealed Bida clay increase in porosity from 16.64% to 35%, Chanchaga clay increase in porosity from 9.98% to 38.38%, Kpakungu clay increase in porosity from 8.12% to 33.37% and Maikunkele clay increase in porosity from 10.50% to 35%. Compressive strength of the clay samples were reduced Bida clay reduced in compressive strength from 51.58N/m^2 to 8.63N/m^2, Chanchaga clay reduced in compressive strength from 65.85%N/m^2 to 29.11N/m^2, Kpakungu clay reduced in compressive strength from 63.59N/m^2 to 20.55N/m^2, Maikunkele clay samples reduced in compressive strength from 59.06N/m^2 to 18.52N/m^2. The refractory temperature of Bida, Chanchaga, Kpakungu and Maikunkele clay samples were increased from 1410°C to 1480°C, 1580°C to 1620°C, 1550°C to 1570°C and 1650°C to 1690°C at 5%wt of additives.

Keywords: Compressive strength, Additives, Porosities, Refractories, Properties.

1.0 INTRODUCTION

Clays by way of a compound inorganic combination has diversities of composition depending on it area of location. The quality of refractory clay depends largely on the physical properties of clay and proper selection of clay affect these physical properties which include Porosities, Compressive strength, Linear shrinkage, Thermal shock resistance, and refractoriness. This gives need on the improvement on some physical properties of selected Nigerian clays.

Refractories have been an essential element in heat engineering plants since the 1960s, where they were successfully used to improve performance and energy efficiency. This is because refractories are chemically and physically stable at high temperatures depending on the operating environment. Good fireclay refractories should always have 24% - 26% plasticity, the shrinkage after firing should be within 6% - 8% maximum and should not contain more than 25% Fe_2O_3 (Atanda *et al.*, 2012)

Fire clays are clays with high refractoriness and possess the capability of maintaining both physical and chemical identity at high temperatures. Clays used for furnace linings in metallurgical industries are classified as refractory clays. However, the degree of refractoriness and plasticity of any clay material is often influenced by the amount of the impurities contained in them. Moreover, the ability of selected refractory clay to withstand high temperature and resist physical and chemical corrosion determines the quality and the suitability of such material for use as furnace lining (Sanni, 2005)

Characterization of the refractory property of Osiele clay, revealed that the clay was silicious alimino- silicate with low content of Iron III Oxide. The water absorption, bulk density and apparent porosity decreased with the firing temperature, whereas the total shrinkage increased as the firing temperature increased. It was concluded

that Osiele clay can be used as refractory material for the lining of furnace particularly for operating temperature in the pre-1100°C range. (Lawal *et al.*, 2008)

Investigation on the effect of additives (sawdust and ashes) on the thermal conductivity of clay, result obtained showed that with sawdust addition the clay was suitable as oven materials as well as good insulator (Folaranmi, 2009)

Termite hills can be used to produce insulating refractory when 25% additives (corn husk and sawdust) are used. However, low values of refractoriness 1200°C were recorded (Ndaliman, 2001)

It was discovered that addition of ash residues from agricultural waste gave an improvement in the apparent porosity and water absorption of the blended clays. (Odo & Mba, 2008)

Clays samples of Ifon, Ipetumodu, and iseyin investigated (Aramide *et al.*, 2014), Clays of Ifon contains low kaolinite (5.63%) which could not be used for making high temperature caliber refractories except with the addition of some additive that will improve on their refractory properties. Thermal conductivity decreases in refractory materials as its porosity increases with the pores acting as non-heat conducting media. Therefore, the refractories used in melting furnaces, are made to have low thermal conductivities, ensure minimal heat loss and maximum heat retention.(Titiladunayo & Fapetu, 2011).

2.0 MATERIALS AND METHODS

Ten kilograms (kg) of clay samples were collected per site from four different locations in Niger state, Nigeria, making a total of four clays samples weighing forty kilograms (40kg). The locations have some ample reserve of Kaolin Clay which could be used for industrial purpose as reported by (Okorafor 2001). The sites are located in four different areas in Niger State which include Bida, Chanchaga, Kpakungu and Maikunkele. The clays were blended with additives and were subjected to physical, chemical and thermal analysis at the Scientific Equipment Development institute (SEDI) Minna, Niger State, to determine the effect of the additives on the physical properties of the clay samples.

Determination of refractory properties

The properties of the pure clays and clays with different additive ratio such as linear shrinkage, bulk density, apparent porosity, compressive strength, thermal shock resistance and refractoriness were carried according to (ASTM, 1985a).

Linear shrinkage

The dimensional changes in length were taken and the results were used to determine the fired shrinkage after firing at 950^{o}C to 1150^{o}C in Daiki scientific furnace (MD010). The linear shrinkage was determined using equations 1. (ASTM, 1985a; Clay Shrinkage Testing, 2010)

$$\text{FIred Shrinkage} = \frac{L_d - L_f}{L_d} \text{ x } 100\%. \quad (1)$$

Where: L_d = Dry length and L_f = Fired length

Bulk density

Bulk density was calculated using a direct volume measurement method. This method exploits the relative density of a substance multiplied by the density of water to obtain the required bulk density. Equation 2 was used to obtain the bulk density in g/cm^3 (ASTM, 1985a; TBDBWD, 2010).

$$\text{Bulk density} = \frac{W_d}{W_s - W_{sp}} \text{ x Density of water} \quad (2)$$

Where W_s = soaked weight, W_d = dry weight and W_{sp} = suspended weight

Apparent porosity

The boiling method was used for this test at 1000°C for 2 hours. The test pieces were subjected to a two-hour boiling followed by an additional four hour water soaking and then weighed W_s. The soaked piece was then suspended from the beam of a balance in a vessel of water so arranged that the test piece under consideration was completely immersed in the water without touching the side of the vessel. The suspended specimen in water weighed as W_{sp}. Porosity was then calculated as a function of the specimen's weight difference between soaked weight and dry weight to specimen's weight difference between soaked weight and suspended immersed weight. The results were obtained by equation 3 (ASTM, 1985a; Calculate Apparent Porosity, 2010)

$$\text{Porosity (P)} = \frac{W_s - W_d}{W_s - W_{sp}} \text{ x } 100\% \quad (3)$$

Where: W_s = soaked weight, W_d = dry weight, W_{sp} = suspended weight

Compressive strength

The compressive strength of each brick was determined in accordance with the Specification of the Standard Organization of Nigeria (SON) as contained in Test for Compressive Strength of Solid Bricks using the Testing Machine. A 40 mm square platen was used on the compressive testing machine. Three test cubes were preconditioned by immersion in cold water at room temperature (29°C ± 2°C) for 24 hours, removed and all traces of water wiped off, and then stored under moist conditions for 24 hours prior to testing. Each test piece was centrally positioned between the platens of the testing machine, and the load was gradually increased until failure (Fayomi *et al.,* 2011). Mathematically, compressive strength can be determined using Equation 4 (Falodun *et al., 2017*)

$$\text{Compressive strength} = \frac{\text{Maximum failure load x Proving ring factor}}{\text{Area sample}} \ (\text{N/m}^2) \quad (4)$$

Thermal shock resistance

This test was carried out with the help of an electrical furnace (Thermodyne 46200) heated at the rate of 5°C/min. The thermal shock resistance was determined by prism spalling test method according to ASTM C- 484 standard in which the spalling resistance was measured by the number of thermal cycles (heating, cooling and testing for failure). The test pieces of refractory bricks were thoroughly dried and placed in the cold furnace and heated at the rate of 5ºC/minute until the furnace temperature got to 1200°C. The samples were then removed using a pair of tongs and cooled in air for 10 minutes, and then observed for cracks. In the absence of cracks (or fracture), the bricks were put back into the furnace and reheated for a further period of 10 minutes and then cooled for another 10 minutes. This process or cycle of heating, cooling and observing for cracks was repeated until cracks were observed. The number of complete cycles that produced visible cracks in each specimen was noted.

Refractoriness

The refractoriness or softening point was determined using the method of pyrometric cone equivalence (PCE) in accordance with ASTM C24-79. The test pieces were mounted on the refractory plaque along with some standard cone whose softening points are slightly above or below those expected of the test cones. The plaque was then inserted into the electric furnace. The temperature was raised at the rate of 5°C per minute during which softening of Orton cone occurred along with the specimen test cone. (Etukudoh *et al.,* 2016).

Raw material beneficiation and production of clay bars for refractory test

The raw clay samples were air dried before processing. The raw dry clay samples were crushed in a mortar to small grain sizes and sieved. The samples were soaked in a plastic container of water and allowed to soak for three days. The dissolved clay was then filtered through a 0.425 mm mesh sieve to get rid of unwanted particles and plant materials. The filtrate was filtered further by the use of a mesh sieve of size 0.18 mm in order to obtain finer particles. The filtrate was allowed to settle for three days after which excess water was decanted off. The clay slip obtained was sun dried for 2 days and then dried in an oven at 100°C.

The processed dried clay was pulverized and then passed again through a 0.18mm mesh sieve. Each of the clay samples was mixed with water and molded using different mould shapes and sizes that suited the respective tests they were to be used for. Bida, Chanchaga, Kpakungu and Maikunkele clays were blended with saw dust ash (SDA), rice husk ash (RHA) and corn husk ash (CHA) were blended at different ratios as shown in table 1 to develop different test samples.

Table 1: Different additive ratio of clay mixture

Clay	250 g	237.5 g		225 g		212.5 g		200 g		187.5 g		175 g	
	0%	5%	12.5g	10%	25g	15%	37.5g	20%	50 g	25%	62.5g	30%	75 g
RHA	-	2	5.00	3	7.5	5	12.5	6	15	8	20	10	25
CHA	-	1.5	3.75	4	10	5	12.5	7	17.5	8	20	10	25
SDA	-	1.5	3.75	3	7.5	5	12.5	7	17.5	9	22.5	10	25

Each of the samples (250 g) was mixed with 35% (0.087 Liters) of water to make the clay plastic for molding. The clay was then molded into shapes using pop moulds with the application of powder lubricant to the surface of the moulds to prevent the test pieces from sticking to the surface. An improvised wooden material was used for transmitting the molding pressure of 2 MPa to the mould when the required quantity of plastic molding mass was put into the mould, wooden plunger was used to extrude out the green brick from the mould. The test samples were sundried, oven dried to 110°C and finally fired to 1150°C before testing for the respective properties.

3. RESULTS AND DISCUSSION

Table 2: Summary of the experimental result

Properties	Bida Clay		Chanchaga Clay		Kpakungu Clay		Maikunkele Clay	
	0%	30%	0%	30%	0%	30%	0%	30%
Linear Shrinkage (%)	9.98	7.81	10.11	8.94	10.25	9.11	10.05	7.22
Bulk Density (g/cm^3)	1.99	1.22	2.23	2.00	2.04	1.90	2.07	1.93
Apparent Porosity (%)	10.24	35.13	4.05	38.33	4.67	33.37	6.72	35.99
Compressive Strength(MN/m2)	67.46	8.63	73.32	29.11	67.60	20.55	63.09	18.52
Thermal Shock resistance(cycles)	11	28	9	22	11	28	23	37
Refractoriness (°C)	1410	1480	1580	1620	1550	1570	1650	1690

Chemical composition

The chemical composition analysis of Bida, Chanchaga, Kpakungu and Maikunkele clay as done using X-ray fluorescence (XRF) and shows that the mined clays are rich in oxides of Alumina. It could be seen that there are oxides of iron, calcium, and titanium. From the result, it is evident that SiO_2 is a major component. Table 3 shows the chemical composition of the selected clay samples.

Table 3: Chemical composition of selected clay samples

Oxide(s)	Bida(%)	Chanchaga(%)	Kpakungu(%)	Maikunkele(%)
SiO_2	44.67	49.45	52.58	54.59
Al_2O_3	33.01	28.58	27.32	29.50
Fe_2O_3	2.1	6.50	4.50	4.50
TiO_2	0.3	0.25	0.10	0.02
CaO	1.90	2.59	2.90	2.10
MgO	1.1	2.41	2.30	1.90
K_2O	2.4	0.45	0.55	0.48
Na_2O	0.3	0.10	0.12	0.04
LOI	14.22	9.67	9.63	6.87

Below are the beneficiation result of all the clay samples

Table 4: Sieve analysis result of Bida clay

Sieve Size Mm	Weight of soil retained(g)	Cummulative mass retained(g)	% Cumulative Retained	% Passing
100	12	12	0.23	99.77
90	14	26	0.50	99.5
75	15	41	0.79	99.21
63	18	59	1.12	98.88
50	211	270	5.12	94.88
37.5	781	1051	19.95	80.05
25	950	2001	37.99	62.01
19	933	2934	55.71	44.29
16	1338	4272	81.11	18.89
12.5	895	5167	98.10	1.9
	100	5267	100	0

Total mass used = 5267 g

Table 5: Sieve analysis result of Chanchaga clay

Sieve Size Mm	Weight of soil retained (g)	Cummulative mass retained (g)	% Cumulative Retained	% Passing
100	26.57	26.57	2.31	97.69
90	73.02	99.59	8.66	91.34
75	122.82	222.41	19.34	80.66
63	136.28	358.69	31.19	68.81
50	99.13	457.82	39.81	60.19
37.5	102.12	559.94	48.69	51.31
25	108.44	668.38	58.12	41.88
19	70.38	738.76	64.24	35.76
16	112.6	851.36	74.03	25.97
12.5	162.25	1013.61	88.14	11.86
	136.39	1150	100	0

Total mass used = 1150 g

Table 6: Sieve analysis result of Kpakugu clay

Sieve Size Mm	Weight of soil retained	Cummulative mass retained	% Cumulative Retained	% Passing
100	16.10	16.10	1.4	98.60
90	64.06	80.16	6.97	93.03
75	133.05	213.21	18.54	81.46
63	97.87	311.08	27.054	72.95
50	137.54	448.62	39.01	60.99
37.5	109.94	558.56	48.57	51.43
25	131.22	689.78	59.98	40.02
19	123.39	813.17	70.71	29.29
16	110.17	923.34	80.29	19.71
12.5	127.07	1050.41	91.34	8.66
	99.59	1150	100	0

Total mass used = 1150 g

Table 7: Sieve analysis result of Maikunkele clay

Sieve Size Mm	Weight of soil retained	Cummulative mass retained	% Cumulative Retained	% Passing
100	64	64	1.22	99.77
90	192	256	4.9	99.5
75	470	726	13.7	99.21
63	693	1419	26.79	98.88
50	497	1916	36.16	94.88
37.5	510	2426	45.78	80.05
25	584	3010	56.81	62.01
19	688	3698	69.79	44.29
16	287	3985	75.20	18.89
12.5	1215	5200	98.11	1.9
	100	5300	100	0

Total mass used = 5300 g

DISCUSSION OF RESULT

The Linear Shrinkage occurred in the fired samples with the percentage of decreasing with increase in the amount of additives, Bida clay reduced from 9.98% to 7.81%, Chanchaga clay reduced from 10.11% to 8.94%, kpakungu clay reduced from 10.25% to 9.11%, Maikunkele clay reduced from 10.05% to 7.22%. Maikunkele clay has the least shrinkage property of 7.22% while Kpakungu clay has the highest shrinkage property of 9.11%. (Arowolo, 2000) pointed out that lower values are more desirable as this means the clay is less suitable to volume change. Figure 1 shows the effect of additives on linear shrinkage at a temperature of 1150°C

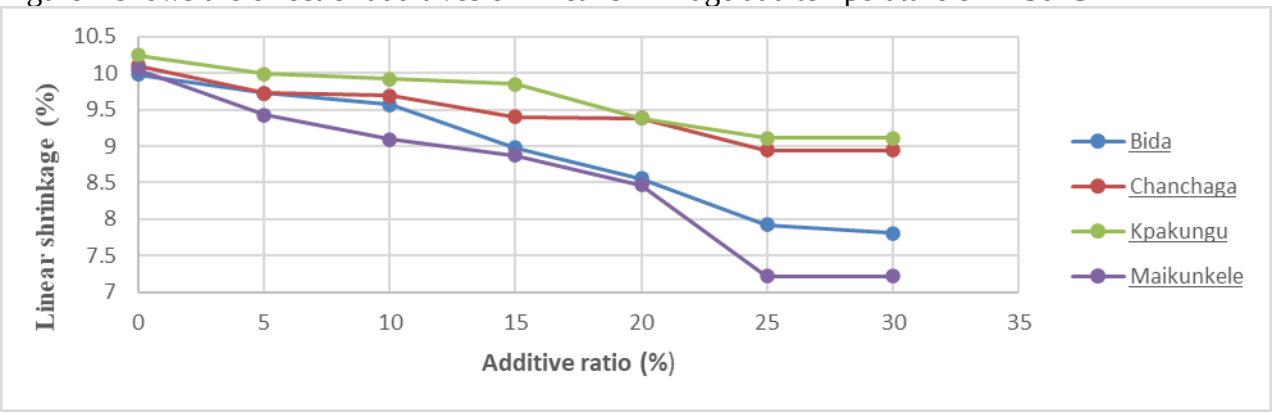

Fig 1: Effect of additives on linear shrinkage at a temperature of 1150^{o}C.

Bulk density of fired clay was inversely proportional to the quantity of additives added.

The bulk density decrease with increase in the amount of additives added. Bida clay has the lowest Bulk density of 1.22g/cm^3 and Maikunkele clay has the highest Bulk density of 1.93g/cm^3. Low Bulk density can be attributed to some extent of mineral composition of the clay (Aliyu *et al.*, 2013). Figure 2 shows the effect of additives on bulk density.

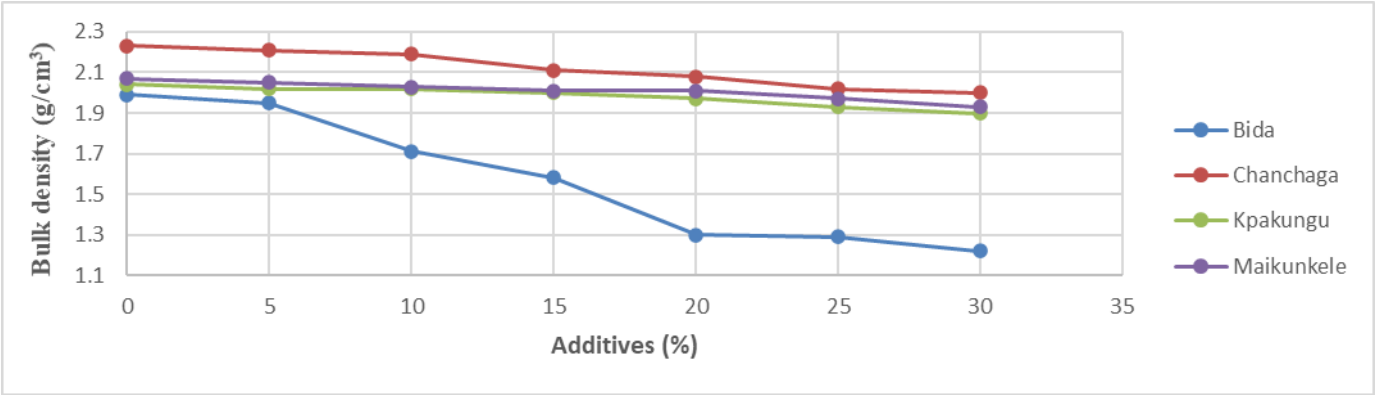

Fig 2: Effect of additives on bulk density at a temperature of 1150^{o}C.

The porosity of a refractory clay material is directly related to the air pocket contained in it hence the higher the porosity of the refractory clay material the higher the insulating property. Bida clay has porposity of 35.13%, chanchaga clay has 38.33%, Kpakungu clay has 33.37% and maikunkele clay has 35.99% ths values falls within the acceptable range of (10 – 30%) for refractories. Fig 3 shows the effect of additives on apparent porosity at 1150°C

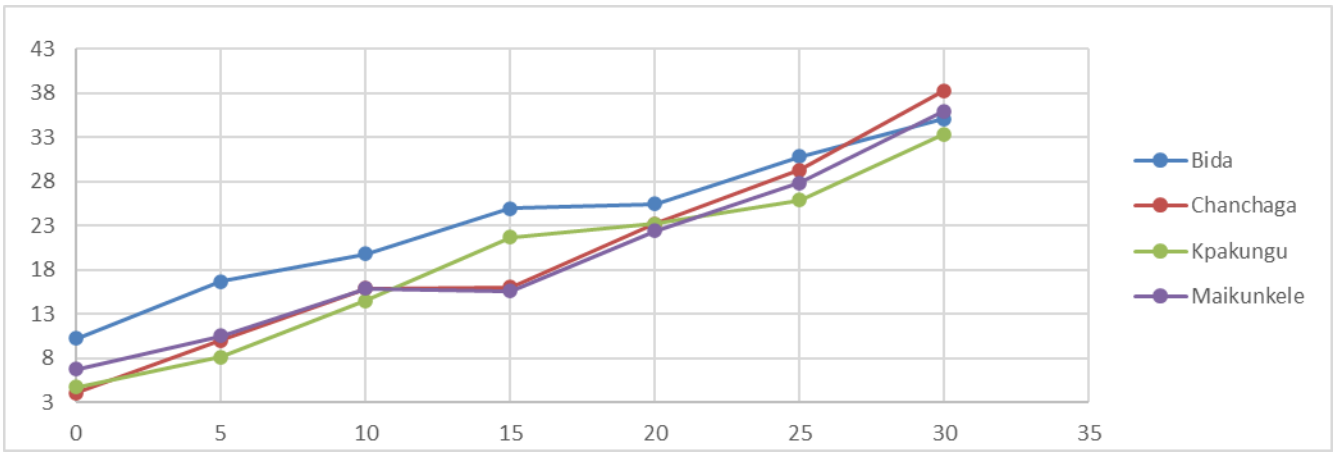

Fig 3: Effect of additives on apparent porosity at 1150^{o}C

The Compressive strength result indicated that the strength of the samples greatly depended on the amount of additives and the firing temperature. The compressive strength was 67.46 MN/m^2 73.32 MN/m^2, 67.06 MN/m^2 and 63.09 MN/m^2 at 0% additives ratio for Bida, Chanchga, Kpakungu and Maikunkele clays at a temperature of 1150°C. when the additives varies from 5% to 30% and the firing temperature from 950°C to 1150°C the compressive strength decrease with increasing additives. At 30% additives Bida clay shows a compressive strength of 8.63 MN/m^2, Chanchaga clay shows 29.11 MN/m^2, Kpakungu clay shows 20.55 MN/m^2 and Maikunkele clay shows 37 MN/m^2. Bida clay had a value in less of 18MN/m^2 at 8.63MN/m^2 which falls short of the 26.5MN/m^2 repoerted by (Ameh & Obasi, 2009) for Nsu clay. Compressive strength of Chanchaga clay,

Kpakungu clay and Maikunkele clay meets the criteria of the TIS77-2545 that define compressive strength not lower than 17MN/m^2. Fig 4 shows the effect of additives on compressive strength at 1150°C

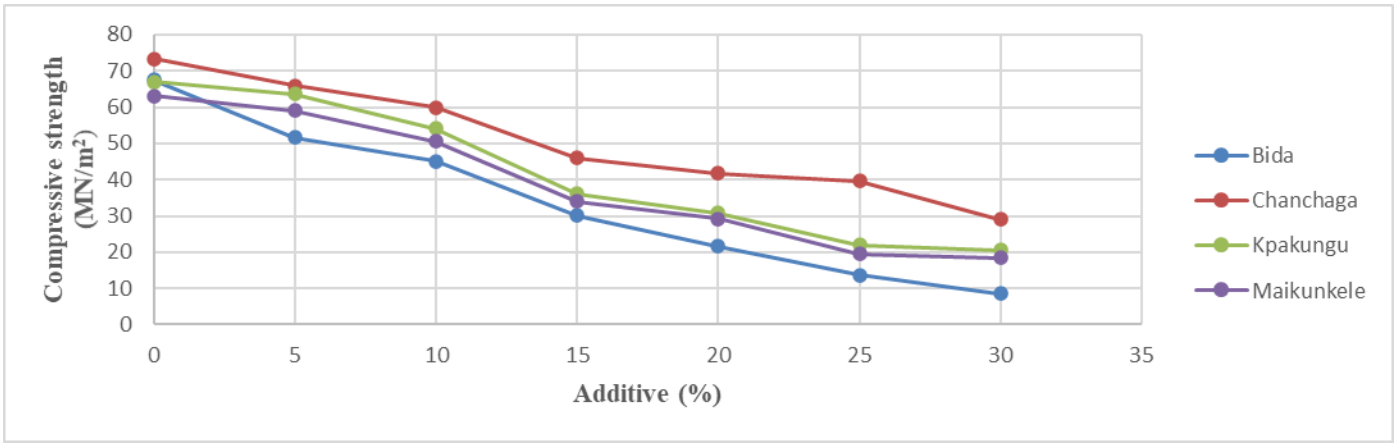

Fig 4: Effect of additive on compressive strength at 1150^{o}C

Thermal shock resistance of the clay samples increases with increase in additives ratio and decrease with rise in temperature. Bida clay show 36$^+$ cycles at 950°C and 28$^+$ cycles at 1150°C. Maikunkele bricks show 56$^+$ cycles at 950°C and 1150°C Kpakungu bricks show 42$^+$ cycles at 950°C and 28$^+$ cycles at 1150°C While Chanchanga clay bricks shows 31$^+$ cycles at 950°C and 22$^+$ cycles at 1150°C all at an additive ratio of 30%wt which gives an excellent thermal shock resistance. The excellent thermal shock resistance exhibited by all the clay samples can be attributed to the insulating property due to uniformly distributed pore at high ratio of additives that burns off at high temperature. Fig 5 shows the effect of additives on thermal shock resistance.

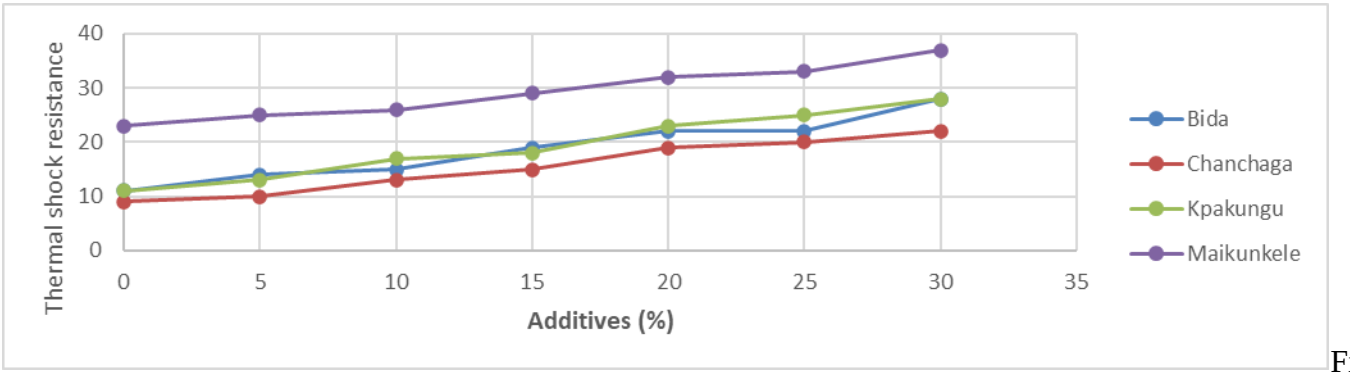

Fig 5: Effect of additives on thermal shock resistance at 1150°C

It was noted that for the clays without additives, the softening point occurred at 1410°C, 1580°C, 1550°C and 1650°C for Bida, Chanchaga, Kpakungu and Maikunkele clay samples respectively while for those blended with the additives ratios of 5%wt to 30%wt were 1480°C, 1620°C, 1570°C and 1690°C for Bida, Chanchaga, Kpakungu and Maikunkele clay samples respectively. This suggests an enhancement in the refractoriness value which may be traced to the presence of useful oxides found in the additives. It was found that combination of two or more additives yielded better refractoriness value than single one (Izwan *et al.*, 2011). Fig 6: shows the effect of additives on the refractoriness of the clay samples.

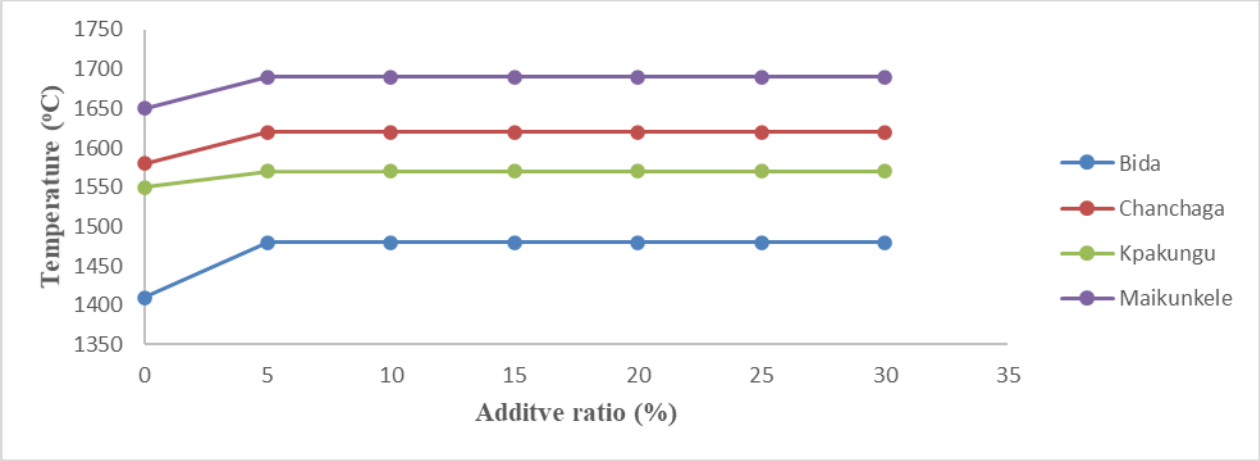

Figure 6: Effect of additives on refractoriness of clay samples

4 CONCLUSIONS

Linear shrinkage occurred in the fired clay samples with the percentage of decreasing with increase in the amount of additives, Maikunkele clay has the least linear shrinkage while kpakungu clay has the highest linear shrinkage.

The porosity of the clay samples increase with increase in additive ratio, the shows a good improvement in the insulating properties of the clay samples. The compressive strength of the clay samples greatly depends on the amount of additives and the firing temperature. Bida clay shows the least compressive strength of 8.63MN/m^2. The fusion temperature of all the clay samples increases at 5% ratio of additives and remain the same for all other ratio of additives. The pyrometic cone equivalent temperature shows beyond 1500°C except for Bida clay which shows 1480°C. Considering the above the additives has a great influence on the refractory clay samples and has improved the refractory properties of the selected clays.

REFERENCE

Al-Amaireh, M. N. (2009). Production of Fire-Clay Refractory Bricks from Local Materials. *European Journal of Scientific Research*, *26*(3), 386–392. Retrieved from http://www.eurojournals.com/ejsr.htm

Aliyu, S., Garba, B., Danshehu, B. G., & Isah, A. D. (2013). Studies On The Chemical And Physical Characteristics Of Selected Clay Samples "Sokoto Energy Research Centre, Usmanu Danfodiyo University, Sokoto., & Department of Forestry and Fisheries, Usman Danfodiyo University, Sokoto" *International Journal of Engineering Research & Technology (IJERT)*, *2*(7). Retrived from www.ijert.org IJERTV2IS70131.

Aramide, O. F., Alaneme, K. K., Olubambi, A. P., & Borode J. O. (2014). Characterization of some clay deposits in South West Nigeria. ([1]Department of Metallurgical and Materials Engineering, Federal University of Technology, P.M.B. 704, Akure, Nigeria., [2,4]African Materials Science and Engineering Network, (AMSEN) a Subsidiary of Regional Initiative for Science Education (RISE)., & [3]Applied Microscopy and Triboelectrochemical Research Laboratory, Department of Chemical and Metallurgical Engineering, Tshwane University of Technology, Pretoria. *Leonardo Electronic Journal of Practices and Technologies*, (25), 46–57. Retrieved from http://lejpt.academicdirect.org

Arowolo M. O. (2000). *Investigation of Local Clays for the Production of Electric Cooker Plate and Electrical Insulator*. "M.Eng Thesis of Department of Mechanical Engineering Federal University of Technology, Minna Niger State. Nigeria".

ASTM C-24 -79. (1985). *Annual Book of American Standard of Testing Methods, part17: Refractories, Glass, Ceramic Materials, Carbon and Graphite product Philidephia*.

ASTM C-484. (2019). Standard Test method of Cold crushing strength and modulus rupture of Refractories. ASTM International west Conshohocken PA.

ASTM. (1985). *Annual Book of American Standard of Testing Methods, part17: Refractories, Glass, Ceramic Materials, Carbon and Graphite product Philidephia*.

Atanda, P., Adeniji, O., & Oluwole, O. (2012). Development of Heat Treatment Refractory Bricks Using Local Nigerian Clays. "[1]Department of Material Science and Engineering Obafemi Awolowo University, Osun State. Nigeria, [2]Department of Mechanical Engineering University of Ibadan, Oyo State". *International Journal of Materials and Chemistry*, *2*(5), 185–191. https://doi.org/10.5923/j.ijmc.20120205.01

Etukudoh, A. B., Akpomie, K. G., Okereke, O. C. B., & Abuh, M. A. (2016). Effect of Cassava peel on the Insulting Properties of Ogugu Clay Deposit. *International Journal of Advanced Engineering Research & Technology (IJAERT)*, *4*(8).

Falodun, E. O., Folorunso, O. D., Oke, R. S., & Borode, O. J. (2017). Investigating the Effects of High Alumina Cement and Silica Sand on the Suitability of Ikere Ekiti Clay for Refractory Applications. *American Journal of Engineering Research (AJER)*, *6*(6), 24–28. www.ajer.org

Fayomi, O. S. I., Ajayi, O. O., & Popoola, A. P. I., (2011). Suitability of local binder compositional variation on silica sand for foundry core-making. "Department of Chemical and Metallurgical Engineering, Tshwane University of Technology, Pretoria, South Africa., & Department of Mechanical Engineering, Covenant University, Ota, Ogun State, Nigeri"). *International Journal of the Physical Sciences*, *6*(8), 1940–1946. https://doi.org/10.5897/IJPS11.324

Folaranmi, J. (2009). Effect of Additives onThe Thermal Conductivity of Clay. *JOURNAL OF SCIENCE*, *14*, 36–42.

Izwan, J., Syamsuhaili, S., & Ramadhansy, P. J. (2011). Chemical and physical properties of fired-clay brick at different types of rice husk ash. In *International Conference of Environment Science and Engineering (IPCBEE)* (pp. 171–174).

Lawal, G. I., Amuda, M. O. H., Ifekoya, D. I., Kuforiji, C. U., & Olokode, O. S. (2008). Characterisation of the Refractory Properties of Osiele Clay. *NSE Technical Transaction*, *43*(2), 21–31.

Ndaliman, M. B. (2001). Some Studies in Refractory Properties of Termite Hills in Nigeria. *Nigeria Journal of Education and Technology(NJET)*, *2*(1), 44–46.

Ndaliman, M. B. (2006). Refractory Properties of Termite Hills Under Varried proportions of Additives. *Leonard Electronic Journal of Practices and Technologies*, (9), 161–166.

Odo, J. U., & Mba, A. C. (2008). Effect of Agricultural waste Ash Additives on Refractory Properties of a Blend of two Nigerian Clays. *Journal of Material and Metallurgical Engineering*, *3*(1), 30–34.

Okoroafor, C. (2001). *Evaluation of some Nigerian Clays for Producing Furnace Bricks*. "M.Eng thesis of Department of Mechaical Engineering Federal University of Technology Minna, Niger State Nigeria".

Sanni, A. G. (2005). *Production of Proto-Type Fireclay Refractories Bricks from Oza-Nagogo Clay*.

Titiladunayo, I. F., & Fapetu, O. P. (2011). Selection of Appropriate Clay for Furnace Lining In a Pyrolysis Process. Journal of Emarging trends in Engineering and Applied Science (JETEAS), *2*(6), 938–945. Retrieved from htpp://jeteas.scholarlinkresearch.org

Development of a Computer Application for Cooling Load Calculation of a Building

[1]Joel C. Nzekwe, [2]James O. Okegbile, [3]Nicholas A. Musa

[1]Department of mechanical engineering, School of Infrastructure, Process Engineering and Technology, Federal University of Technology, Minna, Niger State, Nigeria, joelnzekwe@gmail.com

[2]Department of mechanical engineering, School of Infrastructure, Process Engineering and Technology, Federal University of Technology, Minna, Niger State, Nigeria, ojokegbile@gmail.com

[3]Department of mechanical engineering, School of Infrastructure, Process Engineering and Technology, Federal University of Technology, Minna, Niger State, Nigeria, madonick1@yahoo.com

joelnzekwe@gmail.com, 08105586731

Abstract: This paper presents the development of a computer application for cooling load calculation of a building. The computer application was built in Java programming language and was formulated using the Cooling Load Temperature Difference (CLTD)/ Solar Cooling Load (SCL)/ Cooling Load Factor (CLF) method of cooling load calculation. The computer application was use to estimate the peak cooling load of the case study: Room 103, Engineering complex, Federal University of Technology, Minna to be 10777W sensible and 4545W latent. All assumptions, equations and tabulated data were applied in accordance to ASHRAE proposals on the (CLTD/SCL/CLF) method of cooling load calculation. Also, the calculations were based on the atmospheric condition and parameters obtainable in the month of May at active period of the day, between the 8.00 hour and 18.00 hour of the day. The cooling load of the case study was also calculated manually. Results from manual calculation and results from the computer application were compare and found to be the same.

Key words: *CLTD/SCL/CLF method, Computer application, cooling load, latent, sensible.*

2. INTRODUCTION

Rabiatul *et al.* (2013) stressed that the primary purpose of any building design is to provide a comfortable indoor environment for occupants all the time. Modern house design with appropriate spacing, window sizes, and tree planting are good measures to ensure ventilation, but not enough to provide the perfect atmosphere for human beings all the time. Electrically powered HVAC system installed in buildings, is arguable the only means of attaining the acceptable range of thermal comfort all the time. In Nigeria, about 29% of electrical energy consumption goes into ventilation and cooling process (Arup, 2016). Set against inadequate supply of energy and energy generation in the country. A proper design for ventilation and cooling systems of the indoor environment begins with appropriate calculation of cooling load (Rabiatul *et al.*, 2013). The peak cooling load is used to determine the size of the HVAC systems required (Burdick, 2011). The importance of cooling load calculation is to minimize the energy consumption and to avoid under sizing or oversizing of HVAC systems. An oversized HVAC system will have both increased initial cost of installation (Bhatia, 2014) and purchase of equipment and high cost of operation (Burdick, 2011). Calculation of cooling load is a difficult task especially when it involves building with complex design. But with the advent of computer, applications have been developed to ease the process. Among the recent computer applications are Autodesk Revit, BLAST, Energyplus, HBfort, IBLAST, DOE-2 and Hourly Analysis Program (HAP). The Autodesk Revit uses the RTS method to calculate the cooling and heating load of energy model generated from Building Information Modelling (BIM). Load contributing factors are automatically identified from the model. Energyplus, HBfort, IBLAST uses the Heat Balance Method (HBM) for calculation of loads (Fantu, 2014). DOE-2 uses the weighting function method for load calculation (Fantu, 2014 and Obuka *et al.*, 2015). HAP employs the Transfer Function Method (TFM) in determining heating and cooling load (Carrier, 2005). HAP does not capture every location, hence makes it inapplicable to buildings in areas like Minna, Nigeria.

There has been increasing concerns on the implementation of computer applications on calculation of heating load and cooling load of buildings. Kareem (2008) developed a computer program called Computer Aided Load Estimating for Air Conditioning (CALAC-2004) using QBASIC programming language, for estimating cooling load. Cooling load due to door, wall, roof and ceiling were calculated using the Cooling Load Temperature Difference (CLTD). Cooling load from window and glass was calculated applying the Glass Load Factor (GLF). A constant cooling load by occupants of 67W per person was assumed. The computer program developed, was used to estimate the cooling load of Federal University of Technology, Akure (FUTA) library to be 806.26KW (Kareem, 2008). Sahu (2014) established the results of cooling load calculation of different climate conditions by using CLTD method for a multi-story building which is a part of an institute. The researcher used MS-Excel programme to calculate cooling load items such as, people heat gain, lighting heat gain, infiltration and ventilation heat gain and cooling load due to walls and roofs. It was reported that the results were compared with the standard data given by ASHRAE and CARRIER Fundamental Hand Books and found to be satisfactory. It was also reported that the cooling requirement of summer is about 9% more as compared to monsoon for climate condition of Rourkela. In 2016, Obuka *et al*. (2016) developed a computer application for calculating the latent and sensible cooling load of a single zone in Visual Basic programing language. CLTD/SCL/CLF method was used in the calculation of cooling load. A case study of a lecture room at University of Nigeria, Nsuka, was considered. The software provided input for all load contributing components for a non-residential building except inputs for equipment and skylight.

This paper presents the development of a computer application for cooling load calculation of a building. The computer application will be built in Java programming language and will be formulated using the Cooling Load Temperature Difference (CLTD)/ Solar Cooling Load (SCL)/ Cooling Load Factor (CLF) method of cooling load calculation.

2. MATERIAL AND METHODS

2.1 CLTD/SCL/CLF Method of Cooling Load Calculation

The cooling load due to roof, exterior wall, window and door by conduction heat transfer according to ASHRAE (1997), is written as:

$$q = \mathrm{U} \times \mathrm{A} \times (\mathrm{CLTD}) \quad (1)$$

Where:

q is the cooling load in Watts (W);

U is the coefficient of heat transfer in $\frac{W}{m^2K}$ for wall, glass or roof;

A is the surface area of wall, glass or roof in m^2;

CLTD is the cooling load temperature difference wall, glass and roof, K (ASHRAE, 1997). For geographical location different from the location used to generate the ASHRAE tables, adjustments are made as indicated by ASHRAE (1997).

$$CLTD_{corrected} = CLTD + (25.5 - t_{idt}) + (t_m - 29.4) \quad (2)$$

Where:

$CLTD$ is cooling load temperature difference from ASHRAE (1997) table, K;

t_{idt} is the indoor design temperature, K;

$$t_m = maximum\ outdoor\ temperature - \frac{daily\ range}{2}$$

Solar load through glass (curtain wall) and window (made of glass) according to ASHRAE (1997), is written as:

$$q_{rad} = \mathrm{A} \times (\mathrm{SC}) \times (\mathrm{SCL}) \quad (3)$$

Where q_{rad} is cooling load due to solar radiation in W;

A is the net glass area of the window,m^2;

SC represents shading coefficient for combination of shading device and fenestration.

SCL is solar cooling load in $\frac{W}{m^2}$ (ASHRAE, 1997).

Cooling load from fenestration and curtain wall includes heat gain by conduction and radiation through the windows.

Cooling load due to floor, partition or ceiling according to ASHRAE (1997), is written as:

$$q = \mathrm{U} \times \mathrm{A}(t_{aj} - t_{idt}) \quad (4)$$

Where:

U is the coefficient of heat transfer for floor, partition or ceiling, $\frac{W}{m^2K}$;

A is the surface area of floor, ceiling and partition given in building plans, m^2;

t_{aj} is the temperature of adjacent space, K;

t_{idt} is the inside design temperature, K (ASHRAE, 1997)

The CLTD/SCL/CLF method assumes that the total sensible heat gain from occupants is not converted directly to cooling load. So that the radiant portion is first absorbed by the surrounding (furniture, floor, ceiling wall and partition) then convected to the space at a later time depending on the thermal property of the space. The instantaneous sensible cooling load caused by occupants, according to ASHRAE (1997), is written as:

$$q_{os} = \mathrm{N} \times (\mathrm{SHG}_p) \times (\mathrm{CLF}_p) \quad (5)$$

And the latent cooling load due to occupants according to ASHRAE (1997), is written as:

$$q_{ol} = \mathrm{N} \times (\mathrm{LHG}_p) \quad (6)$$

Where:

$q_{os}$is the sensible cooling load caused by occupants, W;

N is the number of occupants;

SHG_p is the sensible heat gain per person in W;

CLF_p is cooling load factor by hour of occupancy for people;

$q_{ol}$is the latent cooling load caused by occupants, W;

LHG_p is the latent heat gain per person in W (ASHRAE, 1997)

The cooling load caused by electrical lighting fixtures, according to ASHRAE (1997), can be calculated as:

$$q_l = \mathrm{P}_l \times \mathrm{F}_{\mathrm{SA}} \times \mathrm{F}_{\mathrm{UT}} \times (\mathrm{CLF}_l) \quad (7)$$

Where:

$q_l$is the cooling load caused by electrical lighting fixtures, W;

$\mathrm{P}_l$is the watt input for electrical lighting fixtures data or electrical plan, W;

$\mathrm{F}_{\mathrm{SA}}$is special allowance factor, as appropriate;

$\mathrm{F}_{\mathrm{UT}}$is lighting use factor, as appropriate;

$\mathrm{CLF}_l$is the cooling load factor by hour of occupancy for lights (ASHRAE, 1997),

The cooling load caused by motor-driven equipment, according to ASHRAE (1997), is written as:

$$q_e = \eta_e \times \mathrm{P}_e \times (\mathrm{CLF}) \quad (8)$$

Where:

q_e is the cooling load caused by electrical equipment;

$\eta_e$is efficiency factors and arrangements to suit circumstances;

$\mathrm{P}_e$is horsepower rating from electrical plan or manufacturer's data and

CLF is cooling load factor by hour of occupancy (ASHRAE, 1997),

Estimation of cooling load from appliances according to ASHRAE (1997), is written as:

$$q_{sensible} = q_{input} \times \mathrm{F}_{\mathrm{U}} \times \mathrm{F}_{\mathrm{R}} \times (\mathrm{CLF}) \quad (9)$$

Where: F_{U} and $\mathrm{F}_{\mathrm{R}}$are usage factor and radiation factor respectively;

q_{input} is the rated energy input from appliances, W;

CLF is the cooling load factor by schedule hours and hooded or not (ASHRAE, 1997),

Cooling load caused by infiltration and ventilation air according to ASHRAE [11], can be calculated as follows:

$$q_{sensible} = 1.23 \times Q(t_o - t_i) \quad (10)$$

$$q_{lantent} = 3010 \times Q(W_o - W_i) \quad (11)$$

$$q_{total} = 1.20 \times Q(h_o - h_i) \quad (12)$$

Where:

Q is ventilation from ASHRAE standard 62;

t_o and t_i are outside and inside air temperatures, K;

W_o and W_i are outside and inside air humidity ratio, kg of water/ kg of air;

h_o and h_i are outside and inside air enthalpy (ASHRAE, 1997).

2.2 University lecture room profile

The case study is located at longitude 9.5836^0N and latitude 6.5463^0E. On the ground floor of two-storey Engineering Complex, Federal University of Technology, Minna, Nigeria. A BIM software, Autodesk REVIT 2019 was used to model the case study (Room 103, Engineering complex, Federal University of Technology, Minna). The case study has a floor area of $76m^2$ and height of $3.23m$. The lecture room is oriented such that its doors and windows face North or South. East wall is shaded and West wall is a partition wall having no wall opening.

2.3 Design condition and assumptions

The cooling load of the case study was calculated based on the following design conditions:

- Lights remain on from 08:00 hour to 18:00 hour.
- Outdoor design dry-bulb temperature is 37.1^0C.
- Indoor design dry-bulb temperature is 25^0C.
- Daily temperature range is 11.1^0C.
- Relative humidity of 50%.
- Design outdoor humidity ratio 0.02kg of water/kg of air.
- Design indoor humidity ratio 0.01kg of water/kg of air.
- Occupancy period of lecture room is from 08:00 to 18:00.
- Maximum period of occupancy by students for a lecture is 3 hours.
  Occupancy period and hour after the entry of occupants is shown in Table 1.

Table 1: Occupancy period and hour after entry of occupants.

Time of the Day (Hour)	Hours After Entry (Hours)
08:00	0
09:00	1
10:00	2
11:00	3
12:00	1
13:00	2
14:00	3
15:00	1
16:00	2
17:00	3
18:00	1

The lecture room was designed for maximum sitting capacity of 100 students. Components of the case study and their properties are tabulated below in Table 2.

The following assumptions were considered:

- From ASHRAE (1997),$R = 0.65\frac{m^2K}{W}$ with core made of concrete block, corresponds to wall number 4. Wall facing West is partition walls. Temperature of adjacent space to the west partition wall is the same as the indoor design temperature. Shaded walls have similar CLTD as walls facing North (ASHRAE, 1997). Since East exterior wall is shaded, hence its CLTD is the same as North wall.
- Values of Cooling Load Temperature Difference (CLTD) for wall are taken from ASHRAE (1997).

- Values of Cooling Load Temperature Difference (CLTD) for glass are taken from ASHRAE (1997).
- Values of Shading Coefficient (SC) are taken from ASHRAE (1997).
- Values of Solar Cooling Load (SCL) are taken from zone Type D, ASHRAE (1997).
- Rates of Sensible Heat Gain (SHG) and Latent Heat Gain (LHG) from people are obtained from ASHRAE (1997).
- Values of Cooling Load Factor (CLF) for people are taken from zone Type D, based on 10 hours from 8:00 hour to 18:00 hour in space, ASHRAE (1997).

Table 2: Given or Measured Parameter

S/N	Load Component	Parameter
1	Wall	Principal wall material: 230mm hollow sandcrete block covered with plaster; Wall thickness = 300mm; From Arup (2016), $U = 1.6\frac{W}{m^2K}$and Thermal Resistance, $R = 0.65\frac{m^2K}{W}$.
2	Floor	Terrazzo of thickness = 25mm; Floor area = $76m^2$ Conductance, U = $71\frac{W}{m^2K}$. (ASHRAE, 1997).
3	Window	16 Projected Aluminium windows of sizes by 1190mm by 1190mm, 1190mm by 600mm and 880 by 600mm. Glass thickness = 8mm; frame thickness = 25.4mm; $U = 5.8\frac{W}{m^2K}$.
4	People	101 people (100 seated students and one lecturer standing).
5	Light	6 26W fluorescent tubes, Ballast Factor, F_{SA} = 1.2.
6	Fan	4 70W Ceiling fans.

2.4 The computer application

A computer application was developed in JAVA programming language with the aid of Apache NetBeans Integrated Development Environment (IDE), version 11.1. The program comprises 9 Graphical User Interface (GUI). The Figure 1 below illustrates the various GUI of the developed Load App. Each GUI has various unique input parameters with the "PREVIOUS" and "NEXT" button used to toggle back and forth respectively.

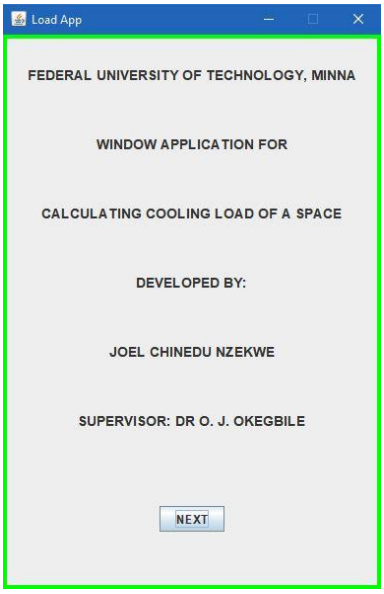

(a): First GUI

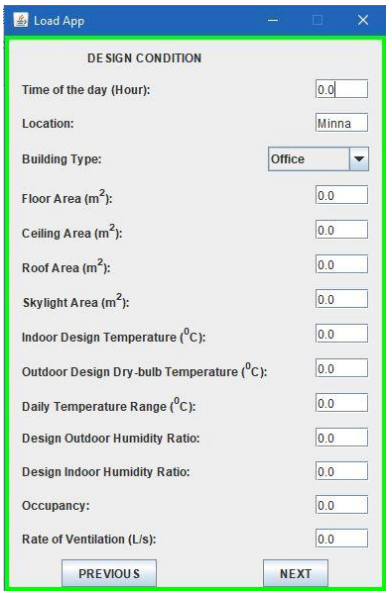

(b): Second GUI

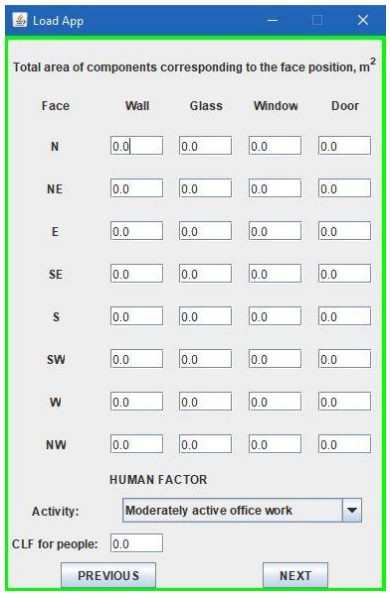

(c): Third GUI

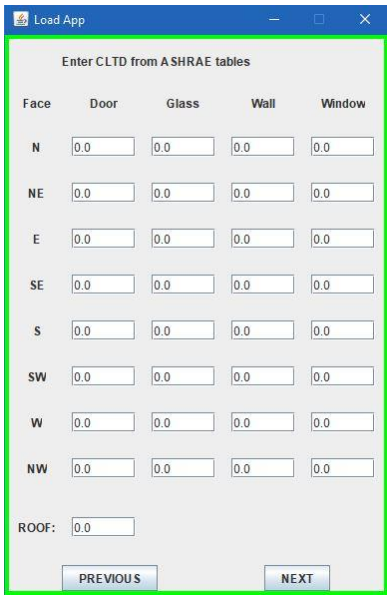

(g): Seventh GUI

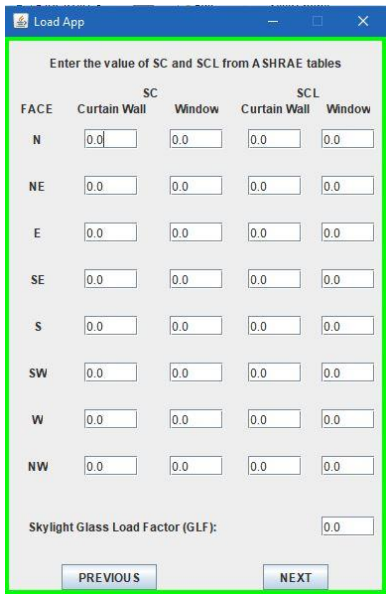

(h): Eight GUI

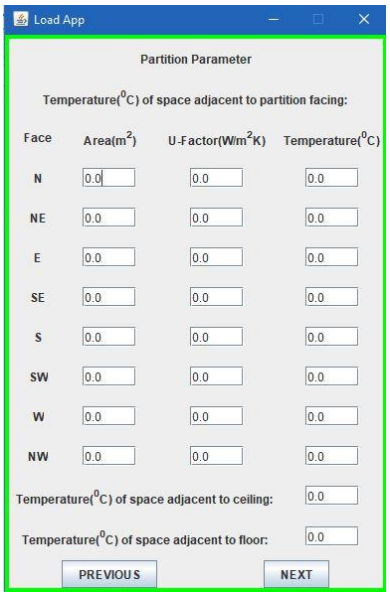

(i): Ninth GUI

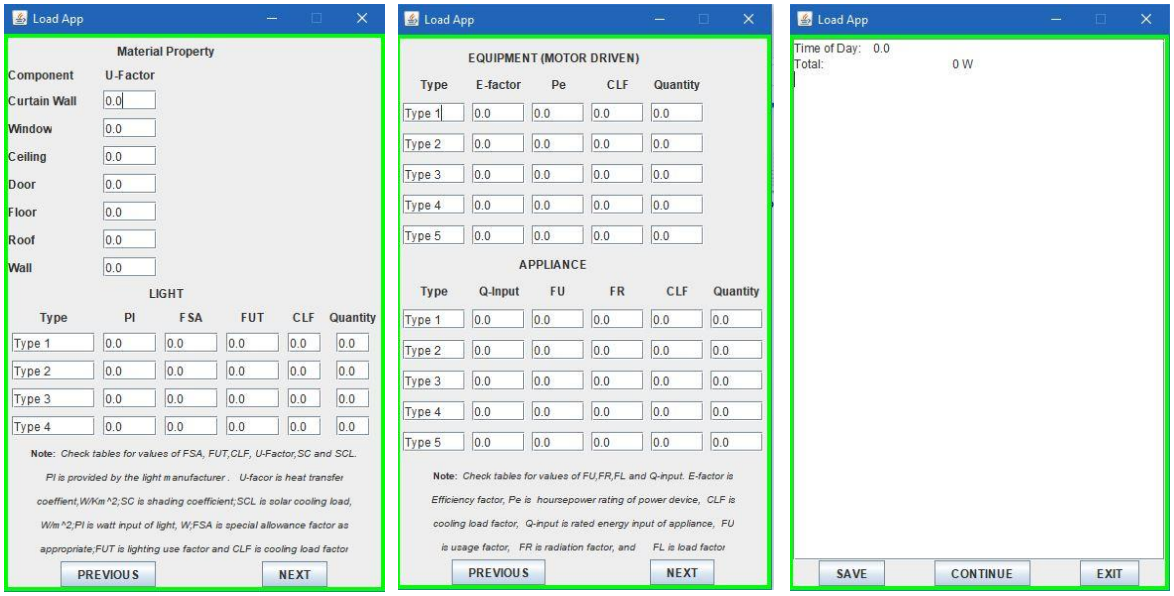

(g): Seventh GUI (h): Eight GUI (i): Ninth GU

Figure 1: Various Graphical User Interface (GUI) of the cooling load computer app

3. RESULTS AND DISCUSSION

Results from the computer application are summarised in Table 3 below. As shown in Table 3, the total sensible cooling increased from 1676W at 8:00 hour to a maximum value of 1077W at 17:00 hour, then drops to 10343W at 18:00 hour while the latent cooling load remains constant Table 3: Cooling loads of the case study at various hour of the day

Time of the day (Hour)	Walls (W)	Windows (W)	People (Latent) (W)	People (Sensible) (W)	Light (W)	Fan (W)	Total Sensible Cooling load (W)	Total Latent Cooling load (W)
8:00	458	1218	4545	0	0	0	1676	4545
9:00	493	1634	4545	4383	124	65	6699	4545
10:00	619	2104	4545	4949	139	73	7884	4545
11:00	789	2625	4545	5303	144	75	8936	4545
12:00	1130	2948	4545	4596	152	79	8905	4545
13:00	1390	3203	4545	5020	155	81	9849	4545
14:00	1776	3048	4545	5515	161	84	10584	4545
15:00	2072	2884	4545	4737	165	86	9944	4545
16:00	2332	2588	4545	5373	168	88	10549	4545
17:00	2458	2404	4545	5656	170	89	10777	4545
18:00	2493	2356	4545	5232	172	90	10343	4545

4545W throughout the day. These maximum values are comparable with 11432W sensible and 4120W latent obtained by Obuka *et al*. (2015) who used computer application to estimate the maximum space cooling load of a zone of 70 students and 5 laptops. Also, the maximum sensible cooling load obtained in this research work is less than 20458.6W and 33541.3W obtained by Suziyana *et al*. (2013) for Computer Laboratory Room and in Excellent Centre Room respectively. From Table 3, cooling load value of 0W at 8:00 hour is in conformity with

the fact proposed by CLTD/SCL/CLF method of cool load calculation that the sensible cooling load is not immediately affected by internal heat source such as people, equipment, appliances and lights (ASHRAE, 1997 and Bhatia, 2004).

4. CONCLUSION

A computer application was developed in Java programming language for cooling load calculations. The application was formulated using the CLTD/SCL/CLF method as proposed by ASHRAE (1997) and was used to estimate the cooling load of lecture room for proper sizing of ventilation and cooling system. Calculations were based on the atmospheric condition and parameters obtainable in the month of May at active period of the day, between the 8.00 hour and 18.00 hour of the day. The calculated maximum space cooling loads are 10777W sensible and 4545W latent.

Acknowledgement

Thanks to my sponsor Petroleum Technology Development Fund (PTDF). God bless Nigeria.

References

Obuka, N. S., Utazi, D. N., Oyechi, P. C., Okoli, N. C., & Eneh, C. O. (2015, January). Determination Of A Nonresidential Space Cooling Load: Vb Program Apprication. *International Journal of Scientific & Technology Research, 4*(01), 59-67.

Suziyana M, D., Nina, S. N., Yusof, T. M., & Basirul, A. A. (2013). Analysis of Heat Gain in Computer Laboratory and Excellent Centre by using CLTD/CLF/SCL Method. *Procedia Engineering, 53*, 655 – 664.

Kareem, B. (2008). Load Estimating for Air Conditioning using Computer Software Approach. *International Journal of The Computer, the Internet and Management, 16* (2), 35-43.

Arup. (2016). *Building Energy Efficiency Guideline for Nigeria.* Abuja: Federal Ministry of Power, Works and Housing.

ASHRAE. (1997). *1997 ASHRAE Hand Book.* Atlanta: American Society of Heating, Refrigeration and Air-Conditioning Engineers, 1997.

Bhatia, A. (2004). *Cooling Load Calculations and Principles.* Stony Point: Continuing Education and Development, Inc.

Burdick, A. (2011). *Strategic Guideline: Acurate Heating and Cooling Load Calculations.* Pennsylvania: IBACOS .

Sahu, S. K. (2014). *Cooling Load Estimation for a Multi-story office building* . M.Tech Thesis submitted to Department of Mechanical Engineering, National Institute of Technology, Rourkela.

Rabiatul, A. N., Sabarinah, S. A., & Azni, Z. A. (2013). Physical Activity and Human Comfort Correlation in an Urban Park in Hot and Humid Conditions. *Asia Pacific International Conference on Environment-Behaviour Studies. 105*, pp. 598-609. London: ELSEVIER.

APEX. (2018). *4 Reasons Why Your School Should Consider Air Conditioning*. Retrieved May 12, 2020, from https://www.apexaircon.com.au/blog/4-reasons-your-schoolshould-consider-air-conditioning.

Housh, W. (2017). *Air Conditioning In Schools – Is It Essential For Learning?* Retrieved May 12, 2020, from https://www.hvac.com/blog/air-conditioning-schools-essential/

Matiak, D. (2020). *The Importance of Airconditioning in Schools*. Retrieved May 12, 2020, from https://randdmechanical.net/the-importance-of-air-conditioning-in-schools/

Carrier. (2005, October 27). *HAP e-Help.* Retrieved from Transfer Function Methodology: http://www.carrier.utc.com

A Review of Availability of Solid Waste for Renewable Energy Generation in Abuja Metropolis

[1]Muhammad T.M, [1]Nasir A.A, [2]Godfrey M., [3]El-Mansur A.A

[1]Department of Mechanical Engineering, Federal University of Technology, Minna, Nigeria, musatogo1307@gmail.com a.nasir@futminna.edu.ng

[2]Quality/Environmental Management System, Sonates Resources Investment Ltd, Abuja, Nigeria, godfreymnet@gmail.com
[3] Centre for satellite technology development, National Space Research and Development Agency, Abuja, Nigeria, elmansur.ahmed@cstd.nasrda.gov.ng

Corresponding author: **Tanko, M.M.** *musatogo1307@gmail.com, +2348035311172*

Abstract

The energy demand in Nigeria especially in Abuja metropolis is high due to dense population. The metropolis is seat of power of Nigeria government requires adequate power supply but its lacking in comparison to developed nation's city capitals. It is high time; solid waste is considered as means of supporting thermal-hydro power supply for efficient electricity. Despite the metropolis high potential of natural and renewable resources that can be adopted in meeting energy demand by the metropolis is rarely considered. This paper reviews and identifying potential availability of solid in Abuja metropolis. It was observed from review that the potential generation of solid waste per year will be 170, 192.3 and 241 G-tonnes for the year 2024, 2029 and 2040 due to growing rate of 3% of the solid waste in the metropolis. Abuja will generate WTE of 135 GWh. It will lead to greenhouse environmental impact in the metropolis. The huge potential of the waste will also economic development of the metropolis, and this will ensure national development sustainability.

Keyword: Waste to Energy; Renewable energy, Municipal solid waste

1.0 INTRODUCTION

Waste generation in the developing nations is growing rapidly and may double in aggregate volume within this decade, driven largely by growth in population and improvements in living standards. If current trends persist, a fivefold increase in global MSW generation is probable by the year 2025 (AfDB, 2002). The Africa projection growths in Municipal solid waste (MSW) generation amongst developing nations is difficult to estimate. Estimates of total quantities of MSW generated in Nigeria are difficult to determine. The estimates of waste generation per capita is investigated by John *et al.,* (2006); Igoni *et al.,* (2007); Kofoworola, (2007); Sha'Ato *et al.,* (2007); and it was observed that waste increased due to population growth in the metropolis. With increasing population growth, rapid urbanisation, rising levels of affluence, and resource scarcity,
waste-to-energy (WTE) is re-establishing itself as an attractive technology option to promote low carbon growth among other renewable energy technologies. WTE is a proven process that provides electricity and steam generation in a sustainable way.
Nigeria is the most populated nation in Africa with a population estimate of approximately 206 million (Simona, 2020), growing annually at an estimated rate of 3% and generating 0.55 to 0.58 kg of municipal solid waste per person per day (Adeyinka, 2005; Oresanya, 2011; Ogwueleka, 2011). Nigeria can be said to be equally experiencing significant waste-related environmental problems which can be minimising through energy conversion. Abuja is a capital of Nigeria in which waste generation is high. Abuja population is growing faster than the authority's capacity of waste collection and disposal, a condition which has led to inadequate waste

management; this is not only in Abuja municipal but all Nigeria cities. The waste generated in Abuja has been enormous due to lack of appropriate techniques for managing generated waste (Olukanni, 2013). Energy availability is perhaps a worse problem than solid waste management in Nigeria of today. Energy is not readily available a condition which cause unfold poverty to Nigerian (Okeye *et al.,* 2007). There were municipal solid waste (MSW) clogs drains which creates stagnant water for insect breeding and floods during rainy seasons in Abuja. The natural organic components of MSW (food and plant wastes) can be composted aerobically that is in the presence of air to generate carbon-dioxide (CO_2), water and a compost product that can be used as soil conditioner from the waste generated but it is not been assessed (Yusuf *et al.,* 2019). There is need to assess the huge deposit of solid waste of alternative source of energy in Abuja metropolis.

Energy can be generated from source of total of 727 estimated trips in weekly basis in different locations in Nigeria Federal Capital, Abuja dumping site. Each waste truck is estimated to have a carriage capacity between 8 to 10 tonnes. In view of the above, the total estimate of tonnes of solid waste evacuated for year 2010 in the Federal capital, Abuja lie between 302,372 to 378,040 tonnes (302472000kg to 378090000kg) and the average solid waste generation rate is also estimated to lie between 0.59 to 0.74 kg/person/day (Abur *et al.,* 2014). The potential energy production and income from energy sales depend heavily on the energy content (net calorific value) of the waste. The amount of energy or heat value in an unknown fuel can be estimated by ultimate analysis, compositional analysis, proximate analysis and calorimetric analysis if the arises. However, this paper presents a review of availability of solid waste for renewable energy generation in Abuja.

2.0 AVAILABILITY OF SOLID WASTE IN ABUJA METROPOLIS

The role of energy in meeting the needs of residential, industrial, transport, agricultural and other sectors in an economy in Sub Sahara Africa economic growth is projected to be at 4.2% GDP (World Bank, 2016a). Energy is the frontier of growth and development in the world and its shortages will leads to crises and poverty. Therefore, it is important to assess the availability of the waste to energy source in Nigeria. The electric power consumption in Nigeria in 2012 was reported at 156 kWh per capita (4) which very low in comparison to Malaysia, South Africa and Venezuela with 4.1, 4.4 and 3.4 MWh per capita respectively in the same year (World Bank, 2016b). Malaysia, South Africa and Venezuela are same developing countries as Nigeria. The meeting of increasing energy demand in Nigeria is insufficient. This is to lead to seeking of alternative energy from MSW. It is readily available in open dumped sites in Nigeria cities. In Nigeria, the National Bureau of Statistics estimates that 55% of Nigerian lack access to electricity and those who have access suffer erratic supply in Nigeria (Castellano *et al.,* 2015; World Bank, 2016a). The World Energy Outlook 2012 reported that of 80 countries, Nigeria ranks 66th with an energy development index (EDI) of 0.11 (World Bank, 2016a, Unaegbu and Baker, 2019).

Inaccessibility of modern energy will limits income generation and this will create a vicious cycle of deprivation that trap people in poverty and poor growth (Sovacool, and Drupady, 2012). The solid waste is a kind of waste that is in form of solid state when generated (Puopiel, 2010).

Solid waste is defined as a discard/useless or unwanted garbage, refuse that include discard material that obtainable from busiest sources such as farm, industry, commercial and social outlet (Abur *et al*., 2014). Puopiel (2010) also defines solid waste as any material that derived from sources that includes domestic, commercial centres, and industry. This waste source may arise from human/animal excrement or faeces and human gadgets that have no value in its functions. The sources of solid waste in Abuja include medical/clinic centres, food

canteen/stores, construction sites, animal slaughters points, markets, schools and homes. The solid wastes are generated but may not properly manage through better techniques. The solid waste generated in the city are refers to municipal waste with appropriate management technique. MSW refers to household waste combined with a minor portion of commercial waste collected together. It is regarded as a source of renewable energy because it contains high proportion of biomass materials such as paper/cardboard, wood, plastic can, glass, polyethene and food (Al. Ansari, 2012). The city of Lagos is the greatest generator of waste followed by Kano and these two cities have the highest densities of population in Nigeria as in Table 1. However, it was observed after these cities, Abuja metropolis is next city of waste generation. Abuja has highest growing waste generation per day in kg/capita/day.

Table 1: Waste Characterisation in Selected Cities in Nigeria (Yusuf *et al.*, 2019)

City	Waste (Gt)	Waste (kg/capita/day)
Abuja	147.9	0.66
Lagos	255.56	0.63
Kano	156.68	0.54
Ibadan	135.39	0.51
Kaduna	114.83	0.58
Port Harcourt	117.83	0.60

According to Odunfa, (2007) the monthly volume of waste sent to landfill in Abuja stands at about 6700 tonnes. Exact actual quantities of waste generated per capita and per household are difficult to come by through neighbouring cities with similar demographic and socio-economic characteristics such as Accra are put at 0.4 kg per capita and density on a wet weight basis of 0.47 t/m^3 . The estimated growth rate of 3%, the quantity of waste generated from the Abuja city will double by 2025 (Ezeah *et al.*, 2009). The waste collection from most households and offices within the municipal area is on a door to door basis. At household levels, waste is stored in container or covered plastic receptacles or black bin bags. For bigger establishments, larger sized receptacles and bring banks are used. Many poorer households, especially those living in the satellite towns and informal settlements at the outer fringes of the city, use any available containers such as baskets and open buckets (which do not meet minimum hygienic conditions) for waste collection before taking them to community bring banks facilities for disposal. It is estimated that about 42% of household municipal solid waste collection in Abuja is carried out with flimsy and open containers (Benneh *et al.*, 1993).

Waste collection from households without any access constraints was carried out on a weekly basis while collection from large organisations and commercial establishments is on daily basis. Equipment used for waste transfer include compacting truck, side loaders, open tippers, pay loaders, roll-on roll-off trucks in Abuja. The

economic analysis assumes that methane constitutes 60% of the volume of biogas produced from MSW. The production potential of methane in Nigeria is illustrated in Table 2. Methane is important gas in engine system either single- multi cylinder or fuel engine plant.

Table 2: Production Potential of Methane in Nigeria (Amoo and Fagbenle, 2013)

City	$m^3/CH_4/Mg$ MSW
Abuja	257
Lagos	296
Kano	231
Ibadan	313
Port Harcourt	168

It was observed from Table 2 that Abuja has generated 257 $m^3/CH_4/Mg$ MSW which is very useful in engine plant. Combined heat and power (CHP) generation, also known as cogeneration, is an efficient, clean, and reliable approach to generating both power and thermal energy from solid waste. When a CHP system designed to meet the thermal and electrical base loads is installed. CHP can greatly increase a facility's operational efficiency while decreasing its energy costs, CHP can also reduce greenhouse gasses, which contribute to global climate change (Hamad, 2013 & 2014). The Conversion of biogas to electricity through WTE technology offers significant increases and efficiency. Therefore, it is a promising technology due to its higher power density and its applicability to a wide range of scales (Pant *et al.,* 2010; Xuan *et al.,* 2013). Biogas can be used as a motive power for the production of electricity using engines. A biogas fuelled engine generator will typically convert between 18% and 25% of biogas to electricity. Biogas engine is depending on engine design and load factor.

Adoption of WTE in Abuja will support development of greenhouse evolution in Abuja. However, the estimated growth rate of 3% per annual of solid waste generation in Abuja in by Ezeah *et al.,* (2009) will contribute hugely as source of renewable energy. Figure 1 was plotted for observing the availability of the solid waste in Abuja and it was drafted from Table 1 by Yusuf *et al.,* (2019) and estimation growth rate observation by Ezeah *et al.,* (2009). Figure 1 illustrates growing rate of waste in giga tonnes per year in Abuja.

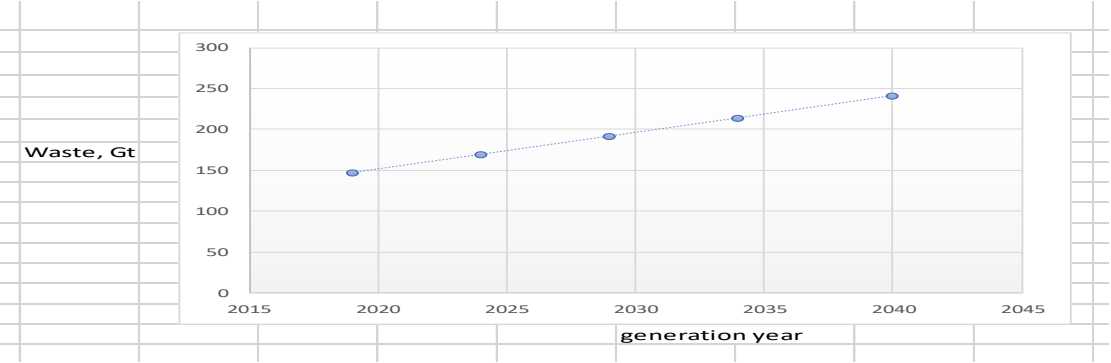

Figure 1: Waste generation per year

From the graph in Figure 1 the potential generation of solid waste per year will be 170, 192.3 and 241 G-tonnes for the year 2024, 2029 and 2040. Abur *et al*. (2014) also estimated waste generation in Abuja to be 387,040 tonnes per year will lead to approximate of 216,742 MWh per year. The adoption of Abur *et al*. (2014) will leads to valuable amount of one tonne gives 0.56 MWh per year and the possibility of energy generation is shown in Table 3.

Table 3: Potential Energy Generation in Abuja

Year	Waste (Gt)	Expected Energy (GWh)
2020	148.3	83.04
2024	170.0	95.2
2029	192.3	107.7
2035	219.0	122.6
2040	241.0	135

In the year 2040, Abuja metropolis will generate energy of 135 GWh through WTE system if really considered. This was predicted based combine effort of study Abur *et al*. (2014) and Yusuf *et al.*, (2019). This potential of availability of the solid waste is huge as source of renewable energy generation for Abuja metropolis. Amoo and Fagbenle (2013) confirmed that the MSW distribution in Abuja is dominated by food wastes that contribute 55% per organic waste. The ash content and ultimate analysis were obtained from a report prepared by the Centre for People and Environment prepared for USEPA. It was also understood that the landfill methane generation potential in Ibadan and Abuja is high among Nigeria cities Nigeria. The moisture content of Abuja was assumed to be the same as in Lagos (Amoo and Fagbenle, 2013). This indicates that the viability of renewable energy source of solid waste is having huge potential in Abuja.

3.0 RENEWABLE ENERGY GENERATION

Globally, the call for renewable energy sources for a sustainable power in an eco-friendly manner is one of the major goals of the United nations and as well as European union among others. Energy from waste is not a new concept, but it is a field which requires a serious attention. There is various energy conversion technologies available to get energy from solid waste, but the selection is based on the physicochemical properties of the waste, the type and quantity of waste feedstock, and the desired form of energy. Conversion of solid waste to energy is undertaken using three main process technologies: thermochemical, biochemical, and mechanical extraction (McKendry, 2002). The Renewable energy generation sources in Nigeria are such as solar; hydro; bioenergy and wind are in abundance to be harnessed in full capacity to its electric power supply issue (Aderoju *et al*., 2017). Currently, the utilization of Municipal Solid Waste (MSW) as a biogenic form of renewable energy source for power generation is on the rise globally.

Nigeria as a nation is blessed with fossil fuels, abundant sunlight, hydro, wind and with huge solid waste deposit especially Abuja cases keep rising daily. The MSW can be consider as source of renewable energy in Abuja due to viable opportunity to providing a sustainable electric power supply to the metropolis growth and development. Energy from renewable energy are very complex systems. In simple term, the process of energy recovery from waste entails harnessing the chemical energy stored in waste materials by converting it to thermal energy at temperatures in excess of 900 ^{0}C to generate steam, then the high temperature, high pressure dry steam is converted to mechanical energy while turning the blades of the turbine, and finally to electrical energy (via the generator connected to the turbine). Efficiency waste to energy plants reduce the volume of waste by up to 95%, producing residual solid material (slag) made of non-combustible waste faction including glass, porcelain, iron scrap, gravel. For health and environmental safety, a proper energy from waste plant is fitted with air pollution control equipment (Hartenstein and Licata, 2000). Energy from solid waste s can be used to generate power and/or heat and they have efficiency ranging from 18 – 27%. Energy from waste can promote a green economy in Abuja metropolis. The optimised energy from waste plant has significant negative overall emission of between 200 to 300kg CO_2 per tonne of waste. This is a clear departure from traditional end-of-pipe treatment for Nigeria - open dumping in unsanitary spaces (Somorin and Kolawole, 2017).

3.1 Economic Benefits of Renewable Energy Generation

A major benefit to be derived from the use of Waste to energy (WTE) will be a reduction in ozone layer depletion. When the electricity generated from the WTE is quantified in monetary terms in the world. It could have attracted revenue of US$ 365.04 billion in 2015. The revenue is projected to reach US$390.14 billion US$ 431.97 billion and US$ 473.82 billion respectively, for the years 2020, 2025, and 2030 in the world (Yusuf *et al.*, 2019). Jobs creation in relation to WTE projects could be done in the areas of design, construction, and operation of energy recovery systems. Renewable energy sources could be included in the energy mix for the power sector. Other benefits include a lower transportation footprint in comparison with more conventional fuels, such as uranium and coal, as the hauling of the garbage will not be much further in terms of the distance covered in comparison to other fuel sources. There will be no additional extraction costs, unlike the case with fossil fuels. The economic benefits of the application of renewable energy are as follows and it can be found useful in adopting renewable energy in Abuja.

i. Operation Costs:
   a) Fixed operating costs (salaries, depreciation, cost of capital)
   b) Variable operating costs (maintenance, utility usage, operation of emissions systems)
   c) Disposal of process wastes (ash from incineration, other unconverted waste).
ii. Revenues:
   a) Tipping fees paid by waste producer
   b) Sales from electricity, heat, and steam
   c) Sales from other co-products (recovered metals, compost).

3.2 Benefits of Energy from Waste in Nigeria

WTE benefits in Nigeria are such as (Unaegbu and Baker, 2019):

i. Improvement of Nigeria's energy supply
ii. It will lead to a sustainable waste management strategy that will end the practice of 'collect and dump' in uncontrolled open dumpsites.
iii. It can contribute to Nigeria meeting her national determined contribution (NDC) decarbonisation targets
iv. It will serve as driver to ensure availability of feedstock (waste) for energy from waste plant will improve waste collection and reduce the amount of waste heaps and litter that defaces cities.
v. A source for carbon credits earning for the country
vi. It will availability of skilled and unskilled jobs for the Nigeria populace

4.0 CONCLUSION

In conclusion, it is clear that Abuja have huge potential of solid waste deposit which tends to increase at 3% per annual. This will serve abundant source of renewable energy with 170 G-tonnes by the year 2024. It will allow to help in rectifying electrical power failure through national grid. The huge potential of the sloid waste will also boost economy development of the metropolis.

REFERENCES

Abur, B.T., Oguche, E.E. & Duvuna, D.A (2014). Characterization of municipal solid waste in the federal capital Abuja, Nigeria. *Global Journal of Science Frontier Research*, 14(2-1.0), 1 – 6.

Adeyinka, M.A. (2005). Environmental statistics: situation in Federal Republic of Nigeria. Dakar, Senegal: *Workshop on Environmental Statistics.*

Aderoju, O.M., Dias, G.A. and Echakraoui, Z. (2017). Assessment of Renewable Energy Sources & Municipal Solid Waste for Sustainable Power Generation in Nigeria. *World Multidisciplinary Earth Sciences Symposium (WMESS 2017), IOP Publishing IOP Conf. Series: Earth and Environmental Science*, 95(1), 12-17.

African Development Bank (2002). *Study on solid waste management options for Africa*. AFDB Sustainable Development and Poverty Reduction Unit, Abidjan, Cote d'Ivoire

Al.Ansari, M.S. (2012). Municipal solid waste management systems in the Kingdom of Bahrain. *International Journal of Water Resources and Environmental Engineering*, 4(5), 150-161.

Abur, B.T., Oguche, E.E. & Duvuna, G.A. (2014). Characterization of Municipal Solid Waste in the Federal Capital Abuja, Nigeria. Global Journal of Science Frontier (H) Research: Environment & Earth Science, 14(2), 1-7.

Amoo, O.M., & Fagbenle, R.L. (2013). Renewable municipal solid waste pathways for energy generation and sustainable development in the Nigerian context. *International Journal of Energy and Environmental Engineering*, 4(1), 42.

Benneh, G., Songsore, J., Nabila, J. S., Amuzu, A. T., Tutu, K. A., Yangyuoru, Y. & McGranahan, G. (1993). Environmental problems and the urban household in the Greater Accra Metropolitan Area, Accra-Ghana. Stockholm Environment Institute, Stockholm, Sweden

Castellano, A., Kendall, A., Nikomarov, M., Swemmer, T. (2015). Brighter Africa: the growth potential of the Sub-Saharan electricity sector. US: McKinsey Report.,

Ezeah, C., Roberts, C. L., Watkin, G. D, Philips, P. S. & Odunfa, A. (2009). Analysis of barriers affecting the adoption of a sustainable municipal solid waste management system in Nigeria. In the proceedings of the 24th International Conference on Solid Waste Technology and Management, 12 - 15 March, 2009. Widener University, Philadelphia, USA, 1556- 1564.

Hamad, T.A, Agll, A.A, Hamad, Y.M., Bapat, S., Thomas., M., Martin, K.B. (2014). Hydrogen recovery, cleaning, compression, storage, dispensing, distribution system and End-Uses on the university campus from combined heat, hydrogen and power system. *International Journal of Hydrogen Energy*.39(1), 647-53.

Hamad, T.A, Agll, A.A, Hamad, Y.M., Bapat, S., Thomas., M., Martin, K.B. (2014). Study of a molten carbonate fuel cell combined heat, hydrogen and power system: End-use application. *Case Studies in Thermal Engineering*, 1, 45–50.

Hartenstein, H. & Licata, A. (2000). Modern technologies to reduce emissions of dioxins and furans from waste incineration. 8th, Annual North American waste-to-energy conference, 93 - 132

Igoni, A. H., Ayotamuno, M. J., Ogaji, S. O. T. & Probert, S. D. (2007). Municipal solid-waste in Port Harcourt, Nigeria. *Applied Energy*, 84(6), 664-670.

John, N. M., Edem, S. O., Ndaeyo, N. U. & Ndon, B. A. (2006). Physical composition of Municipal solid waste and nutrient contents of its organic component in Uyo municipality, Nigeria. *Journal of Plant Nutrition*, 29(2), 189-194.

Kofoworola, O. F. (2007). Recovery and recycling practices in municipal solid waste management in Lagos, Nigeria. *Waste Management*, 27(9), 1139-1143.

Odunfa, A. (2007). Municipal solid waste generation, transfer and disposal in Abuja. Interviewed by: Ezeah, C., via telephone from The University of Wolverhampton, Wolverhampton, 20th December.

Olukanni, D.O. (2013). Analysis of Municipal Solid Waste Management in Ota, Ogun State, Nigeria: Potential for Wealth Generation (Paper presented at the International Conference on Solid Waste Management (ICSW), Widener University, Chester, Philadelphia, 184-196.

Okoye, A.C., Dioha, I. J.,Enzeonu, F.C & Eboatu, A.N. (2007). Energy crisis and poverty: Implication in the environmental status of Nigeria. Paper presented at the National Solar Energy Forum (NASEF) 28th – 29th November, Rockview Hotel.
Oresanya, O (2011). Integrated waste management shifting the paradigm. Paper presented at the 47th Annual International Conference of the Nigerian Mining and Geosciences Society (NMGS), 6-11. Minna (2011)

Ogwueleka, T.C. (2009). Municipal solid waste characteristics and management in Nigeria. *International Journal of Environ Health Science Engineering*, 6(3), 173–180.

Pant, D., Van Bogaert, G., Diels, L., Vanbroekhoven, K. (2010). A review of the substrates used in microbial fuel cells (MFCs) for sustainable energy production. *Bioresource Technology*, 101(6), 1533-43.

Puopiel, F. (2010). Solid Waste Management in Ghana: The Case of Tamale Metropolitan Area. Msc Thesis in Development Policy and Planning, Kwame Nkrumah University of Science and Technology, Ghana.

McKendry, P. (2002). Energy production from biomass (part 2): conversion technologies. *Bioresources Technology*, 83, 47–54.

Sha'Ato, R., Aboho, S. Y., Oketunde, F. O., Eneji, I. S., Unazi, G. & Agwa, S. (2007) Survey of solid waste generation and composition in a rapidly growing urban area in Central Nigeria. *Waste Management, 27(3), 352-358.*

Simona, V., (2020). Population of Nigeria 1950-2020. *Statista*, 1(1), 12-17.

Somorin, T.O., Adesola, S. and Kolawole, A. (2017). State-level assessment of the waste-to-energy potential (via incineration) of municipal solid wastes in Nigeria. *Journal of Cleaner Production,* 164, 804-815

Sovacool, B.K. & Drupady, I.M. (2012). *Energy access, poverty, and development: The Governance of Small-Scale Renewable Energy in Developing Asia*. New York US: Ashgate Publication.

Unaegbu, E. U. & Baker, K. (2019). Assessing the potential for energy from waste plants to tackle energy poverty and earn carbon credits for Nigeria. *International Journal of Energy Policy and Management*, 4(2), 8-16.

Xuan, J., Leung, M.K.H, Leung, D.Y.C. & Ni, M. (2009). A review of biomass-derived fuel processors for fuel cell systems. *Renewable and Sustainable Energy Reviews*. 13(6-7):1301-13.

World Bank., (2016a). Sub-Saharan Africa in "Global Economic Prospects: Spill overs amid Weak Growth". Washington, DC: World Bank, 153-175

World Bank, (2016b). Electric power consumption (kWh per capita). Washington, DC: World Bank.

Yusuf, R.O. Adeniran, J.A. Mustapha, S.I. & Sonibare, J.A. (2019). Energy recovery from municipal solid waste in Nigeria and its economic and environmental implications. *Environmental and Quality Management*, 28(1), 33–43.

Nanoparticle-enhanced vegetable-oil lubricants: Prospects, Opportunities and Limitations

Stephen Y. Tsado [1, *], Sunday A. Lawal [1]

[1] Mechanical Engineering Department, Federal University of Technology, Minna, Niger State, NIGERIA

[*] Corresponding author: steve.tsado@gmail.com

Abstract

Annually, since 2015, an estimated 18MMT (about 50%) of mineral-oil based lubricants find their way into the ecosystem, resulting in adverse environmental and health impact from pollution as a result of spillage during application or handling, leakages during operation, or at point of disposal. This is a rising concern for global economies as this condition continues to predispose the humans, animals and vegetation to risks and hazardous conditions. This undesirable condition has prompted awareness for global economies to shift dependence from mineral-oil based lubricants to environmentally friendly materials, such as biodegradable materials. Vegetable oils have been found from previous researches to be a suitably sustainable alternative to mineral-oil base lubricants. It demonstrates high biodegradability, high lubricity, high viscosity index, and low toxicity. These properties make vegetable oils desirable for use as lubricants. Furthermore, continuously evolving stern environmental regulations and policies around the world is driving favourably, the transition to dependence on nanolubricants. Amongst other biodegradable fluids that are being researched for use as nanolubricants, vegetable oils have a greater contribution, accounting for up to 88.1% of biodegradable oils used in preparation of nanolubricants in 2015. This is indicative of the great potential of vegetable oils as nanolubricants. Despite this, the commercialization and global transition to use of nanolubricants is slow, largely due to some limitations including poor performance at low temperature, poor oxidative stability, interference of edible vegetable oils with the food value chain, and the associated transition implication for lubricant producing companies. Ongoing research efforts to overcome these limitations include varying physical parameter of nanoparticle parameters including shape, size and concentration, and chemical modification of vegetable-oil bases. Despite these limitations, the Compound Annual Growth Rate (CAGR) of vegetable-oil base lubricants between 2016 – 2024 is forecasted to be up to 6.9%. The prospects for the nanolubricant market is a growing one, and can be fully harnessed.

Keywords
Nanoparticles, Lubricants, Vegetable-oil, Tribology, Nanolubricants

1 Introduction

The concepts of motion and friction, wear and tear, lubrication and tribology are very closely related. Motion causes friction and *vice-versa*, which results in wear and tear, both of which are very considerable factors leading to the wastage of energy and materials in machines, with an increased resultant effect on costs and undesirable economic losses, and a significant reduction in mechanical performance of machines (Woma *et al.*, 2019). Both friction, wear and tear can be reduced or managed using lubrication which is the process of introducing a suitable material (fluid or solid – as in graphite) into the interacting surfaces to effectively minimize, reduce or manage the friction, wear and tear being experienced. Tribology is the concept that binds all three together, and it refers to the study of surfaces in an interactive relationship due to their relative motion (Ian, 2016). The schematic presented in Figure 1 represents what this current research refers to as the 'Triangle of Tribology', which is a representation of the relationship between friction, wear, lubrication and tribology.

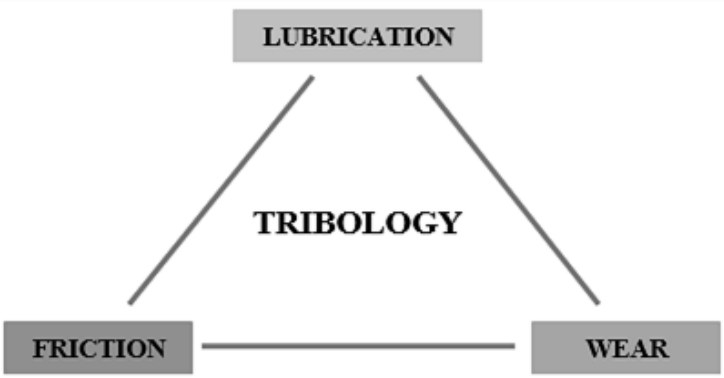

*FIGURE 1: **TRIANGLE OF TRIBOLOGY***

Traditionally, the formulation of lubricants is totally based on the desired specifications of the final product, which is a major consideration for the purpose and environment of application. Typically, lubricants consist of an oil-base (primary constituent), and an additive (secondary constituent) which is essentially to improve or enhance the performance and properties of the base oil to serve the intended purpose of lubrication (Li and Wang, 2015). With continuously growing industrialization, so is the dependence on lubrication, and the continuous need to redesign the formula to suite the ever dynamically growing and changing demands and specifications. A study conducted by Mang and Dresel (2006) revealed that over 10,000 lubricants formula have been developed, satisfying well over 90% of global needs.

Historically, vegetable oils were more commonly used for the purpose of lubrication, until the mid-19th century when the global demand for lubricants and increased specifications due to the increased industrialization activities turned attention to mineral-oil base lubricants (Ajithkumar, 2009). Although these mineral lubricants have been extensively developed and used globally for the purpose of lubrication, they still remain a concern to the environment and health. The rising global awareness of the adverse and undesirable impacts of mineral-oil base lubricants on the environment and the ecosystem at large is driving attention back to the use of vegetable oils (Erhan, *et al.*, 2008[a]). This is not without efforts in enhancing the performance of these oils. Generally, lubricants made from biodegradable oil bases such as vegetable oils, animal oils or oils from microalgae are generally referred to as biolubricants because of their biodegradability property. However, the use of these oils alone as lubricants demonstrates very poor lubricity and tribological properties. To overcome the associated limitations to the use of vegetable or animal oils as lubricants, nanoparticle additives are introduced such as Titanium Oxide (TiO_2), Copper Oxide (CuO), Aluminium Oxide (Al_2O_3), Molybdenum Sulphide (MoS_2).

Nanoparticles have in the recent years been used to enhance the tribological properties of vegetable oils for use as lubricants. When vegetable oils are modified using nanoparticles, they are referred to as nanolubricants, or generally as biolubricants. Several studies have shown the potential of nanolubricants in the lubrication industry. Despite this, the commercialization and global transition to the use of nanolubricants remains very low (Nagendramma, and Kaul, 2012; and Panchal, *et al*., 2013). This study is an effort to identify and delineate the prospects and potential, opportunities and limitations associated with harnessing the use of vegetable-oil base lubricants in the global market.

2 Lubricant Oil Bases

Lubricants are usually composed of a base which serves as the primary constituent of the lubricant oil, and an additive which is the secondary element in the lubricant serves the purpose of enhancing the tribological properties of the lubricant. Oil bases can either be mineral-oil base biodegradable-oil base (vegetable-oil, animal oil, or microalgae oil). Lubricants formulated using biodegradable oils such as vegetable, animal or microalgae are referred to as biolubricants, as the primary constituent is biodegradable. Although biolubricants can be made from either vegetable, animal or microalgae oils, in 2015, vegetable oil recorded 88.1% usage for biolubricants (Market Analysis Report, 2016).

2.1 Mineral-oil base lubricants

Mineral-oil base lubricants are usually made from a formula comprising of 90% mineral-oil plus 10% additives depending on the specifications of its application. Mineral-oil base lubricants have often time been used as automotive lubricants, industrial lubricants including hydraulic oils, metalworking fluids, greases, industrial gear oils, process oils and marine oils. Over the years, dependence on mineral-oil base lubricants have increased considerably (see section 2.3). Albeit that this condition predisposes the environment, vegetation, humans, animals and nature (life) in general to adverse risks and potential health hazards, as 50% of total global lubricants consumed on a year-to-year basis end up in the ecosystem either as incompletely combusted fluids from exhausts, or from direct spillage during usage, or during disposal (Ajithkumar, 2009).

Challenges associated with the use of mineral-oil base lubricants

A major challenge associated with the mineral-oil base lubricants is connected with the adverse environmental and health impact. According to Madanhire, and Mbohwa, (2016), about 50% of consumed lubricants globally end up in the ecosystem either through spillage during application/usage, incomplete combustion, or at disposal point. From the foregoing, it is observed that between 2015 to 2019 where an average consumption of 36MMT of lubricants was recorded globally in each year, an average 18MMT of lubricants find their way into the ecosystem annually, with a safe estimation of about 90MMT emitted into the ecosystem just between 2015 to 2019 alone. In other to understand this impact, Etkin (2010) stated that between 36.9 to 61 million litres of lubricating oil used in marine end up in ocean water annually. It is noteworthy that the oil reserve is fast depleting, and this is a major concern for manufacturers and the industrial sector who depend vastly on lubricants (see 3.2 for more details on global lubricant demand).

2.2 Vegetable-oil base lubricants using nanoparticle additives

When vegetable oil is used as base with nanoparticles as additives, the final product is otherwise referred to as nanolubricants. In this combination, vegetable-oil serves as the primary constituent, and nanoparticles as the additives for enhancing the tribological properties and performance of vegetable-oils for use as lubricants. This properties of the final lubricant prepared, largely, is dependent on the type of vegetable-oil used, and the type of nanoparticle used. It has been found that the shape, size and concentration of nanoparticles are very critical parameters of consideration in the preparation of nanolubricants (Zulkifli *et al.*, 2013). Nanolubricants possess significantly high lubricity (ability of the lubricant to reduce friction (including heating), wear and tear), and are biodegradable. These properties make them very desirable. Additionally,

Awoyale *et al.,* (2011) reported that nanolubricants possess high viscosity index (HVI) when compared to mineral-oil base lubricants, and are less costly, and possess low toxicity too.

Preparation of Nanolubricants

There are various methods that can be adopted in the preparation of nanolubricants. This review shall focus on two methods namely, two-step method, and one-step method.

i. **Two-Step Method:** This method, as the name implies, involves two steps in the process of preparation of nanolubricants. The first step in this process is the preparation of the nanoparticles to be used, using either physical or chemical preparation processes. The second process involves the dispersal of the desired shape and size of the powdered nanoparticle into the vegetable oil to be used as base for the nanolubricant. This can be achieved using intensive magnetic force agitation (IMFA), ultrasonic agitation, high-shear mixing, homogenizing, and ball milling (Yu and Xie, 2012). This process has proven to be the most economic method for preparing nanolubricants in large scale. Conversely, a major disadvantage or limitation of this method is the tendency of nanoparticle to aggregate, usually due to the large surface area. Although surfactants have been found to enhance the stability of nanoparticles in fluids, they have functional limitations specifically in high-temperature application. Other methods have been developed to overcome the limitations associated with the two-step method.

ii. **One-Step Method:** This method was developed by Eastman *et al.* (2001) to overcome the limitations associated with the two-step method, which is chiefly the tendency of nanoparticles to aggregate, making the nanolubricants prepared to be unstable. This process involves a single step of concurrently making the nanoparticles while dispersing it in the fluid. This process reduces the tendency of nanoparticles to aggregate, and hence, increases stability of the nanolubricant prepared. This process also allows for uniformly dispersed nanoparticles in the vegetable-oil base. There are two forms of carrying out the one-step method, which is either physical or chemical, although the physical method cost more to undertake compared to the chemical method. A significant limitation of the one-step method is the incomplete stabilization process of nanoparticles, which remain in the nanolubricant as residual which act as impurity.

2.2.1 Other non-oil bases

Although the common lubricants used are oil base lubricants which can either be mineral-oil base or vegetable-oil base, the use of other material base that are non-oil exist. These include the use of water-based lubricants, and gas-based lubricants, as well as solid lubricants as in graphite.

3 Statistical Assessment of Global Demand and Supply Trends of Lubricants and Demand Forecast

3.1 Global Lubricant Consumption % (GLC)

In a study conducted in 2004 and reported in Bartz (2006[b]) on global consumption of lubricant (mineral-oil base), a major insight into the global demands and consumption of lubrication can be grasped. The result of this study can be summarized in the Table 1.

*TABLE 1: **GLOBAL PERCENTAGE LUBRICANT CONSUMPTION (2004)***

Type of lubricant consumed		Percentage consumption (%)
Automotive lubricants		53
Industrial lubricants:		
i)	Hydraulic oils	12
ii)	Other industrial oils	10
iii)	Metalworking fluids	5
iv)	Greases	3
v)	Industrial gear oils	2
	Total	**32**
Process oils		10
Marine oil		5

The information presented in Table 1 depicts that the automotive industry alone accounts for more than half the total global demand and consumption of lubricants, with a 53% consumption recorded in 2004. Garside (2019[a]) reported that automotive/transportation industry accounted for 57.7 % of global consumption of lubricants.

3.2 Global Lubricant Demand (GLD)

Garside (2020[b]) reported the global lubricant (mineral-oil base) demand between the years 2000 – 2019. This study reported the following global demand for lubricants as presented in Table 2, and are indicative of the significant dependence on lubricants globally. According to the researcher, the total GDL reached a high of 36.9MMT in 2006, and in 2019, a near value of 36.8MMT was recorded.

*TABLE 2: **GLOBAL LUBRICANT DEMAND (2000 - 2019)***

Year	2000	2001	2002	2003	2004	2005	2006	2007	2008	2009	2010	2011	2012	2013	2014	2015	2016	2017	2018	2019
GLD (MMT)	36.4	**35.6**	35.7	35.4	35.4	36.1	36.5	36.9	36	36	32.2	34.5	35.1	35	35.4	35.6	35.7	36.1	36.4	36.8

(in million metric tons – MMT)

Source: Statista 2020

The statistics indicate that within the last seven (7) years, the demand for lubricants globally have steadily increased, from 35 MMT in 2013 to 36.8 MMT in 2019, a whooping difference of 1.8 MMT. This is easily traceable to increased industrial activities and energy demand, including the direct impact of the global manufacturing industry. Lubricants literally keep the global industrial sector moving.

3.3 Application of Nanolubricants in lubrication

The automotive and industrial markets are the two major applications of nanolubricants globally. Historically, vegetable oils were commonly used as media for lubrication, and remained the primary media for lubrication until the 19th century (Ajithkumar, 2009). Following the increased industrial activities of the industrialization era, the requirements needed to be satisfied by materials used as lubricants changed, which soon made the vegetable oils no longer suitable for this purpose. This led to the wide use and acceptance of mineral oil for lubrication in the second half of the nineteenth century. The need to enhance the properties of vegetable oils so it can function suitable as lubricants gave rise to the research efforts of nanoparticle additives, and are thus referred to as nanolubricants.

In the automotive industry, nanolubricants have applications as engine oils (nanolubricants-based engine oils), and transmission fluids. In the industrial or manufacturing sector, nanlubricants have applications as process oils including cutting fluids, metalworking fluids, etc.).

Much like the conventional mineral-oil base lubricants, the nanoparticle-enhance vegetable-oil base lubricants have a wide range of applicability. This cuts across the automotive and transport sector, aerospace, marine and manufacturing/industrial sector. This includes applicability in metalworking processes such as grinding, milling, drilling, etc. where it is used as metalworking fluid (MWF), cutting fluid, etc.

While other biodegradable oils can be used in preparing nanolubricants, vegetable oils recorded a leading high of 88.1% raw material for the preparation of nanolubricants in 2015 (Market Analysis Report, 2016). In the same study, a forecast period of 8 years (2016 – 2024) was used to forecast the growth rate of the nanolubricant market. It reported a growth rate of 7.6% over this forecast period.

The Table 3 presents the main areas of application of some commonly used vegetable-oil base lubricants. The table shows that vegetable oils are used as greases, engine oil, gear lubricants, hydraulic fluids/oils, diesel fuels, biodiesel, transmission fluids, in the automotive sector, while they are commonly used as metalworking fluids in the manufacturing and industrial sector.

*TABLE 3: **VEGETABLE OILS AND MAIN APPLICATIONS***

Base oil	Main Applications
Castor oil	Greases, gear lubricants
Coconut oil	Engine oil
Olive oil	Engine oil
Rapeseed oil	Greases, hydraulic fluids, chainsaw oils
Palm oil	Greases, metalworking fluids
Soybean oil	Engine oils, hydraulic oils, transmission fluids, biodiesel fuel, etc.
Sunflower oil	Greases, diesel fuels

The Table 3 presents the physicochemical properties of vegetable-oil bases commonly used in the preparation of nanolubricants and other biolubricants. Similarly, table 4 presents the physicochemical properties of mineral-oil bases used for the preparation of lubricants. In comparison, the vegetable oils displayed better properties than the mineral oils. This superior performance are key factors that increase the global market demand for nanolubricants, in addition to its biodegradability and low emission levels. The Table 4 shows viscosity is one of the major properties of vegetable oils, which means that they offer high lubricity, good metal adherence, and a high viscosity index.

Table 4: Physicochemical properties of commonly used vegetable oils for nanolubricants and biolubricants

Base oil	**Viscosity 40ºC (cSt)**	**Viscosity 100ºC (cSt)**	**Viscosity Index**	**Pour Point (ºC)**	**Flash Point (ºC)**	**Oxidative Stability (min)**	**Coefficient of Friction**	**Wear (mm)**
Castor oil	220.6	19.72	220	-27	250	-	-	-
Coconut oil	24.8	5.5	169	21	325	-	0.101	0.601
Cottonseed oil	33.86	7.75	211	-	252	-	-	-
Jatropha oil	35.4	7.9	205	-6	186	5	-	-
Lesquerella oil	119.8	14.7	125	-21	-	-	0.045	0.857
Moringa oil	44.9	-	-	-	204	28.27	-	-
Palm oil	52.4	10.2	186	-5	228	-	-	-
Passion fruit oil	31.78	-	-	-	228	7.5	-	-
Pennycress oil	40.0	9.3	226	-21	-	-	0.054	0.769
Olive oil	39.62	8.24	190	-3	318	-	-	-
Rapeseed oil	45.60	10.07	180	-12	252	-	-	-
Rice bran oil	40.6	8.7	169	-13	318	-	0.073	0.585
Sesame oil	27.33	6.3	193	-5	316	-	-	-
Soybean oil	28.86	7.55	246	-9	325	-	-	-
Sunflower oil	40.05	8.65	206	-12	252	-	-	-

(Source: McNutt, J. and He, Q.S, 2016)

*TABLE 5: **PHYSICOCHEMICAL PROPERTIES OF COMMONLY USED MINERAL OILS FOR LUBRICANTS***

Lubricant	**Viscosity 40ºC (cSt)**	**Viscosity 100ºC (cSt)**	**Viscosity Index**	**Pour Point (ºC)**	**Flash Point (ºC)**	**Oxidative Stability (min)**	**Coefficient of Friction**	**Wear (mm)**
ISO VG32	>28.8	>4.1	>90	-6	204	-	-	-
ISO VG46	>41.4	>4.1	>90	-6	220	-	-	-
ISO VG68	>61.4	>4.1	>198	-6	226	-	-	-
ISO VG100	>90.0	>4.1	>216	-6	246	1640.26	-	-
Paraffin VG45	95	10	102	-	-	-	-	-
Paraffin VG460	461	31	97	-	-	-	-	-
R150	150	-	-	-	195	931.16	-	-
SAE20W40	105	13,9	132	-21	200	-	0.117	0.549
AG100	216	19.6	103	-18	244	-	-	-
75W-90	120	15.9	140	-48	205	-	-	-
75W-140	175	24.7	174	-54	228	-	-	-
80W-140	310	31.2	139	-36	210	-	-	-

(Source: McNutt, J. and He, Q.S, 2016)

Viscosity Index:

Level	Low	Medium	High	Very High
Value	<35	35 – 80	80 – 100	>110

Advantages of vegetable-oil base lubricants:

Considering the tribological properties and the physicochemical properties of vegetable-oil base lubricants, vegetable-oil base lubricants possess some superior advantages over mineral-oil base lubricants. According to Hsien, (2015), the following are advantages of vegetable-oil base lubricants.

- Low emission levels due to high boiling point
- Significantly high biodegradability
- High lubricity
- Low volatility
- High stability
- Increased tool life (metalworking process)

- High viscosity index
- High safety on floor (Health and Safety considerations)

It is noteworthy that although the physicochemical properties of vegetable-oil base lubricants can be viewed broadly as in table 4, the properties of the lubricant are very much dependent on the specific area of its application, these include their properties when used as engine oil, hydraulic fluids, compressor oil, for metalworking fluids, etc.

Engine oils: When vegetable-oil base lubricants are used as engine oils, they display low volatility, low emissions, and good lubricity for the reduction of friction and wear in the engine. Generally, palm oil, castor oil and coconut oil have been found to be very efficient in use as engine oils for two-stroke engines, with castor oils recording a 5% reduction in emissions (Signh, 2011), although palm and coconut oils demonstrated high efficiency similar to mineral-oil base lubricants when used in four-stroke engines. When these oils are used over prolonged periods, their performance significantly drops, and this was traceable to the absence of additives (Mannekote, and Kailas, 2011). It was found that when used as engine oils, vegetable-oil base lubricants reduce emissions, and has the potential to significantly improve the performance of the engine.

Hydraulic Fluids: Hydraulic fluids essentially serve the purpose of energy/power transfer in a hydraulic system, and in the provision of lubrication for the system. For use as hydraulic fluids, the parameter of interest is the compressibility, such that lubricants to be used in a hydraulic system must display low compressibility (Regueira, *et al*, 2011). Vegetable oils used for hydraulic fluids display desirable properties including low compressibility, fast air rate of air release (which is very desirable to release trapped bubbles in the transmission line), and appropriate viscosity for use in hydraulic systems. Soybean oil demonstrated significantly high power transmitting power when compared to the performance of mineral-oil base hydraulic fluids (Arumugam, *et al*, 2014). In comparison with mineral-oil base hydraulics, rapeseed, palm, moringa, passionfruit, and rubber seed oils are some vegetable oils that have demonstrated superior performance as hydraulic fluids (Yunus, *et al.*, 2004; Silva, *et al.*, 2015; Kamalakar, *et al.*, 2013).

Metalworking Fluids: These fluids are used in machining processes including cutting, shaping, drilling, etc. They serve as lubricant and coolant to the process. Bartz, (1998) reported that a major concern with the use of mineral-oil based metalworking fluids is with the health, safety and environmental impact from its use and disposal. Raynor, *et al.*, (2005) reported that soybean oil is very suitable for use as metalworking fluids and minimizes this impact. In a study by Syahir, *et al.* (2017), it was reported that the use of vegetable-oil based metalworking fluids was beneficial in significantly reducing surface roughness, with a ripple effect in reducing the temperature, and minimizing tool flank wear. In the same study, it was reported that several studies have reported increased tool life of up to 40% in addition to improved surface finish and accuracy, traceable to use of vegetable-oil base metalworking fluids. According to Belluco, and Chire, (2004), and Tazehkandi, *et al.* (2015), the following properties were analysed using differenct vegetable-oil based metalworking fluids for: tool wear, cutting forces, tool life, and heat transfer efficiency levels. The studeis recorded high improvement in tool life. They generally demonstrate low volatility, good antirust capacity, good emulsifiability, good lubricity.

3.3.1 Testing the suitability of nano-lubricants using Four-Ball Tester

One of the methods of testing the suitability and functionality of prepared nanolubricants is the use of a four-ball tribotester. The tribotester is often used in the determination of the following tribological properties of the prepared nanolubricant: wear resistance, extreme pressure, and friction behaviour of lubricants. The apparatus is made up of four small balls made of steel, with an arrangement similar to an equilateral tetrahedron (see Figure 3). In this arrangement, the fourth ball (which is the rotating specimen) is attached to the spindle of the tribotester. During rotational motion, the ball makes contact with the remaining three balls held in fixed positions in the lubricant pot where the sample of the nanolubricant to be tested is introduced.

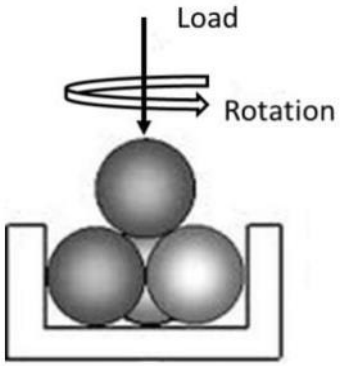

Figure 2: Arrangement of four-balls in the lubricant pot

The procedure for carrying out this test involves a series of steps. First, the balls are to cleaned using suitable liquid such as Acetone to remove unwanted materials on the surfaces. A ball is further attached to the spindle, while the others are placed in the lubricant/ball pot. The locking ring and nut is used to hold the balls firmly in position. 10ml of the prepared nanolubricant to be tested introduced into the lubricant pot until the balls are just submerged underneath the nanolubricant. Once completed, the setup is then placed on an anti-friction disc which can move up and down freely. The following parameters are recorded: (i) load (N); (ii) duration (sec); (iii) temperature (°C); (iv) rotational speed (rpm); (v) frictional torque; and (vi) real time applied load. These parameters are used to compute the desired tribological properties being tested for, using formulas.

3.4 Prospects for Nanolubricants

The continuously rising agitation and concerns about the adverse environmental impact of using mineral-oil based lubricants is leading global economies to develop policies to regulate the use of such lubricants. Attention is being continuously drawn to adopting environmentally friendly lubricants. The U.S. EPA has developed and adopted regulations that mandate all marine vessels to obtain the mandatory Vessel General Permit (VGP) for plying in the U.S. waters. This also enforces the utilization of acceptable and environment-friendly lubricants (nanolubricants or biolubricants) in all oil-to-sea interfaces. Application of nanolubricants in the transportation and the manufacturing industries are leading to a significant growth of global demand of nanolubricants. The favourable characteristics of nanolubricants including its biodegradability properties, high flash points, constant viscosity, and lower emission levels are driving the growth and applicability of nanolubricants

in these industries at global levels, in response to stringent standards on emission guidelines and regulatory framework (Market Analysis Report, 2016).

In 2015, the global nanolubricants market recorded a demand size of 630 kilo tons. Of this, vegetable-oil based automotive engine oil accounted for 200 kilo tons. In 2019 alone, the market size value of nanolubricants recorded an estimated 2.18 billion USD, and an estimated reach of USD 2.28 billion in the current year (2020) (Market Analysis Report, 2020). In the same report the global market value is expected to record a forecasted Compound Annual Growth Rate (CAGR) of 6.9% between 2016 to 2024, with an estimated market demand reach of 1,115 kilo tons by 2024.

3.5 Limitations and Potential Futuristic Drawbacks to Research Development

Although it has been established that vegetable-oil base has great potential in lubrication industry, it has not gained sufficient global commercialization as compared to mineral-oil base lubricants. The commercialization of vegetable-oil base lubricants globally is met with some limitations or challenges. Some of the major issues associated with biolubricants were highlighted by Nagendramma and Kaul, (2012), and Panchal, *et al*., (2013): (i) High heterogeneity; (ii) Poor oxidation stability; and (iii) Poor lubrication properties at low temperature. Additionally, Erhan, *et al.,* (2006[b]) identified that a major drawback for biolubricants is associated with its poor oxidative stability, and their poor performance at lower temperatures. He further established that most vegetable oils solidify at about -10^{o}C, thus making them difficult to use. Moreover, Syahir, *et al.,* (2017) highlighted a major challenge to the exploitation of vegetable oils for use in the lubrication industry. He reported that previous studies were carried out using vegetable oils that has the potential to interfere with the stability of the food chain as they were rather edible. Some of these include palm oil, coconut oil, soybean oil, amongst others. This can result in a major imbalance in the food value chain, as the demand for commercialization of these vegetable-oil base lubricants can compete significantly with the demand for food.

Moreover, the transition from mineral-oil base lubricants to biolubricants is largely an enormous process for lubricant producing companies. The process of transition might require efforts, time and costs expended towards machineries, capacity building and training for operators at production plants, etc. (Juan, *et al.,* 2020). These transition requirements might pose a major drawback for companies to fully embrace the biolubricant technology.

3.6 Opportunity for improvement

Continuously evolving environmental regulations for use of environmentally friendly lubricants for the automotive and manufacturing industries are paving ways for the evolution of biolubricants, and its global acceptability. Aside the grossly desirable properties of biolubricants, these regulations are driving the development and demand levels of biolubricants.

Syahir, *et al.* (2017) has highlighted that the use of edible vegetable oils can become a major challenge to the commercialization of vegetable-oil base lubricants as it might compete with the food value chain. This is an opportunity that can be harnessed for improvement by the shift of emphasis from edible vegetable oils to non-edible vegetable oils. Few studies have carried out to check the suitability of non-edible vegetable oils such as Jatropha oil, Castor oil, etc. for use as lubricants and as suitable alternatives to edible oils. Mata, *et al.* (2010) highlighted that very recently, possibilities of

harnessing oil content (more than 70% oil content in some cases) from microalgae. Additionally, more studies can be carried out to compare the performance of various vegetable oils using varying sizes, shapes and concentration of additives such as non-toxic inorganic oxides nanoparticles, nanofibers, etc.

In addition to the above, there is need to further research on the chemical modification of starting oils or vegetable-oil base suitable for formulating lubricants with superior desirable properties. These research efforts include the esterification, hydrogenation reactions, epoxidation and branching reactions of the vegetable oils are other possibilities for optimal performance of vegetable-oil base lubricants in the lubrication industry. The chemical modification of vegetable-oil base can significantly improve the properties and performance of the final lubricant formulation, at this might enhance the stability of the resultant biolubricant.

4 Conclusion

The rising concerns of the adverse environmental impacts of continuous use of mineral-oil base lubricants from spillage, disposals, leakages, and handling are favouring continuous research and development efforts towards achieving suitable sustainable alternatives to the use of mineral-oil base lubricants globally. Vegetable-oil base lubricants and other biolubricants have demonstrated potential for suitably replacing mineral-oil base lubricants. This is easily traceable to pertinent physicochemical properties they possess including high viscosity index, biodegradability, high lubricity and good metal adherence. Global lubricants market forecasted a CAGR of 6.9% for vegetable-oil base lubricants between 2016 – 2024. Regardless of the potential displayed in vegetable-oil base lubricants, the global commercialization and transition to vegetable-oil base lubricants are low, compared to the use of mineral-oil base lubricants. A major challenge associated with the development of biolubricants is poor oxidative stability. To conquer this, researches have been done and are still being carried out to chemically modify the vegetable oils in order to attain oxidative stability, including the use of esterification, hydrogenation, epoxidation and branching reactions. Further studies in research and development for improving the performance of vegetable-oil base as lubricants are needed to harness its potential.

5 References

Ajithkumar, G. (2009). Analysis, modification and evaluation of the cold flow properties of vegetable oils as base oils for industrial lubricants.

Arumugam, S., Sriram, G., and Ellappan, R. (2014). Bio-lubricant-biodiesel combination of rapeseed oil: An experimental investigation on engine oil tribology, performance, and emissions of variable compression engine. *Energy*, 72, 618–627

Awoyale, A. A., Odubiyi, O. A., & Eloka-Eboka, A. C. (2011). Production and Testing of Biodegradable Grease from Black-Date (Canarium schweinfurthii) *Oil*, pp. 223-233.

Bartz, W. J. (2006[b]). Automotive and industrial lubrication. *International Colloquium Tribiology: Technische Akademie Esslinge*, 15.

Belluco,W. and De Chire, L. (2004). Performance evaluation of vegetable-based oils in drilling austenitic stainless steel. *J. Mater. Process. Technol*., 148, 171–176.

Dowson, D., (1998), History of Tribology, Professional Engineering Publication Limited, Bury St. Edmunds, Suffolk, U K.

Eastman J. A., Choi S. U. S., Li S., Yu W., and Thompson L. J. "Anomalously increased effective thermal conductivities of ethylene glycol-based nanofluids containing copper nanoparticles," *Applied Physics Letters*, vol. 78, no. 6, pp. 718–720, 2001.

Erhan, S.Z.; Sharma, B.K.; Liu, Z.; Adhvaryu, A. (2008[a]). Lubricant base stock potential of chemically modified vegetable oils. *J. Agric. Food Chem.*, 56, 8919–8925.

Erhan, S.Z., Sharma, B.K., and Perez, J.M. (2006[b]). Oxidation and low temperature stability of vegetable oil-based lubricants. *Ind. Crops Prod.*, 24, 292–299.

Etkin, D.S. 2010. Worldwide analysis of in-port vessel operational lubricant discharges and leaks. Proc. 33rd Arctic and Marine Oilspill Program Technical Seminar: p. 529-554

Garside, M. (2019). Lubricant demand worldwide in 2018 by region. *Lubricant Industry Factbook* 2019-2020, *Lubes'n'Greases*, 32.

Garside M. (2020). Global lubricant demand 2000-2019.

Hsien, W.L.Y. (2015). Utilization of vegetable oil as Bio-lubricant and additive. In *Towards Green Lubrication in Machining*; Hsien, W.L.Y., Ed.; Springer: Berlin, Germany; Volume 1, pp. 7–17.

Juan A. C., Daniel B.P., Rosana M.A.S., Francisco M.T., Celio L.C., and Enrique R. (2020). An Overview of the Biolubricant Production Process: Challenges and Future Perspectives. *Processes*, 8, 257

Kamalakar, K., Rajak, A.K., Prasad, R.B.N., and Karuna, M.S.L. (2013). Rubber seed oil-based biolubricant base stocks: A potential source for hydraulic oils. *Ind. Crops Prod*., 51, 249–257.

Li, W. and Wang, X. (2015). Bio-lubricants derived from waste cooking oil with improved oxidation stability and low-termperature properties. Journal of Oleo Science, 64(4), 367-374.

Madanhire, I. and Mbohwa, C. (2016). Mitigating Environmental Impact of Petroleum Lubricants. *Springer International Publishing*

Mang, T. and Dresel, W. (2006). Lubricants and lubrication. Weinheim, Chichester.

Mannekote, J.K., and Kailas, S.V. (2011). Experimental investigation of coconut and palm oils as lubricants in four-stroke engine. *Tribol. Online*, 6, 76–82.

Market Analysis Report, (2016). Retirieved from: http://www.grandviewresearch.com/industry-analysis/biolubricants-industry

Mata, T.M., Martins, A.A., and Caetano, N.S. (2010). Microalgae for biodiesel production and other applications: A review. *Renew. Sustain. Energy Rev*., 14, 217–232

McNutt, J. and He, Q.S. (2016). Development of biolubricants from vegetable oils via chemical modification. *J. Ind. Eng. Chem*., 36, 1–12.

Nagendramma, P. and Kaul, S. (2012). Development of ecofriendly/biodegradable lubricants: An overview. *Renew. Sustain. Energy Rev.*, 16, 764–774.

Panchal, T., Chauhan, D., Thomas, M. and Patel, J. (2013). Synthesis and characterization of bio lubricants from tobacco seed oil. *Res. J. Agric. Environ. Manag*., 3, 97–105.

Raynor, P.C., Kim, S.W., and Bhattacharya, M. (2005). Mist generation from metalworking fluids formulated using vegetable oils. *Ann. Occup. Hyg*., 49, 283–293.

Regueira, T., Lugo, L., Fandiño, O., López, E.R., and Fernández, J. (2011). Compressibilities and viscosities of reference and vegetable oils for their use as hydraulic fluids and lubricants. *Green Chem.*, 13, 1293–1302

Silva, M.S., Foletto, E.L., Alves, S.M., de Castro Dantas, T.N., and Dantas Neto, A.A. (2015). New hydraulic biolubricants based on passion fruit and moringa oils and their epoxy. *Ind. Crops Prod.*, 69, 362–370.

Singh, A.K. (2011). Castor oil-based lubricant reduces smoke emission in two-stroke engines. *Ind. Crops Prod*., 33, 287–295.

Syahir, A.Z., Zulkifli, N.W.M., Masjuki, H.H., Kalam, M.A., Alabdulkarem, A., Gulzar, M., Khuong, L.S., and Harith, M.H. (2017). A review on bio-based lubricants and their applications. *J. Clean. Prod.*, 168, 997–1016.

Tazehkandi, A.H., Shabgard, M., and Pilehvarian, F. (2015). On the feasibility of a reduction in cutting fluid consumption via spray of biodegradable vegetable oil with compressed air in machining *Inconel 706. J. Clean. Prod*., 104, 422–435.

Woma, T. Y., Lawal, S. A., Abdulrahman, A. S., Olutoye, M. A., & Ojapah, M. M. (2019). Vegetable Oil Based Lubricants: Challenges and Prospects. Tribology Online, 14(2), 60-70.

W. Yu and H. Xie (2012). A Review on Nanofluids: Preparation, Stability Mechanisms, and Applications. *Journal of Nanomaterials*, vol. 2012.

Yunus, R., Fakhru'l-Razi, A., Ooi, T.L., Iyuke, S.E., and Perez, J.M. (2004). Lubrication properties of trimethylolpropane esters based on palm oil and palm kernel oils. *Eur. J. Lipid Sci. Technol*., 106, 52–60.

Zulkifli, N. W. M., Kalam, M. A., Masjuki, H. H. and Yunus, R. (2013). Experimental Analysis of Tribological Properties of Biolubricant with Nanoparticle Additive. Procedia Engineering. 68: 152-157.

Development and Optimization of the production process of Gasket from Plant Fiber Hybrid

N. K. Ugwuneji[1,] S.A. Lawal[2]

[1]Mechanical Engineering Department, Federal University of Technology Minna, Niger State

[2]Mechanical Engineering Department, Federal University of Technology Minna, Niger state

Corresponding Author: [1]08068899366; nnaemekaugwuneji@gmail.com

Abstract

This study investigates and improves the production process of gasket paper sheets from agricultural waste materials by employing the principles of papermaking. It uses sawdust as base material, sugarcane and banana stem fiber as the fiber reinforcement, cationic starch as binder and kaolin as filler in the paper at a loading level of 20% by weight in all samples and propylene glycol as an additive. The investigation of the effectiveness of the gasket paper to be produced will be based on compressibility, heat resistance and fluid absorption. This study will try to solve the issue of weak gaskets by producing good efficient gaskets able to maintain a leak-free seal throughout its lifetime. It hopes to eliminate the need for importation of gaskets and move the dependency to locally made ones, thereby creating job opportunities through these new areas of investment.

Keywords: *sawdust, sugar cane fiber, kaolin, banana stem fiber*

1.0 INTRODUCTION

In Nigeria, over 52 metric tons of agricultural wastes accumulate in urban areas and only 30% of them are collected and properly disposed by waste contractors leaving the rest to rot, litter and pollute the environment. Proper utilization of agricultural wastes and residues can vastly reduce the level of environmental pollution while increasing the availability of locally made products, thereby converting waste to wealth. Discarded plant products and residue, like sugar cane fibers, and banana stem, contribute to the pollution of the environment just like other agricultural wastes. There is therefore a serious need for effective waste management of such waste through recycling in order to create new products like gaskets from them. In the automotive, petroleum, oil and gas and other industries where mechanical parts are fitted together, gaskets are commonly used. A gasket is a material used to seal one component of a device from another and fill the space in between in order to prevent liquids, gases and other contaminants from getting to where they are not wanted (Oladele & Adewuyi, 2009). A gasket can also be described as a sealing element placed between two flange faces and held in a position by the compressive forces of a set of bolts located around the circumference of the flange blades (Peter Smith, 2007). Gaskets can come in all shapes and sizes with a wide range of materials to choose from each designed to perform sealing functions for specific purposes (Martin et al., 1985; Duffy 1998). Because a gasket will fill the space between these surfaces, gaskets are made from materials that are able to deform and fill any slight irregularities in the mating surfaces. They are also made in different designs based on individual usage, budget, chemical content and physical parameters (Bickford, 1995).

Ipambese (2010) produced homemade gasket papers through the compression of bambara-nut shells and palm kernel fibers and by also employing the basic operations of papermaking. Kaolin was used as filler in the paper at a loading level of 24.8% by weight in all the samples, other additives utilized were cationic starch and polyethylene glycol in the percentages of 1 to 7 by weight of the samples. Park et al (2018) used an eco-friendly manufacturing process to make low density compressed sheet gaskets which were used to maintain gaslight properties regarding gases and liquids. The main raw materials were latex, organic and inorganic textile, and fillers. Kokusan Parts Industries (2019) produced cylinder head gaskets through some organized processes beginning with First Pressing where the product shape was punched out of the coil material. The second process consisted of an automated line with four presses connected by a transfer robot. Cleaned products underwent heat treatment to enhance functionality before painting the surface. James (2016) manufactured gaskets by mixing of raw materials, forming and packing. The raw materials were mixed so as to obtain a uniform blend of the mixture, adequate dispersion of pigments, uniform degree of dispersion and viscosity. Oladele et al (2009) sun dried natural fibers (bamboo, coconut husk, sponges and wood) and pulverized them in a ball mill and sieved with a sieve aperture size of 850µm. Fifteen different compositions were obtained and homogeneous pastes were produced by mixing the pulverized fibers with Top Bond white glue.

This study is aimed at creating a market opportunity for indigenous manufactured gaskets by improving the targeted performances quality to a level that they can compete favorably with the imported ones. This will be achieved by improving the choice of the gasket material and by producing efficient gaskets capable of maintaining a leak-free seal during its lifetime. Finally, it will reduce the level of pollution caused by agricultural waste by creating alternative sources of raw materials and thereby improve the economy by the conversion of waste to wealth.

2.0 MATERIALS AND METHODS

2.1 Materials: The materials used in the production process of the gasket material includes sugar cane bagasse, sawdust, banana stem fiber, kaolin, propylene glycol, cationic starch, caustic soda, water, cellulose sanding sealer, the mould, wooden platen, deckle, commercial gasket paper, mortar and pestle. Equipment used include a hydraulic press, electric furnace, digital balance and vernier caliper.

2.2 Methods: The production process begins with the construction of a mould. A rectangular wooden frame measuring 20cm by 20cm was constructed, with wire mesh covering the bottom and capable of producing a gasket paper with an area of 20cm by 20cm. Also constructed were a deckle and platen. The next phase was the pulp preparation where sugarcane bagasse and banana stem fibers sourced from sugar cane sellers and a farm respectively were cleaned and sundried for about 2 hours.

Figure 1: Raw Sugarcane bagasse and Banana stem

Then the banana stem was chopped into bits and cleaned of its bark before being soaked in water for 30 minutes in order to soften the banana fibers. Caustic soda equaling 20% by weight of the dry weight of the fiber was added to boiling water and the fiber cooked at 1000°C for at least 3 hours while being checked and stirred at 30 minutes interval to ensure uniformity. This application of alkaline (caustic soda) removes impurities from the fiber, loosens the fiber structure at the same time dissolves the non-cellulose parts of the fiber. The percentage of the alkaline to be mixed depends on the strength of the fiber structure, this can be determined by the water retention capacity of the fiber. At the end of the 3 hours the fibers were removed from heat and rinsed thoroughly with water to remove all caustic soda until the water was clear. The same process of boiling and rinsing was performed on the sugar cane bagasse. The boiled chopped stem of banana and sugar cane where then pounded separately in a mortar using a pestle to detangle the fibers and reduce it to a mushy pulp. Two sets of gasket paper samples each were produced from the banana pulp, the sugar cane bagasse pulp and the combination of the two pulps. Kaolin and sawdust were added as fillers to each of the pulps at 20% by weight of 125 grams of the entire mixture, while additives like epoxy resin and propylene glycol were added to the individual pulps. Propylene glycol was added in 5% by weight of 125grams in the entire mixture. For the epoxy resin, the resin and the hardener were added in the ratio 3:1.Paste mixture was poured into the mould and deckle and shaken to settle into the desired shape.

A piece of cloth was placed on the mould after the deckle was removed and the mould flipped over to transfer the paste to the surface of the cloth. This was done for all the paste mixtures. The clothes carrying the pastes were then stacked and compressed with a weight of 50kg by a universal press for 5 minutes with the aid of a platen. This was done to achieve stronger fiber to fiber bonding and to give a flat and smooth surface. The clothes with the gasket paper were placed in the sun to dry so as to remove any remaining water. After drying, the gasket paper was carefully peeled off from the cloth and coated with the cellulose sanding sealer.

2.3 Evaluation of the gasket papers sheets

Tests were carried out at the Sheda Science and Technology Complex (SHETSCO) Abuja to determine the effectiveness of the gasket paper sheets produced. These tests include compressibility and recovery, fluid absorption and heat resistance tests. Compressibility and Recovery test are carried out to determine the behavior of the gasket materials under applied crushing loads and to determine the maximum internal pressure that the materials can withstand. Compression test is carried out using loads of 5kN to 10kN. Each of the loads was exerted upon a particular specimen, applied as a distributed load and the percentage reduction in thickness recorded. The thickness of the gasket before and after compression was measured using a micrometer screw gauge and the percentage reduction in original thickness was determined

Liquid Absorption Test was carried out on the gasket materials to observe the performance of the gasket material when applied in water, petrol and oil. This also includes determination of the percentage of liquid absorption. Samples were wholly immersed in water, petrol and Quartz SAE 40W engine oil for 30 minutes. They were then cleaned and weighed in a digital balance to determine the mass of liquid absorbed into the specimens. The tests were then carried out for 60 minutes, 90 minutes, 120 minutes, 160 minutes and 180 minutes.

Heat Resistance test was carried out to determine the heat resistance of the samples produced and the commercial gasket sheet. It was also done to determine the maximum temperature at which the gasket will fail (get burnt). The samples and commercial gasket paper were cut to the same size of 4cm by 6cm each and placed in an electric furnace. The furnace temperature was initially set at 50^{o}C and then increased by 10^{o}C after every five minutes. The produced samples and the commercial gasket paper were brought out every 10^{o}C increment and five minutes of exposure and visually observed to determine the temperature at which the specimens got burnt.

Figure 2: Universal Testing Machine

Figure 3: Samples in the Electric Furnace

Figure 4: Samples being wholly immersed in engine oil, petrol and water respectively

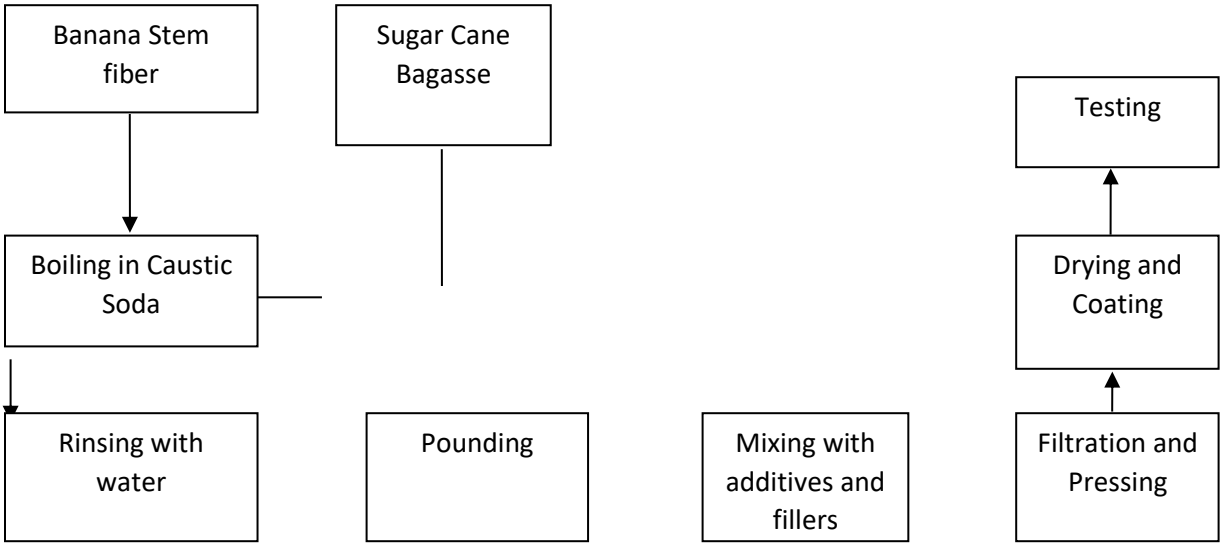

Fig 5: Flow chart for the production of gasket materials

3.0 RESULTS AND DISCUSSION

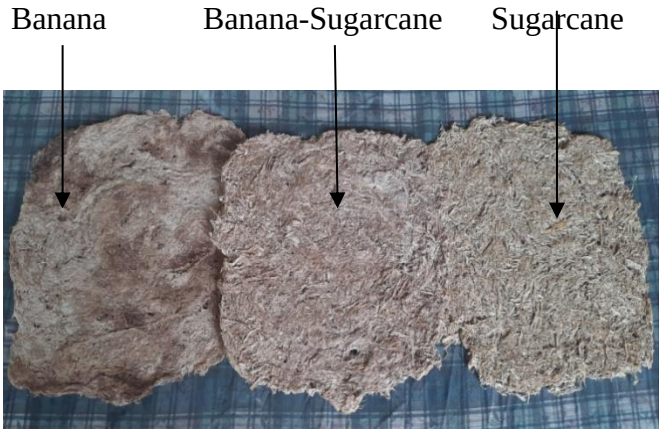

Figure 6: Gasket material samples produced

3.1 Compressibility and Recovery Test

Table 3.1: Compressibility and Recovery test results

	Force (Intended Force)	Max Force (Actual Force Applied)	Original Thickness	Max Elongation	Max Extension	Max Stress	Thickness after Recovery
	F	FH	LO	dHL	AH	RH	
	N	N	mm	mm	%	N/mm²	mm
BANANA	0	0	0	0	0	0	0
	5	4998.22	7	5.6	79.97	2.21	6
	6	5989.86	7	4.67	66.85	2.64	4
	7	7000.61	6	5.79	96.52	3.09	4
	8	7995.38	6	5.96	99.42	3.53	4
	9	9004.6	7	5.45	88.98	3.98	5
SUGARCANE	0	0	0	0	0	0	0
	5	4996.97	6.5	7.23	96.46	2.21	5
	6	5998.09	7.5	7.39	98.71	2.65	6
	7	6983.33	7.5	7.79	104.06	3.08	7
	8	8000.97	7.5	8.03	107.04	3.53	8
	9	9005.17	7.5	8.04	107.27	3.98	9
BANANA AND	0	0	0	0	0	0	0
	5	4976.56	6.5	6.97	107.3	2.2	5

SUGARCANE COMPOSITE	6	5961.34	6.5	7.49	120.24	2.63	6
	7	7012.52	6.5	7.78	120.11	3.1	7
	8	8003.3	6.5	8.11	124.75	3.53	8
	9	9019.83	6.5	7.94	122.24	3.98	9

3.2 Fluid Absorption Test

The result of the Fluid Absorption Test using Engine oil, Petrol and Water respectively is shown below:

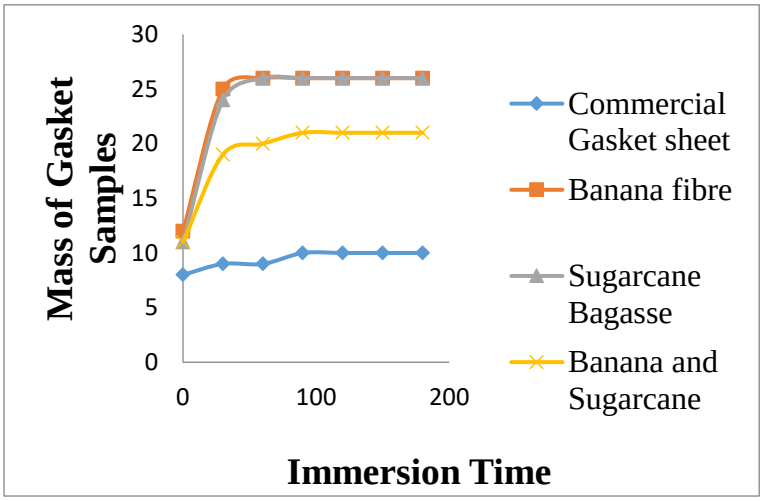

Figure 7: Mass of Gasket samples immersed in Engine oil against Time of immersion

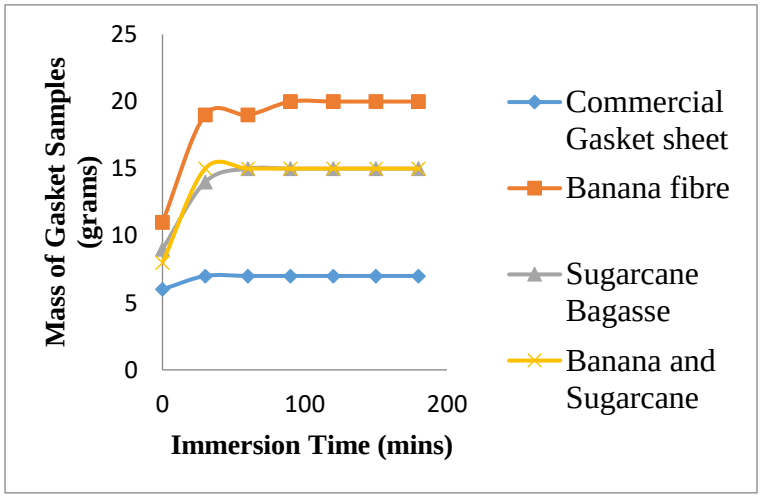

Figure 8: Mass of Gasket samples immersed in Petrol against Time of immersion

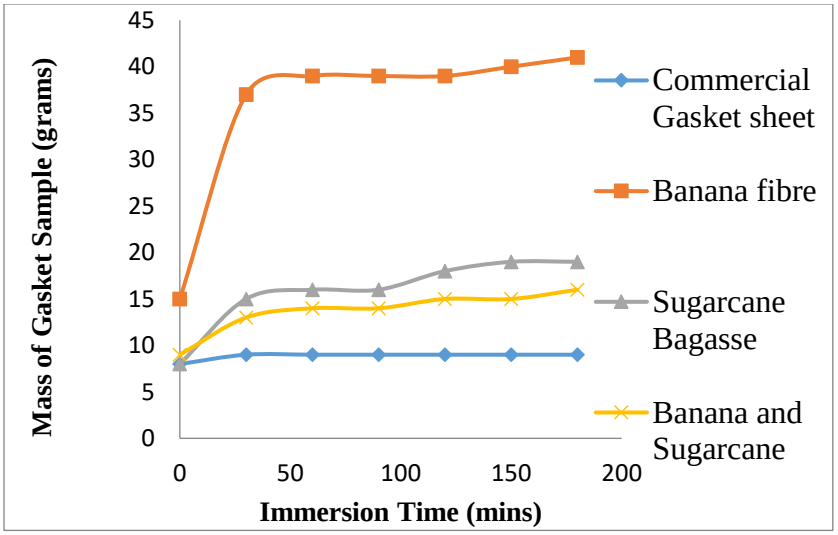

Figure 9: Mass of Gasket samples immersed in Water against Time of immersion

3.3 Heat Resistance Tests

The Heat Resistant Test Results are represented in the graph below:

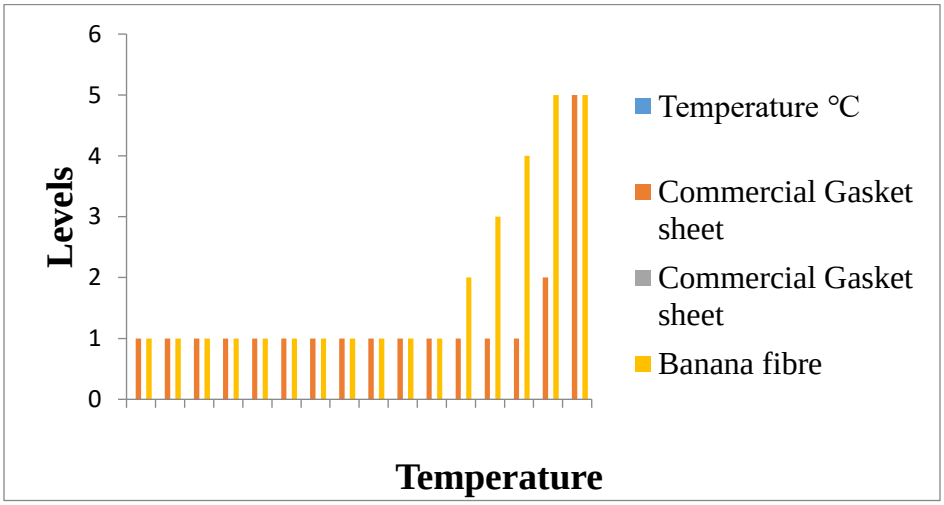

Fig 3.4: Heat Resistance of Gasket Samples in an Electric Furnace

Key:

Level 1 – Normal, Level 2 – Slight Change in Colour, Level 3 – Colour changes to Brown,

Level 4 – Burnt Partially, Level 5 – Burnt Completely

4.0 CONCLUSION

The following findings were made in the course of the study:

(a) The average percentage compressibility and recovery of sugarcane is more than that of banana, while the average percentage compressibility and recovery of the banana-sugarcane composite is more than that of the banana and also that of the sugarcane

(b) The banana and sugarcane composite absorbs less fluids compared to the banana and sugar cane bagasse gasket material samples

(c) The banana and banana-sugarcane composite gasket material samples were more resistant to heat than the sugarcane bagasse material sample

Based on the findings mentioned above, the following conclusions were drawn at the end of the study:

(i) The banana and sugarcane composite material was the best gasket material produced and therefore a better choice of combination of plant fiber for the production of gaskets.

(ii) This research provides a step by step guide to producing effective and efficient gasket stem materials as well as their testing and comparisons

(iii) This research provides a useful outlet for the recycling of agricultural wastes in Nigeria through the use of such waste as banana and sugarcane bagasse in gasket making.

References

Bickford, John H. (1995), An introduction to the design and behaviour of bolted joints, 3rd edition; Marcel, Delkiler pp 5

Ikpambese, K.K. (2010). Production of Gasket Paper Sheets from Bambara Shell and Palm Kernel fiber

James. (2016). Profile on the production of formaldehyde. Kokusan. (2019). Production System | Kokusan Parts Industry | Manufacturer of Automotive Parts and Sealing Parts Including Cylinder Head Gaskets and Heat Insulators. Retrieved August 13, 2019, from https://www.kbk-k.co.jp/en/technique/production.html

Martin, W.S. and Martin, T.S. (1985). "Auto Mechanics Fundamentals", The Good-heart Willcox Company, Inc, pp 48-49

MES. (2017). Gaskets - Basics, Types, Working Principle, Calculation of bolt load - Mechanical Engineering Site. Retrieved May 19, 2019, from http://www.mechanicalengineeringsite.com/gaskets-basics-types-working-principle-calculation-bolt-load/

New Age Encyclopedia (1978), Encyclopedia Britanica, U.S.A, 15th Edition pp 966-987

Oladele, I., & Adewuyi, B. (2009). Development of Automobile Gaskets from Local Fibres. Journal of Science and Technology (Ghana), 28(3). https://doi.org/10.4314/just.v28i3.33115

Park, S., Lee, H., Lee, S., Kim, S., Yoo, Y., 2018. Journal of Material Sciences and Engineering

Manufacturing of Sheet Gasket using a Paper Making Process without Organic Solvents

Peter Smith. (2007). Gaskets - an overview | ScienceDirect Topics. Retrieved May 19, 2019, from The Fundamentals of Piping Design website: https://www.sciencedirect.com/topics/engineering/gaskets

APPLICATIONS OF ARTIFICIAL INTELLIGENCE TECHNIQUES IN METAL CASTING -A REVIEW

[1,2] Suleiman L. T.I., [1]Bala K.C., [1]Lawal S.A., [1]Abdulllahi A.A., [3]Godfrey M.,

[1]*Department of Mechanical Engineering, Federal University of Technology, Minna, Nigeria,*
iliyasu.sule@futminna.edu.ng , katisna.bala@futminna.edu.ng , lawalsunday@futminna.edu.ng
aliuaabdullah@futminna.edu.ng
[2]Department of Petroleum Resources (DPR), Minna, Niger State
iliyasu.sule@futminna.edu.ng
[3]*Quality/Environmental Management System, Sonates Resources Investment Ltd, Abuja, Nigeria, godfreymnet@gmail.com*

Corresponding author: **Suleiman L.T.I.,** *iliyasu.sule@futminna.edu.ng, +234806639063*

Abstract

Process control and monitoring of product quality during metal casting operation(s) cannot be overemphasised. In addition, algorithms, models and optimisation techniques can be developed in metal casting processes to minimise casting defects through artificial intelligence. This review paper explores the applications of artificial intelligence (AI) in metal casting process. The evolution, fundamentals concepts of the AI methods/tools covering Fuzzy Logic (FL), Case Based Reasoning (CBR) and Artificial Neural Networks (ANN) are discussed accordingly. Furthermore, applications of these methods/tools in aspects of casting process optimisation, product quality monitoring/control of defects, intelligent design and materials selection are critically reviewed. The structure of this article provides clear understanding of the concept to foundry engineers, researchers and stakeholders in metal casting industry for enhancing net-shape casting with high reliability and integrity.

Keyword: Algorithm, Artificial Intelligence, Casting defects, Manufacturing, Metal Casting, Optimization; Soft Computing

1.0 INTRODUCTION

Metal casting is one of the oldest processes of manufacturing and it is assumed that it is as old as mankind. It is also known as net shape process. In the last three decades, a lot of advancements have been taken place in the field of metal casting. However, green sand casting remains one of the most versatile casting processes due to readily available and cheap raw materials; flexibility with respect to shape, size and composition; and the possibility of recycling the moulding sand (Singha and Singh, 2015). The sand casting process starts with preparation of mould, pouring molten metal into a sand mould, allowing the metal to solidify, and then breaking away the sand mould to remove a casting product. Out of the various steps involved in the casting process, moulding and melting processes (pouring of molten metal) are the most important stages. Improper control at these stages results in defective castings (Tiwari *et al.*, 2016). Casting is a process of pouring molten metal into the cavity of a mould and allowed to solidify into a required shape. Casting as a process involves a relationships of many parameters such as mould temperature, moisture content, permeability of sand, type of binders, pouring temperature and gating system. These parameters significantly have effect on the mechanical properties of the cast. In the past the foundry engineer has used the manual methods in producing cast products. This has led to defective cast and resulted in cast rejection (Lei and Su, 2019). In casting industry, the cast parts defects caused by solidification shrinkage, improper feeding, heat transfer mechanism between the cast and the mould and the sand mixture represent a major cause for casting defects and rejection. The defects can be minimised through

artificial intelligence. Artificial intelligence (AI) is a fourth industrial revolution of computational analysis (Schwab, 2017; Pan, 2016), distinguished by the shift of agency and control from humans to technology, and thus transforms our previous understanding of human-technology relations. This revolution and its implications highlight new theoretical and empirical questions that need to be addressed by organizational researchers on workforce structures, designs, decisions and analysis (Brynjolfsson *et al.,* 2018; Danaher, 2017; Huang and Rust, 2018; Kaplan, 2015; Kellogg *et al.,* 2019; Pfeffer, 2018; Wirtz *et al*., 2018). However, this paper presents review of applications on artificial intelligence.

2.0 Artificial Intelligence

2.1 Development of the AI Algorithm and Models

Numerical analysis is constantly used in casting industry for a better understanding of both the critical aspects related to heat transfer and fluid flow phenomena. This relationship between metallographic structures and formation of microstructure defects in the cast parts has employed numerical analysis in the past decades (Das *et al.,* 2015). Some of the thermo physical properties necessary for obtaining very accurate results by using numerical analysis are very often totally missing in case of some alloys which have a very high commercial interest for casting industry. The casting technologies have many advantages as the flexibility of manufacturing some complex geometry. Furthermore, by controlling the casting process can be obtained, through a single processing operation, a cast part which corresponds to the imposed mechanical properties and quality level. Thus, the application of numerical analysis in casting is good while thinking towards application of AI in casting will act as programming of machine learning in controlling the precision parameters of casting process.

Due to computational time consumption during analysis in controlling parameters of casting process will require better algorithm that will speed up defects control in casting. The algorithms such as genetic algorithm (GA), ISRES (Improved Stochastic Ranking Evolutionary Strategy) and ESCH (Evolutionary Strategy with Cauchy Distribution) are samples of AI algorithms that is being applied engineering application. The latter is a meta-heuristic version of an Evolutionary Strategy (ES) workflow, using a Cauchy random number function to generate each individual, instead of the usual uniform distribution function available in almost all programming languages (Bertelli *et al.,* 2014).

In casting industry, the casting part defects caused by solidification shrinkage represent a major cause for rejection. Some researchers stated that pore formation is determined by the heat transfer mechanism between the cast and mould, shrinkage solidification or improper feeding of the mould. The type of mould used in metal casting depends heavily on the type of casting to be produced, the alloy involved and the complexity of the shape to be cast. Heat transfer between the solidifying casting and mould is critical for high quality casting. In addition, heat transfer between the casting and the mould is primarily controlled by conditions at the mould-metal interface. The quality of castings in a green sand mould are influenced significantly by its properties, such as green compression strength, permeability, mould hardness and others which depend on input parameters like sand grain size and shape, binder, water etc. Thus, applying AI into this moulding process will minimise defects.

Lee *et al.* (2018) stated that the prediction of internal defects of metal casting immediately after the casting process saves unnecessary time and money by reducing the amount of inputs into the next stage, such as the machining process, and enables flexible scheduling. This research is intended to look at Artificial Intelligence, which has proven to be one of the most important tools in decision making in Energy industry, with the industry increasingly becoming more digitalized, data generated, processed, and analysed are used for product design, planning, and

production control. This makes the Energy industry more reliable, flexible and efficient in production processes. Artificial Intelligence has been a central focus for many researchers in the last 3 decades. Casting defects which occurred as a result of inaccurate process parameters, mould design, sand mixtures, and processes and procedures could be resolved with the aid of Artificial Intelligence. Hence, optimising the processes and procedures offers tremendous potential for the Energy industry via predictive production and maintenance. This will reduce defect in casting and cast rejection, thereby avoiding wastages in terms of cost, production time faster and energy consumption and can be used to study industrial scale Problems.

2.2 Applications of AI in Casting

Artificial Intelligence (AI) could be defined as the simulation of human intelligence in machines programmed to think like humans and mimic human's actions. This term may also be applied to a machine that exhibits traits associated with a human minds or brain such as learning and problem solving skills. In today's scenario of competition and precision, where we are talking about six sigma lots of efforts are being made by the foundry engineers to reduce rejection of defective castings. And very high cost and time is associated with analysis and prevention of defects in castings because previously they were dependent on the conventional trial and error methods that lead to huge losses. Therefore, use of computational intelligence methods in the field of sand mould design, defect identification, evaluation, analysis, and casting process planning with the objective casting quality assurance is increasing day by day (Rai and Ganguly, 2018).

2.3 Optimisation, monitoring and control of casting process parameters and defects

AI has been adopted in optimisation, defect monitoring and control, process parameters in casting base on different algorithm approach. The algorithm includes the prediction of internal defects of metal casting process (Lee *et al*., 2018). This saves unnecessary time and money by reducing the amount of inputs into the next stage, such as the machining process, and enables flexible scheduling. Bayesian inference algorithm was employed by Sata and Ravi (2016) in analysing investment-casting defect. Sata and Ravi (2016) proposed the process to predict and prevent various defects, based on the computation of posterior probabilities of process parameters using Bayesian inference methodology. The inference was based on AI. It overcomes the limitations of other approaches used so far for the purpose, including ANN and casting process simulation. Unlike an ANN model, which presents challenges in the selection of training model and requires a large amount of input data for the purpose, the proposed approach can be directly applied to existing data. In comparison with casting process simulation, which requires a 3D model of casting, thermo-physical property data for the casting alloy, accurate specification of the boundary conditions, followed by mesh generation, solver computation, post-processing, and interpretation of results, the proposed approach is much simpler to apply by foundry engineers.

Moreover, the proposed approach cannot only identify the cause of casting defects but also highlight the range of process parameters that should be avoided to minimize the occurrence of those defects. The relative ease and speed compared to other methods make this approach particularly useful for such industrial applications. Automatic localization of casting defects with convolutional neural networks was introduced in Ferguson, Lee & Law, (2017) identified several different convolutional neural network (CNN) architectures can be used to localize casting defects in X-ray images. The advantage of transfer learning is allowed to localized models to be trained on a relatively small dataset. In an alternative approach, a defect classification model on a series of defect images and then use a sliding classifier method to develop a simple localization model. This compares localization accuracy and computational performance of each technique. Promising results were shown for defect localization

on the machine database of X-ray images called (GDXray) dataset and establish a benchmark for future studies on this dataset (Ferguson *et al.,* 2017).

Das *et al.,* (2015) brought about methodology for modelling and monitoring of centrifugal casting process. In this a study, a process monitoring strategy has been devised for a centrifugal casting process using data-based multivariate statistical technique, namely, partial least squares regression (PLSR). The practical implication of the study involves development of a software application with a back-end database which would be interfaced with a computer program based on PLSR algorithm for estimation of model parameters and the control limit for the monitoring chart. It would help in easy and real-time detection of faults. Based on a case study, the PLSR model constructed for this study seems to mimic the actual process quite well which is evident from the various performance criteria (predicted and analysis of variance results (Das *et al;* 2015).

2.4 Intelligent Design and Materials Selection

Decision support systems in the metal casting industry by Prasad and Ratna (2018); the study adopted a framework developed by Ngai *et al.,* (2009) on selection of material is a AI application of artificial intelligence techniques in metal casting. The necessary time needed for casting a large, intricate and geometric object can be significantly shortened by computer aided development methods. Optimising metal casting by means of artificial intelligence avoids costly changes as a result of casting defects and reduces post processing operations and the quality of cast product increased. Artificial Intelligence help the engineer to predict accurately the process parameters, mould design and sand mixtures required to produce a non- defective cast. It gives the engineer an insight into the kind of facilities they would use for prevention of defects in castings thereby avoiding the trial and error methods that leads to huge financial loss. Hence, Artificial Intelligence helps engineers in modelling a conservative design decisions when building a production platform. Overdesigned equipment essentially results in wastages in terms of money. For instance, one millimetre error in diameter of a casting can bring a lost on the scale of millions of dollars in capital investment. Hence, AI is a vital factor for cost reduction, wastages and competitiveness. This invariably helps in improving the productivity of the oil and gas industry via production concept, planning, design as well as quality of products.

2.5 Method for Steelmaking and Continuous Casting Production Process

The heuristic rescheduling method for steelmaking and continuous casting production process with multi refining modes developed by Yu *et al*., (2016) is effective rescheduling of casting process. This challenge and presents a comprehensive analysis of start-time delay disturbance, its consequences, and strategies to resolve conflicts. A heuristic rescheduling algorithm is then proposed to allow the system to remain alert to this type of disruption in real SCC production, and to quickly react it with an optimal rescheduling plan that has the minimum total waiting time. The proposed methodology and algorithm are applied to and illustrated through both a simulated prototypical SCC system and Shanghai Bao Steel plant, a real industrial setting. (Yu *et al.,* 2016). The inverse modelling of heat transfer is a useful tool in analysing contact heat transfer at the ingot surfaces during the casting process. The determination of the boundary conditions involves an experimental work consisting in the evaluation of the thermal history, generally at the casting surface, experimentally provided by infrared pyrometers. Additionally, numerical simulations, based on the solution of the 2D transient heat conduction equation, are performed in order to be inversely solved in response to the measured thermal data furnished by the sensor.

2.6 Challenges and Future Works

Numerical analysis is constantly used in casting industry for a better understanding of both the critical aspects related to heat transfer and fluid flow phenomena and the relations between them and the metallographic structures and the formation of microstructure defects in the cast parts. (Das et al., 2015). Some of the thermo physical properties necessary for obtaining very accurate results by using numerical simulation are very often totally missing in case of some alloys which have a very high commercial interest for casting industry. The casting technologies have many advantages as the flexibility of manufacturing some complex geometry. Furthermore, by controlling the casting process can be obtained, through a single processing operation, a cast part which corresponds to the imposed mechanical properties and quality level. This new concept near-net-shaping can be applied in casting by controlling the precision parameters of the process. The accuracy of data as well as the sheer volume is basic information required for evaluating data, recognizing patterns for analysis. AI is replacing the data and forming a databases using digital monitoring to optimize casting products. This will reduces casting defects and costs, as well as efficiency increment in casting.

4.0 CONCLUSION

In conclusion this review deals with the applications of artificial intelligence techniques in metal casting in a real factory setting. The artificial intelligence can help in simulations, manufacturing, advanced planning and scheduling casting systems. Subsequently, AI also help in machine learning algorithms such as decision tree, random forest, artificial neural network, and support vector machine which can be used for casting product quality prediction Finally, AI is feasible in performance model of casting through quality process, cost and time which is very important in casting manufacturing process.

REFERENCES

Bertelli, F., Silva-Santos, C. H., Bezerra, D. J., Cheung, N., & Garcia, A. (2014). *An Effective Inverse Heat Transfer Procedure Based on Evolutionary Algorithms to Determine Cooling Conditions of a Steel Continuous Casting Machine. Materials and Manufacturing Processes, 30(4), 414–424.* doi:10.1080/10426914.2014.952038

Das, A., Mondal, S. C., Thakkar, J. J., & Maiti, J. (2015). A methodology for modeling and monitoring of centrifugal casting process. International Journal of Quality & Reliability Management, 32(7), 718–735. doi:10.1108/ijqrm-07-2013-0122

Ferguson, M., Ak, R., Lee, Y.-T. T., & Law, K. H. (2017). *Automatic localization of casting defects with convolutional neural networks. 2017 IEEE International Conference on Big Data (Big Data).* doi:10.1109/bigdata.2017.8258115

Gavarieva, K. N., Simonova, L. A., Pankratov, D. L., & Gavariev, R. V. (2017, September). Development of expert systems for modeling of technological process of pressure casting on the basis of artificial intelligence. In *IOP Conference Series: Materials Science and Engineering* (Vol. 240, p. 012019).

Hetmaniok, E., Słota, D., & Zielonka, A. (2015). *Restoration of the cooling conditions in a three-dimensional continuous casting process using artificial intelligence algorithms. AppliedMathematicalModelling, 39(16), 4797–4807*

Kittur, J. K., Manjunath Patel, G. C., & Parappagoudar, M. B. (2015). Modeling of Pressure Die Casting Process: An Artificial Intelligence Approach. International Journal of Metalcasting, 10(1), 70–87.

Kujawinska, A., Rogalewicz, M., Piłacińska, M., Kochański, A., Hamrol, A., & Diering, M. (2016). Application of dominance-based rough set approach (DRSA) for quality prediction in a casting process. *Metalurgija*, *55*(4), 821-824.

Lee, J., Noh, S. D., Kim, H. J., & Kang, Y. S. (2018). Implementation of cyber-physical production systems for quality prediction and operation control in metal casting. *Sensors*, *18*(5), 1428.

Lei, Z., & Su, W. (2019). Research and application of a rolling gap prediction model in continuous casting. *Metals*, *9*(3), 380.

Marani Barzani, M., Zalnezhad, E., Sarhan, A. A. D., Farahany, S., & Ramesh, S. (2015). *Fuzzy logic based model for predicting surface roughness of machined Al–Si–Cu–Fe die casting alloy using different additives-turning. Measurement, 61,150–161.*

Mishra, N., & Rane, S. B. (2018). *Prediction and improvement of iron casting quality through analytics and Six Sigma approach. International Journal of Lean Six Sigma.*

Pan, Q.-K. (2016). *An effective co-evolutionary artificial bee colony algorithm for steelmaking-continuous casting scheduling. European Journal of Operational Research, 250(3), 702–714.* doi:10.1016/j.ejor.2015.10.007

Peng, K., Pan, Q. K., Gao, L., Zhang, B., & Pang, X. (2018). An improved artificial bee colony algorithm for real-world hybrid flowshop rescheduling in steelmaking- refining-continuous casting process. *Computers & Industrial Engineering*, *122*, 235- 250.

Prasad, D., & Ratna, S. (2018). *Decision support systems in the metal casting industry: An academic review of research articles. Materials Today: Proceedings, 5(1),1298– 1312.*

Qin, H., Fan, P., Tang, H., Huang, P., Fang, B., & Pan, S. (2019). *An effective hybrid discrete grey wolf optimizer for the casting production scheduling problem with multi- objective and multi-constraint. Computers & Industrial Engineering, 128, 458–476.*

Radiša, R., Dučić, N., Manasijević, S., Marković, N., & Ćojbašić, Ž. (2017). Casting improvement based on metaheuristic optimization and numerical simulation. *Facta Universitatis, Series: Mechanical Engineering*, *15*(3), 397-411.

Riaz, F., Kamal, K., Zafar, T., & Qayyum, R. (2017). *An inspection approach for casting defects detection using image segmentation. 2017 International Conference on Mechanical, System and Control Engineering (ICMSC).*

Sata, A., & Ravi, B. (2016). *Bayesian inference-based investment-casting defect analysis system for industrial application. The International Journal of Advanced Manufacturing Technology, 90(9-12), 3301–3315.*

Singha, S. K., & Singh, S. J. (2015). Analysis and optimization of sand casting defects with the help of artificial neural network. *Int J Res Eng Technol*, *4*, 24-29.

Yu, S., Chai, T., & Tang, Y. (2016). *An Effective Heuristic Rescheduling Method for Steelmaking and Continuous Casting Production Process With Multirefining Modes. IEEE Transactions on Systems, Man, and Cybernetics: Systems, 46(12), 1675–1688.*

PERFORMANCE EVALUATION OF SOLAR ENERGY CLOTH IRONING SYSTEM

[1]Emmanuel .N. Ogbonna, [2]James O.Okegbile

[1]Department of mechanical engineering, school of Infrastructure Process Engineering and Technology, Federal University of Technology, Minna, Niger State, Nigeria, nkembest21@gmai.com

[2]Department of mechanical engineering, school of Infrastructure Process Engineering and Technology, Federal University of Technology, Minna, Niger State, Nigeria, ojokegbile@gmai.com

Nkembest21@gmail.com 07069000930 & 08122078778

Abstract: Charcoal is mainly used in the ironing of clothe in rural areas. This is a non-renewable energy. There is need to develop a solar cloth ironing system to replace this non-renewable energy source with negative impact on the environment. The iron received its heat from concentrated parabolic reflective dish. The design of the iron was based on the mass of aluminum required to be heated to a temperature of 155 ^{o}C in a period of 30 minutes.. Hourly readings of solar radiation of Benin on horizontal surface were collected from February to April 2020. These readings showed that the highest value of Benin solar radiation obtained in February was 365.35 MJ/m^2. Daily maximum and minimum temperature readings of Benin were also collected for the same period; showed that the highest value of 123.7367 ^{o}C was obtained in February 2020. Similarly, temperature reading of the parabolic dish was taken for three months. The readings for the three months (February to April, 2020) were taken from 8:00am to 5:00pm. Hence, sad iron temperature readings of April were taken from 8:00 am to 2:00pm daily. Readings of time taken to use sad iron to iron 100% cotton clothes of consecutive 1 to 6 yards were taken. Result of the response of the linear mode of the linear model of the SPSS 22.0 software for 100% cotton material of different sizes. . The Model F-value of 52.45 implies the model is significant since Values of "Prob > F" less than 0.0500 indicate model terms are significant. The R-square value of 0.929 (92.9 %) also confirms the significance of the data since 0.929 is very close to unity (1). From the foregoing the model below was generated from the software to determine ironing time for 100 % cotton material in terms of sad iron temperature and material size (yards) . In a similar development, the model was generated from the software to determine ironing time for 100% polyester material in terms of sad iron temperature and material size (yards) after establishing the significant of the obtained data. From these models, the observed and the estimated ironing periods were statistically and graphically analyzed to arrive at a decision which makes the model acceptable. From the economic point of view, the sad iron was economically compared to charcoal and electric cloth ironing systems. The results obtained from the comparisons showed that the sun of initial purchase and running costs of electric, charcoal and sad irons, after being used for ten years were ₦47,658, ₦34, 200 and ₦20, 000 respectively which revealed that the sad iron was economical than the others.

Key words: *Parabolic dish collector, sad iron, renewable energy & domestic solar ironing*

INRODUCTION

(Ozturk, 2007) conducted several experimental researches on solar parabolic cookers and analyzed the performance parameters in terms of thermodynamic laws. Ozturk experimentally examined energy and exergy efficiencies of a simple design and the low cost parabolic reflective concentrators under the climatic conditions of adana which is located in southern turkey. the energy output of the parabolic reflector was determined to be 20.9–78.1w, whereas its exergy output was in the range of 2.9–6.6 w. the results showed that the energy and exergy efficiencies of the parabolic reflector were calculated between 2.8–15.7% and 0.4–1.25%, respectively (Ozturk, 2004).

A parabolic dish reflective concentrator was also investigated from the exergy viewpoint by (patella, 2005). According to the results, the exergy efficiency of the system was relatively very low approximately 1% while the energy efficiency ranged from 6% t0 19%.

Similarly, (Shukla, 2009) presented the energy and exergy efficiencies of two types of parabolic solar cookers which were tested in summer and winter in the climatic conditions of India. the results showed that the energy output of the community and domestic solar cookers varied from 2.73 to 43.3w and 7.77 to 33.4 w, respectively whereas the exergy output of the cookers ranged from 1.92–2.58w to 0.65–1.45w, respectively. On the other hand, the energy efficiencies of the community and domestic solar cookers were in the range of 8.3–10.5% to 7.1–14.0%, respectively .Al-soud, et al., (2010) designed, operated and tested a parabolic reflector with automatic two

axes sun tracking system. The test results showed that the water temperature inside the cooker's tube reached 90°c when the maximum registered ambient temperature was 36°c.

In another recent review carried out by Hereza, et al. (2018), the work presented a review on the fundamentals of solar reflectors with a detailed description of the influence of several key-parameters on their performance. Exergy and exergy analysis were presented and environmental and economic studies were also developed. the economic study was carried out to compute the payback period for different solar heating system (solar box cooker, solar panel cooker, parabolic solar cooker and evacuated tube solar cooker with thermal storage, etcetera) for several scenarios in Lebanon (home, hotel, restaurant snack), the results confirmed that the payback period decreased from 96 to 24 months in home, restaurant, hotel and snack. The authors also reviewed the environmental study and pointed out that there is decrease of carbon dioxide production on the utilization of solar heating devices. The carbon dioxide emission decreased from 60.55 to 30.27 kg/month, 6055.2 to 3027.6 kg/month, and 3996.43 to 1998.21 kg /month and from 908.28 to 454.14 to kg/month in home, restaurant, hotel and snack respectively.

The aim of this project work is to evaluate the performance of domestic solar energy cloth ironing system, while the objectives are as follows:

1. Evaluating performance of the solar system in domestic ironing
2. Determination of effect of temperature on ironing time
3. Comparing it's cost to cost of electric and charcoal ironings

On the contributing to knowledge, the work also brought in a new technology to the fabrication of cloth pressing iron by introducing a sad aluminum iron, which iron that is not hollow but rather complete solid in structure. Aluminium being light in weight, a very good conductor of heat, has good surface finishing ability as suggested by (cue & cue,2013).

MATERIALS AND METHODS

The equipment listed below were used in carrying out this research work.

Materials:

i. Sad pressing iron. ii. Parabolic solar dish (Dia.=600, thickness 2) iii. Reflector. iv. Focus stand (L=300, W=40) v. Clamps. vi. Stand (L=2000, Dia.=50). vii. Black mild steel sheet mental (thickness 3, L=100, W=50) viii. Abro Silicon gum ix. Glass (4mm thickness, black)

All dimensions are in mm.

Equipment:

i. Reference Thermometer ii. Solarimeter (Solar Meter) iii. Digital Stop Watch

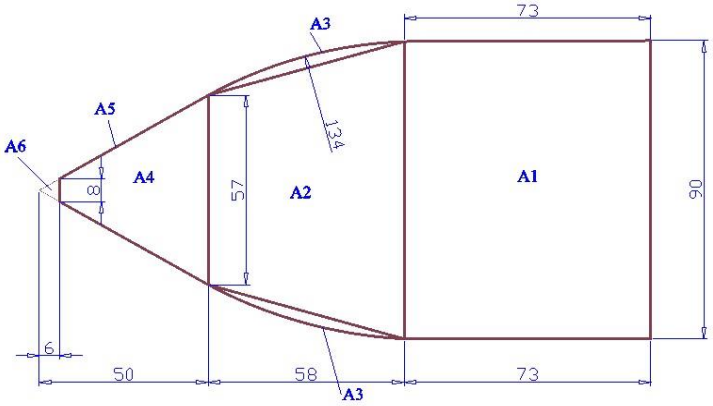

All dimensions in mm

Figure 1: The base of the Sad Iron

This enables easy calculations of the ironing surface area of the iron; Aabs.

$$A_{abs} = A_1 + A_2 + 2A_3 + A_4 \quad (2.1)$$

Where A_1 = Area of rectangle = L x B, L is length = 73 mm, B is breadth = 90 mm, A1= 73 X 90 = 6570 mm^2, A_2 = Area 0f trapezium = $^1/_2$(a+b) h, where a = 90, b = 57, h = 58,

Substituting the values of a, b, and h into A_2 gives

$A_2 = {}^{1}/_{2}(90+57) \times 58 = 4263\ mm^2$ (2.2)

A_3 = Area of segment $= \frac{1}{2} r^2 \left[\left(\frac{\pi}{180}\right)\theta - sin\theta\right]$

Where r = 134 mm, $\theta = 26°$

Substituting into A_3 gives

$$A_3 = \frac{1}{2} \times 134^2 \times \left[\left(\frac{\pi}{180}\right)26 - sin26\right] = 2772 \quad (2.3)$$

$$2A_3 = 2 \times 2772 = 5544\ mm^2$$

But $A_4 = A_5 - A_6$

When $A_5 = \frac{1}{2} b_1 h_1$

$$A_6 = \frac{1}{2} b_2 h_2 \quad (2.4)$$

$b_1 = 57\ mm, b_2 = 8\ mm h_1 = 50\ mm, h_2 = 6\ mm$

So $A_4 = \frac{1}{2}(b_1 h_1 - b_2 h_2) = {}^{1}/_{2}(57x50 - 8x6) = \mathbf{1401\ mm^2}$

Summing all the components areas;

$A_{abs} = A_1 + A_2 + 2A_3 + A_4 = 17{,}783\ mm^2$ (2.5)

Design Analysis

Dimension of the parabolic dish reflector

The Height of the reflector of a symmetrical parabola are related by equation (El Quedermi, et al, 2009) expressed as

$$h = \frac{R_{rim}^2}{4f} \quad (2.6)$$

Where f is focal length, R_{rim} is the rim radius, h is parabolic dish depth.

The relationship between focal length with the rim angle and aperture diameter of the parabolic dish can be found in terms of the dish dimension (Yahuza, et al., 2016). The relationship is expressed as: -

$$\varphi_{rim} = tan^{-1}\left[\frac{{}^{8f}/_{D_{ap}}}{16\left({}^{f}/_{D_{ap}}\right)^2 - 1}\right] \quad 2.7$$

Where φ_{rim} is Rim angle,

The aperture opening area A_{ap} is expressed as

$$A_{ap} = \frac{\pi D_{ap}^2}{4} \quad 2.8$$

Where Dap is aperture diameter

Surface area of the parabolic dish

The expression for the determination of the surface area of the parabolic dish is given by El Quedermi, et al. (2009) as : -

$$A_s = \frac{8\pi}{3} f^2 \left[\left[1 + \left[\frac{D_{ap}}{4f}\right]^2\right]^{3/2} - 1\right] \quad (2.9)$$

Where A_s is Surface area, f is focal distance

The volume of the dish can be determined as thus: -

$$V_c = \frac{1}{2}\pi R_{rim}^2 h \quad (2.10)$$

Where V_c is dish volume, R is rim radius, h is height of the parabolic dish

Calculations involving solar radiation

The extra-terrestrial solar radiation in Nigeria can be calculated as given by F0laranmi (2009) as:

-

$$R_X = I_{XC} A_{CL} \quad (2.11)$$

Where R_X is Extra-terrestrial radiation, I_{xc} is solar constant = 1353 KWh, A_{CL} is c0ntinental area = 9.3277 x 1011 (m^2)

Energy Balance

The expected power of the parabolic reflector (Q_C) is given by Yahuza, et al. (2016):

$$Q_C = I_{XC} \times A_{ap} \rho \quad (2.12)$$

Where I_{XC} is solar constant = 1353 kWh (Yahuza, et al., 2016), A_{ap} is aperture opening area = 0.282 m^2 ρ is reflectance of the mirror = 0.98 (Yahuza, et al., 2016)

Quality of material required for the sad iron

By the definition of specific heat capacity, when the temperature of an object increases, it has gained energy (Revision Science, 2018). The amount of energy depends on: -the temperature change (ΔT), the mass of the object (m), the specific heat capacity (c)

The specific heat capacity is different for different materials. It is the energy needed to increase the temperature of 1 kg of the material by 1°C and is measured in J/kg °C. The energy required can thus be expressed as: -

$$E = m \times C \times \Delta T \quad (2.13)$$

Where E is Energy, m is mass, c is specific heat capacity and ΔT is temperature change

The energy supplied can als0 be expressed as: -

$$E = W \times t \quad (2.14)$$

Where E is energy supplied, W is power and t is time

Combining equations 2.20 and 2.9 and simplifying give

$$m = \frac{t \times W}{C \times T} \quad (2.15)$$

Where m is mass of Aluminium to be molded to form the sad iron, and W is Power supplied to the sad iron from the parabolic dish

Design Calculation and specification

The values of the input parameters for designing the critical components of the solar powered sad iron system are given below.

Table 2: Design specification of the input parameters

Parameter	Specification
Aperture diameter of dish, D_{ap}	0.6 m
The depth of the parabolic dish, h	0.05 m
Focal length of the parabolic solar dish	0.45 m
Solar constant, I_{XC}	1353 kWH
Continental area, A_{cl}	9.3277 x 10^{11} m^2
Reflectivity of the mirror, ρ	0.98 (Yahuza, et al., 2016)
Aperture opening area, A_{ap}	0.282 m^2
Bright sunshine hours	9 h0urs
Power supplied, W	374.843 W
Efficiency range, 40%-60%	187.4215 W (Magal, 1993)
Specific heat capacity of aluminium, c	621.096 J/kg/K
Ironing cloth temperature, T	155 ^{0}C
Time taken to heat iron to required temperature, t	30 minutes
Mass of the sad iron to moulded, m 2.36 kg	2.36 kg

The design procedures of various parts of the system with their detail explanation are given as follows:

Parabolic dish focal distance, f

The focal distance f, of the parabolic dish is expressed as:

$$f = \frac{D_{ap}^2}{16h} \quad (2.16)$$

Substituting for D_{ap} and h gives:

$$f = \frac{0.6^2}{16 \times 0.05} = 0.45 \text{ m} \quad (2.17)$$

Rim angle, $\boldsymbol{\varphi_{rim}}$

From equation (2.20), Rim angle, φ_{rim} is expressed as

$$\varphi_{rim} = tan^{-1}\left[\frac{{}^{8f}/_{D_{ap}}}{16\left({}^{f}/_{D_{ap}}\right)^{2}-1}\right] \quad (2.18)$$

Substituting various parameters from the specification table gives

:

$$\varphi_{rim} = 36.87^{0} \quad (2.19)$$

Aperture opening area, A_{ap}

From equati0n (3.8), the aperture opening area, A_{ap} is expressed as:

$$A_{ap} = \frac{\pi D_{ap}^{2}}{4} \quad (2.20)$$

Substituting value of D_{ap} gives:

$$A_{ap} = \frac{3.124\times 0.6^{2}}{4} = 0.2827 \text{ m2} \quad (2.21)$$

Extra-terrestrial radiation, R_X

From equation (2.22) extra-terrestrial radiation, R_X for Nigerian is expressed as

$$R_X = I_{XC}A_{CL} \quad (2.22)$$

Substituting various parameters from the specification table gives:

$$R_X = 1.262 \times 10^{15} Wh/m^{2} \quad (2.23)$$

For an average of nine hours of bright sunshine hours

$$R_X = 9 \times 1.262 \times 10^{15} = 1.1353 \times 10^{16} W/m^{2} \quad (2.24)$$

Expected power of the parabolic reflector, Q_C

From equation (3.12) the expected power of the parabolic reflector, Q_C is expressed as:

$$Q_C = I_{XC} \times A_{ap}\rho \quad (2.25)$$

Substituting values of I_{xc}, A_{ap}, and ρ parameters gives:

$$Q_C = 1353 \times 0.2827 \times 0.98 = 374.843\ W \quad (2.26)$$

Design of Sad iron

From equati0n (3.15), the mass of Aluminium to be molded to form the sad iron (m) is expressed as:

$$m = \frac{t\times W}{C\times T} \quad (2.27)$$

Substituting various parameters from the specification table gives:

$$m = \frac{30\times 60\times 187.4215}{921.096\times 155} = 2.36\ kg \quad (2.28)$$

From the above, the mass of the sad iron to be molded for this work is designed to be **2.36 kg.**

Selection of type of pressing iron to use

The faulty electric irons were used due to the fact that the proposed sad irons are out dated and relatively scarce and the cost of making it locally by molding and casting will be relatively higher than the cost of purchasing faulty electric iron. These particular faulty electric irons were used because they have almost the same heat absorption and retention rates with the sad irons, after experiments were carried out to determine the heat absorption and retention of both types of irons it was discovered that the two types of the irons have negligible differences in terms of heat absorption and retention rates.

Data collection

The data used in this work were collected from Nigeria meteorological agency, (NIMET) Benin Airport office, Benin City, Edo state. The data are solar radiation, minimum and maximum temperatures of Benin City, for the period of three months, from February to April 2020. The below are some data tables of the data collected.

Table 3: Minimum and Maximum Temperature of Benin City

Days/Months	Maximum Temperature			Minimum Temperature		
	February	March	April	February	March	April
1	36	35	32	24	28	24
2	37	36	34	24	25	24
3	34	32	35	21	23	26
4	36	34	32	23	26	26
5	33	35	35	24	26	24
6	36	36	34	24	24	26
7	37	38	35	24	24	26
8	38	35	34	23	26	26
9	35	35	35	25	26	26
10	35	35	32	26	27	26
11	36	35	34	25	24	27
12	36	35	36	24	23	26
13	36	35	34	23	26	27
14	37	34	35	23	25	26
15	36	35	35	24	24	27
16	36	35	34	26	26	27
17	35	35	34	26	28	28
18	36	36	34	26	27	26
19	36	34	32	26	27	26
20	36	33	35	26	27	25
21	37	30	35	28	26	26
22	35	34	33	27	26	22
23	36	32	33	27	26	24
24	37	30	34	27	23	26
25	26	33	33	27	25	26
26	35	33	31	26	24	26
27	37	33	34	27	26	24
28	36	34	33	28	26	22
29	34	35	32	26	25	25
30		34	31		26	25
31		33			27	

Table 4: Summary of the Measured Solar Radiation Parameters from February to April 2020 for Benin City.

Month	$\bar{}$(MJ/m^2)
February	302.65
March	346.06
April	354.69
	Mean $\bar{}$= 334.47

The sad iron was placed on a focal support attached to the parabolic dish which lined with pieces of glass of 4mm thickness. The sad iron was placed on the focal support with a distance of 450mm away from the dish, this distance was determined by carrying out several iterations and the optimal position for maximum possible heat was obtained to be within the range of 450mm to 490mm

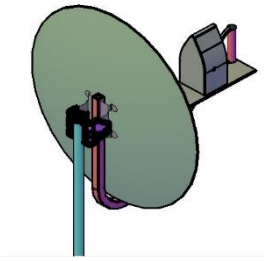

Figure 2: Assembled Drawing of the solar ironing system

The whole unit comprising of the b0th the reflective dish and the focus support are rotated to the direction of the Sun. If the sad iron is to be used before noon, the system is rotated to the East, while if it is in the afternoon, the system is rotated to the west facing the Sun. Thereafter, the reflective dish lock nut is tightened to restrict any further rotation.

Table 5: Data obtain from daily Maximum Temperature Reading of Sad Iron from February to April 2020 in Benin City.

Days of the Month	Maximum Temperature			Days of the Month	Maximum Temperature		
	February	March	April		February	March	April
1	36	35	32	17	35	35	34
2	37	36	34	18	36	36	34
3	34	32	35	19	36	34	32
4	36	34	32	20	36	33	35
5	33	35	35	21	37	30	35
6	36	36	34	22	35	34	33
7	37	38	35	23	36	32	33
8	38	35	34	24	37	30	34
9	35	35	35	25	26	33	33
10	35	35	32	26	35	33	31
11	36	35	34	27	37	33	34
12	36	35	36	28	36	34	33
13	36	35	34	29	34	35	32
14	37	34	35	30		34	31
15	36	35	35	31		33	
16	36	35	34				

RESULTS AND DISCUSSION

Results of monthly mean minimum and maximum ambient temperatures (˚C)

The monthly mean minimum and maximum ambient temperature from February to April 2020 in Benin City is presented in Figure 3 below. This chart showed that February had the higher values of average maximum temperatures of 36.51 ˚C. The lowest minimum monthly average temperature was also observed in the months of February.

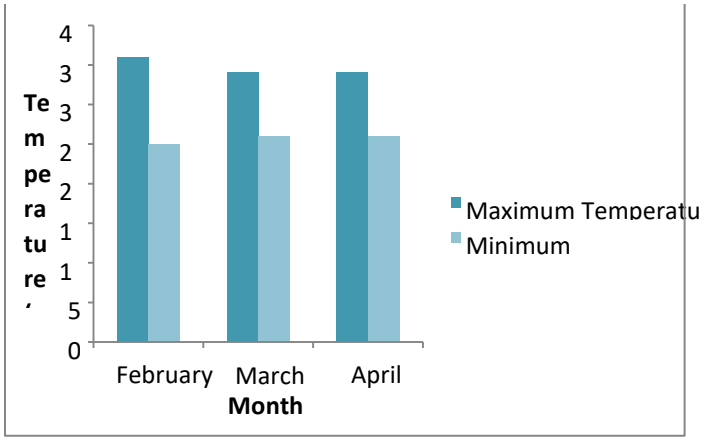

Figure 3: Monthly mean Minimum and Maximum Ambient Temperatures (^{0}C) from February to April 2020 for Benin City.

Results obtained from Ironing Different Sizes of Cloth Material

Results from sad iron temperature readings when ironing different sizes (yards) of 100 % cotton and 100 % polyester materials

Figure 4: shows the plot of the results obtained from sad iron temperatures readings when ironing 100 % cotton and 100 % polyester materials of different sizes of 1 to 6 yards. The results obtained showed that the lowest ironing temperature for 100 % cotton material was observed to be about 84 $^{\circ}$C, while the lowest ironing temperature to iron 100% polyester material was at an average temperature of 100 $^{\circ}$C. The 100% cotton material of sizes 2, 3, 4, 5 and 6 yards were ironed at average temperature of 115.0 $^{\circ}$C, 93.2°C, 128.7°C, 110.1°C and 133.1°C respectively. Ironing temperatures for 100% polyester materials were 105.2°C, 100.0^{0}C, 121.1^{0}C, 131.6^{0}C, 115.0^{0}C and 141.6°C for 1 to 6 respectively. It was observed that the ironing temperatures were not in an orderly manner; this was so because the ironing temperatures depend on the daily temperature of Benin City at the period of the experiment. It was also noted that the minimum ironing temperature required to iron 100 % cotton material is lesser that 0f 100% polyester material. This means that it takes a higher temperature of sad iron to iron 100 polyester materials than 100 % cotton material. Consequently, in a given size 0f cotton material, the temperature needed to iron the material is directly proportional to the polyester contents of the cotton material. Finally, there is similarity in the trend of the curves of both 100% cotton and 100% polyester materials as shown in Figure 5

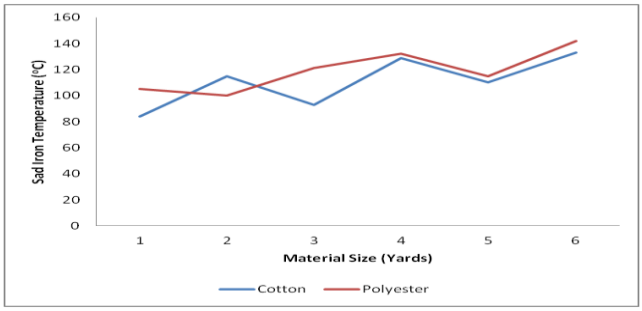

Figure 4: Experimental ironing temperatures against different sizes (yards) of 100 % cotton & polyester materials

Results from time taken to iron different sizes (yards) of 100 % cotton material

Figure 5, shows the plot of results of time taken to iron different sizes (yards) of 100 % cotton and polyester materials. The results obtained showed that the lowest ironing time for 1 yard of both cotton and polyester materials were 3.1 and 4.8 minutes respectively. The average ironing times for 2 yards were 4.7 and 6.4 minutes for 100% cotton and 100% polyester materials. The average ironing time for 3, 4, 5 and 6 yards of 100% cotton materials were 6.7,6.05, 8.9 and 11.9 minutes respectively. While it took average periods of 5.3, 5.1, 8.0 and 8.4 minutes to iron 3, 4, 5 and 6 yards of 100% polyester material respectively Details of the readings is presented in appendix 5.

The experimental results obtained from time taken to iron different sizes (yards) of 100 % cotton material, it was observed that the higher the sad iron temperature, the lesser the ironing time for a particular material size. Also to a large extent, the time taken to iron a cloth of a given size of material depended on the temperature of the sad iron which directly depended on the daily ambient temperature.

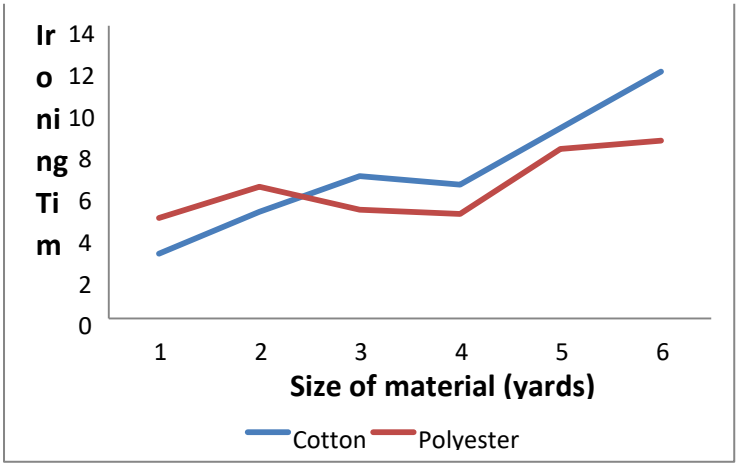

Figure 5: Plot of experimental ironing time against different sizes (yards) of 100 % cotton & polyester materials.

Generation of models for the estimation of ironing time

Analyses of the results obtained from these experiments using SPSS 22.0 software is presented below:

Ironing 1 – 6 Yards of 100 % Cotton Material

Table 5, below presents the result of the response of the linear model of the SPSS 22.0 software for 100% cotton material of different sizes. The Model F-value of 52.45 implies the model is significant since Values of "Prob > F" less than 0.0500 indicate model terms are significant. The R-square value of 0.929 (92.9 %) also confirms the significance of the data since 0.929 is very close to unity (1). From the foregoing the model below was generated from the software to determine ironing time for 100 % cotton material in terms of sad iron temperature and material size (yards):

$$t_c = 1.48 + 1.64Y - 0.041T \quad (4.1)$$

where t_c is the time taken to iron 100 % cotton material in minutes, T is sad iron temperature, ^{0}C and Y is material size in yards.

Table 6: Response Surface Regression Model

Model Summary

Model	R	R Square	Adjusted R Square	Std. Error of the Estimate	Statistics		
					Mean Square	F	Sig.
Cotton	0.964	0.929	0.911	0.909	49.703	52.445	0.002

Ironing 1 – 6 yards of 100 % polyester material

Table 6, shows the result of the linear model of the design expert software for 100% polyester material of different sizes. The Model F-value of 13.42 implies the model is significant since Values of "Prob> F" less than 0.0.0168 indicate model terms are significant. The R-square value of 0.9328 (93.28 %) also confirms the significance of the data since 0.8703 is very close to unity (1). "Adeq Precision" measures the signal to noise ratio. A ratio greater than 4 is desirable. A ratio of 9.338 indicates an adequate signal, which confirms that the model can be used to navigate the design space. From the foregoing the model below was generated from the software to determine ironing time for 100 % polyester material in terms of sad iron temperature and material size (yards): -

$$t_p = 0.93 + 1.88Y - 1.97T \quad (4.2)$$

Where t_p is the time taken to iron 100 % polyester material in minutes, T is sad iron temperature, ^{0}C and Y is material size in yards.

Table 7: Response Surface Linear Model
Model Summary

Model	R	R Square	Adjusted R Square	Std. Error of the Estimate	Statistics		
					Mean Square	F	Sig.
Polyester	0.911[a]	0.830	0.788	0.6727	0.830	19.560	0.011

Observed ironing time and estimated ironing time

The results of the estimated ironing time for 100% cotton material and 100 % polyester material using respective models for each are presented in this section. Figure 6 shows the result of the observed and modeled time to iron 100% polyester material of 1 to 6 yards.

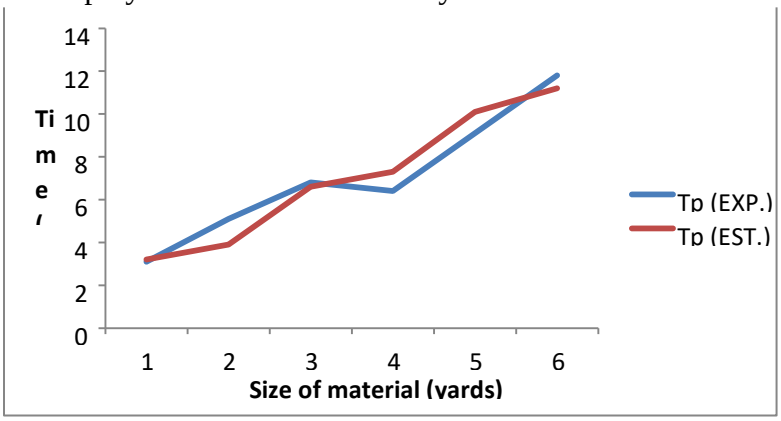

Figure 6: Observed Ironing Time and Estimated Ironing Time for 100 % cotton material

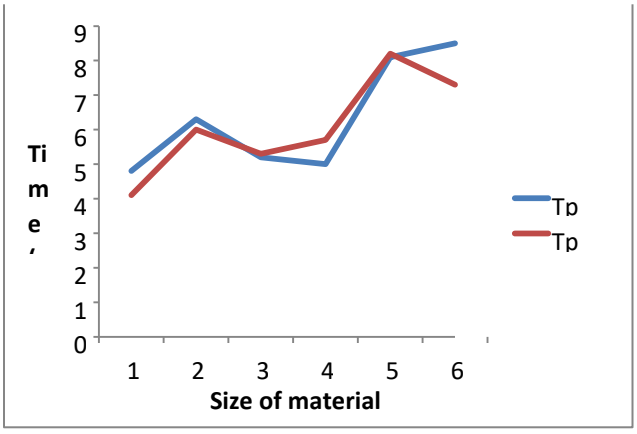

Figure 7: Observed Ironing Time and Estimated Ironing Time for 100 % polyester material

From the Figure 7, above, it can be observed that there is strong correlation between the experimental observed values and the model estimated values of the ironing time as being estimated from the generated model equations.

CONCLUSION

Economic Benefit of Using Sad Iron for Ten Years

Table 8 shows the consumption of different pressing irons after being used to iron clothes for ten years. The table showed that the initial cost price of the electric iron was ₦ 10, 000, the charcoal iron was purchase at the cost price of ₦ 3, 000 and the sad iron was purchase at a total cost of N 20, 000. The table also showed a ten years running cost of using the electric, and the charcoal irons at the rates of ₦ 37, 908 and ₦ 34, 200 respectively, while the sad iron does not have a running cost. Finally, the sun of initial purchase and running costs of electric, charcoal and sad irons after being used for ten years are ₦ 47, 658, ₦ 34, 200 and ₦ 20, 000 respectively. From these analyses, the cost of running sad iron is about 57% lesser than using the charcoal iron.

Table 8: Different Iron Types and their Consumption for Ten Years

Type of iron	Cost price	Considered Usage hours (10 years)	Running cost/hour	Total running cost	Total Cost (₦)
Electric Iron	₦ 10, 000	1560 hours	24.14	37,658	₦ 47, 658
Charcoal Iron	₦ 3, 000	1560 hours	20.00	31, 200	₦ 34, 200
Sad Iron	₦ 20, 000	1560 hours	0	0	₦ 20, 000

REFERENCES

Gebhardt, F. S. and Herlinger, k.(2000). Fibers Survey in Ullmann's Encyclopedia of Industrial Chemistry, Wily-VCH, Weinheim. doi:10.1002/14356007.a10_451

Hereza, A,. Ramadana, M. & Khaleda, M (2018). Review on solar cooker systems: economic and environmental study for different Lebanese scenarios. Elsevier – Renewable and sustainable Energy Reviews. 81 (2018), 421-432

Butti, K. & Perlin J. (1980). A golden thread: 2500 year of Solar Architecture and Technology. The Cheshire Books, University of Michigan. 116 – 143.

El Quedermi, A. R., Ben-Saleh, M, Askri, F., Ben-Narallah, M., Aloui F. (2009), Experimental Folaranmi J (2009) Design construction and testing of a parabolic solar steam generator. Leonardo Electronic J Practices and Technologies, 115-133.

Cuce, E. & Cue, P. M. (2013). A comprehensive review on solar cookers, Elsevier – Applied Energy-102 (2013) 1399-1421.

Butti, K. & John P. (1980) A Gold Thread: 2500 Year of solar Architecture and Technology, Cheshire Books, Palo Alto.

Ghai M. L. (1953). Design of reflector type direct solar cookers. J Sci Ind Res. 1953, 12A, 165-175.

Al-soud, M. S., Abdallah, E., Akayleh, S., & Hrayshat, E.S. (2010). A parabolic solar cooker with automatic two axes sun tracking system. Applied Energy. 87,463-470

Humboldt State University Arcata (2000). Campus Center for Appropriate Technology, CA 95521. Retrieved 22-12-2017 from www.humboldt.edu/-ccat

Leverette, M. M. (2016). How to Select the Correct Ironing Temperature for All Fabrics.
Laundry and laundry rooms expert. http://laundry.about.com/od/ ironing/a/irontemp.htm) Retrieved 22-122017.

DESIGN ANALYSIS OF WATER-COOLED SOLAR PANEL SYSTEM

Abubakar Jibril,[1] A. B. Hassan[1], Alkali Babawuya[2], M. M. Muhammadu[1] and [1]Aminu O. I.

Department of Mechanical Engineering, Federal University of Technology, Minna
Department of Mechatronics Engineering, Federal University of Technology, Minna

Corresponding Author: abuzhim2015@gmail.com, 07037070547.

Abstract

Photovoltaic cells otherwise known as solar panel, converts irradiance into electrical energy. During this process of conversion, the temperature of the PVC increased as it absorbs solar irradiance lead to a reduction in its output power. This problem affects the performance of the PVC especially in the hotter regions of the world. In this research, a water cooling system was designed to the PV panel in order to reduce its temperature. The objective of this research is to carryout design analysis of the system for possible fabrication and performance evaluation. The design analysis results shows an insulator thickness of 5.5 mm and a theoretical water temperature of 62.3^{o}C was attained, which implies a 5.2^{o}C reduction in PVC temperature.

Keywords: PV Module, Pressurized Fluid, Flow rate, Heat exchanger, Cooling.

1.0 Introduction

The use of solar photovoltaic (PV) electric systems is growing rapidly in the sustainable renewable energy market and is expected to play an important role in the future sustainable energy mix (Saira, Samia, Atta, Hazeema,, & Anab, 2018). On the other hand, the initial capital cost of the PV modules and systems has always been a major barrier to the widespread use of this technology over the globe. The initial price of solar PV systems can be reduced by producing more power with the same PV module. The PV module's power output can be increased by increasing the incident solar radiation falling on a PV module according to the inherent characteristics of the PV cells. The distribution of solar radiation is not constant throughout a day. Photovoltaic panels absorb incident solar energy converting directly a small part of it into electrical energy. A limited wavelength of the incoming irradiation on the PV cells is converted into electrical energy with an electrical efficiency of 15 %–20 %, while the remaining energy is wasted as thermal energy causing the major problem of heating of PV modules, consequently increasing its surface temperature and thus decreasing the electrical efficiency (Huan-Liang, 2014).The efficiency of the energy conversion depends strongly on the type of the solar cell and its technology, as well as the operating and environmental conditions such as surface temperature of PV panel, solar irradiation intensity, air temperature and its humidity, air dust, and mass flow rate of cooling fluids (Chandra, Goel,, & Ray, 2015).

the development of new technologies of the PV panels and the improvement of existing available ones are necessary to increase the panel electrical efficiency by decreasing its high surface temperature utilizing appropriate cooling techniques. The reduction in the electrical power of the PV module is 0.65% per 1 deg of temperature increase within the range from 22℃ to70℃ (Arjyadhara & Bhagbat, 2017). In addition, the conversion efficiency and power output of the PV panel decrease by 0.08 % and 0.65 %, respectively, per 1 deg of temperature increment up to 80℃ (Swar, Mohammed,, & Mustafa, 2017).

Cooling of PV panels can be achieved by either passive or active cooling systems. Active and passive cooling systems may coexist in order to obtain better efficiency. The passive cooling system of the PV panels that is achieved by three basic heat transfer mechanisms such as free convection, conduction, and radiation depends on the buoyancy-driven flow of the working cooling fluid in a duct. The drawbacks of the passive cooling system are dependent on the environmental conditions, its low heat transfer rate, low thermal conductivity, and hence limited temperature reduction. The active cooling system that is performed using liquid or air is comprised of a supplementary device, such as pump to circulate liquids or fan to force air to the panels to extract heat away from the system (Kasaeian, A.,2017). Generally, the active cooling system is used for both increasing the electrical

power output of the PV/T module and supplying available heat to nearby users. Mainly, there are three fundamental working fluids that are employed for the combined PV/T active cooling system: air, water, and refrigerant. The essential advantages of the water cooling system rather than other cooling systems are availability, reliability, low cost, no environmental impact, high thermal conductivity hence higher heat transfer rate, and higher temperature reduction of
/solar energy is one of the most abundant renewable energy resources, but is it characterized with very low conversion efficiency. Another major problem of energy from PV modules is the larger percentage of the solar radiation that incident on the solar panel is converted to heat energy, Therefore, this research seek to develop a water cooling system for a solar panel. Hoping that, this will cool the solar panel thereby improving its electricity conversion efficiency and also harvesting the excess heat to heat up a water for domestic use.

(Bahaidarah, Abdul, Gandhidasan, & Rehman, 2013) investigated the thermal behavior of a PV panel integrated with a water cooling system by producing a 3D models of the PV panels without and with water cooling system and simulated them using ANSYSCFX. The thermal performances of the PV panels without and with water cooling system has been compared and the effect of the inlet water temperature in the cooling case has also been studied detail in method section. A water pump of 373 Watts was used to pump the water flow over the surface of the PV panel from an insulated tank. The experimental measurement of the PV panel with cooling system shows a temperature reduction 7.3 °C in as compared to that without cooling system. This leads to the electrical efficiency of the PV panel with water cooling system has increased 9 %, with a reduction in temperature. Similarity, (Abiola-Ogedengbe, 2016) applied a water-closed circulation to the PV panel to overcome the overheating issues. But in this research work a water pump drained water on the surface of the PV panels and hot water has flowed back into the water tank and circle continues in that manner. The result obtained shows that the PV panel with cooling system has increased an additional 11.6 % of the output power from the PV panel without the cooling system by reducing the temperature of the PV panel.

Photovoltaic (PV) panel is directly converted solar irradiance into electrical energy. The temperature of the PV panel increased as it absorbs solar irradiance lead to a reduction in its output power, (Leow, et al., 2019).This undesired impact can be prevented through the use of a cooling system with PV panel. (Leow, et al., 2019), designed a water cooling system for a PV panel, so as to reduce its temperature. (Saira Iqbal, etal 2016) investigated the effect of water cooling of the energy conversion efficiency of PV cell inclined at 45^{o} using Polycrystalline solar panel having area of $1.2m^2$ 36 x 27 cm^2 of area and a power of 12watt (12v and 0.68A), a battery, a 5L water tank. A knob connected to a hose were used to regulate the water flow. Sponge was used to absorb the water flowing over the panel. Pyranamter was used to monitor water temperature and that of solar panel. The volyage and current from the soalr panel were measured with the used of voltmeter and ammeter. A 8 Watt bulb was used to load and discharge the battery used for the study. The result obtained are 0.50 V and 0.10 A. The efficiency of solar panel against mass flow rate in used ranges between 7% - 12% and the highest PV temperature recorded was 48^{o}.

2.0 Material And Method

2.1 Materials

	Materials	Specification
i	Solar Panel	80 W
iii	DC Pump	12V, 3-6 W
iv	Stand	Mild steel
v	Robber Hose	1.03 cm

2.1 Model description

The sun ray is incident on the solar panel resting on a mild steel stand and the ray heat up the panel, inside the solar panel of 80W are coiled copper tube of 9.5mm diameter.

A DC Pump was used to pump water that flow through the copper tube which in turn cools the solar panel that is already heat up. The water then flows into the heat exchanger tank and heat exchange would take place i.e the water in the tank would heat up and the water from the coiled copper tube would get cool off. The cycle would continue and by so doing the solar panel cools up and in turn would increase the efficiency of PV and intermittently the output of the PV would be recorded.

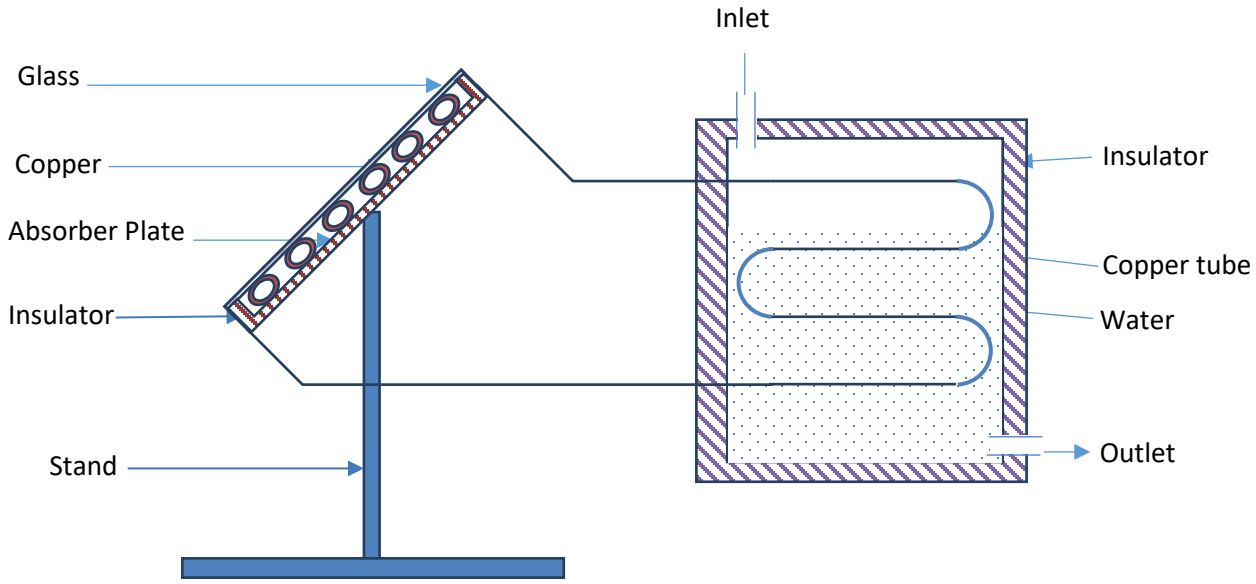

Figure 1: Schematic of the PVC Cooling system

2.2 Solar Collector Design

The solar collector convert the solar energy to heat energy, for other useful purposes. The collector is comprise of the absorber plate, the glass, the insulator cover, the fluid tubes and the frame. (see Figure 1). The design analysis of the collector requires the determination of the amount of heat absorbed through radiation by the solar panel into the copper tubes and the insulator thickness required for maximum retention of the absorbed heat.

The useful heat gain from working fluid from the environment is given by equation 1

$$Q = mC_p(T_o - T_i) \qquad \text{(Kartini, Ag-Sufiyan, Halim, \& Jedol, 2017)} \qquad 1$$

Where $\dot{m}$, C_p, T_0, T_i, is the mass flow rate, specific heat, Outlet and Inlet temperature of working fluid. The Hottel-Whiller equation for the useful heat gain from solar collector is given by equation 2.

$$Q_U = A_P F_R[I_R(\tau\alpha) - U_L](T_o - T_i) \qquad 2$$

Where A_p, F_R, T_a, U_I, I_T, $(\tau\alpha)$ are the area of the absorber plate, Heat removal factor, ambient tem- perature, overall heat loss coefficient, incident solar radiation and the transmittance absorptance product. Heat removal factor in equation 2 is defined by equation 3;

$$F_R = \frac{\dot{m}C_p}{U_L A_p}\left[1 - exp\left(-\frac{FU_L A_p}{\dot{m}C_p}\right)\right] \quad 3$$

Where F' is the collector efficiency factor. And the thermal efficiency of solar collector is calculated from equation 3.8;

$$\eta_e = \frac{Q_U}{I_T A_p} \quad 4$$

2.3 **Heat Exchanger Design**

The function of the heat exchanger in this system is to absorb heat from the solar panel and discharge the heat into reservoir tanks via copper pipe. According to Jaya, (2019), "The temperature difference (ΔT) is not constant throughout the heat exchanger it varies with the length of heat exchanger." The rate of heat transfer in a heat exchanger was expressed by equation 5;

$$Q = UA\Delta T_m \quad \text{(Efstratios, 2015)} \quad 5$$

Where;
Q= Heat transfer rate (kJ/h) (Btu\h);
A = Heat transfer area (m^2) (ft^2);
U= Overall heat transfer coefficient (kJ/h.m^2.°C) (Btu/h°F);
ΔTm= Log mean temperature difference (°C) (°F).

$$\Delta T_m = \frac{(T_1 - T_2) - (T_2 - t_1)}{ln\frac{T_1 - t_2}{T_2 - t_1}} \quad 6$$

Where;
T1 = Inlet tube side fluid temperature;
t2 = Outlet shell side fluid temperature;
T2 = Outlet tube side fluid temperature;
t1 = Inlet shell side fluid temperature.

Where the mean temperature difference (ΔTm) between the hot and cold stream is obtained by using equation 7.

$$T_m = \frac{DT_o - DT_L}{\ln\left({}^{DT_o}/_{DT_L}\right)} \quad 7$$

The overall heat transfer coefficient (U) for the heat exchanger based on the heat exchanger tube outside surface was obtained using equation 8,

$$U_o = \frac{{}^{1}/_{A_0}}{\frac{1}{h_i A_i} + \frac{ln{}^{d_o}/_{d_i}}{2K_w L} + \frac{1}{h_o A_o}} \quad 8$$

When designing a vapor absorption air conditioning system there is a need of mass flow rate at each point to be determined.

According to tubular exchange manufactures association (TEMA) the following specifications are used in the design of a heat exchanger.

0.0666 < (Shell diameter/Tube length) < 0.2
1.25 < Pitch/Outer diameter of tube < 1.5

$$\text{Number of tubes} = \frac{\pi CTP.D^2}{4CL.P^2} \quad 9$$

3.0 Results of the design analysis

The result of the design analysis of PVC cooling system obtained are in shown in Table 1.

S/NO	QUANTITY	VALUE	UNIT
1.	Amount of heat absorbed, Q	351.74	W/m^3
2.	Insulation thickness	5.5	Mm
3.	Efficiency	66.8%	
4.	Area of collector, A_C	0.0855	m^2
5.	Area of copper tube, A_c	0.0339	m^2
6.	Number of coil copper tube, n	9	

4.0 Conclusion

The design analysis of a water cooling system to determine its effect of the performance of a solar panel output was conducted. The system are made of copper tubes laid behind the PVC and water runs through it, with the aid of a heat exchanger. The design analysis result gives the dimension for the fabrication of the PVC water cooling system. The system was designed using an 80 watt solar panel and a 20 liters water tank/heat exchanger. The PVC and the heat exchanger insulator thickness was determine to be 5.5 mm and a theoretical water temperature of 62.3^{o}C was attained, which implies a 5.2^{o}C reduce in PVC temperature.

References

Abiola-Ogedengbe, A. (2016). *Experimental investigation of wind effect on solar panels.* Ontario, Canada: ,A master drgree thesis, The University of Western Ontario London, .

Arjyadhara, P., & Bhagbat, P. (2017, December). Experimental Analysis of Factors Affecting the Power Output of the PV Module. *International Journal of Electrical and Computer Engineering (IJECE), 7*(6), 3190~3197.

Bahaidarah, H., Abdul, S., Gandhidasan, P., & Rehman, S. (2013). Performance evaluation of a PV (photovoltaic) module by back surface water cooling for hot climatic conditions. *Energy Journal, 59*, 445-453.

Chandra, R., G. V., & Ray, C. B. (2015). Thermal performance of a two-pass PV/T air collector. *, Proc. SESI, Baroda*, (pp. 63-69).

Efstratios, C. (2015). *Modelling and Analysis of Water Cooled Photovoltaics.* Strathclyde: A Masters degree thesis, University of Strathclyde.

Huan-Liang, T. (2014). Design and Evaluation of a Photovoltaic/Thermal-Assisted Heat Pump Water Heating System. *Journal of Energies, 7*, 3319-3338;. doi: doi:10.3390/en7053319,

Kartini, S., Ag-Sufiyan, A. H., Halim, R., & Jedol, D. (2017). Evaluation on Cooling Effect on Solar PV Power Output Using Laminar H2O Surface Method. *INTERNATIONAL JOURNAL of RENEWABLE ENERGY RESEARCH, 7*(3).

Leow, W. Z., Mohd, I. Y., Amelia, A. R., Muhammad, I. M., Safwati, I., Muhammad, I. F., & Rosmi, A. &. (2019). Effect of Water Cooling Temperature on Photovoltaic Panel Performance by Using omputational Fluid Dynamics (CFD). *Journal of Advanced Research in Fluid Mechanics and Thermal Sciences, 56*(1), 133-146.

Saira, I., Samia, A., Atta, U. M., H. A., & Anab, D. (2018). Effect of Water Cooling on the Energy Conversion Efficiency of PV Cell. *American Scientific Research Journal for Engineering, Technology, and Sciences (ASRJETS)*.

Swar, A. Z., M. H., & Mustafa, I. (2017). A review of photovoltaic cells cooling techniques. *E3S Web of Conferences 22*.

NUMERICAL ANALYSIS OF HYDRO-DYNAMICS PROPERTIES OF TURBINE PENSTOCK IN SHIRORO HYDROELECTRIC POWER PLANT

Yahaya Giwa and Bako D. M.

Department of Mechanical Engineering, Federal University of Technology, Minna

Corresponding Author: Yahaya.giwa@yahoo.com

Abstract

Penstocks are very important component of hydroelectric power generation. They transport water at high pressure from the reservoir to the water turbine. This high pressure and penstock geometry have effect on the turbine performance. Therefore, a numerical analysis of the hydrodynamic characteristics of the water in the penstock is very important to the design and maintenance of the penstock. Some fluid flow equations such as Navier Stoke equation, continuity and Bernoullis equations were applied in this study. Also, a computational fluid dynamics was used to validate the results from the numerical modelling of the flow in the penstock. The results shows that the water velocity is higher at the bend were the penstock descend into the ground. The pressure difference in the penstock varies with the reservoir head. And drops increasingly as it travels through the penstock with a pressure difference of 7000 bar. The pressure at the penstock outlet is more than the atmospheric pressure, which mean high pressure at the end of the penstock. The velocity of the water in the penstock increases up to about 6.4 m/s, and starts to drop after the penstock length of 250 m.

Keywords: penstock, hydrodynamics, numerical, turbine, pressure, velocity.

1. Introduction

The Shiroro Hydroelectric power station (SHEP) is one of the seven power stations in Nigeria. Shiroro Hydroelectric power station is situated in Niger State and is located about 65km northeast of Minna. The actual power station is situated downstream of the confluence of the River Kaduna and River Dinya. To convert the potential energy of the water fall at a certain height into mechanical power and then later to electrical power, a penstock is used. There are four (4) penstock used in the SHEP which are buried in the ground. The hydropower plant efficiency η_a depends on the design of the water conduits (penstock) and the operating conditions.

The penstock is the long pipe that carries the water flowing from the reservoir towards the power generation unit, comprised of the turbines and generator. The water in the penstock possesses kinetic energy due to its motion and potential energy due to its height. The total amount of power generated in the hydroelectric power plant depends on the height of the water reservoir and the amount of water flowing through the penstock (Amit *et al,* 2014). Hence it becomes extremely important that water is brought with minimum head loss from the source to the inlet of the turbine. This ensures higher hydraulic efficiency of the overall plant and structural safety.

The penstock orientation and pressure head contributes to the differences between penstock inlet and outlet pressure, hydrodynamic properties which then affect the pressure delivered to the turbine and also penstock life. These properties also affects the turbine output and service life of the penstock. Recently, unit 411G4 penstock scroll casing of Shiroro Hydro-electric power plant shown in Figure 1 buckled at the lower neck of up to about 2.83m radius. And this block the water way up to about 80%, thereby starving the turbine of the required water tongue and thereby causing inefficiency in the operation of the unit 411G4. To prevent this problem from occurring in the future designs, a numerical approach is proposed to determine the penstock performance (hydrodynamic characteristics).

Figure 1.1: Buckling of underground Penstock (SHEP, 2020).

Determining the hydrodynamic properties of the turbine penstock at the Shiroro hydro-electric power generating station reveals the deficiencies in design or operations of the plant. This will prove to be vital information to the running and performance of the water turbine at the Shiroro hydro electricity generation station. The dynamic characteristics of penstock and its governing equation of the fluid flow can be used to determine its performance. Numerical modeling of the penstock will help to study hydrodynamic response of the system to varying pressure level from the water reservoir. For stability of power system it is necessary to minimize hydraulic transient. When there is load change in the system, change in mechanical power occurs due to sudden opening of gate or due to sudden flow of water in the penstock (Alex *et al,* 2018; Alex and Linus, 2017). To reduce the transient in the mechanical power optimal value of penstock parameter is required. This research work will be focus on the effect of the hydrodynamic properties of Penstock. The MATLAB Simulink were used to solve the resulting governing equation.

2.1 Reviewing the previous literature shows that Tchawe *et al.* (2018) studies the variation of flow through the intake of a penstock on the structure of a dam in Cameroon. The study was based on a 2D numerical approach using FLEUNT 6.3.26. The study shows that the shape of the structure upstream and the intake has a real impact on the structure of flow. And also the flow rate of water that arrives upstream varied the Reynold number at 25.9 x 10^6, 28.8 x 10^6 and 30.27 x 10^6. The study visualized the velocity profile at a distance of x=13, x = 15, x= 17m and x= 23 m.

Santiago *et al*. (2010) carried out the CFD the internal flow in a Francis turbine from a numerical point of view. A steady state simulation was performed in other to study the turbine and energetic losses in its components and also, a unsteady simulations was performed to investigate the fluctuating pressure dynamics and the rotor-stator interaction of a Francis turbine in Colombia. The employed CFD package was ANSYS-CFX v. 11. The results obtained shows a good agreement with experiments data, especially for the characteristic curve. The study focused on turbine discharged coefficient and energy coefficient at 72.55% opening. This work focuses on the turbine and not turbine penstock. Nicolet and Alligne (2011) on modelling, simulation and analysis of the transient behaviour of a 340 MW pump turbine in case of emergency shutdown in generation mode with particular attention to the possible draft tube water column separation. A simplified model of a pumped storage power plant was developed and setup in EPFL software SIMSEN. The model developed also includes a penstock feeding a 340MW pump-turbine with the related rotating inertia and a tailrace tunnel. The results show the influence of the tailrace tunnel length and diameter on the minimum pressure in the draft tube was investigated through a parametric study without water column separation model. The result obtained shows that the used approach is not suitable as valve characteristic to reproduce a rapid discharge drop resulting from the turbine runaway. The study presented by Tchawe *et al.* (2018); Santiago *et al*. (2010) Nicolet and Alligne (2011) are guides to this present paper but differ in approch due to Numerical analysis adopted by the present study. However numerical model gives better outcome (Ibrahim *et al*, 2014; Juan, 2018; Monika, 2015).

3.0 MATERIALS AND METHODS

3.1 Model Description of the Turbine Penstock At Shiroro Hydro

A typical structure representing turbine penstock of the Shiroro-hydro the dam is shown in Figure 3.1. The water is transported from a reservoir, where it is stored, through a tunnel known as intake race / conduit / headrace closer to the powerhouse where the turbine and generator is installed.

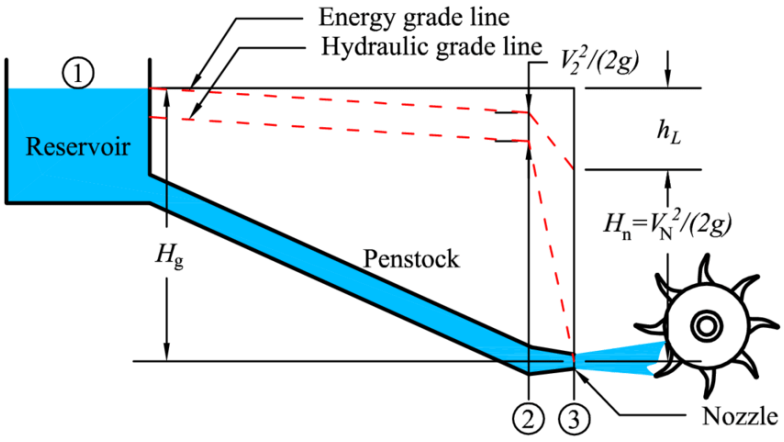

Figure 3.1: Schematic of the penstock layout.

The simulation is for Francis turbine used by SHEP and the control of the flow rate through the turbine is done by manipulating the guide vane. The turbine is rotating an axis which also holds the rotor of the generator producing electricity to the power grid. Normally, a synchronous generator is used.

3.2 Simplifying assumptions

Knowing that water is an incompressible fluid, we will impose some assumptions for our work:

- The turbulence is isotropic;
- The resistance of the air is negligible;
- The parietal effects are neglected (2D work).

3.3 Numerical Modeling of the Penstock

To study the hydrodynamics properties of the penstock, velocity, pressure and temperature profile were developed. Consider the section 1-1 to 2-2 of the penstock as a pipe section with pressure as a driving force, let P_1 and P_2 be the inlet and outlet pressure respectively. P_1 will be equal to P_2, if there is no frictional resistance by the penstock (pipe). Equation 1 is true based on this assumption (Uzma, 2014):

$$F_\mu = P_1 A - P_2 A \qquad 1$$

$$\frac{F_\mu}{A} = P_1 - P_2 \qquad 2$$

Dividing equation 2 by the specific weight of the water in the penstock.

$$\frac{F_\mu}{A\omega} = \frac{P_1 - P_2}{\omega} \qquad 3$$

And

$$h_f = \frac{F_\mu}{A\omega} \qquad 4$$

Which means that ;

$$h_f = \frac{P_1 - P_2}{\omega} \quad 5$$

When the penstock has a circular cross section (A = πD^2),

$$h_f = \frac{4fLV^2}{\omega D^2} \quad 6$$

Which can be expressed in terms of flow discharges,

$$h_f = \frac{6.5\, fLQ^2}{D^5} \quad 7$$

The hydrodynamic characteristics of flow in a penstock were studied using equations 8-11, i.e. continuity equation, Naviar stoke equation and Bernoulli's equation respectively. The general solution procedure for Navier Stoke equation are itemized as follows:

- Coordinate system – cylindrical and symmetry.
- Driving force - pressure flow.
- Boundary condition : $@r = a, V_z = 0.$ $@r = 0, V_z = finite.$
- Guess the form of solution.
- Simplified equation of motion.

1. Conservation of mass (Continuity Equation 8)

$$\frac{\partial \rho}{\partial t} + \frac{1}{r}\frac{\partial(\rho r V_r)}{\partial r} + \frac{1}{r}\frac{\partial(\rho r V_\theta)}{\partial \theta} + \frac{\partial(\rho V_z)}{\partial z} = 0 \quad 8$$

$$V_z = -\frac{a^2}{4\mu}\frac{\Delta P}{L}\left(1 - \frac{r^2}{a^2}\right) \quad 9$$

The equation 9, give the solution of the velocity profile inside the penstock.

3.4 Volumetric Flow Rate

The flow rate, Q of a fluid through a pipe (penstock) is given by;

$$Q = \frac{\pi a^4}{8\mu}\frac{\Delta P}{L} \quad 10$$

Where: a= acceleration; ΔP= change in pressure; μ= friction coefficient; L= Penstock length

3.5 Bernoulli's Equation

Bernouli's equation 11 represents work and energy of the moving fluid as follows (Douglas 2015**)**

$$P_1 + \frac{1}{2}\rho v_1^2 + \rho g h_1 = P_2 + \frac{1}{2}\rho v_2^2 + \rho g h_2 \quad 11$$

Where: P= pressure at inlet (1) & outlet (2); v= velocity at inlet (1) & outlet (2); h= height at inlet (1) & outlet (2); ρ= density, g= acceleration due to gravity.

3.6 CAD Simulation of Penstock

1. **The CFD Analysis**
   CFD analysis of the turbine penstock starts with geometric model preparation, i.e a 2D model were created and converted to 3D base on the details shown in Table 3.1

Table 3.1: Unit 4 Penstock Features.

S/No	Description	Parameters
1	Penstock Length	330 m
2	Penstock Head	97m
3	Penstock diameter	6.325 m
4	Penstock thickness	32mm
5	Discharge rate	181.3 m^3/s
6	Inlet pressure	10 bar
7	Inlet Water Temperature	20^oC

2. **Meshing**: Meshing of the geometry model was carried out by dividing the model into small sub parts for CFD analysis called mesh. The shape of the mesh elements used was rectangular. The Boundary Conditions (BC) for computational domain are such as: given radius, $@r = a, V_z = 0$.. $@r = 0, V_z = finite$.

4 Results and Discussion of the Results

4.1 Numerical Modeling Results

The solution of the numerical model of the hydrodynamics of the water flow in penstock was solved using the input parameters as given in Table 3.1. The velocity profile and contour plot at the entrance region of the penstock are shown in Figure 7.

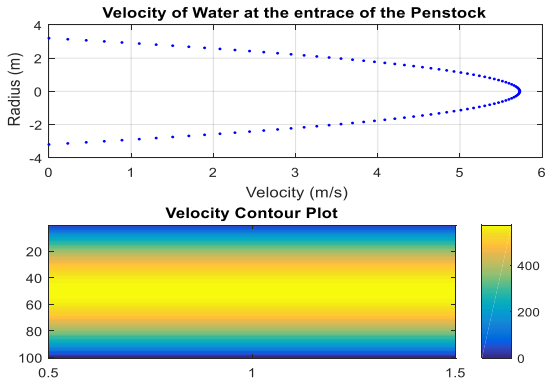

Figure 7: Velocity Profile and Contour of the water. as It travels in the Penstock.

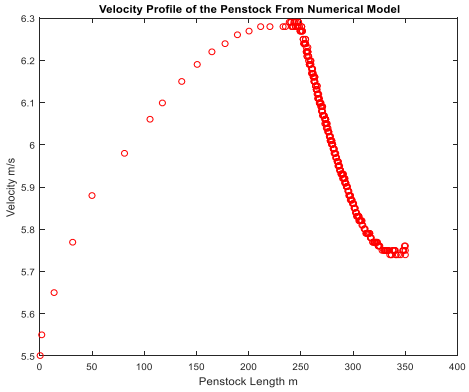

Figure 8: Velocity Profile of the Water as it travels in the penstock

Figure 7, presented the velocity profile at the entrance of the penstock as defined by the equation 9. This shows that at the penstock wall were the r=R, the flow velocity approaches 0, and approaches max when r=0. the figure shows the normal flow in a pipe profile. The velocity of water as it enters the penstock reaches a maximum of 5.7265 m/s. Figure 8 –10 shows the profile of hydrodynamics properties under study for the turbine penstock as the water flows across the penstock length.

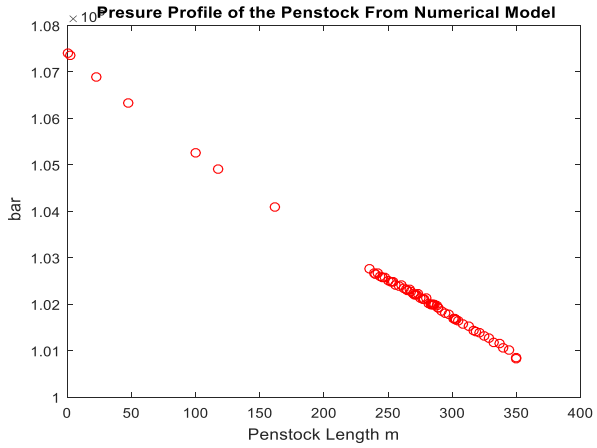

Figure 9: pressure Profile of the Water as It travels in the Penstock.

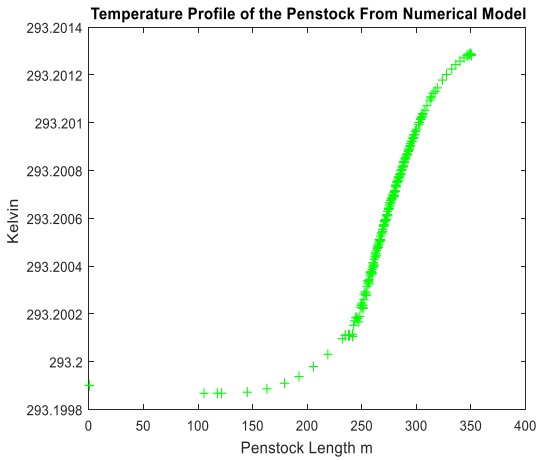

Figure 10: Temperature Profile of the Water as It travels in the Penstock.

The velocity of the water inside the penstock increases up to about 6.4 m/s, and starts to drop after the penstock length of 250 m. The velocity of the water linearly drops as it is exiting the penstock to as low as 5.75 m/s.
The pressure profile of the flow in the penstock was computed using equation 11. The result shown in figure 9, indicates that the water pressure drops linearly as its passes through the penstock. A pressure difference of 0.07 x 10^5 bar was recorded from Figure 9, between the penstock inlet and outlet lids. Also from the graph, it was noticed that the pressure is more concentrated from where the penstocks descends in to the turbine. There was no significant increase in the water temperature as it flows through penstock. From Figure 9, its appears that only pressure of the water will have significant impact of the penstock structure. And this appear more at the elbows of the penstock.

4.2 CFD Results

The results of the computational fluid dynamics carried out on the hydrodynamics properties of the water flow in turbine penstocks are presented in Figures 11- 14. Figure 11 presented the absolute velocity profile in the penstocks. This shows that the water from the reservoir has high velocity at the middle of the penstock and slows down as it approaches the bend. The overall water velocity increases up to the time is gets to bends and the velocity decreases until it exit the penstock. Also from the Figure 11, it shows that the water at the penstock walls have less velocity as compare with the water at the center of the pipe. A highest water velocity reached is about 6.5 m/s.

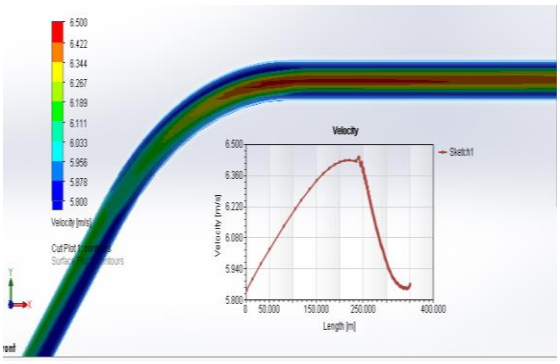

Figure 11: Velocity Profile of travelling water

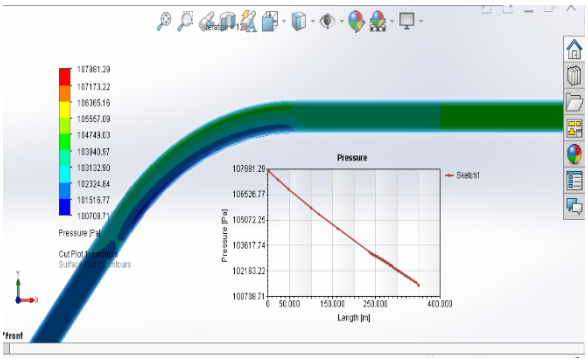

Figure 12: Pressure Profile of the water flow

The pressure profile of the flow in the penstock is shown in Figure 4

this reveals that the water has a higher pressure from the beginning of the penstock and decrease towards the end of the penstock. The contour plot in Figure 12, shows a high pressure (stress) at the upper side of the penstock elbow. This predict the failure of the SHE unit 4 penstock show in Figure 1. Also from the plot the graph shows some turbulent after the water pass 250m length of the penstock. Temperature of the fluid is one of the hydrodynamics properties of the fluid flowing in a pipe. Figure 13 presents the color contour and temperature profile of the water inside the penstock, and this shows that the temperature of the water has not change significantly.

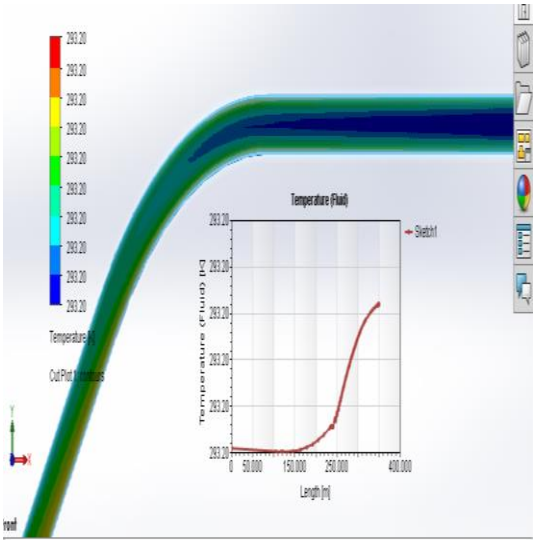

Figure 13: Temperature Profile of the Water Flow in the Penstock.

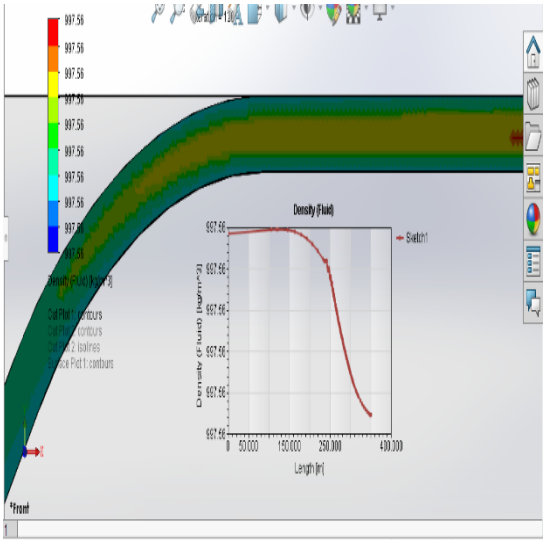

Figure 14: Density Profile of the Water Flow in the Penstock.

The density profile of the water in Figure 14, has almost the same opposite profile with that of the temperature in Figure 13. There is no significant change in the density of the water. Although, the water is slightly lighter as it descend into the exit of the penstock. The color contour shows that the water is hotter at the center of the penstock from the entrance region and well mix at the exit region.

Conclusions

In this work numerical and Computational Fluid Dynamics (CFD) approach has been used to predict the hydrodynamic characteristics of one of the turbine penstock at SHEP. This study was conducted in other to ascertain the likely cause of failure of the penstock. The hydrodynamics properties examined are the pressure, velocity, temperature flow rate and the density of the water flowing through the penstock from the reservoir. The pressure difference in the penstock varies with the reservoir head. And drops increasingly as it travels through the penstock with a pressure difference of 7000Pa. The pressure at the penstock outlet is more than the atmospheric pressure, which mean high pressure at the end of the penstock. The velocity of the water in the penstock increases up to 6.4 m/s, and starts to drop after the penstock length of 250 m.

References

Alex, O. E., & Linus, A. (2017). Experimental Investigation of the Influence of Penstock Configuration and Angle of Twist of Flat Blades on the Performance of a Simplified Pico-Hydro System EJERS. *European Journal of Engineering Research and Science, 2*(7).

Alex, O. E., Matthew, E., & & Taofeek, A. Y. (2018). Athens Journal of Technology and Engineering. *Influence of Penstock Outlet, Number of V-Blades, Flat Blade Lateral Twist Angle and Hub to Blade Ratio on the Performance of a Simplified Pico Hydropower System, 6*(2), 115-140.

Amit, A., Hiren, P., & Sunil, P. (2014, May). Analysis of the penstock for pit turbine using computational fluid dynamics. *IOSR Journal of Mechanical and Civil Engineering (IOSR-JMCE), 11*(3), 2278-1684.

Ibrahim, M., Zied, D., & Mohamed, S. A. (2014). *Numerical Study of the Hydrodynamic Structure of a Water Savonius Rotor in a Test Section Laboratory of Electro-Mechanic Systems (LASEM),*. Soukra, Tunia: National School of Engineers of Sfax (ENIS), University of Sfax.

Juan, C. A. (2018). *Analysis of Hydrodynamic Forces on High-Head Slide Gates Using Computational Fluid Dynamics.* A Masters Degree Thesis, Universidad Nacional de Colombia .

Laura, C., Gustavo, U., Adam, A., & & Marcelo, R. (2016). Experimental and Numerical Simulations Predictions Comparison of Power and Efficiency in Hydraulic Turbine. *, Hindawi Publishing Corporation Modelling and Simulation in Engineering, 20*(1).

Mohammed, T. G., & Rasim, A. K. (2013). Hydro Power. In *Hydro Power*.

Monika, S. (2015, May-June). Modeling of Hydraulic turbine for analyzing effect of penstock parameter variation on mechanical power. *International Journal of Engineering Research and General Science, 3*(3).

.NICOLET, C., & ALLIGNE, S. &. (201, November). Parametric study of Water column Separation in Francis Pump-turbine draft tube, SHF. *Pumped storage Powerplants», Lyon*, 23-24.

Santiago, L., Manuel, G., & Brian, Q. &. (2010). CFD and Numerical simulations of Francis turbines. *5*(1), 24 - 33.

Tchawe, T. M., Tcheukam-Toko, D. K., & & Djiako, T. (2018, July). Numerical study of flow in the water inlet of the penstock. , *International Journal of Current Research, 10*(7), 71061-71066.

Uzma, N., Muhammad, N. A., & Rukh, G. (2014, December). Dynamic Model of Turbine System of Micro Hydroelectric Scheme for Stability Analysis. *International Journal of Electrical & Computer Sciences IJECS-IJENS, 4*(6).

Comparism of NIFFR Improved smoking kiln with the Traditional Smoking Kiln

[1]Ayuba A. B., [2]Olufemie O. A., [2]S. S. Lawal, [1]Aminat I. M. and Ayuba E. J.

[1]National Institute for Freshwater Fisheries Research, P.M.B. 6006, New Bussa, Nigeria
[2]Department of Mechanical Engineering, Federal University of Technology, Minna
[3]Department of Mechanical Engineering, Niger State Polytechnic, Zungeru.

***Corresponding Author:** aababanna@gmail.com 08054361324*

Abstract: Fish drying has been the traditional method of processing and preserving fish in developing countries. Traditional fish smoking using the Banda and the drum ovens has been adopted in the past. However as a result of the hazard and time consuming involved in traditional smoking of fish, the need for modern and mechanized fish smoking kiln is encouraged. The Design and fabricated of NIFFR Improved 200kg batch capacity smoking kiln was used for smoking fish. The smoking kiln uses either firewood or charcoal as heat source for drying of fish. Trials were conducted on the newly fabricated smoking kiln, and the output shows low consumption of heat source, the smoked fish were better than those from the traditional fish smoking kilns in term of appearance. Batch smoking operation is concluded within 36 hours with the consumption of 5kg fire wood. An excessive heat loss is minimized by the rock wool used as insulating material. Heat transfer was as a result of transient conduction and temperature of the smoking chamber was maintained at 140^{o}C.

Key words: *Fish smoking, mesh wire, rook wool, damper,*

1. INRODUCTION

Fish drying or dehydration is a process of the removal of water from fish or fish products by evaporation, salting, application of pressure and using absorbent pads. Fish drying is the oldest method of fish preservation as observed by Eyo (1997). The main purpose of dehydration is to extend the shelf life of fish by reduction in water activity. Water plays an important role in the suitability of fresh and dried fish, it act as a solvent for chemical, microbiological and enzymatic reactions Olokor, *et, al.* (2007)

Fresh fish when out of water deteriorate fast except immediate step are taken to preserve its quality, despite the subsistence nature of our capture fisheries in Nigeria. Tawari (2006), also reported that most of the fish processing community in Nigeria employed traditional technique and they have been in existence for more than ten years. As much as 50% post harvest losses are recorded, the result of this is economic losses to fish farmers, fish processors and marketers is quite enormous.

The need to mechanised fish processing technique has drawn the attention of national agricultural research to devote utmost interest and resources to engineering research in fish processing operation, to reduce labour operation and unsanitary fish handling procedures that may be involve in fish smoking operations. Eyo A. A., (1999). Thus it is imperative to process and preserve some of the fish caught in the period of abundance, so as to ensure an all year round supply. This will invariably reduce post harvest loses, increase the shelf life of fish, and guarantee a sustainable supply of fish during off season with concomitant increase in the profit of the fish entrepreneurs. (Eyo, 2002).

JUSTIFICATION FOR THE STUDY

Consequently, the presences of these carcinogenic components in smoked fish make it not acceptable in international market (EFSA, 2005).It has also been observed that the existing NIFFR smoking kiln has low carrying capacity with low heat retention, which usually take long period of time before drying fish successfully. Consequently, the presences of these carcinogenic components in smoked fish make it not acceptable in international market (EFSA, 2005).It has also been observed that the existing NIFFR smoking kiln has low carrying capacity with low heat retention, which usually take long period of time before drying fish successfully.

MATERIALS AND METHOD

The materials used for this research work are

Galvanize metal plate 1.0mm and mild steel metal plate 0.8mm

Angle bar 1.0 inch

Iron pipe 1x1 inch

BRC wire mesh 2x1inch

Rook wool

Electrode

Hinge

The smoking cabinet is made up of two layer metal wall, lagged with insulating material called rock wool. The rock wool helps to prevent heat loss from the inner heating chamber of the smoking kiln. Galvanize metal plate with thickness of (1.0mm) was used for the outer wall of the smoking kiln, while mild steel plate with thickness of 0.8mm was used for the inner wall of the smoking kiln with structural dimension of (1.2 x 1.5 x 0.9) meters. The heating chamber is located in the lower part of the smoking kiln with a dimension of (0.3x 0.3) m. Above the heating chamber is the damper plate which is made up of stainless steel with thickness of (0.9mm) measured (0.7x 0.6)m which allow heat transfer to the mesh tray and prevent direct fire from burning the fresh fish product during smoking operation. At the same time the damper serve as a receptacle for the collection of melted fat and oil.
The smoking chamber is divided into two cabinets; each cabinet is measured (0.76 x 0.7) m. The racks are made of one inch angle bar and galvanize wire mesh (2 x 1)'' welded together. Each chamber of the smoking kiln contain ten racks with dimension (0.6 x 0.6) m
The smoking kiln has a dome shape at the top where the chimney is located. The chimney is made of galvanize metal plate with dimension 4 x 20 inch covered with a cap for opening and closing to enable the release of smoke from the chamber during smoking operation. The modified smoking kiln has the batch capacity of 200kg of fresh fish per batch operation as shown in plate 3 while plate 1 and 2 shows the traditional smoking kiln

The smoking kiln utilizes fire wood or charcoal as heat source. During operation heat is uniformly distributed to all parts of the smoking cabinets

Plate 1: Mud smoking kiln

Plate 2: Drum smoking kiln

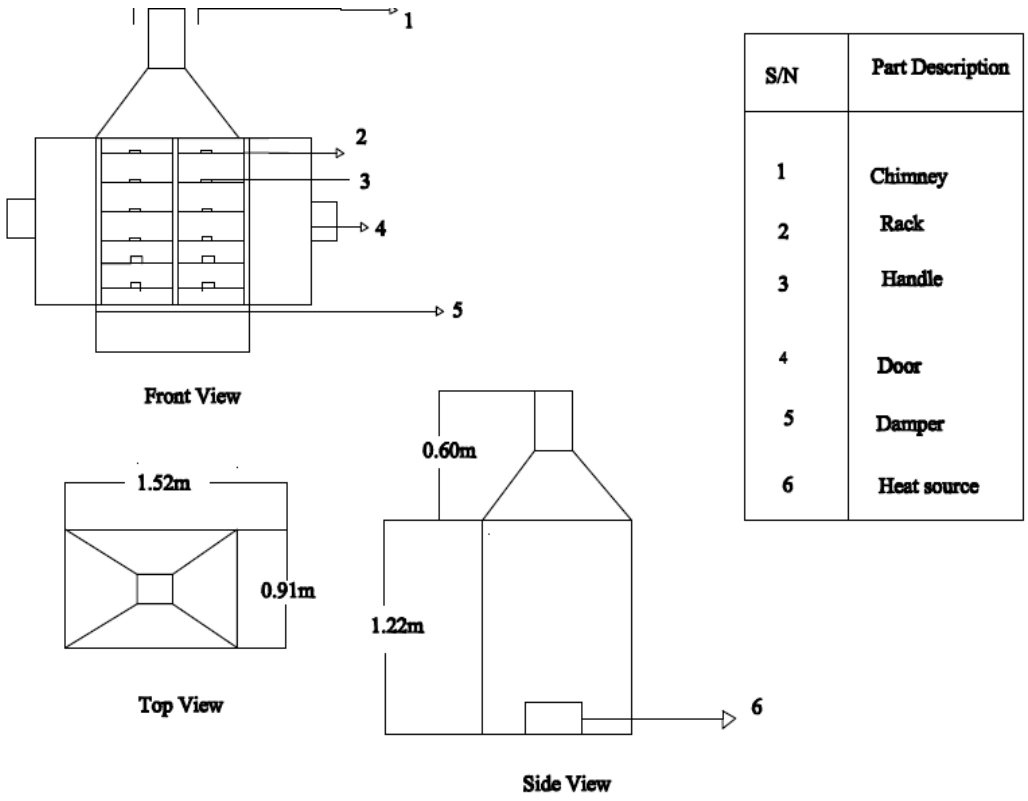

S/N	Part Description
1	Chimney
2	Rack
3	Handle
4	Door
5	Damper
6	Heat source

Fig. 1: Design of NIFFR Improved Smoking Kiln

Plate 3: Fabricated NIFFR Improved Smoking Kiln

Fish processing and smoking operation

The fresh fish used for this study was*Clariasgariepinus*species harvested from a fish farm in New-Bussa, Niger State. The fish were degutted and washed, then placed in a bowl of brine solution for 30 minutes. The brining solution was prepared with 250g of table salt in 3.5 litres of water 12kg of fish each. The fish were removed from the brining solution to drip and arranged on the racks then placed in the pre-heated kiln for smoking operation. The smoking chambers were pre-heated to initial temperature before the fish were loaded in the kiln. The

temperature inside the smoking chamber of the newly fabricated smoking kiln and the traditional mud kiln was monitored and recorded using a data logging machine. Smoking operation was concluded within 36 hours.

Result and discussion

Table 1: Temperature measurements at different time around the improved and traditional smoking kiln

Time	Ambient	Improved NIFFR KILN		Traditional Kiln	
	Temp. (^oC)	Chamber Temp. (^oC)	Outer wall Temp. (^oC)	Chamber Temp. (^oC)	Outer wall Temp. (^oC)
1:00	38	130	45	39.6	10
2:00	36	135	40	39.6	30
3:00	34	140	45	45.0	20
4:00	32	150	50	47.8	35
5: 45	30	135	30	40.2	25

It was observed that there is build up of temperature within the improved NIFFR smoking kilnfar above the ambient temperature. A much lower temperature was recorded from different location in the traditional smoking kiln. The differences in temperature account fr the variation in processing time between the two types of smoking kiln. However heat transfer from the heating chamber to the smoking chamber was a situation of transient heat conduction. The magnitude of distribution of heat within the walls of the NIFFR Improved smoking kiln increases as temperature increase in the smoking chamber. This agrees with Okouzi *et al*., 2015 and Cenger, 2006 that heat transfer is proportional to temperature difference.

Heat retention in the NIFFR improved smoking kiln was encouraging as the kiln was able to retain heat for up to six hours provided the door are permanently locked and heat source extinguished. This attribute was as a result of the rock wool insulating material in between the two walls of the smoking kiln. This attribute has been observed in other smoking kilns such as the NIFFR/WAAPP hybrid smoking kiln and NIOMR smoking kiln. Other smoking kiln such as the drum smoking kiln and mud smoking kiln lack this attribute as resultant heat losses are excessive.

In terms of fuel wood consumption the smoking kiln utilizes 5kg of fire wood to complete one batch smoking operation.

Conclusion

In this research a portable and easily maintained fish smoking kiln with 200kg batch capacity was designed, fabricated and tested for smoking. Its performance was evaluated, the result shows that its performance is better than the mud and the drum smoking kiln in terms of low carbon content and high batch capacity of smoked fish products. Smoked fish from the smoking kiln had a characteristic golden brown colour.
The heat temperature from the burning wood can be easily controlled by constant observation and monitoring as the wood is burning. Smoked fish from the fabricated smoking kiln were easily identified from there appearance.

REFERENCES

Cengel, Y.A (2006) Heat and mass transfer: A practical approach. 3rd Edition Mcgraw-Hill Co. 900p.

EyoA.A (1997) Post harvest lesser in the fisheries of kainji lake. A consultancy report submitted to Nigeria-German (GTZ) Kainji lake fisheries promotion project, March 1995.

Eyo A. A., (1999) The effect of traditional handling, processing and storages methods of the quality fish in small scale fisheries in Nigeria In: Proceding of 13th Annual Confrence of fisheries Society of Nigeria p.50

Eyo A. A. (2002) Fish Technology. National Institute for Freshwater Fisheries Research p. 95

Okouzi, S.A, Omojowo, F. S, Ayuba, A. B, Mohammed, A and Olugbenga, B. O. (2015). Evaluation of conduction heat losses in NIFFR-WAAPP hybrid smoking kiln. In: proceeding of 30th FISON conference p 577-579

Olokor, J.O., Ihuahi, J.A., Omojowo, F.S., Falayi, B.A. and Adelowo, E.O. (2007). Introduction to Fish Handling and Preservation. In: Handbook of Practical Fisheries Technology, Fisheries Technology Division, NIFFR, New Bussa, pp. 1-21.

TawariC.C (2006) Effectiveness of agricultural agencies in fisheries management and production in Niger Delta. Phd thesis River State University of Science and Technology, Portharcourt, Nigeria

Design Analysis and Fabrication of PCM Solar Oven

Nasamu Yusuf and Nicolas Musa
Department of mech, Federal University of technology, Minna

Author email:

Abstract:
Renewable energy resources are have become more importance because they are sustainable and due to the fast depletion of conventional resources. Owing to the lower efficiencies of renewable devices, much researches are focus in improving their efficiency. The concept of utilizing phase change materials (PCMs) has attracted wide attention in recent years and this is because it has the potential to improve its performance. This is the motivation behind the design and fabricate of a PCM solar oven. The use of a latent heat storage system using phase change materials (PCMs) is an effective way of storing thermal energy and has the advantage of high-energy storage density and the isothermal nature of the storage process. The experimental results show that this system is capable of successfully storing and utilizing thermal energy for balking applications where temperature is below 75 ◦C.

Keywords: baking, oven, phase change material, solar, radiation

1. Introduction

According to statistics, 50% of the commercial sources of energy like petrol, gas, and electricity are used in our daily consumption. Humans should take advantage of other sources of energy; renewable energy is one of the alternative available energy sources. It is also essential to encourage the community to start using alternative energy sources for the sake of cleaner environment. Solar cooker is now an invention that uses solar energy for late evening cooking (Nagaraj, Hatim, & Haitham, 2016).

Solar cooking has been identified as an appropriate technology as it has numerous advantages such as no recurring cost, potential to reduce drudgery of firewood collection, high nutritional value of the cooked food and high durability of the cookers (Muthusivagami & Velraj, 2010). Solar cookers are heat exchangers designed to use solar energy in the cooking process. All solar cookers use the basic principles of concentrating light and heat from the sun into a small cooking area, converting light to heat and trapping the heat by isolating the air inside the cooker from the air outside the cooker using the Greenhouse Effect. The efficiency of Solar cookers increases with the temperature of the heat source. To achieve high temperatures in solar thermal energy plants, solar radiation is concentrated by mirrors or lenses - a technique called Concentrated Solar Power (CSP) (Wikipedia, n.d.). The dependency of the collector performance on temperature makes the whole system performance sensitive to temperature (Duffie & Beckman, 2013). Solar cookers are broadly categorized under two groups: Solar cookers without energy storage and solar cookers with storage.
Energy consumption for cooking in developing countries is a major component of the total energy consumption, including commercial and non-commercial energy sources (Sharma et al. 2008). Wood fuel in Nigeria is the most abundant source of energy. **Ogunsawa and Ajala (2002) and Zaku et al. (2013)** reported that over 70% of the country's households depend directly on wood fuel as their main sources of energy, with daily consumption estimated at 27.5 million kg/day.
Cooking with the sun's power is a fun way to use a renewable resource, and with excellent results. Food cooked in solar ovens retains its moisture and nutrients as it cooks slowly, and does not burn as with other types of heat. Many organizations are introducing solar cooking to the world's less developed regions to prevent deforestation in fuel-starved areas. They hope also to release the women and their children who must spend their days trying to gather fuel instead of working or going to school. High-performance parabolic solar ovens and vacuum tube ovens can attain temperatures above 290°C (550°F). They can be used to grill meats, stir-fry vegetables, make soup, bake bread, and boil water in minutes. Vacuum tube type ovens can heat up even in the clouds and freezing cold. Conventional solar ovens attain temperatures up to 165°C (325 °F). They can sterilize water or prepare most foods that can be made in a conventional oven or stove, including bread, vegetables and meat over a period of hours.

Solar ovens use no fuel. This saves cost as well as reducing environmental damage caused by the use of fuel. Since 2.5 billion people cook on open fires using biomass fuels, solar ovens could have large economic and environmental benefits by reducing deforestation. (Chukwuneke, Nwuzor, & Digitemie, 2018)

The demand for wood fuel, charcoal combined with the high cost of kerosene has pushed the low income earners residing in towns to use charcoal as the cheaper option. The use of liquid petroleum gas (LPG) and electricity for cooking and lighting is out of reach to most Nigerians due to the high cost.

Wood energy is becoming scarce and more expensive and is of great concern since deforestation leads to serious consequences such as soil erosion, floods and desertification **(GoK, nd)**. Petroleum fuels are the most important source of commercial energy in Nigeria, and are mainly used in the transport, commercial and industrial sectors. Nigeria uses a lot of resources on imported petroleum products, hence there is need for alternative sources of energy.

Direct solar ovens use solar radiation directly in the cooking process, while the indirect solar ovens use solar radiation to heat thermal fluids that transport heat to the place of the cooking process (Hussein & Nada, 2008). These ovens have been used effectively with partially overcast skies and will typically reach temperatures of 150^{o}C (Wikipedia, n.d.).

When higher temperatures are required it becomes necessary to concentrate solar radiation. This is achieved using focusing or concentrating solar collectors (Sharma & Singh, 2008). The use of the reflectors is to increase the irradiance on the receiver thereby increasing heat production (Kwan & Bannerot, 1984). Solar energy is intermittent by its nature and at night there is no sunshine. Unreliability is the biggest retarding factor for extensive solar energy utilization (Sharma et al., 2008). Food have been found to cook faster in the period between two hours before and two hours after the local solar noon than it does in either the early morning or the late afternoon (Wikipedia, n.d.)**.** Most of the meals are prepared late in the evening when there is no enough solar energy for cooking.

The application of solar ovens is restricted if they are not equipped with energy storage system since it is impossible to use solar energy in cloudy conditions, evenings and at night (Kenisarin & Mahkamov, 2007). Energy storage may be in form of sensible heat of a liquid or solid medium, as heat of fusion in chemical systems, or as chemical energy of products in a reversible chemical reaction (Duffie & Beckman, 2013) and (Sharma & Singh, 2008)

The technical concept of solar cooker can be evaluated by thermal storage potential and energy is stored by raising the temperature of a storage medium; therefore, phase change materials (PCM) play important role in the present scenario. These materials has the ability to store large amounts of thermal energy under isothermal conditions, which means they can deliver or store energy at constant temperature and excrete the heat whenever there is a difference in the degree of the temperature.

In this study, latent heat storage using phase change material were investigated. PCMs have a high thermal energy storage capacity. They store large amount of energy while changing from the solid to liquid phase and release the energy while changing from liquid to solid phase at a particular temperature.

Energy storage not only reduces the mismatch between supply and demand but also improves the performance and reliability of the energy systems and plays an important role in conserving energy. The effects of solar energy on the economy and employment are highly beneficial (Sharma et al., 2009). The use of solar energy would save a lot of time and money for the user and this could be effectively diverted for increased productive activities and monetary gains which means better living standards and overall prosperity.

In this study a solar box oven with latent heat storage unit was investigated to improve the efficiency of the oven and reduce the cost by use of locally available materials.

2.0 Materials and Method

2.1 Materials Used

The solar oven with internal energy storage using PCM has the following elements that was considered in developing the energy balance of the solar oven:

Table 1: Materials used.

S/No	Components	Function	Reason for Selection
1	Solar Reflector	To concentrate solar radiation in to the oven	High reflective index.
2	Plywood	To support the reflector	Strong and corrosion resistance
3.	Glass	To seal the oven from the outside and to allow light rays into oven chamber	High transparency and transmissivity
4	Wood	Glass holder	Moderate strength
5.	Fiber glass	To reduce heat loss to the environment	Low thermal conductivity.
6.	Sheet metal	To cover the oven body	Strength
7.	Foil	Use inside the oven	Food grade
8.	Al-sheet	PCM container	High thermal conductivity and moderate strength
9.	Rollers	Portability	
10	Tray	To carry the drying object	Strength and resistance to corrosion.
11.	Tray stand	To support the ray	Strength

2.2 Design Concept

The solar oven was designed to use solar radiation and a phase change material (PCM) as latent heat storage (for baking oven). The schematic of the solar oven is shown in Figure 1. During the day, the solar radiation is reflected into oven chamber for drying. And a phase change material is used to store the solar energy in the form of heat energy and release during the later hours for use. The over has a container for the PCM, a reflector, glass top, insulated body and drying tray. The insulator is covered with a galvanized sheet metal. The solar oven was designed in a box shape 450mm x 450mm x 450mm.

2.3 Design Consideration

A number of factors were considered during the design of solar oven. This includes over capacity, baking temperature, resistance to corrosion etc.

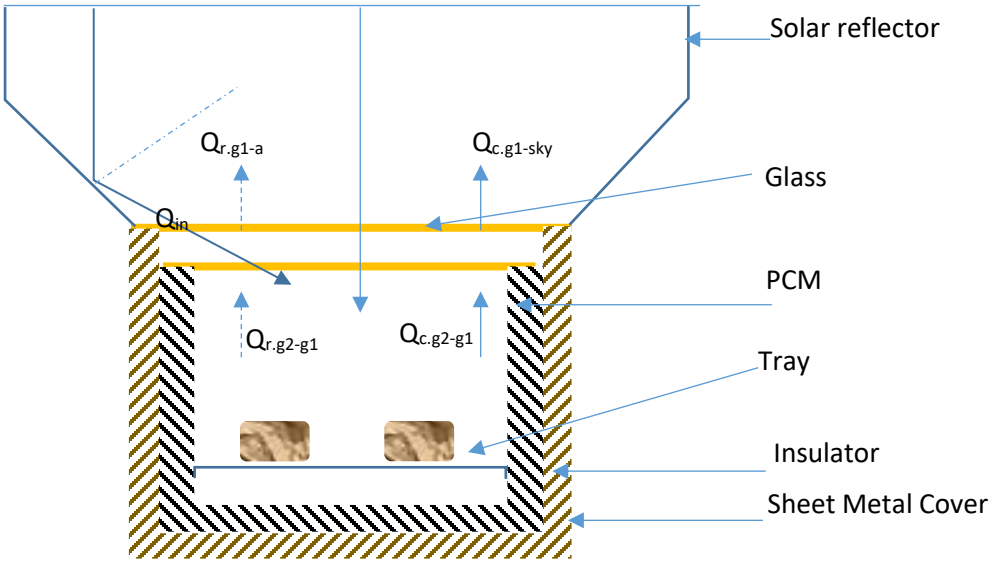

Figure 1: Schematic of the PCM Solar Oven Concept.

2.4 Design Analysis

The solar oven is locked air tightly; this allows reaching considerable temperatures in the test fluid inside the baking chamber. The mathematical model was developed by considering the energy gain into the oven and energy lost to the environment for each of the elements listed above. The following assumptions (Punia, Marwal, Sengar, & Dashora, 2012) were made in balancing the energy for the oven shown in Figure 3.4, so as to simplify the model.

1. The solar radiations received by the vertical walls of the vessel are negligible.
2. There is good thermal contact between the vessel and absorber plate.
3. The temperature gradient across the thickness of covers and cooking vessel has been neglected. (Adewole, Popoola, & A., 2015)
4. The heat exchange through air enclosed in the cooking vessel is negligible.
5. The energy absorb or given off by each element of the solar oven are:

The energy balance equations for each of the components of the solar oven involve in the energy transmission were according to (Punia, Marwal, Sengar, & Dashora, 2012).

The Upper Glass Cover: The energy balance equation for upper glaze cover may be written as

$$M_{g1}\frac{dT_{g1}}{dt} = I_{in}\alpha_g A_c + Q_{r,g2-g1} + Q_{c,g2-g1} - Q_{r,g1-sky} - Q_{c,g1-amb} \quad 1$$

Where;

$$Q_{r,g2-g1} = h_{r,g2-g1}A_c(T_{g2} - T_{g1}) \quad 2$$

$$Q_{c,g2-g1} = h_{c,g2-g1}A_c(T_{g2} - T_{g1}) \quad 3$$

$$Q_{r,g1-sky} = h_{r,g1-sky}A_c(T_{g1} - T_{sky}) \quad 4$$

$$Q_{c,g1-amb} = h_{c,g1-amb}A_c(T_{g1} - T_{amb}) \quad . \quad 5$$

The Lower Glass Cover:

$$M_{g2}\frac{dT_{g2}}{dt} = I_{in}\alpha_g\tau_g A_c + Q_{r,p-g2} + Q_{r,v-g2} + Q_{c,a-g2} - Q_{r,g2-g1} - Q_{c,g2-g1} \quad 6$$

Where;

$$Q_{r,p-g2} = h_{r,p-g2}(A_c - nA_{vb})(T_p - T_{g2}) \quad 7$$

$$Q_{r,v-g2} = h_{r,v-g2}nA_{vb}(T_p - T_{g2}) \quad 8$$

$$Q_{c,a-g2} = h_{c,a-g2}A_c(T_a - T_{g2}) \quad 9$$

For Sill Air in the Baking Chamber:

$$M_a \frac{dT_a}{dt} = Q_{c,p-a} + Q_{c,v-a} - Q_{c,v-g2} \quad 10$$

where;

$$Q_{c,p-a} = h_{c,p-a}(A_c - nA_{vb})(T_p - T_a) \quad 11$$

$$Q_{c,v-a} = h_{c,v-a}nA_v(T_v - T_a) \quad 12$$

Baking Tray:

$$M_t \frac{dT_t}{dt} = I_{in}\alpha_g\tau_g A_c + Q_{pcm} - Q_{c,t-b} - Q_{r,t-g2} - Q_{c,t-a} \quad 13$$

$$Q_{pcm} = UnA_{tc}(T_{pcm} - T_t) \quad 14$$

$$Q_{c,v-b} = h_{c,v-b}nA_v(T_v - T_b) \quad 15$$

Baking Material:

$$M_b \frac{dT_b}{dt} = I_{in}\alpha_g\tau_g A_c + Q_{co,t-b} - Q_{c,b-a} \quad 16$$

$$Q_{c,b-a} = h_{c,b-a}(A_c - nA_{vb})(T_b - T_a) \quad 17$$

$$Q_{co,t-b} = k_t A_{tb}(T_t - T_b)/x \quad 18$$

PCM:

$$M_{pcm} \frac{dT_{pcm}}{dt} = I_{in}\alpha_g\tau_g A_c + Q_{r,pcm-g2} - Q_{c,pcm-a} - Q_u - Q_t \quad 19$$

$$Q_t = (U_b A_c + U_s A_s)(T_{pcm} - T_{amb}) \quad 20$$

$$U_b = \left[\frac{xb}{ki} + \frac{1}{h_{c,g1-amb}}\right] \quad 21$$

$$U_s = \left[\frac{xs}{ki} + \frac{1}{h_{c,g1-amb}}\right] \quad 22$$

3.0 Results and Discussion of the Results

The design and fabricated solar oven in Figure 2, was tested between 9:00am - 4:30 pm, and the results is presented in Figure 3. The solar oven has a baking chamber of 450 mm cube with two drying trays with door located at the top of the oven. From the test results, the maximum oven temperature of the oven and PCM recorded is 63.5^{o}C, but this is dependent on the solar radiation of the test day. The oven is yet to be evaluated using only the PCM, this will be carryout in another test yet to be conducted.

Figure 2: Fabricated PCM Solar Oven.

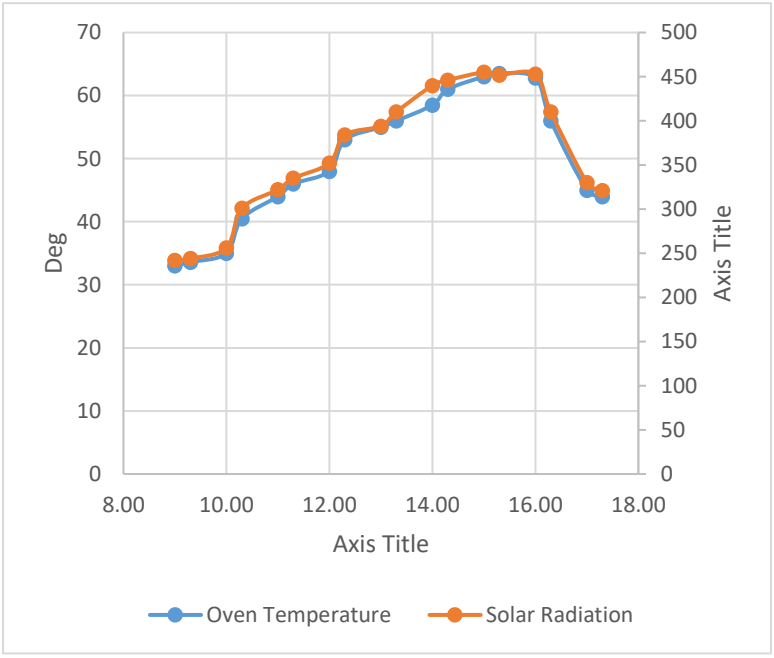

Figure 3: Experimental Results.

4.0 Conclusions

This paper presented the design analysis and fabrication of a solar oven with PCM as a thermal energy storage system using potash alum as a phase change material. Our preference of potash alum as a phase changing material over other materials is due to its easy availability at a lower price along with better thermal energy storage compatibilities for low baking temperature. The essence of the using a PCM is to enhance the performance of the oven when the solar radiation is low or absent. The test results shows that the oven can be used to bake some flour products, since a temperature of 64^{o}C was recorded.

References

Adewole, B. Z., Popoola, T. O., & A., A. A. (2015). Thermal Performance of a Reflector Based Solar Box Cooker. *Implemented in Ile-Ife, Nigeria, International Journal of Energy Engineering, 5*(5), 95-101. doi:10.5923/j.ijee.20150505.02

Chukwuneke, J. L., Nwuzor, I. C., & Digitemie, I. E. (2018). Design and Fabrication of a Dual Powered Baking Oven. *Advances in Research, 16*(4), 1-8.

Duffie, J. A., & Beckman, W. A. (2013). *Solar Engineering of Thermal Processes* (4 ed.). London: John Wiley & Sons.

Hussein, H. M.-G., & Nada, S. (2008). Experimental investigation of the novel indirect solar cooker with indoor PCM thermal storage and cooking unit. *49*(8), 2237-2246.

Kenisarin, M., & Mahkamov, K. (2007). Solar Energy storage using phase change materials,. *Journal of Renewable and Sustainable Energy Review, 9*(11), 1913–1965.

Kwan, B. M., & Bannerot, R. B. (1984). Improved Optical Design of Non tracking Concentrators. *Journal of Solar Energy Engineering, 106*(3), 271-278.

Muthusivagami, R. M., & Velraj, R. &. (2010). Solar cookers with and without thermal storage. *A review. Renewable and Sustainable Energy Reviews, 14*(2), 66-70.

Nagaraj, N., Hatim, A. J., & Haitham, A. (2016). "Solar Cooker Study under Oman Conditions for Late Evening Cooking Using Stearic Acid and Acetanilide as PCM Materials. *Journal of Solar Energy*.

Punia, R. C., Marwal, V. K., Sengar, N., & Dashora, P. (2012). Numerical Modeling of a Box-Type Solar Cooker. *International Journal of Advances in Science and Technology,, 4*(4).

Sharma, Y. C., & Singh, B. &. (2008). *Advancements in development and characterization of biodiesel: a review.* London: John Wiley.

Wikipedia. (n.d.). Retrieved from www.wikkipedia.com.

Appendix : CAD Model

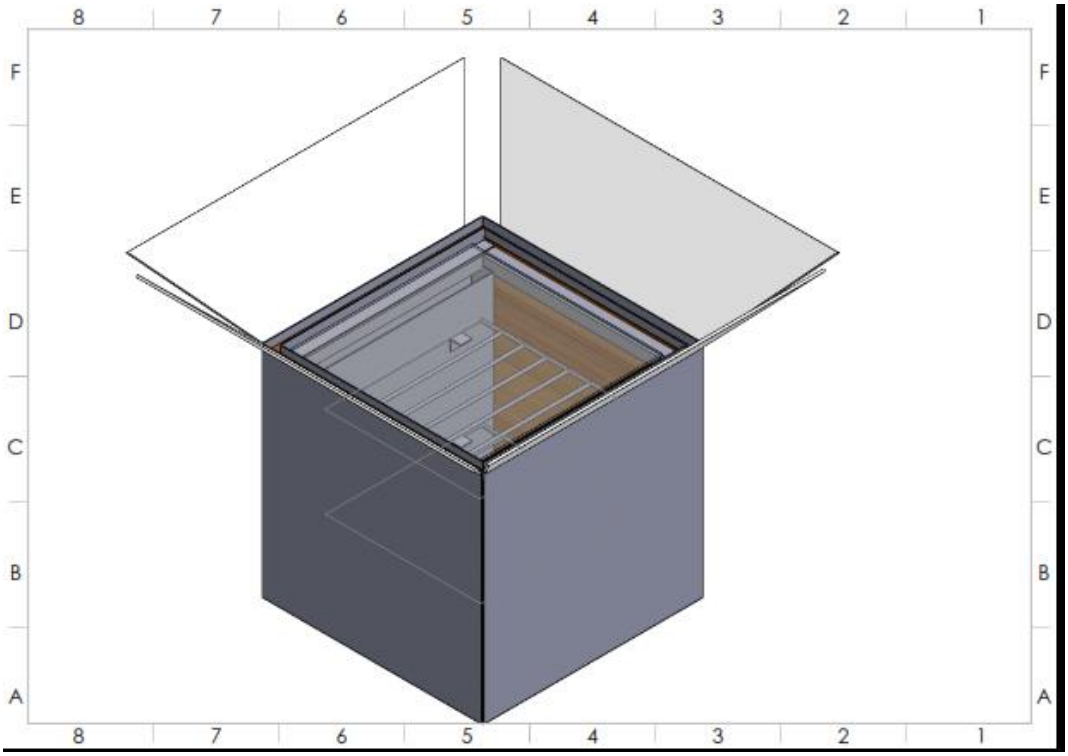

Isometric Projection of PCM Solar Oven.

Optimization of Rectangular Fins Cooled by Force Convection Using Computational Fluid Dynamics.

[1]Idris J. M., [2]Ayo S.A.

Department of Mechanical Engineering, School of Infrastructure and Process Engineering Technology, Federal University of technology, Minna, Nigeria, idrisjamiu6@gmail.com

Abstract: The trends in electronics are toward decreasing size and cost, while increasing speed. Performance and reliability of operating devices can be achieved by increasing heat dissipated. As heat loads increase, the thermal management to keep junction temperatures within safe operating limits is becoming more critical. The heat sink optimization study allowed for a determination of the heat sink geometry, which would produce a minimum thermal resistance, while producing the highest heat dissipation. A flat plate heat sink with 50 mm x 58mm with different configurations was modeled using Solidworks and a thermal analysis was performed. The result of the thermal analysis was used to optimize the fin geometries. The fin geometries considered are the pitch, fin height, numbers of fin and fin thickness. An Aluminum alloy was used as fin material to cool a motor driver (IRFP150N) with a heat power of 50W. It is found from the results that the best design with larger heat dissipation capacity is when fin thickness is small, wider pitch and taller fin height. And this consists of (7) fins with (0.3 mm) fin thickness and 7mm pitch

Key words: (heat Sink, Flat plate, CFD, cooling, optimization, fin thickness).

INTRODUCTION

One of the challenges of electronic devices is thermal management, because overheating of electronic devices has become a major issue especially in devices and a Metal-Oxide Semi-Conductor Field Effect Transistor (MOSFET) drive electronics. This problem is also witness by many home, office and industrial appliance such as power inverters, stabilizers, personal computers, cellular phones etc. therefore, most of these devices require effective means of extracting the excess heat from the electronic device. Heat sink dissipates the heat from the electronic devices. Air-cooled heat sinks have been commonly used as a means for overseeing heat-related issues of electronics because of their adequacy and cost effectiveness. Air-cooled heat sinks are susceptible to relatively low heat transfer coefficients and have large base temperature variations (Mohan & Govindarajan, 2011).

Heat sink is a passive heat exchanger which transfers generated heat by an electronic or a mechanical device to a fluid medium that are often air or liquid coolant, the heat is then dissipated away from the device thereby allowing temperature control of the device. In personal computers, heat sinks are used to cool the central processing units, some chipsets and RAM modules. Heat sinks are designed to maximize its surface area in contact with the cooling medium around it which is sometimes air. Velocity of air, material choice, extrusion design and surface treatment are factors affecting the performance of heat sink. There are several design and arrangement of heat sink which are but not limited to the following;

- Straight rectangular uninterrupted fins
- Straight rectangular interrupted fins
- Inclined rectangular fins
- Knurled fins
- Triangular fins
- Pinned fins

In this study, a straight rectangular uninterrupted fin is considered with varying parameters of fin height, fin width; inter fin spacing as well as air flow rate to determine the performance of the fin. Recently in electronics a very complicated designs of air cooled heat sinks are used which dissipates heat to the surrounding by flow of large volume of air. The major challenges associated with heat sinks are; due to constraint in space, air should be blown at very high velocities and to maintain such velocities, big size fan has to be employed. Also air flowing at a very high velocity creates noise. More so, in air cooled units, there is no active cooling device so temperature below ambient condition is unattainable. Therefore, working at high speeds in the high ambient conditions had become extremely difficult. Processor and chips cooling is one of the bottlenecks in many electronics, so there is need for the design of effective cooling techniques. (Paulo & Heitor, 2011)

The study of rectangular fin by varying geometric parameters using numerical analysis as well as simulation will reveal the optimum and effective design techniques which will provides effective passive cooling and mitigate damaged caused by excess heat generated in electronic devices as well as other engineering applications

John et al. (2010) observed that heat sinks with circular pin fins perform better than heat sinks with square pin fins at low Reynolds number. Consequently, at high Reynolds number, heat sinks with square pin fins perform better than that with circular pin-fin. Further (Rubio-Jimenez et al., 2012) concluded that heat sinks with offset micro pin fin are good option for cooling the IC chips. John et al. (2010) observed that at low Reynolds number, the heat sinks with circular pin-fins shows better performance compared with heat sinks having square pin-fins and vice versa. (Rubio-Jimenez et al., 2012) concluded that the heat sink having offset micro pin fin is a good option for cooling the IC chips. Tullius et al. (2012) studied numerically the effect of fin shapes in mini channels and established that the optimal fins shape is dependent on the flow rate of the fluid through the channel. Jadhav et al (2019) investigated geometrically enhanced heat sinks through experiment by using water and concluded that water has many potential to cool the high heat generating microprocessors. Shyu et al., (2017) numerical study concluded that by locating a rectangular pin fin in a microchannel heat sink, a reasonable heat transfer could be achieved (Jadhav et al., 2018).

Flow velocities, fluid type selection, material choice for heat sinks with different channel surface modifications are some of the related areas of heat sink where research is being carried out. It was observed by many researchers that the use of fins in micro channel enhances the thermal performance. Most researchers reported that elliptical pin fins usually exhibit poor thermal performance, but the pressure drop offered by the elliptical pin fins is minimum among the different pin fin shapes under consideration (Jadhav et al., 2018).

MATERIAL AND METHODS

Model Description

The geometry flat plate heat sink used for cooling in the research is shown in Figure 1. The work seeks to optimize the fin parameters such as the height, fin thickness, the pitch and numbers of fin. The heat sink is used for cooling IRFP150N which generate up to 50W and can operate at a maximum temperature of 150^{o}C. The heat sinks are produced from an Aluminum alloy (AL6061). A thermal simulation of the heat sinks was carried out using Solidworks with difference configuration shown in Table 1.

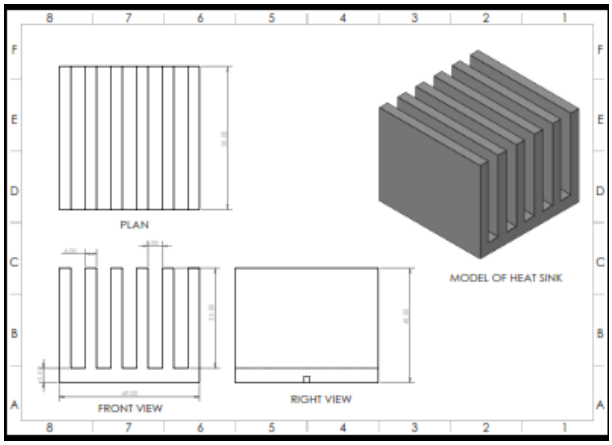

Figure 1: Geometry of the Heat Sink

Governing Equations

The Conservation of Mass, Momentum and Energy within an infinitesimal small fluid element are the fundamental governing equations of all Computational Fluid Dynamics simulations. The Conservation of Momentum laws (equation) are also known as Navier-Stokes equations, (Piyush, Bhushan, & Praveen, 2016). The governing equations for heat transfer and fluid flow are often formulated in a general form for the simplification of discretization and programming, which has achieved great success in thermal science and engineering. These equations speak physics. They are the mathematical statements of three fundamental physical principles upon which all of fluid dynamics are based:(1) mass is conserved;(2) F = ma (Newton's second law); (3) energy is conserved. The purpose of this section is to present basic equations of fluid motion.

Continuity equation

$$\frac{D\rho}{Dt} + \rho\nabla.\overline{V} = 0 \qquad (1) \qquad \text{(Hansa, et. al, 2019)}$$

The fluid density remains unchanged for all compressible flows, i.e. independent of time and space. And hence $\frac{D\rho}{Dt} = 0$ and therefore, the continuity equation is given as $\nabla.\overline{V} = 0$. (2)

Momentum equation;

The momentum of the moving fluid in x,y and z directions are expressed by equation 3 – 5.

$$for\ x-component: \frac{\partial\rho(\rho u)}{\partial t} + \nabla.(\rho u.\overline{V}) = \frac{\partial p}{\partial x} + \frac{\partial\tau_{xx}}{\partial x} + \frac{\partial\tau_{xy}}{\partial y} + \frac{\partial\tau_{zx}}{\partial z} + \rho f_x \qquad (3)$$

$$for\ y-component: \frac{\partial\rho(\rho v)}{\partial t} + \nabla.(\rho v.\overline{V}) = \frac{\partial p}{\partial y} + \frac{\partial\tau_{xy}}{\partial x} + \frac{\partial\tau_{yy}}{\partial y} + \frac{\partial\tau_{zy}}{\partial z} + \rho f_y \qquad (4)$$

$$for\ z-component: \frac{\partial\rho(\rho w)}{\partial t} + \nabla.(\rho w.\overline{V}) = \frac{\partial p}{\partial z} + \frac{\partial\tau_{xz}}{\partial x} + \frac{\partial\tau_{yz}}{\partial y} + \frac{\partial\tau_{zz}}{\partial z} + \rho f_z \qquad (5) \qquad \text{(Ejehson, et. al, 2016)}$$

Energy equation

$$\rho\frac{D}{Dt}\left(e + \frac{V^2}{2}\right) = \rho q + \frac{\partial}{\partial x}\left(k\frac{\partial T}{\partial x}\right) + \frac{\partial}{\partial y}\left(k\frac{\partial T}{\partial y}\right) + \frac{\partial}{\partial z}\left(k\frac{\partial T}{\partial z}\right) - \frac{\partial(up)}{\partial x} - \frac{\partial(vp)}{\partial y} - \frac{\partial(wp)}{\partial z} + \frac{\partial(u\tau_{xx})}{\partial x} + \frac{\partial(u\tau_{yx})}{\partial y} + \frac{\partial(u\tau_{zx})}{\partial z} + \frac{\partial(v\tau_{xy})}{\partial x} + \frac{\partial(v\tau_{yy})}{\partial y} + \frac{\partial(v\tau_{zy})}{\partial z} + \frac{\partial(w\tau_{xz})}{\partial x} + \frac{\partial(w\tau_{yz})}{\partial y} + \frac{\partial(w\tau_{zz})}{\partial z} + \rho\vec{f}.\vec{V} \qquad (6)$$

Design of Experiment/Optimization Technique

Design of experiments (DOE) is a statistical technique for quickly optimizing performance of systems with known input variables such as an electronics cooling system. Use of DOE in the heat sink design is to obtain optimum thermal characteristics. In the design of the heat sink there must be identified factors having the greatest impact on improving the capacity for heat dissipation. The geometrical factors of the structure of the heat sink, which are selected as design parameters, are the height of the fins, the fin thickness, the number of fins and pitch of the heat sink. Full Factorial Experiment for four factors for each one on two levels is used as a tool for the realization of DOE. Table 1 shows the four design parameters, whose influence is analyzed.

Table 1: Design Variables

S/No	Factors	Level 1	Level 2
1	No of Fin	6	7
2.	Fin Thickness (mm)	3	4
3.	Fin Height (mm)	35	40
4	Pitch (mm)	5	6

Thermal Simulation method

1. 3D model of the Heat sinks having different configurations was created.
2. A thermal study was from the simulation icon.
3. Materials were defined for both the heat source and the heat sink.
4. And thermal loads/restraints were defined, i.e. the power source (50W) and the mode of heat transfer (convection).
5. Contact settings were also defined between the heat sink and the heat source.
6. For assemblies and multi body parts, the proper contact settings were defined.
7. Fine mesh was created for the model and then the study was run.

RESULTS AND DISCUSSION

CFD Results

Table 2, shows sixteen (16) different configurations used for the thermal analysis of the heat sink and the responses recorded from the CFD results. i.e. the heat sink total surface area, the minimum and maximum temperature of the heat sink and total heat dissipated by the heat sinks. The results were extracted from the color plots in Figure 2. From results configuration run number 1 has the heat sink highest temperature, while run number 16 has the heat sink lowest temperature. This two heat sinks also have the smallest and largest surface area for dissipating the heat.

Table 2: Responses from the CFD analysis results

Run	No of Fin	Fin Thickness (mm)	Fin Height (mm)	Pitch (mm)	Area (m^2)	Tmin (^oC)	Tmax (^oC)	U ($W/m^{2o}C$)	Q=UCT
1	6.000	3.000	35.000	5.000	2.748	79.100	151.000	14.294	2824.233
2	6.000	3.000	35.000	7.000	2.859	86.600	120.000	14.294	1364.946
3	6.000	3.000	40.000	5.000	3.067	82.600	115.000	14.307	1421.718
4	6.000	3.000	40.000	7.000	3.177	80.400	114.000	14.307	1527.253
5	6.000	4.000	35.000	5.000	2.858	87.600	104.000	14.294	670.039
6	6.000	4.000	35.000	7.000	2.967	84.700	117.000	14.294	1369.856
7	6.000	4.000	40.000	5.000	2.858	87.500	119.000	14.307	1288.124
8	6.000	4.000	40.000	7.000	2.964	84.800	122.000	14.307	1577.568

9	7.000	3.000	35.000	5.000	3.208	80.600	113.000	14.294	1485.711
10	7.000	3.000	35.000	7.000	3.340	77.800	111.000	14.294	1585.037
11	7.000	3.000	40.000	5.000	3.579	79.800	113.000	14.307	1700.021
12	7.000	3.000	40.000	7.000	3.711	71.900	107.000	14.307	1863.600
13	7.000	4.000	35.000	5.000	3.334	78.700	110.000	14.294	1491.643
14	7.000	4.000	35.000	7.000	3.466	76.100	109.000	14.294	1629.969
15	7.000	4.000	40.000	5.000	3.844	73.300	105.000	14.307	1743.401
16	7.000	4.000	40.000	7.000	3.840	71.100	105.000	14.307	1864.394

The results of the thermal analysis conducted on the 16 heat sink configuration are shown in Figure 2. The graphs indicate the highest and the lowest temperature recorded for each heat sink configuration.

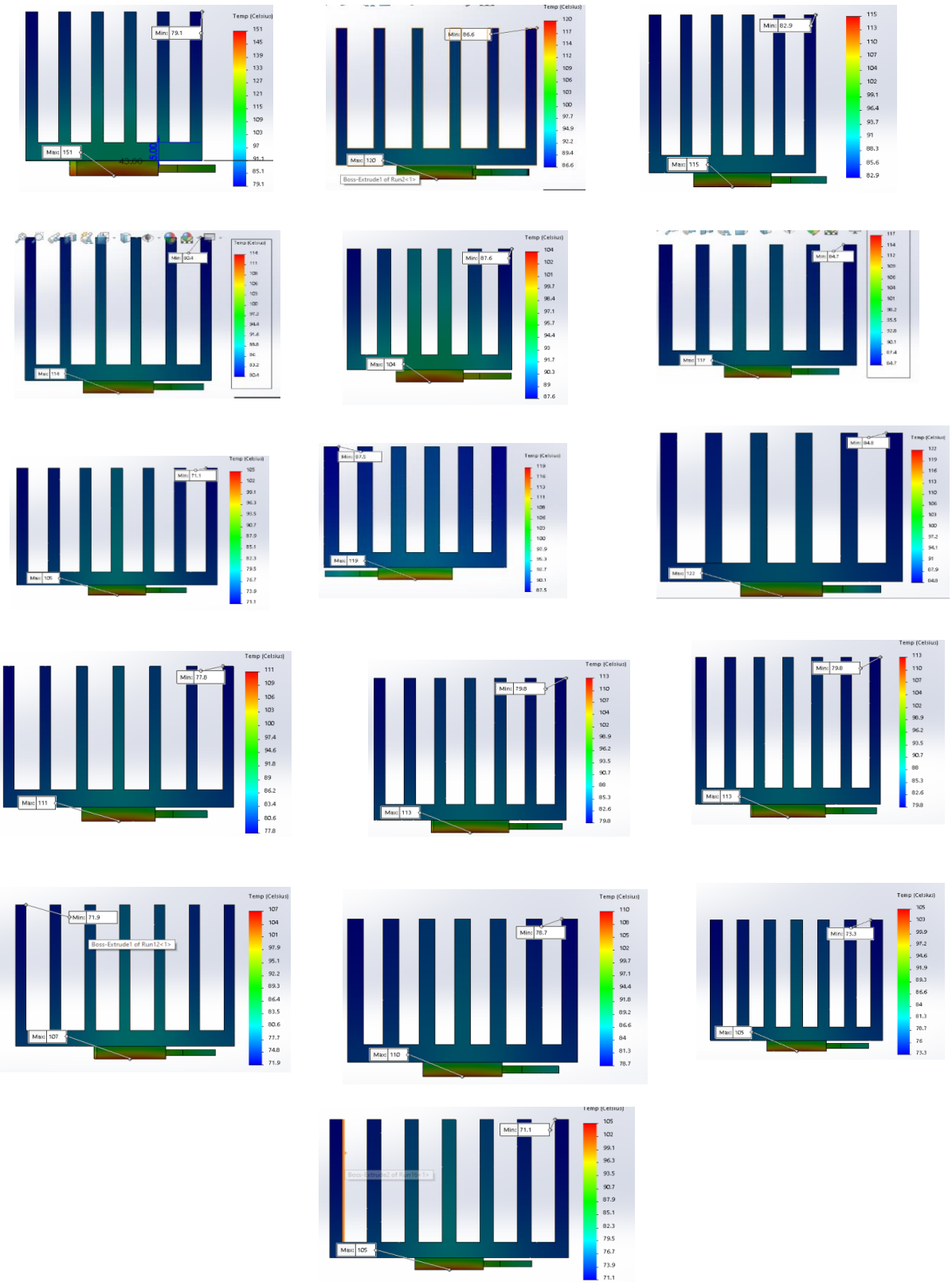

Figure 2: Temperature Color May of the Heat Sinks.

Optimization Results

The optimization of the design variables were carried out using Minitab 17 software and the key results are the main effect plots, interraction plots and contour plots, as shown in Figures 3-5. The graphs (Figure 3) reveals that the heat sinks with 7 numbers of fins dissipate more heat than the heat sinks with 6 numbers of fins. Also, the heat sinks that have 3mm thickness perform better than the heat sinks with 4mm thickness and lastly, the heat sinks with 7mm pitch have higher heat capacity that the heat sinks with 5mm pitch.

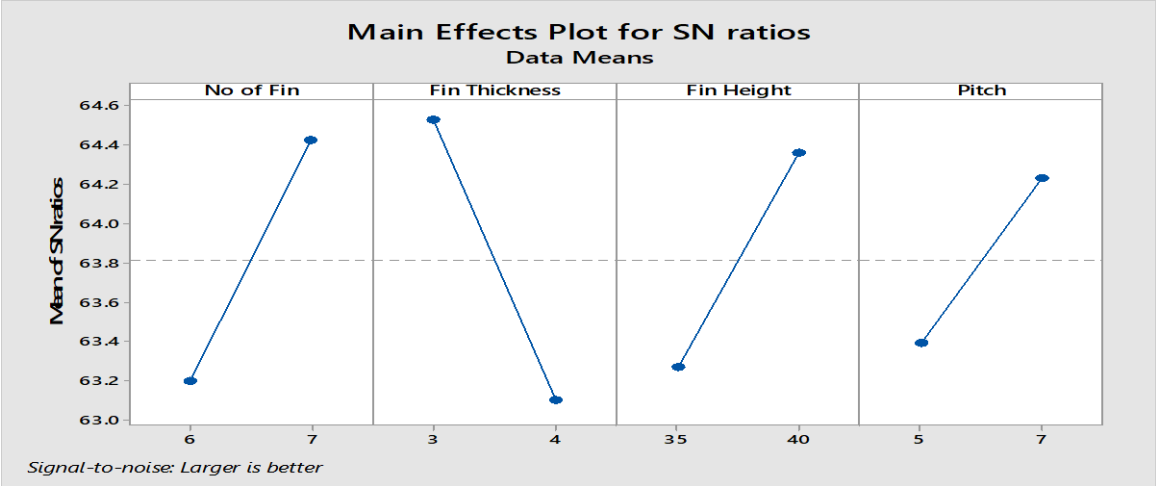

Figure 3: Main effect for SN Ratio.

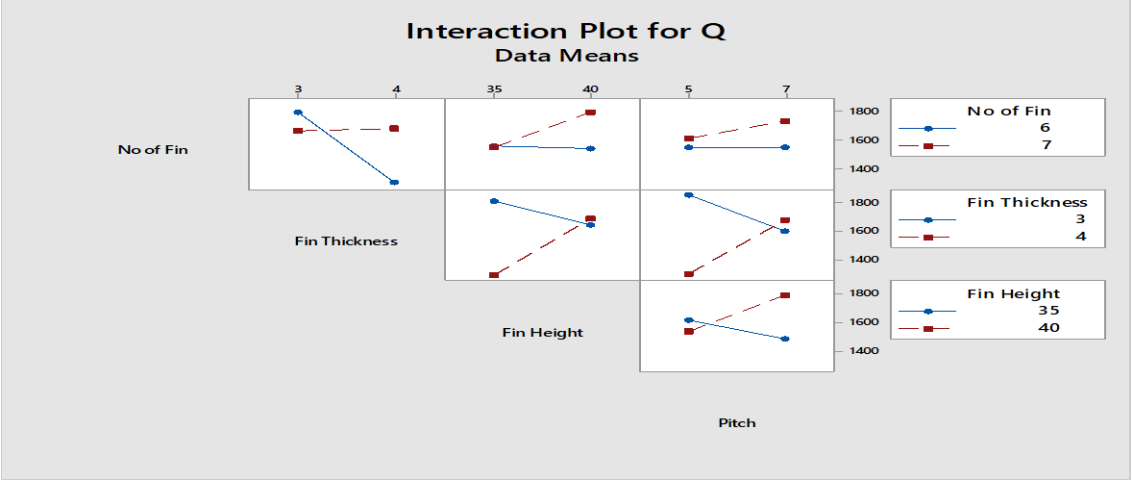

Figure 4: Interaction Plots for Quantity of Heat Dissipated.

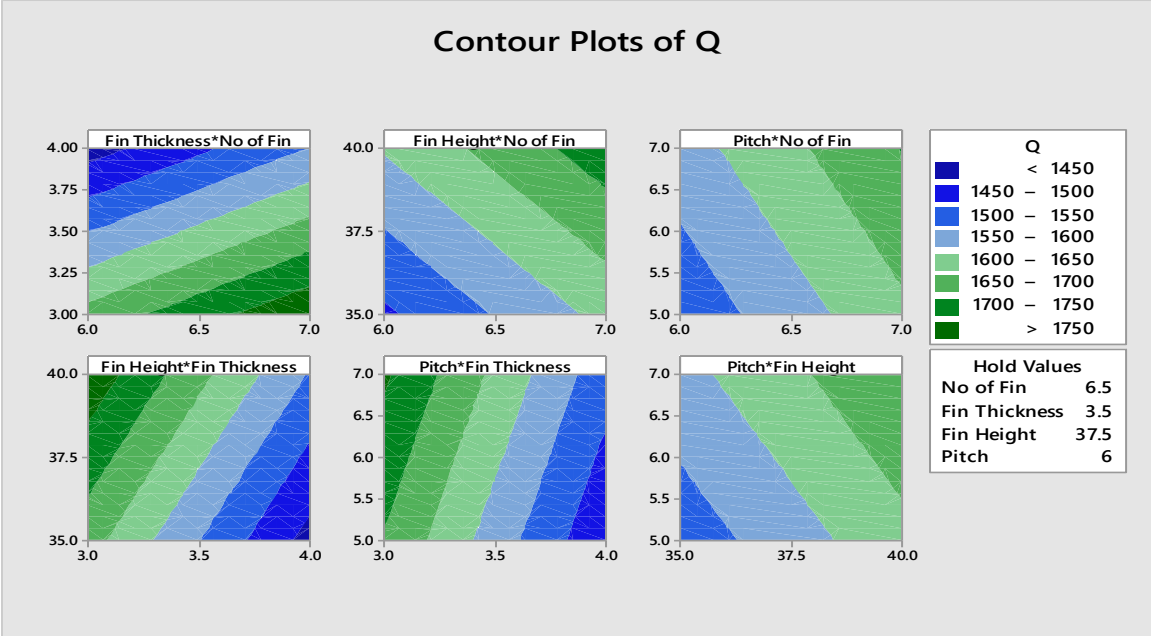

Figure 5: Contour plot the design variables and the Amount of Heat dissipated.

Figure 5, reveals the possible comfort zones for the combinations of the design variables. This shows that the small fin thickness and higher numbers of fins, higher fin height vs higher number of fins and higher number of fins with longer fin height will dissipate more heat than vise visa combinations. Similarly, slimmer fins that are taller, wider pitch with thinner fins and taller and wider fins will produce a cooler heat sink than other configurations.

CONCLUSION

The objective of this paper is to optimize the geometry of the flat plate heat sinks with different configurations for cooling motor drivers like IRFP150N and thereby produce an optimum thermal performance heat sinks by using the design variables from the IRF150N datasheet. The flat plate heat sink model was used to explore the optimal dimensions of heat sink cooled under forced convection. A 2^4 full factorial design was used with CFD thermal analysis to achieve the objectives of the research work. It was found from the results that the best design of a (50 x 50 x 5) mm aluminum heat sink with a temperature input of (50^0C) consists of (7) fins with (0.5 mm) fin widths. The optimum design variable obtain are 3mm fin thickness, 40mm fin height, 7 numbers of fin and 7mm pitch.

REFERENCES

Ejehson, P. S., Asha, S., Erukpe, A. P., Joseph, M. I., Imah, F. (2016). Investigation and Optimization of Heat Removal from a Micro-Processor Using Solid Works 2013 and Ansysy Workbench. *Scholars Journal of Engineering and Technology (SJET), 4*(9), 418-429.

Hansa, G., Prerna, L., Pranjali, S., Y. P. (2019). Thermal analysis and experimental validation of pin fins with peripheral protrusions. *IOP Conf.erence Series: Materials Science and Engineering*, 1-12.

Mohan, R., Govindarajan, P. (2011). Experimental and CFD analysis of heat sinks with base plate for CPU cooling. *Journal of Mechanical Science and Technology*, *25*(8), 2003-2012. Retrieved from www.springerlink.com/content/1738-494x DOI 10.1007/s12206-011-0531-8

Paulo, C..,Heitor, R. A. (2011). Optimization of forced convection heat sinks with pumping power requirements. *International Journal of Heat and Mass Transfer*, *54*, 1441 - 1447. Retrieved from journal homepage: www.elsevier.com/locate/ijhmt

Piyush, L., Bhushan, A., Praveen, C. (2016). Thermal Analysis of Heat Sink with Fins of Different Configuration Using ANSYS workbench 14.0 . , *International Journal of Engineering Sciences & Research*

Jadhav, S. V, Pawar, P. M., Ronge, B. P. (2018). *Analysis of Pin-Fin Geometry Effect on Microchannel*. *8*(4), 653–666.

Jadhav, S. V., Pawar, P. M., & Ronge, B. P. (2019). Effect of pin-fin geometry on microchannel performance. *Chemical Product and Process Modeling*, *14*(1), 1–15. https://doi.org/10.1515/cppm-2018-0016

Shyu, J. C., Chang, T., & Lee, S. C. (2017). A numerical study on natural convection heat transfer of handheld projectors with a fin array. *Energies*, *10*(3). https://doi.org/10.3390/en10030266

Rubio-Jimenez, C. A., Kandlikar, S. G., & Hernandez-Guerrero, A. (2012). Numerical analysis of novel micro pin fin heat sink with variable fin density. *IEEE Transactions on Components, Packaging and Manufacturing Technology*, *2*(5), 825–833. https://doi.org/10.1109/TCPMT.2012.2189925

John, T. & Mathew, B. & Hegab, Hisham. (2010). Parametric study on the combined thermal and hydraulic performance of single phase micro pin-fin heat sinks part I: Square and circle geometries. International Journal of Thermal Sciences - INT J THERM SCI. 49. 2177-2190. 10.1016/j.ijthermalsci.2010.06.011.

Tullius J.F, Tullius T.K, Jour TY, Bayazitoglu, Yildiz. (2012). Optimization of Short Micro Pin Fins Mini Channels. International Journal of Heat and Mass Transfer.55. 3921-3932. 10.1016/j.ijheatmasstransfer.2012.03.022

Design Analysis of a Rice Destoning Machine.

[1]Alfa N, and [2]Egbe E. A. P.

[1]Mechanical Engineering, School of Infrastructure Process and Engineering Technology, Federal University of Technology Minna, Nigeria, alnuhu@gmail.com

[2]Mechanical Engineering, School of Infrastructure Process and Engineering Technology, Federal University of Technology Minna, Nigeria, evus.egbe@gmail.com

[1]alnuhu@gmail.com and 08034983830.

Being a paper presented at the 5th National Conference of The Nigerian Institution of Mechanical Engineering (Minna Chapter).
19th December 2020

Abstract: Rice is a staple food of well over 90 % of the world's population it supplies a quarter of the entire calorific intake of the human race. This means rice has been of very great economic importance. Foreign materials get into rice during harvesting, handling and transportation. These unwanted materials must be significantly reduced or completely removed for good market value for grains and their products. The paper aims at presenting the analysis carried out on the design of a rice destoning machine where standard design data were generated for fabrication and subsequent performance evaluation of the machine. The major components that ensure the efficient running of the machine have been accounted for in the analysis.

Key words: *Design Analysis, Design Data, Electric Motor, Performance Evaluation, Rice Destoning*

1 INTRODUCTION

Rice is a very popular food consumed around the world, with more than 120 million Nigerians depending on it as a staple food in their diet. It is consumed in various forms but most popularly boiled as grains (Ojediran et al., 2019). The popularity is not over-emphasized as more than 5 billion people consume it globally on regular basis according to Ojediran et al. (2019).

Nigeria is the largest producer of rice in Africa according to (Udemezue and Osegbue, 2018), as the consumption rate in the country is high owing to the population of the country and the naturally arable land available. The country has a total of 91.07 million hectares, 77% of which is arable but only 44% is cultivated. More than 60% of Nigerians are farmers (Ajala and Gana, 2015), most comprise of small-scale farmers operating an average of 1 to 2 hectares of land. The consumption needed in the country is not being met with this form of farming technique. The annual consumption rate of the country is now 7.9 million (Udemezue, 2018), with the system of farming practiced only 5.5 million tonnes is realised (Udemezue and Osegbue, 2018).

Nigerian rice production process is mostly manual or inefficient methods, allowing contamination, especially during drying, winnowing, and milling process (Ojediran *et al.,* 2018). Contaminants introduced may range from pebbles from drying on the ground, chaffs left from improper cleaning after milling and even sticks.

There is a need for mechanisation of the process so that the rice produced will be commensurate with the quality of the imported ones. Machines have been developed over the years for rice cleaning and de-stoning. Adejuyigbe and Bolaji (2012) with the capacity of 31.84 g/s had 98.3 % efficiency, Gbabo et al. (2015) designed and tested a destoner powered by a 2hp motor and Ojediran et al. (2018) developed a motorized rice destoner that has high efficiency at separating 5 to 7mm impurity. These machines are mostly plagued by grain losses and low destoning efficiency if the feed rate is not properly regulated.

2 BASIC COMPONENTS

2.1 Machine Parts Description

The machine comprises of the following components: hopper, screen, reciprocating screen unit, centrifugal blower, driving and driven assembly and a discharge outlet.

2.2 Hopper
The hopper is pyramidal in shape, fabricated from mild steel sheet It forms the feeding chute through which stone contaminated milled rice is fed into the reciprocating screen, it has a feed gate at the base to regulate the discharge into the de-stoning unit by bolts and nuts for easy maintenance.

2.3 Reciprocating screen
The reciprocating screen arrangement consists of four reciprocating arms; each arm has a bearing at both ends and the ends are attached to the frame and the other to the reciprocating screen. The reciprocating screen bears the separating screen that is fixed on the blower casing. Beneath it is a connection to the cam (an eccentric mechanism) which energised the reciprocating screen in both horizontal and vertical oscillatory motion as it rotates. The reciprocating screen is arranged at an angle (which is also adjustable) to facilitate the flow of material on the screen.

2.4 Centrifugal blower
The direction of air intake of a centrifugal fan is parallel to its axis of rotation, while its discharge is perpendicular to the axis of rotation. Centrifugal fans was used in producing the require airflow needed for separating the stones from the rice grain.

2.5 Blower housing
It is made of mild steel. It accommodates the blower blade and the shaft. The blower provides the air blast for aero-dynamism.

2.6 Driving and driven assembly
A single-phase electric motor of 1hp (0.746KW) with its pulley and eccentric shaft pulley as well as a blower pulley was used. The electric motor, eccentric shaft and blower where connected by a V – belt.

2.7 Discharge Outlets
The de-stoning machine contained two discharge outlets that contain the clean rice and the stone in the reverse order.

2.8 Machine Frame
The machine frame is the unit of the machine on which all other components are mounted. It provides support for the machines during operation and when not in operation. Considering weight and strength while choosing the right material for the frame. In this work, angle steel bar of 50 × 50 × 4mm (thick) is used to provide the required rigidity.

3 METHODOLOGY
The materials selected for the fabrication of the machine are mild steel sheet for the hopper, main enclosure and the outlet, mild steel for both shafts and frame structure. Angle bars were used for the frame. Figure (1) and (2) represent the conceptual model designed in SolidWorks modelling software.

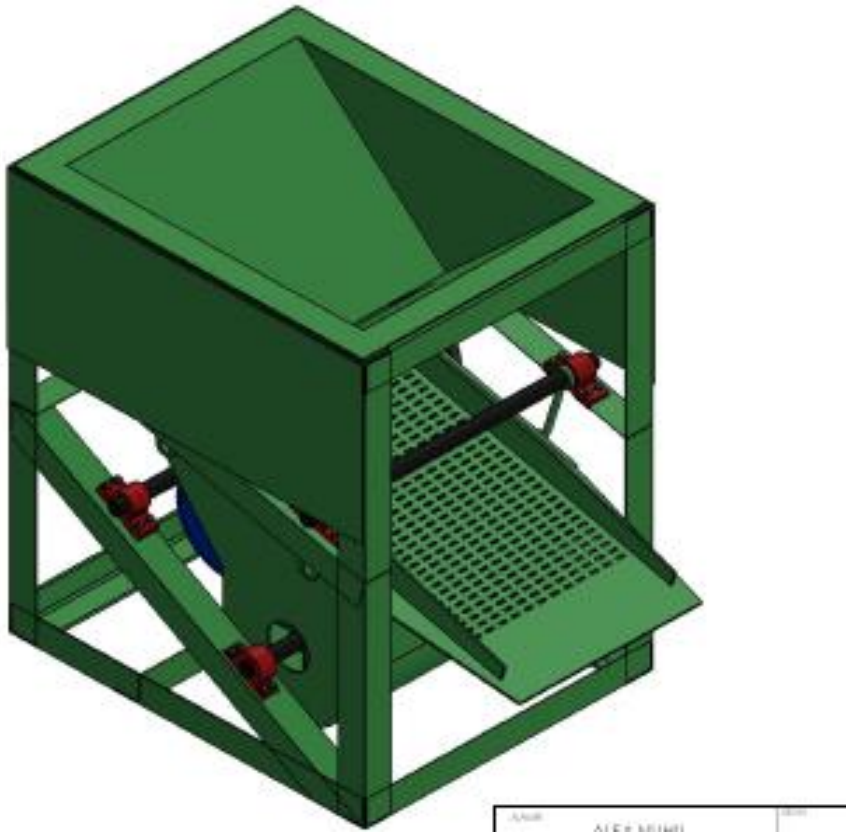

Figure 1: Isometric view of the designed destoning machine

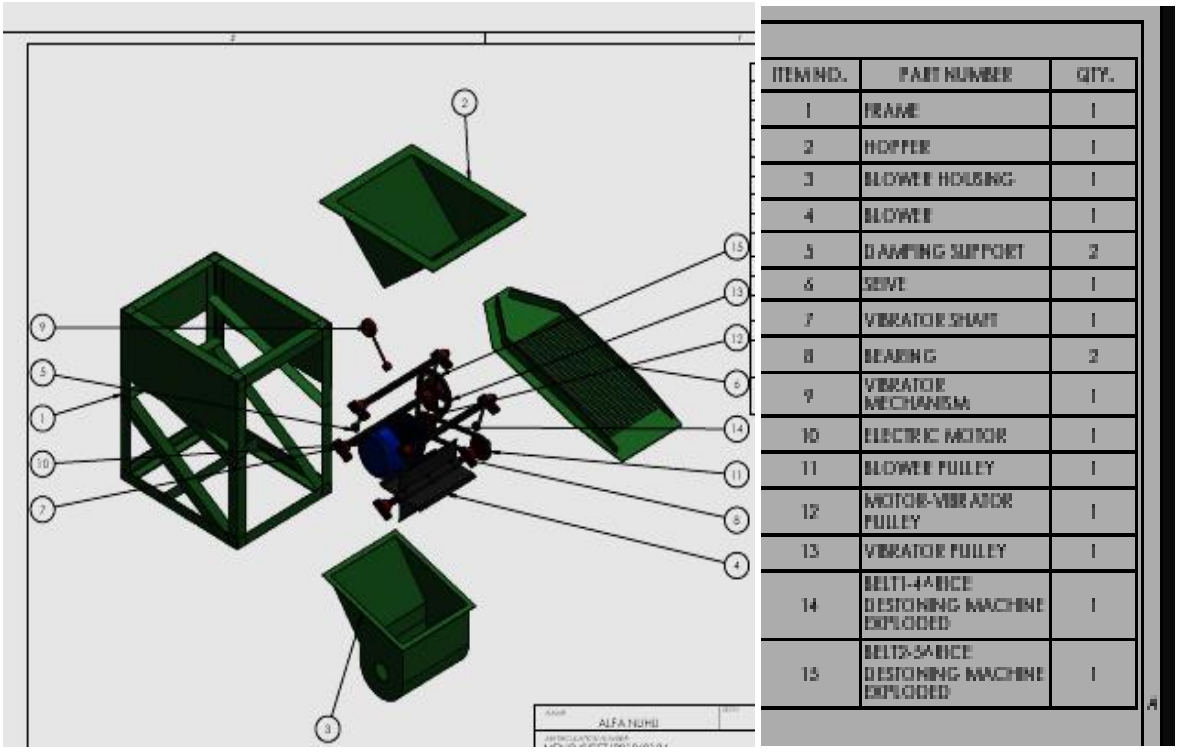

ITEM NO.	PART NUMBER	QTY.
1	FRAME	1
2	HOPPER	1
3	BLOWER HOUSING	1
4	BLOWER	1
5	DAMPING SUPPORT	2
6	SIEVE	1
7	VIBRATOR SHAFT	1
8	BEARING	2
9	VIBRATOR MECHANISM	1
10	ELECTRIC MOTOR	1
11	BLOWER PULLEY	1
12	MOTOR-VIBRATOR PULLEY	1
13	VIBRATOR PULLEY	1
14	BELT1-4 RICE DESTONING MACHINE EXPLODED	1
15	BELT2-5 RICE DESTONING MACHINE EXPLODED	1

Figure 2: Exploded view of the designed destoning machine

3.1 Design Analysis and Calculation

The design analysis was carried out to evaluate the necessary design parameters, for consideration in the selection of the various rice de-stoner components. This is so that it performs efficiently and to avoid failure during the required working life of the machine.

3.1.1. Determination of the Hopper Capacity

The hopper used was pyramidal in shape with a rectangular feed discharge gate which can be regulated for efficient de-stoning of the mass coming into the de-stoning unit, the volume of the hopper can be determined with Equation (1) as given by Ojediran *et al.,* (2018).

$$volume\ of\ pyramid\ V_h = \frac{1}{3} \times Base\ area \times height \quad (1)$$

$$volume\ of\ pyramid\ V_h = \frac{1}{3} \times (0.15 \times 0.03) \times 0.3$$

$$V_h = 4.5 \times 10^{-4} m^3$$

3.1.2 Determination of Mass Flow Rate

To determined mass flow rate of the grain through the hopper process engineers must often estimate the flow of powder, or more generally bulk solids, that they can get out of a hopper through gravity unloading (Engineering Resources for Powder Processing Industries, 2020). Angle of pour can be determined from the coefficient of friction (μ) between rice and the material for the hopper this give the minimum angle at which the rice will flow through the hopper outlet. From literature, the frictional coefficient for mild steel was determined and found out to be 0.436 as shown in Table 3.1 and according to (Ismaila, *et al.,* 2013).

Table 3.1 Show the result of the mean value for the coefficient of friction of rice on materials

Material	Rice
Wood	0.273
Stainless Steel	0.449
Mild Steel	0.436
Glass	0.086

Source: (Kayode *et al.,* 2018)

Using Johanson Equation to determine the mass flow (m) through the hopper outlet as suggested Equation 3.2 by (Ismaila, *et al.,* 2013). According to (Aremu, *et al.,* 2014) average bulk density of rice was 563 kg/m^3

$$\dot{m} = \rho_b \times A \sqrt{\frac{B \times g}{2 \times (1+m) \times \tan\theta}} \quad (2)$$

$$\dot{m} = 0.6343 kg/s$$

The mass flow rate *(m)* is 0.6343 kg/s which is equivalent to 2.2835 t/hr

3.1.3 Determination of the Screen Capacity

To determine the capacity of the machine the screen capacity was determined using the formula for calculating the volume of a rectangular shape as suggested by Gbabo, *et al.,* (2015).

$$V_{sc} = L \times B \times H \quad (3)$$

Taking length, width and height as $0.4 \times 0.25 \times 0.05\ m$ from Equation 3.2

$$V_{sc} = 0.4 \times 0.25 \times 0.05$$

$V_{sc} = 5 \times 10^{-3} m^3$

3.1.3 Determination of Vibrating Sieve for rice

Physical properties of rice grain are considered in order to design the sieve at the first stage of the separation and final stage, Figure (3) shows the dimension of the average rice grain and Figure (4) is the arrangement of the holes that make up the sieve with the dimension.

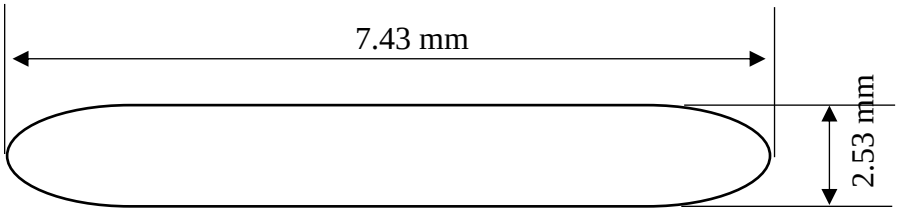

Figure 3: Rice dimension average size

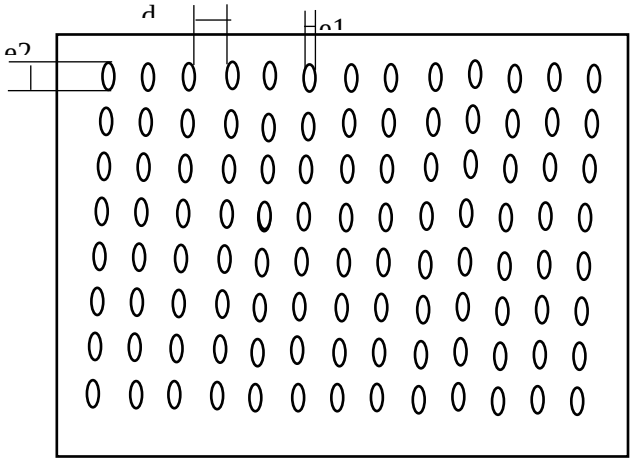

e1=2.8 mm; e1= 8.4 mm

Figure 4: Dimension of rice sieve

The dimension of the sieve can be determined by using the Table (3.2), considering the wmaximum length and width of rice grain, the following parameters can be determined (Ismail et al., 2013). The distance between the openings can be determined from the Equation (4) suggested by Usman et al. (2018).

Table 3.2: Physical properties of Sandri variety

	Variety			
Property	**Mean**	**Max**	**Min**	**CV (%)**
Length (mm)	7.43	8.31	7.26	1.02
Width (mm)	2.53	2.62	2.11	0.33
Thickness (mm)	2.75	2.97	1.88	0.68
Equivalent diameter (mm)	3.48	3.87	3.21	0.42
Sphericity (%)	4.352	4.631	4.107	0.31
Thousand weight of grain	28	31	23	3.41
Porosity (%)	46	49	41	1.08
Bulk Density (kg/m^3)	541	589	520	3.02
True density (kg/m^3)	1108.98	1218.06	1048.47	35.70
Angle of repose (°)	34	36	31	0.28

$$d = \sqrt{\frac{D^2(3\pi - 2C_o)}{C_o}} \quad (4)$$

Where D= maximum diameter of rice grain size (2.6 mm), C = coefficient of opening (3.5)

$$d = \sqrt{\frac{(2.53)^2(3\pi - 2\times 3.5)}{3.5}}$$

$$d = 2.10\ mm$$

3.1.4 Determination of the Weight of the De-stoning Unit

Equation 2.4 is used to suggest the weight of the destoning unit and its content (rice) which was determined to know the amount of load being exerted on the shaft. Hence, the weight of the unit is expressed as and also taken density of mild steel is approximately 7.85 g/cm^3 (7850 kg/m^3) and density of rice is 1452 kg/m^3).

$$F = m \times g \quad (5)$$

$$M = \rho v \quad (6)$$

For the weight of the content, that is rice from Equation 2.

$$M_{rice} = \rho v$$

$$M_{rice} = 1452 \times 4.5 \times 10^{-4}$$

$$M_{rice} = 0.65\ kg$$

Therefore $F_1 = 0.65 \times 9.81 = 6.38N$

For the purpose of this design, the weight of the rectangular frame needs to be calculated

For the pair length of the screen we have

$$M_{frame} = 2(sectional\ area\ \times length \times density\ )$$

$$M_{frame} = 2[(0.05 \times 0.004) + (0.046 \times 0.004)] \times 0.4 \times 7850\ ]$$

$$M = 2(1.21\ ) = 2.42kg$$

Also for the pair width side, we have

$$M_{frame} = sectional\ area\ \times length \times density$$

$$M_{frame} = 2[(0.05 \times 0.004) + (0.046 \times 0.004)] \times 0.25 \times 7850]$$

$$M_{frame} = 2[0.75] = 1.5\ kg$$

$$F_{frame} = (2.42 + 1.5) \times 9.81 = 38.46N$$

The sieve mass was also calculated, a metal sheet of 0.4×0.25×0.0015 m

$$M_{sieve} = \rho v$$

$$M_{sieve} = 7850 \times 0.4 \times 0.25 \times 0.0015 = 1.1775$$

$$M_{sieve} = 1.18\ kg$$

Since the sheet metal was perforated with a diameter of 2.1 mm the mass of the sieve will be the average of the sieve size.

Therefore

$M_{sieve} = 0.59\ kg$

$F_{sieve} = 0.59 \times 9.81 = 5.79N$

$F_2 = F_{frame} + F_{sieve} = 44.25N$

$F = F_1 + F_2 = 44.25 + 6.38$

$F = F_1 + F_2 = 44.25 + 6.38$

3.1.5 Determination of Required Power

The total sum of the various power needed to drive centrifugal blower and the reciprocating unit in a pendulum motion was taken into consideration, as well as the torque which will be calculated using the Equations (7) and (8) according to Ojediran *et al.,* (2018).

$P = T\omega$ (7)

$T = Fr$ (8)

Both speed and pulley sizes were determined from the relationship as shown in Equation (9)

$N_1 D_1 = N_2 D_2$ (9)

3.1.6 Determination of the Shaft Angle of Twist

Equation (10) was used to ascertain if the diameter of the shaft is safe to carry the applied load, angle of twist of a solid shaft it was determined using the formula given Ojediran *et al.,* (2018).

$\theta = \frac{584 M_t L}{G d^4}$ (10)

wherein θ is the angle of twist of the shaft in degrees; M_t is the twisting moment (Nm) l is the length of the shaft (m), G is the torsional modulus of elasticity, Nm^{-2}; d is the shaft diameter of the eccentric mechanism or the blower (m).

3.1.7 Design of Centrifugal Blower

The blower must be efficient for providing the appropriate air velocity needed for the separation of the rice-stone mixture. The theoretical airflow rate Q_T is given as (Usman *et al.,* 2018).

$Q_T = V D_p W$ (11)

Where,

V = velocity of air (ms^{-1}); D_p = depth of air (m); and W= width over which air is required. The actual air flow rate (Q_A) needed will be higher than the analytical and is obtained using the Equation (12) as provided by (Adejuyigbe & Bolaji 2012)

$Q_A = \frac{Q_T}{\eta}$ (12)

Where η is the efficiency of the blower

3.1.8 Determination of Amplitude and Frequency of Vibration

Equation (13) according to Olugboji & Jiya (2014) explains that for a system of forced vibration with a single degree of freedom (SDOF), the amplitude is given as amplitude of steady-state vibration, X.

$$X = \frac{\frac{F}{K}}{[\{1-(\frac{\omega}{\omega_n})^2\}^2+\{2\xi(\frac{\omega}{\omega_n})\}^2]^{0.5}} \quad (13)$$

Where, F = magnitude of excitation force, k = stiffness of spring (suspension reeds)
X = amplitude of steady-state vibration, m = mass of system, ξ = coefficient of damping, ω = frequency of excitation force and ω_n = natural frequency of vibration of the system, given by Equation (14).

$$\omega_n = \sqrt{\frac{k}{m}} \quad (14)$$

Where,
m is the mass of the system in (kg); f is the frequency of vibration given as Equation (15)

$$f = \frac{\omega}{2\pi} \quad (15)$$

4 CONCLUSION

Nigerian rice production process is mostly manual or inefficient methods, allowing contamination, especially during drying, winnowing, and milling. Contaminants introduced to the rice in the process are numerous hence the need for a rice destoning machine. The design analysis of a rice destoning machine was achieved in the analysis which is the aim of the paper. The major components that are required for the efficient running of the machine have been accounted for in the analysis. Hopefully, the analysis will be used for further study; this includes the fabrication and performance evaluation of the machine.

References

Adejuyigbe, S. B. & Bolaji, B. O. . (2012). Development and performance evaluation of a rice destoning machine using vibrating sieves. *Journal of Natural Sciences, Engineering and Technology*, 11(2), 94–105.

Ajala, A. S. & Gana, A. (2015). Analysis of challenges facing rice processing in Nigeria. *Journal of Food Processing*, 1-7, doi.org/10.1155/2015/893673.

Aremu, D. O., Babajide, N. & Ogunlade, A. (2014). Comparison of Some Engineering Properties of Common Cereal Grains in Nigeria. *International Journal of Engineering Science Invention (www.ijeci.org)*, 3(4), 10 - 14.

Gbabo, A., Ndagi, B., Kuku, A. M. & Abdullahi, L. . (2015). Development and testing of a rice de-stoning machine. *International Journal of Engineering Research and Science and Technology*, 4(3),135–141.

Ismail, S. O., Ojolo, S. J., Orisaleye, J. I. & Okuofo, O. S. (2013). Design of a Rice De-stoner . *International Journal of Mechanical Computational and Manufacturing Research*, 2(3), 54-64.

Ojediran, J. O., Okonkwo, C. E., Alake, S. A., Alhassan, E. A. & Olayanju, T. O. (2019). Design, development and evaluation of a motorised grader. *Journal of Food Processing Engineering*, 1-8.

Olugboji, O. A. & Jiya, J. Y. (2014). Design and fabrication of rice de-stoning machine. *Food Science and Technology* , 2(1), 1-5.

Sulaiman, I., Egbe, E. A. P., Alkali, B., Kolo, Y. B. & Enock, O. I. (2017). Development of a horizontal shaft hammer mill. *2nd International Engineering Conference* (pp. 365-369). Minna: IEC2017.

Udemezue, J. C. & Osegbue, E. G. . (2018). Analysis of Rice Production and Consumption Trends in Nigeria. *Annals of Reviews and Research*, 1(5), 1-4.

Udemezue, J. C. (2018). Analysis of Rice Production and Consumption Trends in Nigeria. *Journal of Plant Sciences and Crop Protection*, 1(3), 1-6.

Usman, M., Balogun, A. L. & Oyebanre, O. D. (2018). Design, fabrication and testing of a rice de-stoning machine. *International Conference of Science, Engineering & Environmental*, 3(1), 1-12.

TECHNO-ECONOMIC ANALYSIS OF A HYBRID POWER SYSTEM (DIESEL, SOLAR PV AND WIND) FOR A GAS MANUFACTURING PLANT IN NIGERIA

[1]Abubakar Yakubu Khartum, [2]Abdulkarim Nasir, [3]Effiom Victor Essien

[1]Mechanical Engineering, School of Infrastructure Process and Engineering Technology, Federal University of technology Minna, Minna, Nigeria, babayaks8069@gmail.com

[2]Mechanical Engineering, School of Infrastructure Process and Engineering Technology, Federal University of technology Minna, Minna, Nigeria, a.nasir@futminna.edu.ng

[2]Mechanical Engineering, School of Infrastructure Process and Engineering Technology, Federal University of technology Minna, Minna,Nigeria, victoressien2000@gmail.com

Abstract: Techno-economic analysis of a hybrid power system was conducted for an industrial gas manufacturing plant (BelAir) sited in Kontagora area of Niger State. The plant just like most other manufacturing plants in Nigeria is faced with high production costs due to majorly epileptic power availability; the plant does experience around five (5) hours of electricity power supply in a day. This is not sufficient to meet its operational needs. With the current power scheme, the firm will not sustain its operations going forward. HOMER Pro was employed to optimize the best hybrid power combination for this company. Load profile analysis for the firm was done and a peak load of 233.89KWp was obtained. A 500kW (400KVA) diesel generator, 1kW generic flat plat solar PV, and 3kW wind turbine respectively were selected and used for the optimization study. The meteorological data for wind and solar were downloaded from the National aeronautics and space administration (NASA) database. Sensitivity analysis was equally performed on diesel price, nominal discount rate, and inflation rate. The result shows that a hybrid power system consisting of a diesel generator and solar PV is the optimal solution. The optimal architecture has a Levelized cost of energy (LCOE) of ₦146.45, a total net present cost (NPC) of ₦4,198,250,000, and a return on investment (ROI) of 7.6%. It was concluded that the manufacturing company of this type can improve on their existing power scheme by leveraging on the available renewable energy resources.

Key words: Techno-economics analysis, optimization, hybrid power system, sensitivity analysis

1.0 INRODUCTION

In Nigeria, the availability of energy plays a major role in every aspect of our political and socio-economic life. Inadequate supply of energy restricts socio-political development, limits economic growth, inclusive growth in particular, and adversely affects the quality of life of citizens, both in urban and rural areas. So, improving energy supply results in improving standards of living, consequently, lead to an increase in food production and storage, increase industrial output, provision of efficient transportation, adequate shelter, improve healthcare, and enhancements in other human services.

Finding a solution to the industrial growth stagnation that Nigeria faces today requires long-term potential actions for sustainable development. A sustainable energy system may be defined as a cost-effective, reliable, and environmentally friendly energy system that effectively utilizes local resources and networks (Arif Hepbasli, 2008). For providing a sustainable energy supply, renewable energy sources appeared to be one of the most efficient and effective solutions. Each type of renewable energy system (i.e., solar, hydroelectric, biomass, wind, ocean, and geothermal energy) also has special advantages that make it uniquely suited to certain applications. The benefits of renewable energy include a decrease in external energy dependence, a decrease in transmission losses, etc. Besides, almost none of the renewable energy sources release gaseous or liquid pollutants during operation which also provides a significant advantage over the conventional systems. Now, BelAir gas

manufacturing plant is an industrial gas plant sited in Kontagora area of Niger State. This plant is responsible for the production of compressed oxygen gas, compressed Nitrogen gas, and acetylene gas. The plant just like most other plants in Nigeria is faced with high production costs due to majorly epileptic power availability; the plant does experience around five (5) hours of electricity power supply in a day. Currently, a 365kva generator is employed to supply the machinery with power and to keep operations running. Meanwhile, the operations hitherto, are not without glaring issues; lack of enough diesel fuel storage capacity, fluctuation, and unpredictable cost of diesel fuel are some of the contending factors affecting the company's growth. If the company's operations continue at this rate, the company may not able to meet up with paying of salaries, and eventually may fold up. Thus, for this reason, this study was aimed at conducting a techno-economic of a hybrid power system, to see the possibilities of investing in more economically and environmentally friendly alternatives. The aim was achieved by collecting data relating to wind speed, solar irradiation, and the technical and economic information of relevant technologies proposed for the work. Different architectures were then optimized with HOMER software, which was then followed by techno-economic analysis. Most work conducted on techno-economic analysis does not address the issue of applying autonomous grids for manufacturing companies; this work will attempt to conduct a techno-economic analysis of a hybrid power system for a company. It is with a conviction that the outcome of this work will be positive and proffer options for the company to change its course and travel on the path of positive growth. However, before embarking on this study, some reviews were done and articulated below.

An assessment of technical and economic feasibility for a hybrid PV-wind-diesel-battery energy system in a remote community of north-central Nigeria was conducted. The assessment considered designing a hybrid PV/wind/diesel/battery energy system for rural electrification in Giri village, Gwagwalada Nigeria with latitude 8.9508_ N and longitude 7.0767_ E. The study estimated the village's load profile based on the number of households, schools, and the basic health center in the village. The electrical load of 80 households for Giri village was examined; a primary school and a health center load demand were also examined for the same village. The peak and average consumption of the houses is 64.29 kW and 451.20 kWh/day, while the peak load and average consumption of the school and health center is 2.34 kW and 23.68 kWh/day with a load factor of 0.17. 10% hour to hour and 15% day to day random variables were used to enable the load data to have some degree of variability at different times of the year. The load data is served into the HOMER software for the graphical representation of the hourly and monthly load profiles. The data for solar global horizontal irradiation (GHI) and the data for wind speed respectively were from the National aeronautics and space administration (NASA) using the latitude and longitude of the location via HOMER software. The solar global horizontal irradiation data ranges from 4.27 kW/m^2/day to 6.11 kW/m^2/day respectively. The month of August has the least solar radiation with 4.27 kW/m^2/day and the month of March has the highest solar radiation value of 6.11 kW/m^2/day. For this study, the average WS of the study area is 3.19 m/s at 10 m high. The wind speed for the entire year varies between 2.66

m/s and 3.85 m/s. The optimum configuration comprises 160 kW PV panels, 50 kW generator, 320 units of batteries, and 80 kW converter, it has a total NPC of $1.01 m and COE of $0.110/kWh (Hasan et al., 2020). Consequently, an analysis on Techno-Economic-Environmental Suitability of an Isolated Micro-grid System Located in a Remote Island of Bangladesh was carried out. This work considered a municipal of 770 families and 30 different types of shops were considered. The primary loads considered were three energy-efficient lamps (compact fluorescent bulb, 15W each), one fan (ceiling fan, 50 W), one television (TV, 80 W), and one refrigerator (80 W) for every family. Some daily arbitrariness of 20% and 15% noise from time step to time step was added. The resultant annual peak load was summed up to be 324 kW, and the primary load to be 2792 kWh/day. For this research, the meteorological data was fetched from the National Renewable Energy Laboratory (NREL). Average daily radiation is 4.55 kWh/m2/day. The result shows that the PV-wind-diesel-battery hybrid system is the most feasible, having the lowest COE and NPC (Hasan et al., 2020). In a similar vein, an economics and environmental impacts assessment of a hybrid PV system in Arid Climate Considering Different Types of Solar Trackers was studied. The work evaluated and compared the performance of six different tracking systems for photovoltaic (PV) with diesel, battery hybrid system. The monthly average GHI of the selected location is downloaded from KACARE for three years. The daily solar irradiation ranges between 4.150 kWh/m^2 and 8.158 kWh/m^2; whereas, the annual average daily solar irradiation for this area is 6.3 kWh/m^2. The work considered a hypothetical load for a large residential load with daily consumption of 90kW/day located in the vicinity of Riyadh city, Saudi Arabia. Economic, technical, and meteorological data were inputted into HOMER software for simulation. Their result shows that the PV system around Riyadh city with a tracking system is economically better than the fixed angle system. Among the considered tracking system, the VCA system is the most preferred due to low NPC and LCOE values with a high return on investment (ROI) as well as low carbon dioxide (CO_2) emissions due to high renewable energy penetration (Yahya et al., 2018). Thus, from the reviews, most of the works on the techno-economic analysis of hybrid power systems are directed at residential loads. Though they are welcoming studies, however, manufacturing activities growth in Nigeria are stunted due to lack of electrical power availability and so far, no significant study on the possibilities of a hybrid power system for manufacturing industries has been established. Hence, this work attempted to conduct a techno-economic analysis for a gas manufacturing company situated in Kontagora area of Niger state Nigeria. The map of the study area is shown in figure 1 below.

Figure 1: Map of study site

2.0 MATERIAL AND METHODS

In achieving the objectives of this study, several steps were taken as shown in the figure 2.0 below.

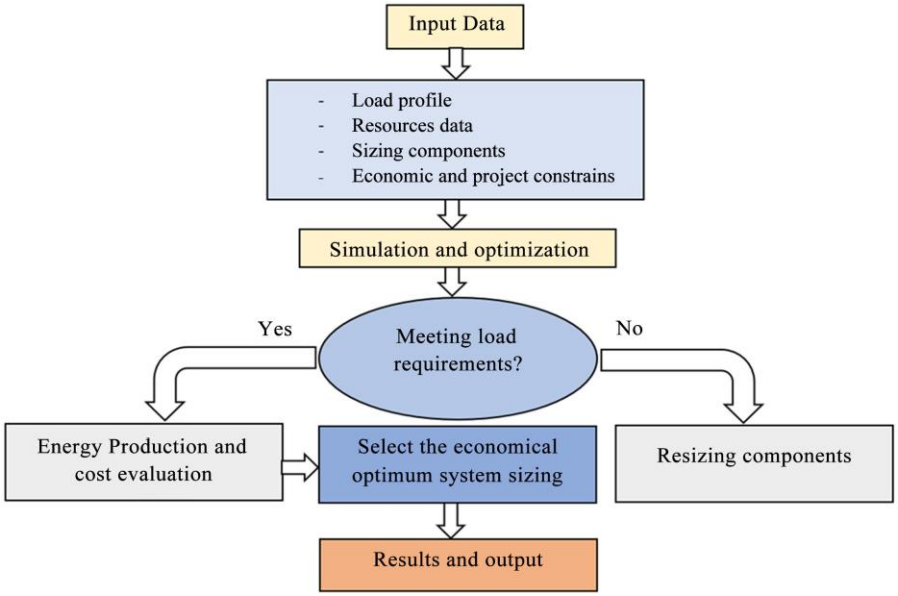

Figure 2.0: Flow chart of the study (Yahya Z. Alharthi, Mahbube K. Siddiki, Ghulam M. Chaudhry, 2018).

2.1 Load Profile

Load analysis of the company was done through identification of the electrical power equipment that supports its operations. The company's load breakdown and the operation hours for each load are shown in table 2.1 below.

Table 2.1: BelAir gas manufacturing company's load breakdown and the expected operation hours for each load.

S/N	Load	Quantity	Power (kW)	Use (h/day)	Energy consumed (kWh/day)
1	Air Compressor	1	100	24	2400
2	Liquid Oxygen (Lox) Pump	1	5	24	120
3	Molecular Sieve Bed (MSB) Heater	1	20	8	160
4	Lamps for Oxygen plant	6	0.6	12	7.2
5	Air Conditions for Oxygen Plant	2	2.22	16	35.52
6	Carbides' Hopper Drives Motor	2	4	4	16
7	Acetylene Compressor	1	30	10	300
8	Acetylene Generator's Main shaft drive	1	2	10	20
9	Energy Saver for Acetylene Plant	2	0.148	12	1.776
10	Air Condition for Administrative Block	5	5.55	10	55.5
11	Submersible Pump	1	1.11	4	4.44
12	Energy Saver for Administrative Block	7	0.7	13	9.1
	Total	**171.328**			**3129.536**

Consequently, figure 2.1 below demonstrated how the system is often loaded every hour.

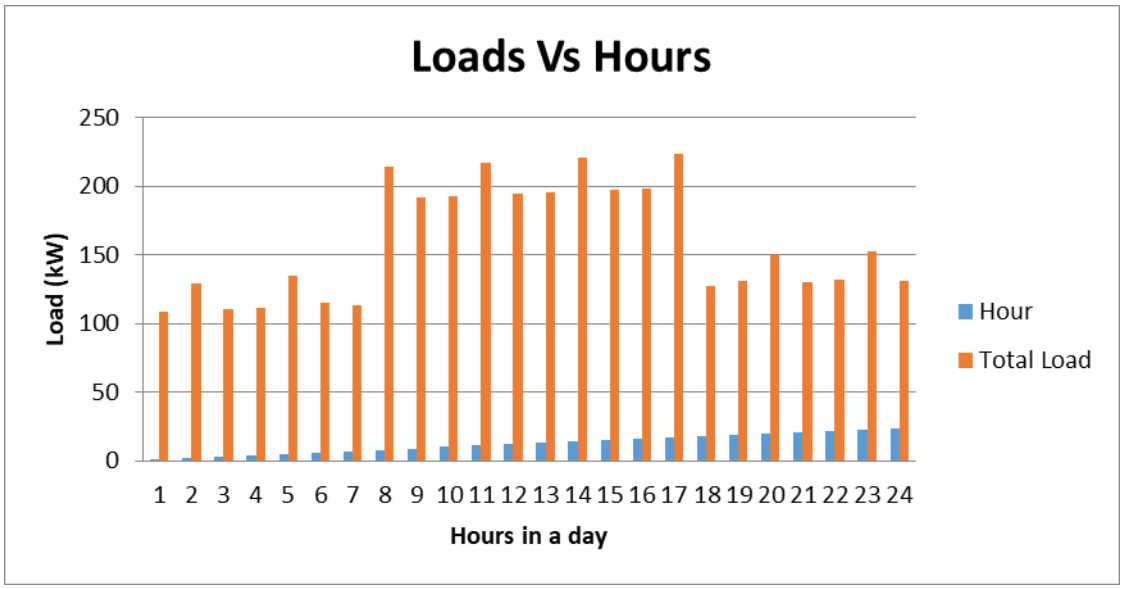

Figure 2.1: Shows how the system will be loaded each hour for 24 hours

These loads were entered on an hourly basis into HOMER Pro for simulation.

2.2 Solar Irradiation data

Monthly average Global Horizontal Irradiation (GHI) data for the study site was downloaded from the NASA database. NASA meteorological data for an average of 22years is what is available on the database. This data serves as input data for the simulation.

2.3 Wind Speed data

Similarly, monthly average wind speed data was downloaded from the NASA database and used for the simulation.

2.4 Techno-economics data

Based on the scaled peak load, some power components were selected and are presented together with their specification as shown in table 2.2.

Table 2.2: Power components for the optimization

SN	Component	kW	Qty
1	Generator	500	1
2	PV	1	0 – 400
3	wind Turbine	3	0-120

In the case of the generator, some sensitivity parameters were initiated. Parameters such as operation life and diesel price were varied to see their respective impact on the cost of energy (LCOE). Diesel generator life spans can range from less than 12,000hrs to 20,000hrs so long as they are well exercised and well maintained (WorldWide Power Product, 2020). The diesel generator lifetime of 15,000 and 876000 running hours was used for the sensitivity study, while diesel prices of 190, 200, and 200 naira were also used. Similarly, for the wind turbine, the hub height of 17, 20, and 24m was used for the sensitivity study.

Now, for capital, installation, and replacement cost of the generator, data from (Mantrac Group, 2020) was used, while, the operating and maintenance (O&M) cost and fuel cost were based on the information from the gas manufacturing company. Also, for the solar PV, the capital and installation costs were based on (Okafor, 2020), while the replacement, and operation and maintenance costs were assumed. Table 2.3 below shows the cost breakdown of the respective components. A project life of 25yrs was considered for this study.

Table 2.3: Costs of the power components

SN	Component	kW	Qty	Capital and installation cost (₦)	Replacement cost (₦)	O&M cost (N)/op.hr &(₦/yr)
1	Diesel generator	500	1	40,000,000	39,360,280	9,153.20
2	Solar PV Panel	160	1	350,000	204,000	10
3	Wind Turbine	3	1	200,000	180,000	50,000

The economics data used for this study were from (Macrotrends, 2020) and are shown in figure 2.2 below. A sensitivity study was equally done on both the nominal discount rate and the inflation rate.

.

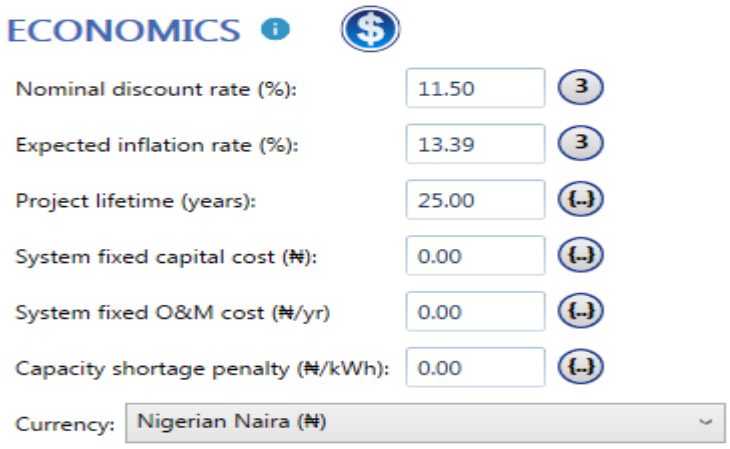

Figure 2.2: Economics parameters

After initiating all the parameters, the configuration shown in figure 2.3 below was simulated and optimum architecture was obtained which is presented in the results and discussion section.

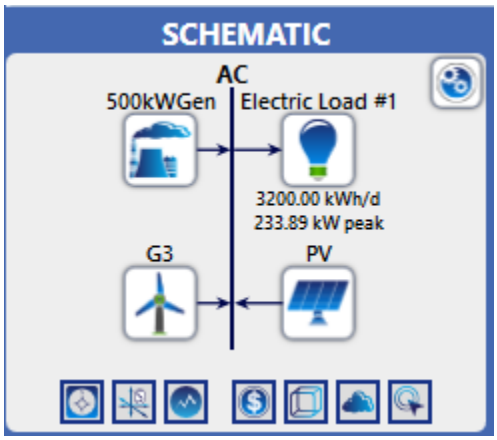

Figure 2.3: The simulated hybrid configuration

3.0 RESULTS AND DISCUSSION

A day-day of 10% and time-step of 5% variability were introduced to the load to give the load more practical representation of what can be obtainable at the gas manufacturing plant. From the HOMER load profile, it can be observed that the maximum peak load is 233.89kWp occurring at 17:00hr. This is because about 67% of the loads are active at this hour as can be seen in the figure 3.0 below.

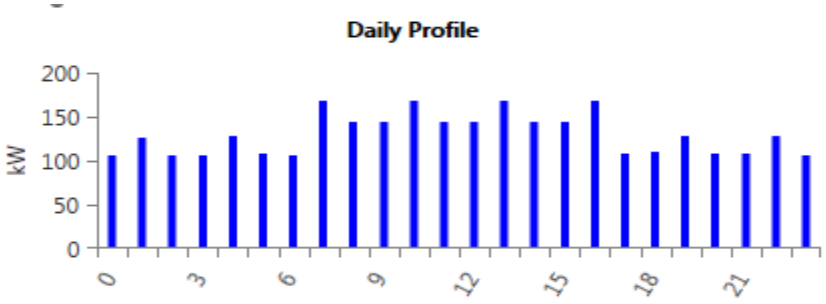

Figure 3.0: Scaled daily load profile of BelAir Gas manufacturing plant Kontagora

The wind speed data collected from NASA for the study site shows that the max wind speed occurs in January while the minimum speed occurs during in October, and the average wind speed is 4.15m/s which is consistent with what was achieved by (Lanre Olatomiwa, Saad Mekhilef, A.S.N Huda & Kamilu Sanusi, 2015), and the profile for monthly average is as shown in figure 3.1. Also, for this site, the maximum GHI value appears in April, while the minimum GHI occurs during August, and average GHI is 5.6kW/m^2/day as can been seen from figure 3.2 below.

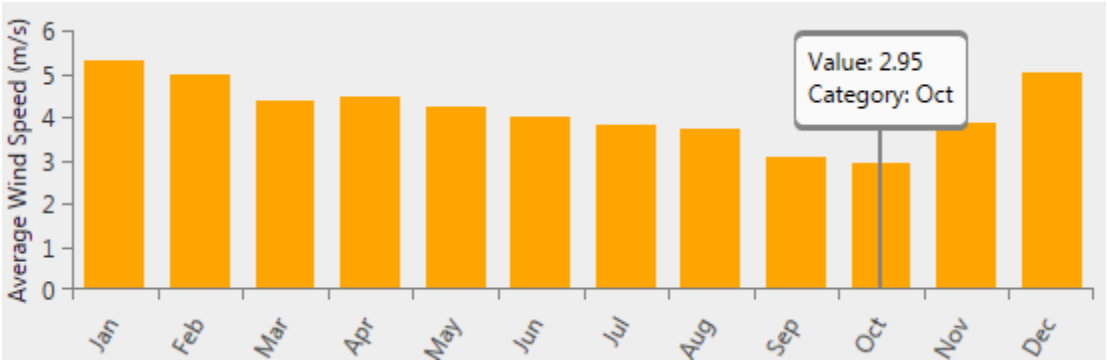

Figure 3.1: Monthly average wind speed for the study site (m/s)

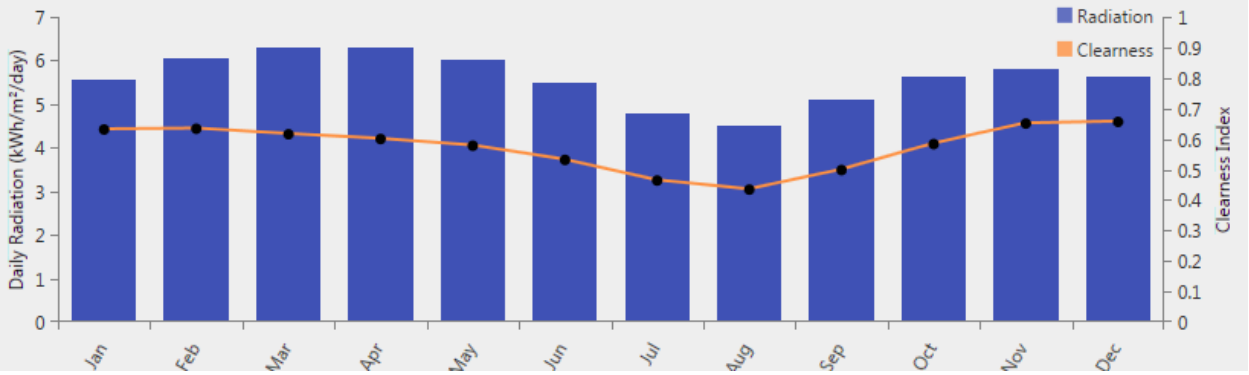

Figure 3.2: Monthly average global horizontal irradiation (kW/m^2/day)

The optimization result revealed that solar PV and generator architecture is the optimum configuration for the gas manufacturing company. This is due to the low net present cost of ₦ 4.2B and low levelized cost of energy (LCOE) of ₦143.45/kWh. The sensitivity result shows that nominal discount rate of 11.5%, inflation rate of 11.4%, generator's operating life of 15,000hrs, hub height of 17m and fuel price of ₦190/ltr are the best sensitivity parameters that gave rise to the optimum configuration. The summary of result for the best hybrid power system option for the gas manufacturing plant is shown in the figure 3.3 below.

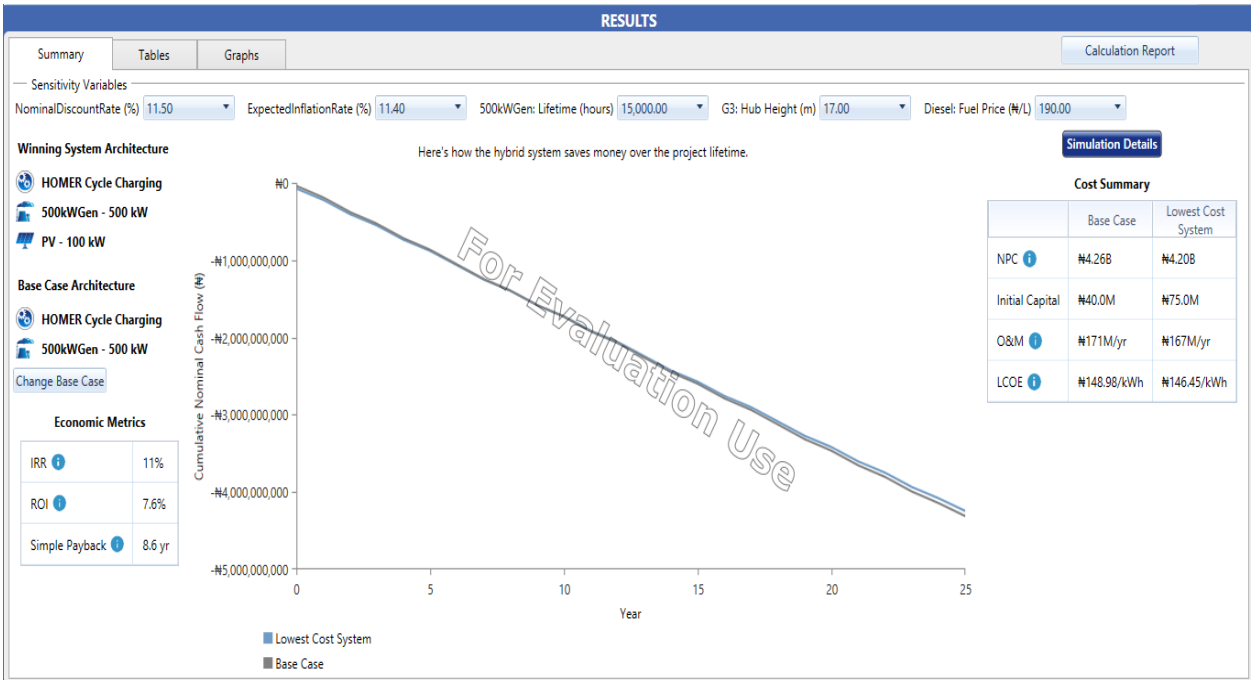

Figure 3.3: Summary of result for the optimum system

4.0 CONCLUSION

In this study, a techno-economic study of all possible hybrid power systems with the existing base case was conducted using certain assumptions. The plant considered in this study was BelAir gas manufacturing company situated in Kontagora area of Niger state. Results illustrate that:

(a) The diesel-alone existing power system is about ₦30M less expensive to install compare to hybrid energy. This is due to the initial cost of PV panels combined in the proposed architecture.

(b) The simple payback period for the proposed system is 8.6years and the return on investment of 7.6%. Also, the cost of energy of the proposed system is ₦146.45/kWh as against ₦148.98/kWh for the base case.

Therefore, similar gas manufacturing companies in Nigeria are encouraged to look at investing in a hybrid power system to reduce their operation cost. However, wind energy is not advised in this region due to low wind power availability. This is also evident in a work by (Lanre et al., 2015), where they pointed out the less potential of wind energy in the area like Kaduna.

RECOMMENDATION

This work does not consider a storage system. Therefore, subsequent work on this can include a storage system.

ORIGINALITY

The Author declare no conflict of interests

REFERENCES

(2020, July 3). Retrieved 11 23, 2020, from WorldWide Power Product: https://www.wpowerproducts.com/news/diesel-engine-life-expectancy/

(2020, 10 1). Retrieved 11 23, 2020, from Macrotrends: https://www.macrotrends.net/countries/NGA/nigeria/inflation-rate-cpi

Mantrac Group. (2020, November 22). Retrieved November 22, 2020, from Mantrac CAT: https://shop.mantracnigeria.com/collections/power/products/deposit-for-600-kva-c18

Arif Hepbasli. (2008). A Key Review on Exergetic analysis and Assessment of Renewable Energy Resources for a Sustainable Future. *Renewable and Sustainable Energy Review*, 593-661.

Hasan Masrur, Harun or Rashid Howlader, Mohammed Elsyed Lotfy, Kaisan R. Khan, Josep M, Guerrero and Tomonobu Senjyu. (2020). Analysis of Techno-Economi-Environmental Sustainability of an isolated Microgrid System Located in a Remote Island of Bangladesh. *Sustainability*, 1-27.

Lanre Olatomiwa, Saad Mekhilef, A.S.N Huda & Kamilu Sanusi. (2015). Techno-economic analysis of Hybrid PV-Diesel-Battery and PV-Wind-Diesel-Battery Power Systems for Mobile BTS: The Way Forward For Rural Development. *Energy Science and Engineering, 3*(4), 271-285.

Okafor, P. (2020, August 3). Retrieved November 22, 2020, from Nigeria Technology Guide: https://www.naijatechguide.com/2008/11/solar-energy-system-components.html

Sani Salisu, M. W. (2019). Assessment of Technical and Economic Feasibility for a Hybrid PV-Wind-Diesel energy System in a Remote Community of North Central Nigeria. *Alexandria Engineering Journal*, 1103-1118.

Yahya Z. Alharthi, Mahbube K. Siddiki, Ghulam M. Chaudhry. (2018). Economic Analysis and Environmental Impacts of a Hybrid PV System In Arid Climate Considering Different Types of Solar Trackers. *Smart Grid and Renewable Energy*, 199-214.

Providing Indigenous Technology for Processing Foods in Post Covid-19 Era for Self-Sustainability

[1]Mahmud J. O., [1]Mustapha S. A.

[1]NASENI Solar Energy Limited, Karshi, Abuja, mustapha.ajibola@naseni.org

Abstract: Innovation being one of the goals of the Sustainable Development Goals to be achieved, is a vital tool to the socio-economic development of Nigeria. Also, because food is inevitable for the survival of human beings, its processing technologies have been a continuous and challenging feat. Meanwhile, many of the technologies meant for processing local foods are foreign which has made Nigeria to be over dependent on imported technologies. Therefore, in the post COVID-19 era nations are to focus on sustaining their socio-economic activities rather than providing for others. There is the need for local Engineers to develop already existing local technologies to process local foods. This will afford Nigeria to continue to be self-reliant. This research work therefore addresses the need for Engineers to invent/innovate indigenous solutions to support local consumption. Selected items currently in use but imported are presented. Also, other items which are locally produced are also presented. Both categories are compared and analyzed. Suggestions are made from the findings. These suggestions are proposed as quick fixes to support local food processing.

Key words: Post COVID-19, Indigenous, Local food processing, Local consumption, Self-sustainability,

INRODUCTION

The Nigerian economy has been monolithic in nature since the advent of crude oil as a result of over reliance on it. In 2016, Nigeria slipped into recession and this lead to the formulation of the economic recovery and growth plan (ERGP) in order to revamp the economy by the year 2020 using indigenously developed Science, Technology and Innovation (STI) **(Mahmud & Mustapha, 2020a)**. While the ERGP is still under implementation and yet to be achieved, a deadly coronavirus pandemic coded (COVID-19) ravaged the world which significantly contributed to another recession Nigeria slipped into in the year 2020 thereby negatively affecting its socio-economic activities (**Madueke, 2020, MBNP, 2017**). With high poverty rate in the country despite the fact that food is inevitable for the survival of human beings, there has been the proliferation of imported food processing technologies **(Eze et al., 2020, United Nations, 2015)**. This research work therefore proposes that there is the need for local Engineers to innovate/invent/develop already existing rudimentary local technologies to process local foods. This will in turn afford Nigeria to continue to be self-reliant in the Post COVID-19 era.

Researchers have identified many challenges facing food processing in Nigeria. As shown in Figures 1&2, over 53.3% of cassava processors in Nigeria still use the traditional crude method and the average level of adoption of more modern technologies for food processing in the country is low, hovering 30% **(Adebayo et al., 2020, Ani et al., 2019, Karim et al., 2014)**. Majority of the Nigerian small business owners in local commercial food processing industry, such as in rice, Jam, yam oil and groundnut battle with poor quality of the output due to the fact that they cannot afford the required technology, as shown in Figure 3, in order to meet up with international standard **(Adebayo et al., 2020, Adebayo and AbdusSalam, 2019, Ajala & Gana, 2015).** This further highlights the calls for an urgent need for the improvement of the indigenous technologies rather than relying on expensive foreign technologies which local farmers cannot afford. It is evident from the reviewed literature that Nigeria has been over relying on foreign technologies in the processing of food it consumes. Wastages of unprocessed or

poorly processed foods have been a major consequence due to the fact that majority of farmers and business owners cannot afford the exorbitant prices of their required food processing machines **(Osowga et al., 2017; Sanusi & Tijani, 2018)**. The research work by **(Mahmud & Mustapha, 2020b)** opined that the building of indigenous human capacity to cater for local challenges is very important. As the Nation coast home to the Post COVID-19 era, there is urgent need for the Nigerian Mechanical Engineers to delve into the research of proffering solutions to the numerous challenges facing food processing in Nigeria via the improvement of already existing crude methods.

Figure 1: Crude methods of peeling and frying cassava **(Karim et al, 2014)**

Figure 2: Crude methods of processing oil **(Olawepo, 2020, Doinggroup.com)**

Figure 3: Modern oil processing machine **(Doinggroup.com)**

Meanwhile, in the post COVID-19 era, many countries of the world will be too occupied by focusing more on rebuilding their socio-economic activities than rendering assistance to others. This calls for the need to adequately boost and develop the local technologies to cater for our needs in the post COVID-19 era. The scope of this work focuses on the calls for the need to adequately prepare indigenous Engineers to proffers indigenous solutions to the challenges in the food processing industry but not design and construction of machines. The remaining section of this work is divided into Material and Methods, Result and Discussion, Conclusion and Recommendations

MATERIAL AND METHODS

Open source literatures were reviewed, details from which were used as a premise to derive result. Ten food processing methods were selected and their technology analyzed. Also, adopted technologies were mentioned as shown in Table 1. This was carried out to symbolize the required disruptive technologies in the post COVID-19 era.

RESULTS AND DISCUSSION

This section presents the result as tabulated in Table 1.

Table 1: Food processing stages with rudimentary and adopted technologies

S/N	Food processing	Local crude technology	Adopted technology
1	Packaging	Jute bags	Polythene bags, paper bags
2	Peeling	Knife that is made of bamboo	Mechanized peeling machine
3	Washing	River/Calabash bowl	Plastic bowl/water tank/pipe born water
4	Frying and roasting	Clay pan placed on wood fire	Solar dryer, modernized roaster
5	Pounding	Local mortar	Mechanized pounder
6	Fermentation	Heavy stone on nylon bag	Batch fermentation in Aluminum tank
7	Extraction/dewatering	Use of filled sack or cloth under heavy stone	Screw/hydraulic jack press/parallel board
8	Stirring	Wooden ladle	Mixer
9	Sieving	Suspended cloth, woven basket	Improved pulverizing machine
10	Grating	Local rough stone, prickly trunk of palms sheets	Hammer mill, disk grater

Peeling is usually one of the early stages in cassava, potato and yam processing into other staple foods or other input materials. In the typical rural areas, peeling is usually done using crude knife made with bamboo or other locally available materials, as shown in Table 1, as they do not have access to or cannot afford modernized peeling machines. The process of washing the peeled farm produce is done usually in an open and public river using local

calabash as they have no access to pipe born water and modernized water tank. In the processing of yam, pounding is done using locally made mortars made from wood due lack of modernized machines. Other processes such as dewatering is carried out with heavy stones on filled sacks as screw jacks are not easily accessible. The rudimentary technologies come with a lot of significant loss in manpower hours due to low output that does not commensurate with the input manpower. It also exposes the processed foods to contaminations and poor output quality and packaging.

The average adoption level of the modernized technologies is still very low. The poor adoption is due to the fact that many of the technologies are: very expensive, require skill and high electrical power to operate and maintain, not close to the rudiment technology used to by rural the communities and small scale business owners. The inevitably continuous use of their rudimentary technologies results in food processing in Nigeria is characterized by not just low output but also inferior quality of processed foods

CONCLUSION

This research work has been able to bring about the challenge for Nigerian Engineers to proffer indigenous solutions to the continuously lingering challenges faced by farmers and business owners in the food processing sector. Although the scope of this work did not cover the design and construction of food processing technologies, the research proposes the need for Nigeria to be self-reliant through disruptive development of local technologies for food processing in Nigeria. This will in turn adequately prepare Nigeria for the live after COVID-19 era where indigenous technologies will sustainably combat local industrial challenges.

RECOMMENDATIONS

Based on the reviewed literature, results and conclusion from this research work, the following are required and hereby recommended:

i. **Local content**: there is the need to completely stir from over dependence of foreign technologies in food processing via local content development. This means that our Engineer should use what we have locally to proffer solutions to local food processing challenges.
ii. **Low cost**: as cost of procuring the imported ultra-modern food processing machines is among the major setback in the industry, there is the need for indigenous Engineers to put the cost of their finished food processing machines into their design consideration.
iii. **Low energy use**: due to the intermittency or complete non-availability of grid electricity in many rural areas where food processing usually takes place, it is recommended that locally designed and manufactured food processing machines should consume low or no electricity.

iv. **Sustainability**: among other factors recommended to be considered for the production of indigenous food processing machine is that such locally produced equipment should be easy to maintain and reinvented.

v. **Government interventions**: the Nigerian Governments at all levels should display the political will by investing in researches geared towards indigenous development of food processing solutions by its Engineers.

vi. **Futuristic**: the designed indigenous technologies should be able to project ahead, the future needs of food processors in the post COVID-19 era.

REFERENCES

Adebayo, S. A., Olorunfemi, O. D., Siyanbola, F. I., Malomo, J. O. (2020). Groundnut Processing Techniques used by Processors in Edu Local Government Area, Kwara State, Nigeria. *FUW Trends in Science & Technology Journal*. 1(5): 117 – 121

Adebayo, F. O., AbdusSalam, R. B. (2019). Jam Making and Packaging in Nigeria, Sub-Saharan Africa: A Review. *African Journal of Food Science and Technology,* 10(1): 5-10

Ajala, A. S., Gana. A. (2015). Analysis of Challenges Facing Rice Processing in Nigeria. *Hindawi Publishing Corporation Journal of Food Processing*. 1-7

Ani, D. P., Ojila, H., Abu, O. (2019). Profitability of Cassava Processing: A Case Study of Otukpo LGA, Benue State, Nigeria. *Sustainable Food Production,* (6): 12-23

Asogwa, I.S., Okoye, J.I, Oni K., (2017). Promotion of Indigenous Food Preservation and Processing Knowledge and the Challenge of Food Security in Africa. *Journal of Food Security*. 3(5): 75-87

Eze, A. E., Okpara, U. H., Madichie, C, V. (2020). Impact of Foreign Aid on Economic Growth in Nigeria. *Socialscientia Journal of the Social Sciences and Humanities.* 1(5): 52 – 64.

Karim, O. R., Oyeyinka, S. A., Adekunle, O. A. (2014). Upgrading Traditional Food Processing Technologies: The Cassava Example in Nigeria. *Food Studies: An Interdisciplinary Journal*. 1(3): 1-67

Madueke, O. (2020). Economic Impact of Covid-19 and Policy Implications for Nigeria. *Journal of Political Science and Leadership Research*, 2(6), 44 – 52.

Mahmud, J. O., Mustapha, S. A. (2020a). Solar Photovoltaic Technology: A Sure Pathway to Nigerian Economic Recovery and Growth. *Conference on Research, Engineering Technology Innovation and Practice (CERTIP)*. 1, 3rd – 6th of November, 2020.

Mahmud, J. O., Mustapha, S. A. (2020b). Developing Indigenous Infrastructure for Local Capacity in Solar Energy. *38th National Solar Energy Forum (NASF 2020) Usmanu Danfodiyo University, Sokoto, Sokoto State*, 23rd – 25th November, 2020. 1-65

Ministry of Budget and National Planning (MBNP) (2017). Economic Recovery and Growth Plan 2017-2020. 1-140

Olawepo, R. A. (2020). Youth, Globalization, and Society in Africa and its Diaspora: Rural Women Farmers and Food Production in Ekiti-Kwara: Motives and Challenges of Operation. 168-181.

Sanusi, M. K., Tijani, S. A. (2018). Utilisation of Modern Processing Technologies among Shea Butter Processors in Niger State, Nigeria. *Journal of Agricultural Extension*. 22(2): 97-109.

United Nations, (2015). Transforming our World: The 2030 Agenda for Sustainable Development. https://sustainabledevelopment.un.org/content/documents/21252030%20Agenda%20for%20Sustainable%20Development%20web.pdf

www.doinggroup.com :

https://www.edibleoilextractionmachine.com/seed_oil_extractor/palm_oil_extraction_machine/palm_kernel_oil_extraction_machine_16.html

DEVELOPMENT OF A 5KG CAPACITY INDUCTION FURNACE FOR MELTING ALUMINIUM

[1*]Arumala J. Paul and [1]Bala, K. C.

[1]Department of Mechanical Engineering, The Federal Polytechnic, Bida. Niger State. Nigeria*
E-mail: saintjap2012@gmail.com

[1]Mechanical Engineering, School of Infrastructure Process and Engineering Technology, Federal University of technology Minna, Minna, Nigeria.
E-mail: chrisbalamaik@yahoo.co.uk

ABSTRACT

Aluminium being the most abundant metallic element, forming about 8% of the solid portion of the earth's crust, is rarely available as rich ores. Hence most countries are dependent on supplies of it being imported. Nigeria, for instance, uses aluminium in all aspects of human endeavour which gives the country abundance of secondary raw material for aluminium production. Most of the furnaces available are either fuel by fossil fuel or are large or expensive. A5kg induction furnace has been developed for melting aluminium. The furnace is designed and fabricated using local materials for small scale production. The heating process is fundamentally based on electromagnetic means and the graphite was selected as the crucible material. A temperature of 775 ^{O}C was achieved in 8 minutes for the furnace which is satisfactory as it is higher than the melting temperature of aluminium (660.4 ^{O}C). Therefore, this fabricated induction furnace can be encouraged to be used in our local foundries, companies and institutions in Nigeria and overseas as a medium for learning, faster production and to encourage local production.

Keywords: *Aluminium, aluminium scraps, crucible, induction furnace, melting temperature.*

1. Introduction

Aluminium is a metallic element that has numerous uses especially in Nigeria, it is used in transportation, machine components and even in cooking utensils. It is used to primarily used to produce pistons, engine and body parts for cars, beverage cans, door and window (frames), bars wires and also for aircraft components (Ekpe et al., 2016).

Aluminium is primarily produced from bauxite ore. Bauxite is a rock formed from a reddish clay material called laterite soil and is most commonly found in tropical or subtropical regions. Bauxite is primarily comprised of aluminium oxide compounds (alumina), silica, iron oxides and titanium dioxide. Approximately 70 % of the world's bauxite production is refined through the Bayer chemical process into alumina. Alumina is then refined into pure aluminium metal (Ekpe et al., 2016).

However, the element is rarely available as rich ores, which leads to countries relying on its importation to satisfy demand (Bala, 2005). Another method of obtaining Aluminium is through secondary production, i.e., recycling. This method according to Ekpe et al. (2016) saves up to 95 % of energy compared to the primary refinement from ore and is also cheaper.

An induction furnace is an electrical furnace where heat energy is transferred directly from the induction coil into the metal to be melted without having contact directly with the metal through the electromagnetic field produced by the induction coil. The emphasis on secondary aluminium processing has caused increase in the development of furnaces for aluminium processing. Most of the furnaces available are either fuel by fossil fuel or are large or expensive, hence the need for developing a small-scale furnace that is made from locally available materials and cheap. The paper is aimed at presenting a developed 5kg induction furnace for melting aluminium and is also introducing a small size model of furnace for our institutions, enrichment of knowledge, technical skill, small scale production of metals in a short-limited time range and also empower the student to be self-employed.

2. Literature review

Historically, the early development of induction furnace started as far back as Michael Faraday, who discovered the principle of electromagnetic induction. However, it was not until the late 1870's when De Ferranti, began experiments on Induction furnaces in Europe. In 1890, Edward Allen Colby patented an induction furnace for melting metals and produced his first steel in the United States in 1907 (Anaidhuno and Mgbenuna, 2015). The first practical usage was in Gysinnge, Sweden, by Kjellin in 1900 and was similar to the Colby furnace. In Germany 1906 the first induction furnace for three phase application was built by Rochling - Rodenhauser. During World War II, the technology grew rapidly to satisfy pressing wartime demands for a quick and authentic method of hardening metal engine parts (Anaidhuno and Mgbenuna, 2015).

The huge economic benefit of the secondary method aluminium production has enabled the continued interest in developing various furnaces for its processing. Bhandari et al. (2018) designed a Crucible Furnaces by using Black Smithy Setup. The furnace was constructed in pit format with fire bricks of 75 mm thickness and a dimension of 220 × 110 mm. The time taken to melt aluminum is 75 minutes and ambient temperature was 30°C, maximum furnace temperature achieved was 1000 °C.

Adeodu et al. (2017) developed of a 30 Kg aluminium diesel-fired crucible furnace using locally sourced materials. The furnace drum had a combustion capacity of 0.1404 m^3 and fitted with a chimney to allow for combustion gas escape. A blower was incorporated in the system, it was designed to discharge air into the furnace at the rate of 0.3 m^3/s with an air/fuel ratio of 400:1. The aluminium crucible furnace is designed to consume 4 litres of diesel fuel with a rating of 139000 kJ/gallon which is required to completely melt 30-kilogram of aluminium over a period of 18 min. the furnace was able to reach a temperature of 780 ^{O}C in 18 minutes.

Bhamare et al. (2017) fabricated a Portable Metal Melting Furnace. The heating medium is LPG gas. The components selected for the manufacturing were metallic plate, insulating material (glass wool), burner, gas cylinder, gas pipe, LPG gas, graphite crucible and gas regulator. The gas cylinder of 5 kg was used with a 1.0 kg/hr regulator. A maximum of 680 ^{O}C was reached by the furnace in 15 minutes.

Meriga et al. (2018) developed a low-cost electrical resistance-based metal melting furnace for casting applications. The furnace was designed to melt metals with temperatures below 1000 ^{O}C. It was tested with aluminium and its alloys and a 700 ^{O}C was achieved in 100 minutes. The charge inserted took 100 minutes to melt.

3. Methodology

The design was considered in two (2) phases; the geometrical and the electrical considerations of the furnace. The crucible used in this project is graphite and other materials are locally available most especially the charge material (aluminium) which can be found littered in our environment, these will help reduce used aluminium and recycle them for other purposes. The heating process is fundamentally based on electromagnetic means, the energy from a coil through which a current flow whereby circulating through the heating coil. The method of fabrication was achieved by cutting with manual hacksaw, drilling with hand drill and joining with electric arc welding machine.

3.1 Design Analysis of the Induction Furnace

3.1.1 Volume of the metal charge intended

The design analysis is based on a 5kg capacity and the shape of the crucible is cylindrical. The volume of the metal charge intended is determined using Equation (1).

$$V_m = \frac{\pi d_m^2 H_m}{4} \quad (1)$$

Where, d_m is the diameter the molten metal will occupy and H_m is the height to be occupied in both in m, with values of 0.07 and 0.13 m respectively.

3.1.2 The thickness of refractory lining

The thickness of the refractory lining of the crucible in the middle of the crucible was determined from Equation (2) according to Bala (2005).

$$B_r = 0.084\sqrt{T} \quad (2)$$

Where, T is the furnace capacity in tonnes. The furnace capacity is 5Kg in Tonnes is equal to 0.005 t, it is obtained as $B_r = 5.94$ mm.

3.1.3 The Height of Furnace from Bottom of the Bath to the Pouring Spout

The height of furnace from bottom of the bath to the pouring spout is given by Equation (3) (Bala, 2005).

$$H_f = (H_m + H_s + b_t) \quad (3)$$

Where, H_s is the height of slag formed in m, b_t is the thickness of bottom refractory lining and is b_t = 25.5 mm for 5kg capacity (Meriga et al., 2018).

The slag height, H_s was calculated using Equation (4) as given by Bala (2005).

$$h_s = \frac{4V_s}{\pi d_m^2} \quad (4)$$

V_s is the volume of slag in one heat, taken as 8% of total charge in m^3. H_f was obtained as 165.89 mm.

3.1.4 Internal Diameter of the Inductor

The internal diameter of the inductor, D_{in} was calculated as 93.88 mm from Equation (5) as stated by Meriga et al. (2018).

$$D_{in} = d_m + 2(B_r + B_{ins}) \quad (5)$$

Where, B_{ins} is the thickness of insulation layer in m (B_{ins} is such that $5 \leq B_{ins} \leq 6$ mm (Meriga et al., 2018).

3.1.5 Height of Inductor Coil

Meriga et al. (2018) gave the relation for determining the height of inductor coil as Equation (6).

$$H_{in} = (1.2 - 1.5)H_m \quad (6)$$

$H_{in} = 0.156$m

3.1.6 Height of Inductor Holding Poles

The Height of Inductor Holding Poles is determined as 162 mm using Equation (7).

$$H_P = H_{in} + 2T_f \quad (7)$$

Where, T_f is the flange thickness, taken as 3mm.

3.1.7 Heat Energy and Electrical Parameters

The required theoretical heat energy (Gandhewar et al., 2011), consumed during the first period of melt is given by Equation (8).

$$Q_{th} = Q_m + Q_{sh} + Q_s + Q_{en} - Q_{ex} \quad (8)$$

Where, Q_m is the amount of heat energy to melt 5kg of charge material in J, Q_{sh} is Amount of heat energy to superheat the melt to temperature of superheat in J, Q_s is the heat required to melt slag forming materials, in J, Q_{en} is the energy required for endothermic process in J and Q_{ex} is the amount of heat energy liberated to the surroundings as a result of exothermic reactions in J. But, theoretically is $Q_{en} = Q_{ex}$ therefore reducing Equation (8).

$$Q_{th} = Q_m + Q_{sh} + Q_s \quad (9)$$

The amount of heat energy required to melt 5kg of charge material is given by Equation (10) as given by Gandhewar et al. (2011).

$$Q_m = MC(\theta_1 + \theta_0) + L_{pt} \quad (10)$$

Where, M is the mass of charge, kg, C is the specific heat capacity of charge material, (for aluminium, C = 1100J/kg K), L_{pt} is the amount of heat to accomplish phase transformation, (for pure aluminium L_{pt} = 0, phase transformation), θ_1 = melting temperature of charge, (for aluminium θ_1 = 660°C) and θ_0= ambient temperature, 25°C.

$$Q_m = 5 \times 1100\ (660 - 25)$$

$$Q_m = 3492500\text{J}$$

Amount of heat energy to superheat the melt to temperature of superheat, Q_{sh} is obtained using Equation (11).

$$Q_{sh} = MC_m\theta_{sh} \quad (11)$$

Where, C_m average heat capacity of molten Aluminum, (= 992J/kg K), θ_{sh} is the amount of superheat temperature, taken as 40°C.

$$Q_{sh} = 5 \times 992 \times 40$$

$$Q_{sh} = 198400\text{J}$$

Heat required to melt slag forming materials, Q_s is obtained using Equation (12) as given by Gandhewar et al. (2011).

$$Q_s = K_s G_s \quad (12)$$

Where, K_s is quantity of slag formed in (kg), taken as 8% of furnace capacity, G_s is the heat energy for slag = 18kJ/kg.

$$Q_s = 0.08 \times 18$$

$$Q_s = 1.44kJ$$

Substituting into Equation (8) yields $Q_{th} = 36910.44$ KJ

3.1.8 Discharge rate of water for coil cooling

Discharge rate of water for coil cooling: from heat, heat balance equation is given as Equation (13) as stated by Bala (2005).

$$Q_p = \text{V}A_W\,\rho_W\,\text{C}_\text{w}\,(\theta - \theta_o) \quad (13)$$

Where, V is the velocity of heat carrying fluid, m/sec, A_w is the cross – sectional area of flow, m^2, ρ_W is the density of heat carrying fluid, Kg/m^3 (1000 kg/m^3), C_w is the specific heat capacity of fluid at constant pressure (4.186 kJ/kg), θ is the outlet temperature of fluid and $\theta_o$is the inlet temperature of fluid

3.1.9 Velocity of heat carrying fluid

Velocity of heat carrying fluid was determined using Equation (14) as stated by Bala (2005).

$$\text{V} = \frac{Q_p}{A_W\rho_W C_W\ (P\theta - \theta_o)} \quad (3.25)$$

Where, $A_w = \frac{\pi}{4} \times (0.006)^2$

$A_w = 2.83 \times 10^{-5} m^2$

$$\text{V} = \frac{3060.32}{2.83 \times 10^{-5} \times 1000 \times 4186(60 - 25)}$$

$$\text{V} = 0.74m/sec$$

3.1.10 Discharge of water from tube or flow rate (m^3/sec)

$$\text{Q} = \text{V}A_w \quad (3.26)$$

$$\text{Q} = 0.74 \times 2.83 \times 10^{-5}$$

$$\text{Q} = 2.09 \times 10^{-5} m^3/\text{sec}$$

3.2 Fabrication of Induction Furnace

A mild steel sheet was chosen for the construction of the furnace unit housing and the transformer seat. The thermal conductivity of mild steel is 40.1w/m$^{o}/_{c}$. A 10 litre water container is conjoined to the transformer for easy flow of water into the induction coil and air-cooling using fan for the control board for heat absorption. A high pressure 360 micro pump is used to pump water from the tank into the coil. The pump is selected because of its ability to lift water at a distance of 2.5 meters and transfer of 2 litres/min. The complete set up of the furnace is given in Figure 1. It consists of the transformer, crucible, gear spinner and cooling unit.

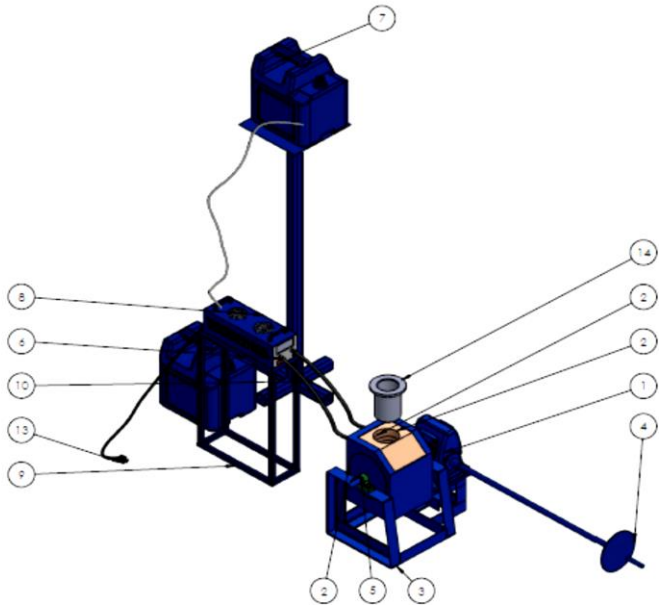

ITEM NO.	PART NUMBER	QTY.
1	MANUAL GEAR	1
2	CRUCIBLE HOUSING	1
3	CRUCIBLE HOUSING FRAME	1
4	GEAR SPINNER	1
5	BEARING	1
6	PIPE	2
7	GALLON	2
8	TRANSFORMER	1
9	TRANSFORMER FRAME STAND	1
10	WATER TANK FRAME STAND	1
11	HOSE	1
12	HOSE 2	1
13	CABLE	1
14	CRUCIBLE	1

Figure 1: Working drawing for Induction furnace

3.5 Components of Induction Furnace

a. The Crucible: The crucible is formed from refractory material, which the furnace coils are lined with. This crucible holds the charge material and subsequently the melt.

b. Inductor Coil: The inductor a tabular copper coil with specific number turns. An alternating current (A.C) pass through it and magnetic flux is generated within the inductor. The magnetic flux generated induces Eddy currents in the metal charge. It is these eddy currents that enables the heating and subsequently the melting process in the crucible

c. Cooling System: As a result of the power supplied to the furnace, its circuit appears resistive, and the real power is not only consumed in the charge material but also in the resistance of the coil. This coil loss, as well as the loss of heat conducted from the charge through the refractory crucible requires the coil to be cooled, with water as the cooling medium - this is to prevent undue temperature rise of the copper coil. To achieve effective cooling, a through-one-way flow system is used. The tubular copper coils are connected to water source through flexible rubber hoses, which are being supplied under particular pressure. The Inlet is at the top, while the outlet is at the lower end. The water flow arrangement in much that after every eight turn the water is discharged and a fresh supply starts immediately.

d. Tilting Mechanism: Tilting of the furnace is to effect pouring of the melt as a last operational activity before casting. Due to the small capacity of this furnace, manually operated tilting mechanism is adopted. The furnace is hinged at the spout edge with a shaft and bearings. And at one side to the bearing is a pinion and gear system to give a gear reduction, so that when the handle is turned clockwise, the furnace is tilted to achieve a maximum angle of 90^{o}C for complete pouring of the molten metal by tilting the furnace upwards.

e. Furnace Transformer: A step-down voltage transformer with various voltage steps tap is required. It has a three-phase primary terminal and single-phase output at the secondary terminal. A voltage supply of 415V, 50Hz frequency is used as the primary power supply. The nominal power output of the transformer ranges from 7KVA to 15KVA. The single-phase secondary terminal of the transformer is connected to the furnace inductor coil by means of a water-cooled Flexible copper coil embedded in a rubber hose.

4. Result and Discussion

4.1 Results

Aluminium scarps were deposited into the crucible and melted, from the first test the maximum temperature attained was 720 ^{o}C in 10 minutes, while the second test carried out attained a maximum temperature of 830 ^{o}C under 5 minutes.

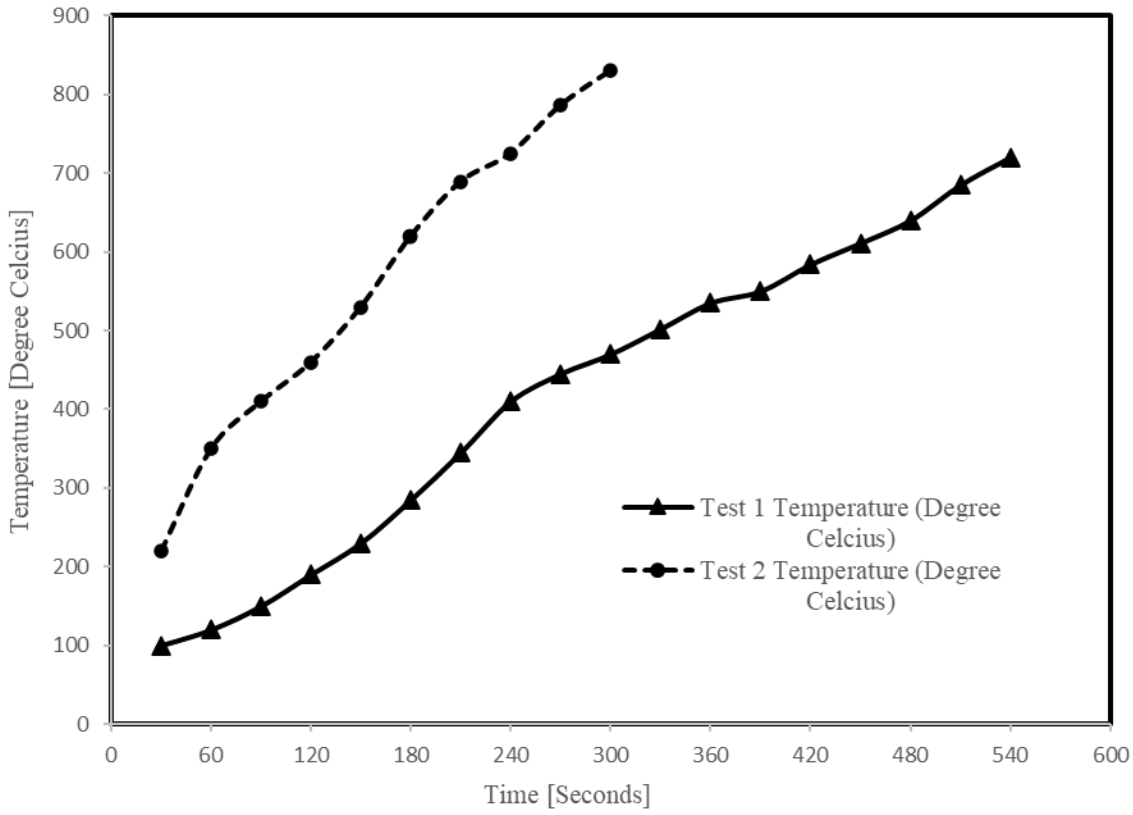

Figure 2: Temperature-Time graph of induction furnace test

4.2 Discussion

For test one carried out the time started up was 30 second and the crucible was heated up to 100 ^{o}C before the aluminium scrap metal was deposit in the crucible. The maximum temperature of 720 ^{o}C in 10 minutes, but the second test carried out attained a maximum temperature of 830 ^{o}C in 5minutes which makes the melting rate higher and faster than test one because the coil was already heated up, so the higher the temperature the faster the metal melts. The fast temperature rise of the second test is due to the preheated condition the furnace was already at when the test was commenced. The furnace was able to achieve an average value of 775 ^{o}C from the mean of the two tests, which is a satisfactory value considering it is higher than the melting temperature of aluminium.

5. Conclusion

The development of a 5Kg induction furnace for melting aluminium scraps was successfully fabricated and tested. A total heat of 36910.44 KJ was determined analytically for the machine and it reached a temperature of 775 ^{o}C in just 7.5 minutes. The temperature achieved is able to heat and melt the metal (aluminium scrap), in other to achieve the required objective.

The development of this machine helped to reduce aluminium scrap in the environment by increase the awareness of waste management and the recycling of the metal. Air pollution was reduced to the minimal when in operation of the machine and the cost of maintenance and labour was low. The metal (aluminium scrap) was melted in a shortest possible period of time with great reduction in energy consumption.

Therefore, this fabricated induction furnace can be encouraged to be used in our local foundries, companies and institutions in Nigeria and overseas as a medium for learning, faster production and to encourage local production.

References

Adeodu, A., Daniyan, I., Babalola, S., Okojie, F. & Aderoba, A. (2017). Development of a 30Kg aluminium oil-fired crucible furnace using locally sourced materials. *American Journal of Mechanics and Applications* , 5(3), 15-21.

Anaidhuno, U. P. & Mgbenuna C. O. . (2015). Development of an Electric induction furnace for heat treatment of ferrous and non - ferrous alloys. *American Journal of Engineering Research (AJER)*, 4(5), 29-35.

Bala, K. C. (2005). Design Analysis of an Electric Induction Furnace for Melting Aluminum Scrap . *AU Journal of Technology*, 83-88.

Bhamare, R., Wagh, S., More, P., Zole, A. & Sonaye, S. Y. (2017). Design and manufacturing of portable metal melting furnace. *International Conference on Ideas, Impact and Innovation in Mechanical Engineering (ICIIIME 2017)*, 5(6), 748-752.

Bhandari, S. S., Badadal, S. B., Kinagi, V. G., Tuljpurkiar, H. S. & Bansode, S. H. (2018). Design and Fabrication of Crucible Furnaces by using Black Smithy Setup. *International Journal of Engineering and Management Research*, 8(4), 131-134.

Ekpe, E. E., Yahaya, B. S. Achema, F. & Fabiyi, M. O. (2016). Design and fabrication of aluminium melting furnace using locally available materials. *American Journal of Engineering and Technology Research*, 16(1), 12-21.

Gandhewar,V. R., Bansod, S. V. & Borade, A. B. (2011). Induction Furnace - A Review. *International Journal of Engineering and Technology* , 3(4), 277-280.

Meriga, V. S. B., Boyina, A. D. & Vadana, C. (2018). Design and fabrication of low-cost electrical resistance based metal melting furnace for casting applications. *Leonardo Electronic Journal of Practices and Technologies*, 32, 41-54.

Techno-economic and environmental risk assessment of flared natural gas in Nigeria

[2]Effiom, Victor Essien, [2]Abubakar, Yakubu Khartum and [3]Nasir, Abdulkarim

[1] Department of Mechanical Engineering, School of Infrastructure Process and Engineering Technology, Federal University of Technology Minna, Minna, Nigeria, victoressien2000@gmail.com

[2] Department of Mechanical Engineering, School of Infrastructure Process and Engineering Technology, Federal University of Technology Minna, Minna, Nigeria, babayaks8069@gmail.com

[3]Department of Mechanical Engineering, School of Infrastructure Process and Engineering Technology, Federal University of Technology, Minna, Nigeria, a.nasir@futminna.edu.ng

Abstract: Techno-economic and environmental risk assessment of flared natural gas in Nigeria was conducted. Despite the penalties attached for flaring gas, oil industries in Nigeria continue to flare gas. Natural gas is one of the most common fuels in gas turbine power plants. It is cheaper to operate the units on natural gas due to better performance. However, the operation of this plant is mostly hindered due to the abrupt supply of natural gas from NLNG. Considering the effects and possible economic benefits of natural gas, this research evaluates the techno-economic and environmental risk assessment of flared natural gas with the view of helping relevant organizations to harness the potentials associated with natural gas and also to be more informed on the environmental consequences of flaring natural gas. Data from the Department of Petroleum and Geregu gas power plant were analyzed using statistical and mathematical methods. The result shows that gas flaring activities have drastically reduced from 1000748082 MSCF in 2001 to 321290.35 MSCF in 2018. Also, data indicates that between 2015 and 2018, the Geregu gas power plant recorded a maximum energy output of 1,676GWH in 2017. A total of 5,103 GWH of electrical energy was generated from 53,242,854,946SCF of natural gas from 2015 to 2018 and about ₦1,576 trillion has been lost to gas flaring between 2015 and 2018 in Nigeria. The amount of water released is the highest, while Sulphur dioxide is the least. In conclusion, a sum, more than enough to finance the Nigerian budget lost to gas flaring.

Key words: Techno-economics analysis, gas flaring, Geregu gas power plant, Environmental risk analysis

1.0 INRODUCTION

Natural gas can be “associated” (found in oil fields), or “non-associated” (isolated in natural gas fields), and is also found in coal beds (as coal bed methane). The natural gas industry is extracting an increasing quantity of gas from challenging resource types: sour gas, tight gas, shale gas, and coal bed methane. Combinations of factors like the high cost of gas processing infrastructure, low quantity of discovered gas in a reservoir, relatively low gas price or absence of a local market for the gas, and unduly inconsistent government policies usually informed the oil-producing industry to flare or vent the associated gas encountered during oil production (Anosike , 2013). In the early days of petroleum exploration, natural gas was not considered a useful product because of the difficulties in transporting it to where it can be utilized or the problems associated with its storage. As a result, gas was simply burned off at the well or vented into the atmosphere, to create rooms for other operations and supposedly to save the whole system from being burnt down by gas explosion (Aregbe, 2017). After Russia, Nigeria has been tagged the second-largest gas flaring country in the world. The Nigerian National Petroleum Corporation (NNPC) estimates that 40% of gas produced in the country is flared and that this accounts for about 11.5% of annual global flaring (Anosike , 2013). Most of the gas is flared by oil companies operating in the Niger Delta region of the country as this is where most of Nigeria’s crude oil is been extracted (Ejiogu, 2013). Niger Delta is the location of a huge oil reserve, which has been extracted for years and had generated an estimated $600 billion since 1960 (Turner, 2005).

Given the lack of infrastructure to capture and use the flared gas as well as the loss in revenue from fines, the government has favored an incentive approach to reduce gas flaring (Ejiogu, 2013). Now, despite the penalties attached for flaring gas, oil industries in Nigeria continue to flare gas knowing very well the flaring is illegal and has dangerous health and environmental consequences, this is obvious when one visits Afam in Portharcourt for

example. Consequently, most gas turbines are designed to burn on dual fuels. Natural gas fuel is one of the most common fuels in gas turbine power plants, for example, the Geregu's gas turbines burn on liquefied natural gas (LNG) fuel. It is cheaper to operate the units on natural gas due to better performance and less environmental discharge of pollutants. However, the operation of this plant is mostly hindered due to the abrupt supply of natural gas from NLNG. So, putting together the effects and possible economic benefits of natural gas, this research evaluates the techno-economic and environmental risk assessment of flared natural gas with the view of helping relevant organizations to harness the potentials associated with natural gas and also to be more informed on the environmental consequences of flaring natural gas.

2.0 MATERIAL AND METHODS

2.1 Data Collection

To proceed with this research, it was necessary to visit the Department of Petroleum Resources (DPR) and Geregu Gas Power Plant for data. Data as regards summary of production and utilization of gas in 2018, total flared gas from 2001 to 2018 among other data were contained in the 2018 Nigerian Oil and Gas Industry Annual Report obtained as a secondary data from DPR Zonal office in Abuja (7 Sylvester U. Ugoh Crescent, Abuja).
Table 2.1 represents the summary of production and utilization of gas in 2018 as exactly contained in the 2018 Nigerian Oil and Gas Industry Annual Report from DPR.

Table 2.1: Summary of production and utilization of gas in 2018

Month	Total Gas Produced (Mscf)	Total Gas Utilized (Mscf)	Total Gas Flared (Mscf)	% Flared
January	258712.89	223937.23	34775.66	13.44
February	243857.13	213943.30	29913.83	12.27
March	257089.89	229258.57	27831.32	10.83
April	242158.64	217216.19	24942.45	10.30
May	240375.58	217751.00	22624.58	9.41
June	210929.63	188244.87	22684.76	10.75
July	238627.16	214175.62	24451.54	10.25
August	260427.56	233805.46	26622.1	10.22
September	242006.42	217837.19	24169.23	9.99
October	248365.83	222594.80	25771.03	10.38
November	215400.08	187654.02	27746.06	12.88
December	251192.75	221434.96	29757.79	11.85
Total	**2909143.56**	**2587853.21**	**321290.35**	**11.04**

Table 2.2: Total amount of gas flared from 2001 to 2018 in Millions of standard cubic feet (Mscf)

Year	Total Gas Flared (Mscf)
2001	1000748082
2002	920927810
2003	801469311
2004	851647802
2005	805517432
2006	820428539
2007	816642948
2008	670786036
2009	536368324
2010	544728832
2011	503944277
2012	465256639
2013	427971368
2014	393839836

2015	330933000
2016	288917198
2017	324192401
2018	321290.35

Amount of natural gas purchased by Geregu gas turbine power plant and corresponding power generation from the utilization of the natural gas for each month from 2018 to 2019 were contained in a primary data obtained from Geregu gas turbine power plant Ajaokuta, Kogi state.

Table 2.3 and Table 2.4 represent the amount of natural gas purchased by Geregu gas turbine power plant in Standard Cubic Feet (SCF) and amount of power generation by Geregu gas turbine power plant in MWH respectively, as exactly contained in the primary data obtained from Geregu gas turbine power plant, Kogi state.

Table 2.3: Amount of natural gas purchased by Geregu gas turbine power plant in Standard Cubic Feet (SCF)

	2015	**2016**	**2017**	**2018**
January	548,577,000	1,477,654,000	994,303,000	1,693,567,783.80
February	836,316,000	850,757,000	1,138,055,182	1,865,539,430.00
March	970,653,000	0	1,057,145,404.60	1,331,432,719.80
April	990,813,000	116,331,000	1,429,068,387.70	1,781,444,945.70
May	835,941,000	373,705,000	1,583,060,999.30	1,054,639,317.60
June	916,812,000	381,630,000	1,929,462,711.40	1,380,341,000
July	880,158,000	486,267,000	1,710,716,938.40	1,272,938,000
August	950,378,000	597,285,000	1,223,280,646.10	616,130,000
September	739,047,000	614,565,000	1,291,145,984.30	785,983,000
October	744,677,000	836,669,000	1,558,062,198.10	787,565,000
November	1,249,440,000	762,641,000	1,688,598,882.90	1,473,070,000
December	1,715,765,000	839,068,000	2,117,619,414.30	2,764,535,000
Total	11,378,577,000	7,336,572,000	17,720,519,749.10	16,807,186,197

Table 2.4 Amount of power generation by Geregu gas turbine power plant in MWH

Month	**2015**	**2016**	**2017**	**2018**
January	82255.1	140008.9	94513.4	160736.4
February	86354.6	81401.7	104445	174253.6
March	95536.1	0	100807.3	123692.3
April	93481.8	10171.4	134261.9	172871.2
May	77906.2	65933.4	150663.3	99773.7
June	88089.3	37377	185193.5	128276.2
July	82531.7	47130.6	159130.9	120890
August	90154.5	58047.1	115512.8	56358.4
September	59190	57414.8	122510.5	74722.5
October	70469.2	80134.2	146822.4	74588.8
November	117407.7	70425.6	161133.2	143965.9
December	162115.1	81341.6	201272.8	262041.1
Total	1,105,491.30	729,386.30	1,676,267.00	1,592,170.10

2.2 Analysis of energy that could have been generated from flared gas

Due to energy loss in the process of electricity generation, it is not expected of the amount of electrical energy to equal the calorific value of natural gas supplied to the gas turbine. Consequently, the amount of natural gas in Table 2.3 and the corresponding electrical energy output from utilizing the natural gas in Table 2.4 were employed to estimate the amount of electrical energy that could have been generated from flared gas.

In this analysis, graphical interpolation was adopted to estimate the energy that could have been generated from natural gas. According to (Stroud & Booth, Engineering Mathematics, 2001), for a function defined by the

following set of data: $f(x_1) = f_1, f(x_2) = f_2$ and $f(x_3) = f_3$, the value of $f(x_{1.5})$ can be estimated from the graph of $f(x)$ against x. Hence, equation of the linear graph of power generated against amount of natural gas purchased was employed in predicting the amount of electrical energy obtainable from natural gas flared.
If two points on a linear graph are given as (x_1, y_1) and (x_2, y_2), according to (Stroud & Booth, Engineering Mathematics, 2001), equation of the graph is written as:

$$y = \frac{y_2 - y_1}{x_2 - x_1}(x - x_1) + y_1 \qquad 2.1$$

With electrical energy generated in MWH and amount of natural gas purchased in SCF represented as x and y respectively, $x_1 = 11{,}378{,}577{,}000$, $y_1 = 1105491.3$, $x_2 = 7{,}336{,}572000$ and $y_2 = 729386.30$, equation 2.1 was used to obtain the equation of the graph.

2.3 Economic and environmental risk assessment of the flare gas.

Assessment of impact of gas flaring on Nigerian's economy was based on cost of electrical energy loss from flared gas. Electricity tariff issued by Nigerian Electricity Regulatory Commission (NERC) from 2015 to 2018 was used to estimate the cost of energy loss due to flared gas.
Also, an in-depth assessment of the environmental impact of flared gas necessitates the analysis of the amount of greenhouse gases released every year from flared gas. According to (Anosike, El-Suleiman, & Pilidis, 2016), typical composition of Nigeria's raw associated gas composition in volume percentage from Nigerian Agip Oil Company (NAOC) Chemical laboratory comprises methane (CH_4) 78.81%, ethane (C_2H_6) 10.46%, propane (C_3H_8) 4.62%, Iso-Butane (C_4H_{10}) 0.79%, N-Butane (C_4H_{10}) 0.97%, Iso-Pentane (C_5H_{12}) 0.31%, N-Pentane (C_5H_{12}) 0.27%, N-Hexane (C_6H_{14}) 0.21%, N-Heptane (C_7H_{16}) 0.1%, Carbon dioxide (CO_2) 2.59%, Nitrogen (N_2) 0.61%, Water (H_2O) 0.26% and Hydrogen Sulphide (H_2S) 0.001%. According to Rajput (2007), gaseous fuel of such composition combust completely in the presence of excess air as described in the following chemical equations:

$$CH_4 + 2O_2 \rightarrow CO_2 + 2H_2O \qquad 2.2$$

$$C_2H_6 + \frac{7}{2}O_2 \rightarrow 2CO_2 + 3H_2O \qquad 2.3$$

$$C_3H_8 + 5O_2 \rightarrow 3CO_2 + 4H_2O \qquad 2.4$$

$$C_4H_{10} + \frac{13}{2}O_2 \rightarrow 4CO_2 + 5H_2O \qquad 2.5$$

$$C_5H_{12} + 8O_2 \rightarrow 5CO_2 + 6H_2O \qquad 2.6$$

$$C_6H_{14} + \frac{19}{2}O_2 \rightarrow 6CO_2 + 7H_2O \qquad 2.7$$

$$C_7H_{16} + 11O_2 \rightarrow 7CO_2 + 8H_2O \qquad 2.8$$

$$H_2S + O_2 \rightarrow SO_2 + H_2O \qquad 2.9$$

Carbon dioxide (CO_2), Nitrogen (N_2) and Water (H_2O) which are present in the natural gas and not represented in combustion equations above, were assumed to be inert in the combustion process and do not react with oxygen at temperature at which gas flaring occurs. However, would reflect in the combustion product. Volume of greenhouse gases such as carbon dioxide (CO_2), steam(H_2O), Sulphur dioxide (SO_2) and Nitrogen (N_2) released into the atmosphere were calculated per MSCF of flared gas.
Evaluation of quantity by volume of greenhouse gases produced was carried out assuming a unit MSCF of flared gas. Equation 2.2 to equation 2.9 were used to evaluate the volume of carbon dioxide (CO_2) and steam(H_2O) produced from complete combustion of the respective MSCF composition of the natural gas.

3.0 RESULTS AND DISCUSSION

3.1 Analysis of Data from Department of Petroleum Resources (DPR) and Geregu Gas Power Plant

Data obtained from Department of Petroleum Resources (DPR) indicates that gas flaring is still in practice during oil exploration. However, the act of gas flaring in Nigeria has been drastically reduced as clearly shown in Figure 3.1 below. From 1000748082 MSCF in 2001 to 321290.35 MSCF in 2018 as indicated in Table 2.2 above.

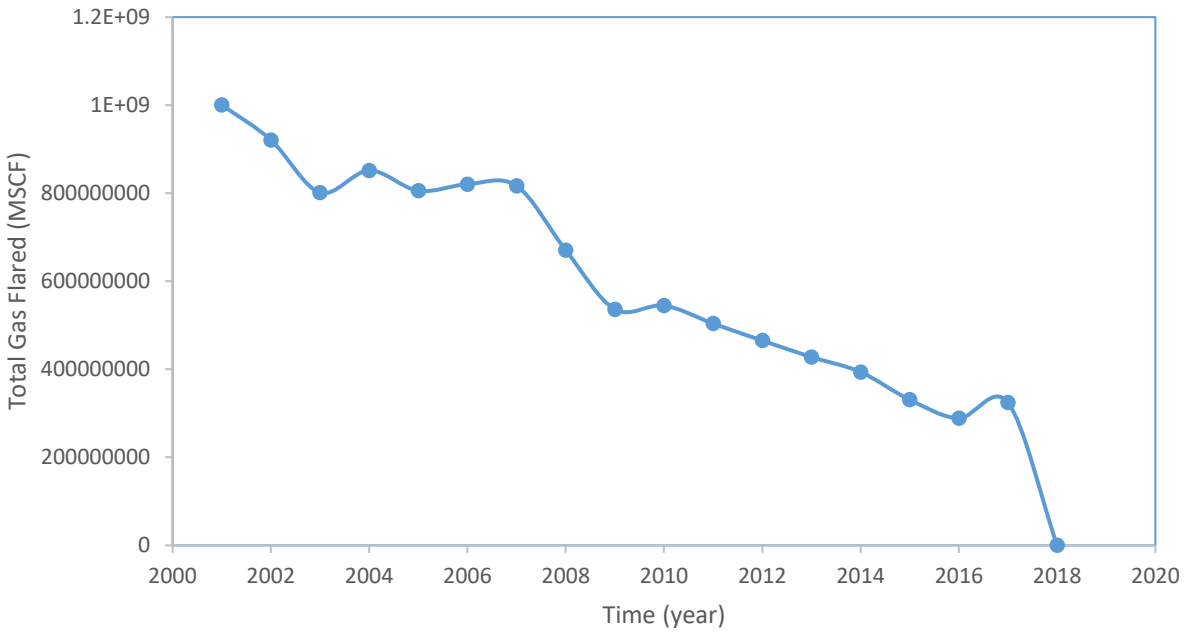

Figure 3.1: Total gas flared in Nigeria between 2001 and 2018

Also data from Geregu Gas Power plant indicates that between 2015 and 2018, Geregu Gas Power Plant recorded a maximum energy output of 1,676,267.00 MWH in 2017 as shown in Table 2.4 which corresponds to maximum amount of natural gas purchased in Table 2.3. Table 2.5 shows the amount of natural purchased and corresponding power generated yearly by Geregu gas turbine power plant.

Table 3.1 Amount of natural purchased and corresponding power generated yearly by Geregu gas turbine power plant.

Year	Amount of Natural Gas Purchased (SCF)	Power Generated (MWH)
2015	11,378,577,000	1,105,491.30
2016	7,336,572,000	729,386.30
2017	17,720,519,749.10	1,676,267.00
2018	16,807,186,197	1,592,170.10
Total	53,242,854,946	5,103,314.70

It can be seen in Table 3.1 above that a total of 5,103,314.70MWH of electrical energy was generated from 53,242,854,946SCF from 2015 to 2018. Also, the minimum amount of power generated corresponds to the minimum amount of gas purchased. This is a clear indication that more gas purchased leads to greater power generated as also illustrated in Figure 3.2 below.

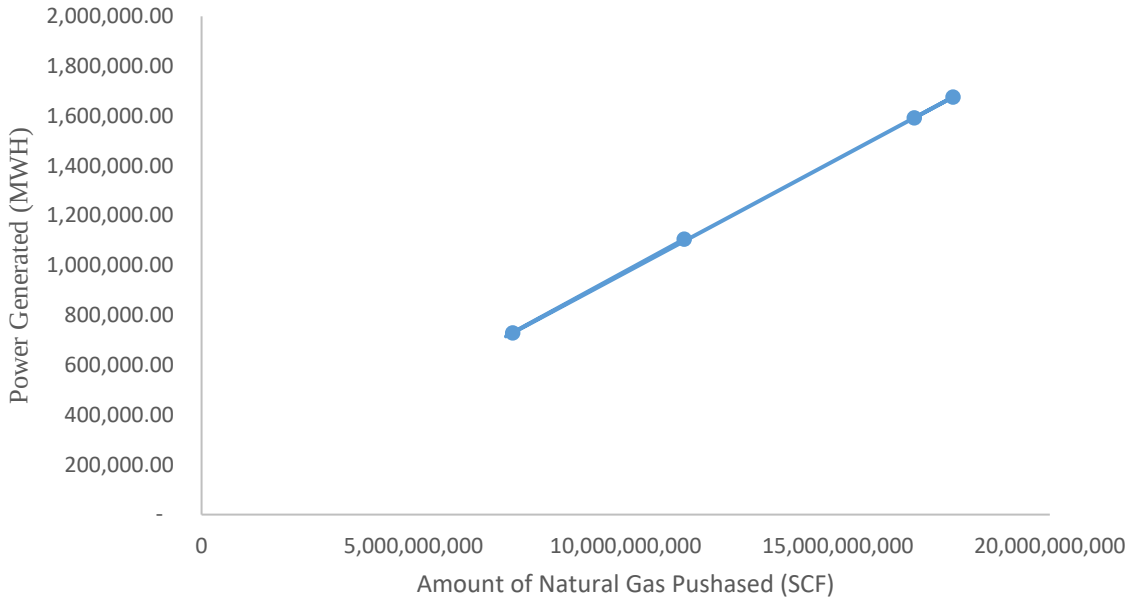

Figure 3.2 Power generated and amount of gas purchased

3.2 Electrical energy that could have been generated from gas flared

As shown in Figure 3.2 above, the graph of Power generated and amount of natural gas purchased by Geregu gas power plant is linear and its equation is:

$$PG = 9.3049 \times 10^{-5}(ANG - 11378577000) + 1105491.3 \quad 3.1$$

Where PG and ANG are power generated and amount of natural gas purchased respectively by Geregu gas power plant. Hence, the estimated amount of electrical energy that could have been gotten from flared gas from 2015 to 2018 is determined from equation 3.1. Table 3.2 indicates Power that could have been generated from flared gas from 2015 and 2018.

Table 3.2 Power that could have been generated from flared gas from 2015 and 2018.

Year	Amount of Natural Gas Flared (SCF)	Power That Could Have Been Generated (MWH)
2015	330933000000000	30793031443
2016	288917198000000	26883503083
2017	324192401000000	30165825447
2018	321290350000	29942471.87
Total	944,363,889,350,000	87872302444

From Table 3.2 it can be seen that an estimated total of 87872302444MWH of electricity could have been generated from 944,363,889,350,000SCF of flared gas.

3.3 Economic impact of the flare Gas

Considering the power that could have been generated in Table 4.2 and Benin DISCO energy charge for residential R2 category from 2015 to 2018 by NERC (Omigbodun, 2015) presented in Table 3.3 below, the lost revenue from flared gas was determined. Table 3.4 depicts the estimated cost of lost electrical energy have could have been generated from flared gas from 2015 to 2018.

Table 3.3: Electricity tariff from 2015 to 2018

Year	Energy charge (₦/kWh)	Fixed Monthly Charge (₦)
2015	18.46	750
2016	17.02	900
2017	18.23	1080
2018	15.23	1296

Table 3.4 Cost of lost electrical energy have could have been generated flared gas

Year	Power That Could Have Been Generated (MWH)	Lost Revenue (₦)
2015	30793031443	568,439,360,446,780.00
2016	26883503083	457,557,222,483,460.00
2017	30165825447	549,922,997,911,770.00
2018	29942471.87	456,023,862,132.10
Total	**87872302444**	**1,576,375,604,704,140.00**

From Table 3.4, it can be seen that about ₦1,576 trillion has been lost due to the flaring of associated natural gas between 2015 and 2018 in Nigeria. Lost revenue in 2015, 2016, 2017 and 2018 are ₦568,439,360,446,780.00, ₦457,557,222,483,460.00, ₦549,922,997,911,770.00 and ₦456,023,862,132.10 respectively as shown in Table 3.4. These lost revenues from flare gas are higher than ₦243 billion in 2015, ₦230 billion in 2016, ₦268 billion in 2017, and ₦233 billion in 2018, obtained by (Omontuemhen, et al., 2019) who evaluated with the global cost of natural gas and financial penalty associated to gas flaring. The differences in value are because evaluation based on revenue from sale of electricity that could have been harnessed from flare gas, apart from basic cost of natural gas would also include electricity generation, transmission and distribution cost in overall cost.

3.4 Environmental Risk Assessment of flare gas

The amount of greenhouse gases released into the environment per Million of Standard Cubic Feet (MSCF) of flare gas is tabulated below in Table 3.5. From Table 3.5, the amount of water released is 2.22291 MSCF per MSCF of flare gas. Carbon dioxide and Sulphur dioxide released are 1.2808MSCF and 0.00001MSCF respectively per MSCF of flare gas as shown in Table 3.5. The amount of water released is the highest, while Sulphur dioxide is the least.

Table 3.5: Amount of Greenhouse Gases Released per MSCF of flare gas

Constituent of Natural Gas	Volume of Constituents per MSCF of Natural gas (MSCF)	Amount of CO_2 released per MSCF of gas flared (MSCF)	Amount of H_2O released per MSCF of gas flared (MSCF)	Amount of SO_2 released per MSCF of gas flared (MSCF)
Methane (CH_4)	0.7881	0.7881	1.5762	0
Ethane (C_2H_6)	0.1046	0.2092	0.3138	0
Propane (C_3H_8)	0.0462	0.1386	0.1848	0
Iso-Butane (C_4H_{10})	0.0079	0.0316	0.0395	0

N-Butane (C_4H_{10})	0.0097	0.0388	0.0485	0
Iso-Pentane (C_5H_{12})	0.0031	0.0155	0.0186	0
N-Pentane (C_5H_{12})	0.0027	0.0135	0.0162	0
N-Hexane (C_6H_{14})	0.0021	0.0126	0.0147	0
N-Heptane (C_7H_{16})	0.001	0.007	0.008	0
Carbon dioxide (CO_2)	0.0259	0.0259	0	0
Nitrogen (N_2)	0.0061	0	0	0
Water (H_2O)	0.0026	0	0.0026	0
Hydrogen Sulphide (H_2S)	0.00001	0	0.00001	0.00001
Total	**1.00001**	**1.2808**	**2.22291**	**0.00001**

Table 3.6 depicts the amount of greenhouse gases released into the atmosphere from flare gas between 2015 and 2018.

Table 3.6: Amount of greenhouse gases released into the atmosphere

Year	Amount of Natural Gas Flared (MSCF)	Amount of CO_2 released (MSCF)	Amount of H_2O released (MSCF)	Amount of SO_2 released (MSCF)
2015	330933000	423858986.4	942200379.5	9422.003795
2016	288917198	370045147.2	822577058.2	8225.770582
2017	324192401	415225627.2	923009199	9230.09199
2018	321290.35	411508.6803	914746.7605	9.147467605

4.0 CONCLUSION

Data collected from the Department of Petroleum Resources during this study revealed the existence of gas flaring in Nigeria. Although, implementation of drastic measures to curtail this act was evident in Table 2.2, as the volume of gas flared continues to drop from 1000748082 MSCF in 2001 to 321290.35 MSCF in 2018. Such volume of wasted natural gas could have been utilized to power a gas plant, typically Geregu Gas Power Plant in Kogi, Nigeria.

Analysis of wasted energy from flared gas between 2015 and 2018, based on the volume of natural gas purchased by Geregu Gas power plant, indicates that an estimate of 87872302444MWH of electrical energy could have been generated from 944,363,889,350,000 SCF of flared gas in Nigeria. Hence, a sum of ₦1,576.4 trillion as lost revenue estimated at the Electricity tariff rate issued by the Nigerian Electricity Regulatory Commission (NERC) from 2015 to 2018. A sum of money, more than enough to finance the Nigerian budget lost due to gas flaring.

Also, greenhouse gases such as water, sulphur dioxide, and carbon dioxide accompany gas flaring.

ORIGINALITY

The Author declare no conflict of interests

REFERENCES

Anosike, N. B. (2013). *Techno-economic evaluation of flared gas reduction and energy recovery using gas-to-wire scheme.* Cranfield: Cranfield University.

Anosike, N., El-Suleiman, A., & Pilidis, P. (2016, March). Associated Gas Utilization Using Gas Turbine Engine, Performance Implication- Nigerian Case Study. *Energy and Power Engineering*, 137-145.

Aregbe, A. (2017). Natural Gas Flaring-Alternative Solutions. *World Journal of Engineering, 5*(01), 139-153.

Arif Hepbasli. (2008). A Key Review on Exergetic analysis and Assessment of Renewable Energy Resources for a Sustainable Future. *Renewable and Sustainable Energy Review*, 593-661.

Ejiogu, A. (2013). Gas Flaring in Nigeria: Cost and Policy. *Energy and Environment, 24*(6), 983-998.

Lanre Olatomiwa, Saad Mekhilef, A.S.N Huda & Kamilu Sanusi. (2015). Techno-economic analysis of Hybrid PV-Diesel-Battery and PV-Wind-Diesel-Battery Power Systems for Mobile BTS: The Way Forward For Rural Development. *Energy Science and Engineering, 3*(4), 271-285.

Okafor, P. (2020, August 3). Retrieved November 22, 2020, from Nigeria Technology Guide: https://www.naijatechguide.com/2008/11/solar-energy-system-components.html

Omigbodun, A. (2015, June 3). *The new electricty tariffs from July 2015*. Retrieved from Vanguard: http://www.google.com/amp/s/www.vanguardngr.com/2015/06/the-new-electricity-tariffs-from-july-2015/amp/

Omontuemhen, P., Akingbade, A., Akinaanu, O., Adigun, B., Omosomi, O., & Ogunremi, M. (2019). *Assessing the Impact of Gas Flaring on the Nigerian Economy.* Nigeria: PwC.

Stroud, K., & Booth, D. (2001). *Engineering Mathematics* (5th ed.). New York: Palgrave.

Stroud, K., & Booth, D. (2013). *Advance Engineering Mathematics* (4th ed.). London: Palgrave Macmillan.

THERMAL ANALYSIS OF FLAT PLATE HEAT SINK WITH FINS OF DIFFERENT CONFIGURATIONS UNDER NATURAL CONVECTION

ONUEGBU J. C. And Ayo S. A.

Department of mechanical engineering, Federal university of technology, minna

Corresponding author: onuegbuchinedu029@gmail.com

Abstract:

This paper investigated the effect of four different configuration of plate fin heat sink subjected to natural convection. Comprehensive thermal performance was studied for each of the heat sinks. The test 1 heat sinks is the normal or control heat sink, test 2, heat sink have its fins tapered and fillet, test 3 has its fins only tapered, while test 4, has its fins filleted. Investigations were performed for variables such as 100W heat source, 303 K ambient temperature and convective coefficient of air 25 W/m^2 K. a temperature color map of the heat sinks were plotted and also, the temperature profile of the center fin for each heat sink. The results show that test 4 has a 11.89% than the other three test 1 configurations.

Keywords: Heat sink, fillet, tapered, temperature, cooling.

1.0 INTRODUCTION

Heat sink is an electronic component or a device of an electronic circuit which disperses heat from other components (mainly from the power transistors) of a circuit into the surrounding medium and cools them for improving their performance, reliability and also avoids the premature failure of the components. For the cooling purpose, it incorporates a fan or cooling device mostly made from Aluminum alloy such as the one used in (Raaid, 2013).

Extended surfaces or fins are commonly found on electronic components ranging from power supplies to transformers. The dissipation and subsequent rejection of potentially destructive self-produced heat is an important aspect of electronic equipment design. The dissipation of heat is necessary for its proper function and component life, (Sandhya & Kishore, 2015). The heat is generated by the resistance encountered by electric current(Sampath, Sawan, & Chithirai, 2015). Many electronics components require proper cooling arrangement during design stage, the operating temperature most exceeds permissible limit, mostly specify in the component datasheet.

2.0 Literature Review

(Zhipeng, Xianghui, Liangbin, & Mengqiao, 2020)presents an effective method for predicting and optimizing the cooling performance of Parallel-Plain Fin (PPF) heat sink module based on the Taguchi method. The numerical simulative analyses of the PPF heat sink module have been constructed to understand the affecting situation of its related modeling parameters. The design parameters evaluated are the outline design of the heat sink module and the wind capacity of fan, and the highest temperature (or thermal resistance) of this module is considered as the performance characteristics. Taguchi method for the design of experiment (DOE) and the analysis of variance (ANOVA) are applied to find the optimized design parameters efficiently. From the numerical simulative analyses, the optimum design parameters to obtain the lowest value of the highest temperature (or thermal resistance) are found, and the highest temperature value has decreased to 8.009 °C and about 15.01% improvement. The result of the analyses of the noise factors has shown that the two noticeable variable factors are the wind capacity of the electric fan and the gap of fin flake. By using Taguchi method for design of experiment (DOE) and the analysis of variance (ANOVA), four noticeable variable factors will be obtained: number of opening slot, copper base surface area, wind capacity of the fan, and the height of the fin flake respectively.

(Arularasan, 2008)have selected an optimal heat sink design in their research work, preliminary studies on the fluid flow and heat transfer characteristics of a parallel plate heat sink have been carried through CFD modeling and simulations. The geometric parameters fin height, fin thickness and fin pitch have been considered in this work. In this research work, optimal design of the heat sink is carried out on a parallel plate heat sink using CFD study. Experimental studies have been performed with a parallel plate heat sink to validate the heat sink model. These results and conclusions drawn in this paper benefit the design engineers involved in electronics cooling.

Kim et al. (2008) have compared the thermal performances of the two types of heat sinks most commonly used in the electronic equipment cooling: plate-fin and pin-fin heat sinks. In order to obtain the fluid flow and thermal characteristics of heat sinks, an experimental investigation is conducted. Based on the experimental results of the present study and the available data from the existing literature, the correlations of the friction factor and the Nusselt number are suggested for each type of heat sink.

Heat sinks with parallel arrangement of rectangular cross section plate fins on a flat base are used preferably in vertical or upward facing horizontal orientations in order to obtain higher natural convection rates (Tari, 2013).

In practice, there is certainly a need for investigating the relationship between the heat sink design variable for easy and effective performance, as there are thousands of applications for heat sinks that require unique configuration, as while was suggested as a viable solution for cooling of flat panel displays with high power components (Tari, 2013). There are several that have been conducted on natural convection heat transfer from flat plate heat sinks (Mittelmann et al. [1]) and Starner and McManus [2]

3.0 Materials and Method

3.1 Numerical computation

In this section, the investigation develops a CFD model to analyze the effect of tapered and fillet profile on the convective heat transfer in plate-fin heat sinks. There are three main steps in CFD analysis: (a) pre-processing, (b) solver execution and (c) post-processing. The former step includes creating the geometry of the desired model as well as the mesh generation, whilst as expected, the results are presented in the last step. Boundary conditions are fed into the model in the solver execution (middle) stage.

3.2 Geometry

In this paper, four (4) sets geometries of the heat sinks were investigated. And their configurations are shown in figure 1. For the plate-fin heat sink with fillet profile, the optimum radius of fillet profile equal to 1.5 mm is considered for the remainder of paper as detailed in (Ammar, 2019). The base dimension measures 40 mm × 39.7 mm, with thickness of 5 mm. The channel width and thickness of fin is assumed to be constant across the length of the base and measures 3.3 mm and 1 mm respectively as shown in Fig. 1. The tapper angle is 3^{o}C. the fin height are between 25mm and 28.5mm. The difference is due to the compensation for the volume of solid material that removed from the base to generate fillet and tappered. For the remainder of paper, the plate-fin heat sink subject to the same thermal condition. Proposed design refers to as a plate-fin heat sink subject to parallel flow so that the air flows into the heat sink along the x-axis.

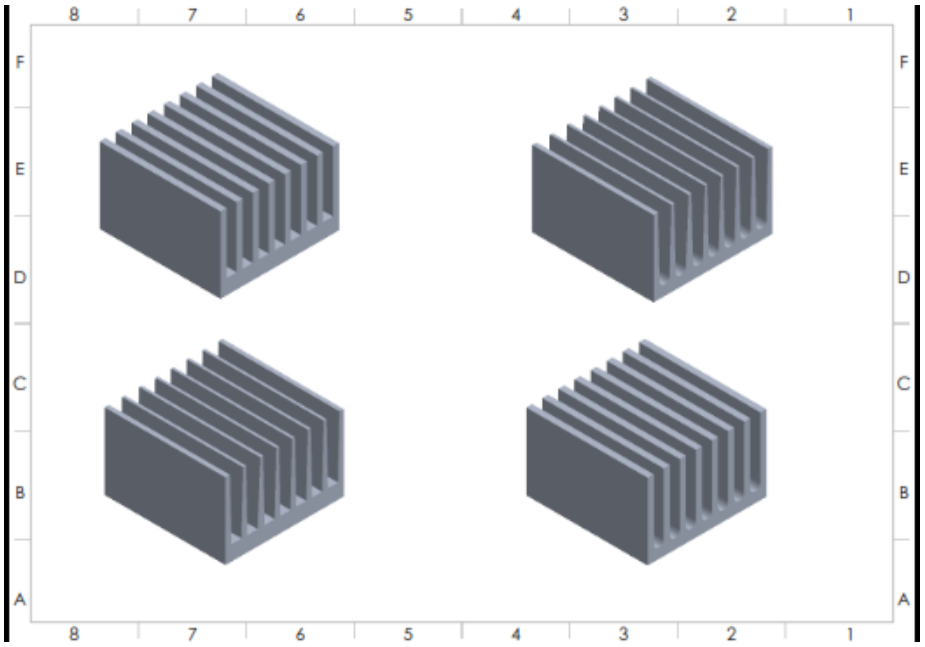

Fig. 1. The geometrical model (a) Conventional design and (b) Proposed designs.

3.3 Mesh generation

In this paper, mesh was generated using Solidworks 2019 software is used to construct the computational grid as well as to discretize and to solve the governing equations of mass and heat transfer. To ensure the accuracy of the simulations, the mesh needs to be generated with care in terms of computational time. To reduce the computation time, the mesh with lower elements were be used.

3.4 Boundary conditions

The boundary conditions of a simulation is similar to the work published by (Babarinde, Adeleke, Ogundeji, Adeyeye, & Ganiyu, 2014)where constant heat power of 150W, convective coefficient of air of 25 W/m^2-K. and an inlet variable value of inlet air flow (i.e. 0.00092, 0.00218, 0.0033 and 0.00433 kg/s) has been applied. the plate-fin heat sink is made from Aluminium alloy 6061. Electrical heaters warm the heat sink up and the temperature distribution at the base of the heat sink at different flow rates is measured by probe.

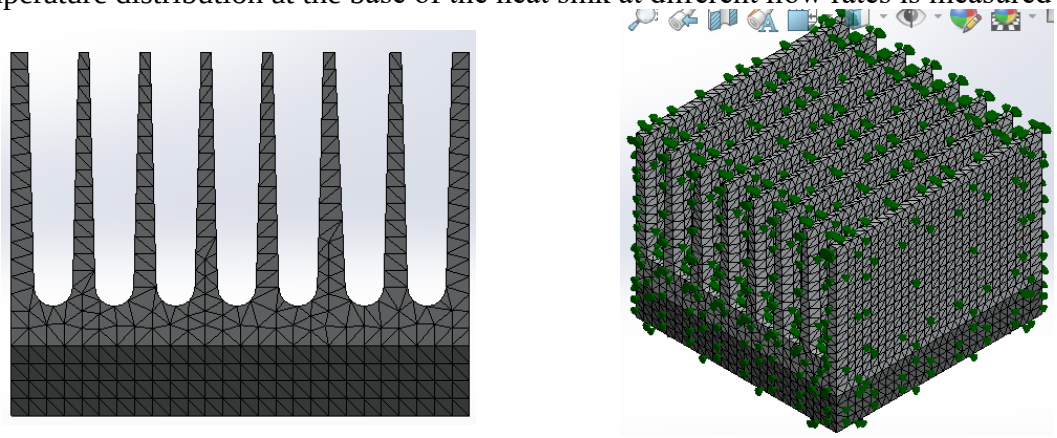

Figure 2: Meshed Geometry

3.5 Heat Sink Resistance Modeling

The primary aim of this research work is to determine the adequacy of the plate heat sink for small electronic coponents. the performance of heat sink is a function of its thermal resistance,(Mohsin & Kherde, 2015). One dimensional method were used to determine the equivalent resistance of the heat sink shown in figure 2shows the global resistance R, in the heat sink and present in equation 1.

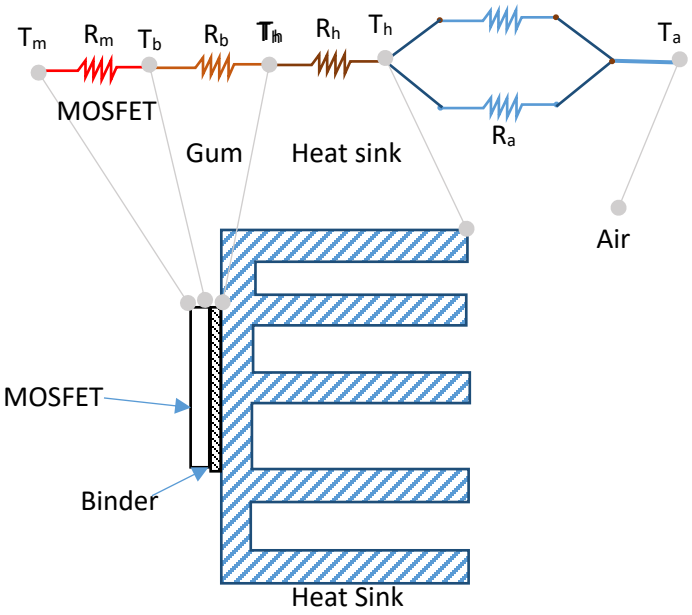

Figure 2: Heat Resistance Circuit.

$R = R_h + R_b + R_m$ 3.1

where

R_m is resistance of the MOSFET, R_b is Resistance of Binder, R_h is Resistance of the heat sink, Ra is Resistance of the air.

The R_h requires an extended analysis because the heat is dissipated to the environment through conduction, convection and radiation from the surface of the heat sink, as presented in figure 3.4

$R_h = R_c + R_v + R_r$ 3.2

And

$$R_c = \frac{t_p}{k.A} \quad 3.3$$

$$R_v = \frac{1}{hA} \quad 3.5$$

$$R_r = \frac{1}{h_r.Ap} \quad 3.6$$

And

$h_r = \varepsilon\sigma(T_h - T_\infty)(T_2^2 + T_\infty^2)$

Where;

$\varepsilon$is emissivity of the surface of the flat plate.

$\sigma = 5.67\alpha w^{-8}$ w/m^2.ic^4

K is plate thermal conductivity (W/k.m), A is heat transfeer area (m^2), t_p is thickness of the binder (m)

3.6 Fin Parameter (m)

Yunus (2008), noted that the fin parameter m of a annular fin of rectangular cross section is given by;

$$m = \sqrt{\frac{2h}{kt_f}} \qquad 3.7$$

3.7 Fin Effectiveness(ε_f)

, noted that fins effectiveness is the ratio of the heat transfer from the finned surface to that of heat transfer from the same surface without fins. Yunus (2008), also noted that the fin effectiveness is calculated by;

$$\varepsilon_f = \sqrt{\frac{kP}{hA_c}} \qquad 3.8$$

Where;

k is thermal Conductivity of the fin material (W/m.K), P is fins Perimeter (m), A_c is fins cross sectional area (m^2)

3.8 Fin Efficiency(η_f)

Fins design are not always likely to be too long so that their temperature does not approach the surrounding temperature at the tip of the fins (Yunus 2008). In order to improve heat dissipation rate of the brake drum; the temperature at the fin tip are considered not to approach the surrounding temperature.

Yunus (2008), relates fins effectiveness and fin efficiency as;

$$\varepsilon_f = \frac{A_f}{A_b}\boldsymbol{\eta_f} \qquad 3.9$$

$$\boldsymbol{\eta_f} = \frac{A_b}{A_f}\varepsilon_f \qquad 3.10$$

Where A_f= Total Surface Area of the Fin

A_b= Base Area of the Fin

4.0 Results and Discussion of the results

The shape of a heat sink contribute to its performance and therefore, the results of the various heat sink configuration used in the research work are shown in Figure 4. Figure 4a, present the results for the normal or control heat sink. Figure 4b, shows the result of the heat sink that have its fin tappered and fillet. And figures 4c and 4d are results of the heat sinks with tappered and fillet fins respectively.

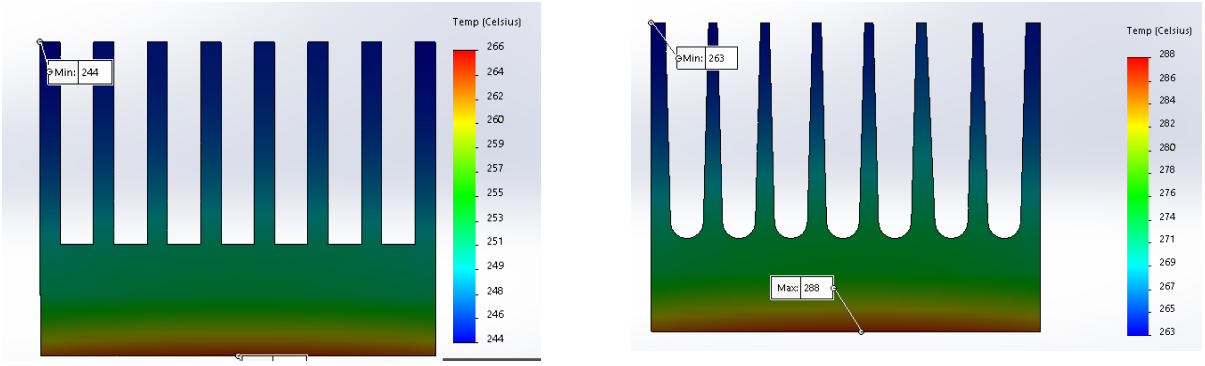

Figure 4: Temperature distribution of the Test 1 and Test 2 of the heat sink.

The minimum temperature for the configurations in Figure 4a, 4b, 4c and 4d are 244ºC, 266 ºC, 270 ºC and 238 ºC respectively, while the maximum temperatures in the heat sinks are ºC, 266 ºC, 288 ºC, 294 ºC and 260 ºC respectively. From this results it is clear that under natural convection test 4 and Test 1 have a better performance,

while test 2 and test 3 have a poorer performance. but test 4 has a better result that all other three heat sinks and it is cooler during operation. This explaination is also confirm on the graph shown in figure 5.

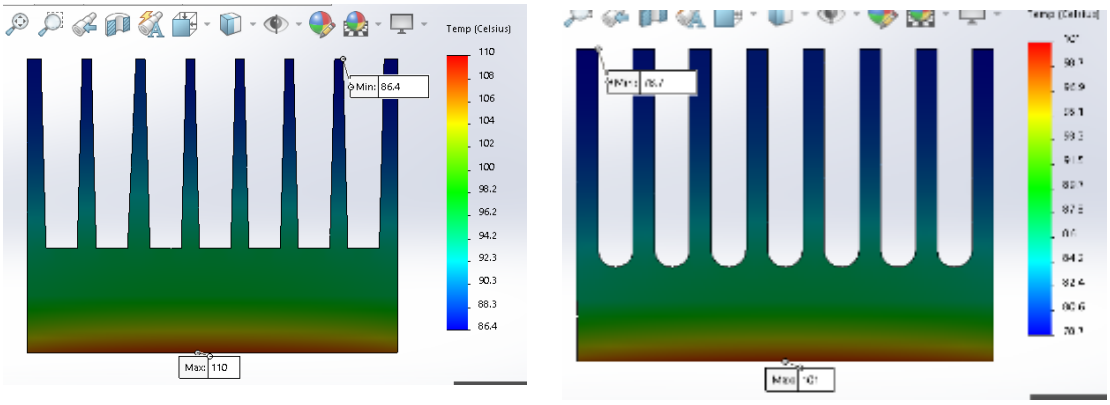

c – Test 3 d – Test 4

Figure 5: Temperature distribution of the Test 1 and Test 2 of the heat sink.

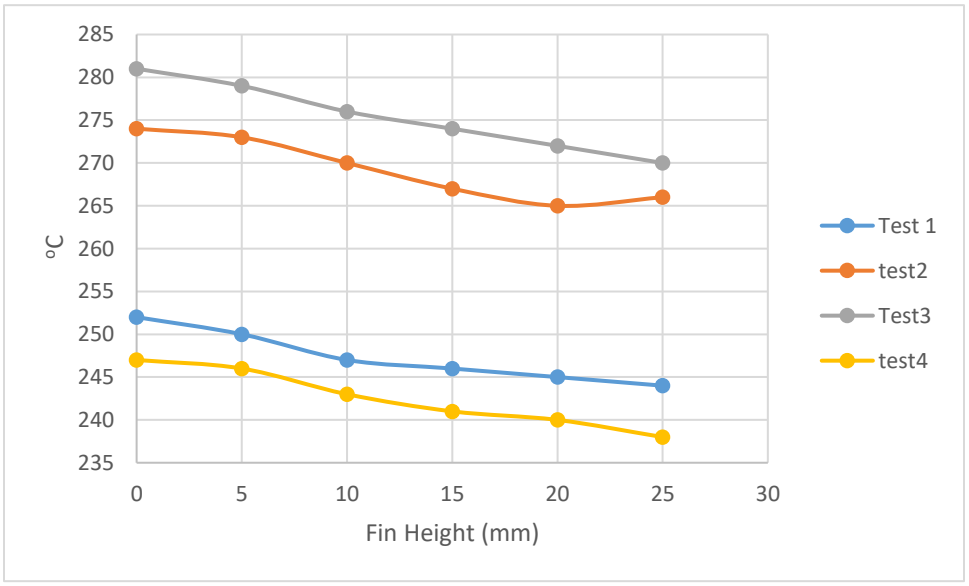

Figure 5: Comparison of the Temperature profile of the middle fin for each heat sink.

Conclusion

The objectives of this study has been successfully achieved by using CFD software. As temperature difference in the heat sink occur in different configurations of the flat plate heat sink used in the study. A 3D model of the heat sinks has been produced and a thermal simulation was conducted on each configuration of the heat sink. The results of the thermal analysis shows that the other of their performance is test 3, test 2, test 1 and test 4 respectively. Test 3 has the highest heat sink temperature of 294^{o}C while test 4 has the lowest heat sink temperature of 238 ^{o}C.and this reveal that fillet has greater important on the heat sink cooling performance.

References

Arularasan, R. (2008). Fluid Flow and Heat Transfer Analysis in AaParallel Plate Heat Sink Using a Commercial CFD Software. *International Journal of Pure and Applied Physics, 4*(2), 97–104. Retrieved from http://www.ripublication.com/ijpap.htm

Babarinde, O. O., Adeleke, B. S., Ogundeji, O. A., Adeyeye, A. H., & Ganiyu, A. L. (2014, June). Design and Construction of 1kVA Inverter. *International Journal of Emerging Engineering Research and Technology, 2*(3), 201-212.

Mohsin, A. A., & Kherde, S. M. (2015, February). Design Modification and Analysis of Two Wheeler Engine Cooling Fins by CFD. *International Journal of Science, Engineering and Technology Research (IJSETR), 4*(2).

Raaid, R. J. (2013). Effect the Form of Perforation on the Heat Transfer in the Perforated Fins. *Academic Research International, 4*(3), 198-207.

Sampath, S. S., Sawan, S., & Chithirai, P. S. (2015). Estimation of Heat Dissipation from Plate with Multiple Tapered and Rectangular Fins. *European Journal of Advances in Engineering and Technology, 2*(5), 123-128. Retrieved from www.ejaet.com

Sandhya, M., & Kishore, P. S. (2015). Heat Transfer Analysis on a Triangular Fin. *International Journal of Engineering Trends and Technology, 19*(5), 279-284.

Tari, L. (2013). Passive cooling assembly for flat panel displays with integrated high power components. *IEEE Transactions on Consumer Electronics 55*, 1707-1713.

Zhipeng, D., Xianghui, L. H., Liangbin, S., & Mengqiao, Z. (2020). Analysis of Flow Characteristics and Pressure Drop for an Impinging Plate Fin Heat Sink with Elliptic Bottom Profiles. *Applied Science, 10*. doi:10.3390/app10010225 www.mdpi.com/